EXPLORING THE EFFECTS OF NUTRIENT DEPRIVATION AND WASTE ACCUMULATION ON T CELLS AND ONCOLYTIC ADENOVIRUSES; IN ORDER TO CREATE IMMUNE ACTIVATORS FOR TUMOUR THERAPY

Sally Frost

Department of Oncology

University College, University of Oxford



A thesis submitted for the degree of Doctor of Philosophy to the Department of Oncology,

University of Oxford, Trinity Term 2020

Supervisor: Professor Len Seymour

A statement addressing the impact of the COVID-19 global pandemic upon this thesis

I was unable to access any laboratories from March 2020 until September 2020, owing to the SARS-CoV-2 outbreak and the nationwide restrictions imposed as a result. All students have been advised to attach documentation of the effects that these restrictions had upon their research.

During this lost time, my main research priorities were as follows:

1) Repeating transfections with siRNAs and shRNAs for reproducibility in pH modulation (Chapter 5)
2) EnAd-shRNA viruses (Chapter 5);
    - To assess the ability for EnAd-shRNA encoded viruses to modulate the pH of culture medium using a real-time pH plate reader (pH-Xtra microplate reader).
    - To repeat viral activity quality control checks to verify results of modified viruses (Figures 5.21-24).
    - To then assess whether modulated conditioned medium of modified virus infected DLD-1 cells would reverse pH-induced suppression of T cells with BiTE.
3) Culturing in Patient 4 (Asc2) (Chapter 3);
    - To identify the potentiating factor in Asc2.
    - To repeat culture experiments and observe changes in CD46 and DSG2 in DLD-1 cells.

If there was time left, then additional experiments were to be conducted as follows:

1) Explore the mechanisms behind T cell inhibition in acid with BiTEs (Chapter 4)
    - Analyse TriTEs with CD28 and compare them to the equivalent BiTE in acid
    - Use flow cytometry and western blots to analyse signalling pathways and metabolism in T cells after activation with BiTE in acid
2) T cell anergy (Chapters 3 & 4)
    - To observe the after effects of BiTE activation on T cells and quantify whether reactivation of exhausted T cells (if they are exhausted) is possible
3) Comparing acidosis targets (Chapter 5)
    - To compare the activity of inhibition of a range of inhibitors including those against NHE1, MCT-1, MCT-4, and CA IX, against siRNA and shRNA used in this study.

Whilst I am unable to present this work, I have made a considerable effort to highlight the gaps that exist within this thesis and to bridge these with analysis of literature which provide possible insights into these experiments as well as to admit the limitations of certain results.

“It is more fun to talk with someone who doesn’t use long, difficult words but rather short, easy words like, ‘What about lunch?’”

- Winnie The Pooh

A. A. Milne

Abstract

High metabolic stress is a hallmark of cancer. Tumours are characterised by a depletion of amino acids and accumulation of lactic acid, both promote an immunosuppressive milieu and may limit success of cancer immunotherapy. One such therapeutic approach is represented by an oncolytic adenovirus, EnAdenotucirev (EnAd), engineered to express a bispecific T cell engager (BiTE) targeting EpCAM. This platform offers a multi-pronged strategy to directly lyse cancer cells and elicit T cell-mediated cytotoxicity, demonstrating anti-cancer activity in *ex vivo* tumour models. However, the impact of nutrient depletion and lactic acid upon EnAd and the EpCAM BiTE are yet to be explored.

Here, we show that the EpCAM BiTE is able to overcome nutrient depletion, likely due to its ability to hyper-activate T cells. By contrast, EnAd replication and cytolytic activity is severely impacted. This was demonstrated using artificial amino acid-depleted media and malignant ascites fluids. The opposite held true for therapeutic activity in accumulated lactic acid; BiTE functionality was severely limited due to acidification, while EnAd was less susceptible and retained its ability to replicate. The use of different BiTE formats did not relieve the inhibition observed. This work is the first to describe the impact of low pH on the activity of BiTEs, and serves to highlight the importance of utilising clinically-relevant models during the pre-clinical development of immunotherapies.

Acidosis represents a hurdle for T cell-activating therapies. We propose that using EnAd to express shRNAs targeting lactic acid production in tumour cells, may reverse pH-induced immune suppression. We targeted LDHA and MCT-4, two components required to extrude lactic acid. We showed that knockdown of LDHA following infection was possible and that the shRNA-encoded EnAd retained its oncolytic and replicative capabilities. Arming oncolytic viruses with anti-acidity agents, alongside those with T cell-activating abilities, may offer a novel approach to overcome metabolic barriers of the tumour microenvironment and combat immune evasion.

Declaration of Authentication

The material presented in this thesis was performed under the supervision of Professor Leonard Seymour, Department of Oncology, Medical Sciences Division, University of Oxford. This work is entirely my own and any contribution made by others has been acknowledged. The work submitted does not form part of another thesis in this or any other university.

Sally Frost

October 2020

Publication Note

Material from the following mini review article in *Cytokine & Growth Factor Reviews* is used in the Introduction (Chapter 1):

- Dyer, A.; **Frost, S**.; Fisher, K.D.; Seymour, L.W. "The role of cancer metabolism in defining the success of oncolytic viro-immunotherapy." *Cytokine and Growth Factor Reviews* **2020**, https://doi.org/10.1016/j.cytogfr.2020.07.006.

Contributions to published work made over the course of this DPhil:

- Pokrovska, T.D.; Jacobus, E.J.; Puliyadi, R.; Prevo, R.; **Frost, S.;** Dyer, A.; Baugh, R.; Rodriguez-Berriguete, G.; Fisher, K.D.; Granata, G.; Herbert, K.; Taverner, W.K.; Champion, B.R.; Higgins, G.S.; Seymour, L.W.; Lei-Rossman, J. "External Bean Radiation Therapy and Enadenotucirev: Inhibition of the DDR and Mechanisms of Radiation-Mediated Virus Increase." *Cancers* **2020**, *12(4),* 798.
- Yousaf, I.; Kaeppler, J.; **Frost, S.;** Seymour, L.W.; Jacobus, E.J. "Attenuation of the Hypoxia Inducible Factor Pathway after Oncolytic Adenovirus Infection Coincides with Decreased Vessel Perfusion." *Cancers* **2020**, *12*, 851.
- Scott, E.M.; **Frost, S.;** Khalique, H.; Freedman, J.D.; Seymour, L.W.; Lei-Rossman, J. "Use of Liquid Patient Ascites Fluids as a Preclinical Model for Oncolytic Virus Activity." *Methods in Molecular Biology* **2020**, *2058,* 261-270.
- Scott, E.M.; Jacobus, E.J.; Lyons, B.; **Frost, S.;** Freedman, J.D.; Dyer, A.; Khalique, H.; Taverner, W.K.; Carr, A.; Champion, B.R.; Fisher, K.D.; Seymour, L.W.; Duffy, M.R. "Bi- and tri-valent T cell engagers deplete tumour-associated macrophages in cancer patient samples." *Journal for Immunotherapy of Cancer* **2019**, *7,* 320.
- Dyer, A.; Schoeps, B.; **Frost, S.;** Jakeman, P.; Scott, E.M.; Freedman, J.D.; Jacobus, E,J.; Seymour, L.W. "Antagonism of Glycolysis and Reductive Carboxylation of Glutamine potentiates Activity of Oncolytic Adenoviruses in Cancer Cells." *Cancer Research* **2019**, *15; 79(2),* 331-345.
- Dyer, A.; Baugh, R.; Chia, S.L.; **Frost, S.;** Iris, Jacobus, E.J.; Khalique, H.; Pokrovska, T.D.; Scott, E.M.; Taverner, W.K.; Seymour, L.W.; Lei-Rossman, J. "Turning cold tumours hot: oncolytic virotherapy gets up close and personal with other therapeutics at the 11th Oncolytic Virus Conference." *Cancer Gene Therapy* **2018**, *Sep 4.*

Acknowledgements

What a wonderful four years it has been, and through it all there has been so much support and fun that even the tougher times haven't seemed half bad and for that I have a lot of people to thank!

Firstly, I'd like to acknowledge how grateful I am to Professor Len Seymour. His continued guidance, good humour, and encouragement have been invaluable to my PhD experience, as well as creating the best lab group that I could have hoped for. I would also like to thank Dr Kerry Fisher for his fantastic ideas and interest in my project throughout. This work would also not have been possible without Ruth Webb and Aubrina Ashton at the NHSBT Oxford Blood Donor Centre, who were a pleasure to see every week.

Much of this work would not have been possible without Dr Janet Lei-Rossman and Dr Brian Lyons; their efforts to help me during my PhD, particularly towards the end, have been instrumental to me managing to complete this thesis. I am so grateful for their scientific know-how and their continued sincerity and friendship. I am eternally grateful to each and every one of Len's Angels, both past and present members. Each one of you has positively influenced my work and life throughout this time. Special mentions to past members, Dr Joshy Freedman and Dr Egon Jacobus, two people who I look up to and who continue to make me laugh and smile every time we speak. To present members, Dr Hena Khalique and Flurin Caviezel; you have no idea how much you have helped me during the struggle of this last year. To my co-thesis writers, Dr Tzveta Povrovska and Dr Arthur Dyer; I wouldn't have chosen anyone else to go through this last six months with than both of you. To Dr Will Taverner, Dr Ellie Scott and Richard Baugh; I am so happy that our PhDs have coincided in this lab. I have made lifelong friends who I would never be without.

I would also like to pass my gratitude to Dr Itziar Serna Martin and Judith Oymans; your enthusiasm and friendship that welcomed me to Oxford made it all the more easy to stay. I miss you both. For their friendship and support I would like to thank Hannah Lake, Olivia Hendry, and Luke Ashton. To Josh and Demelza Abbott-Scott, thank you for coins. To the Scotts, Hamers, and Holsts, I am so grateful for your continued motivation and love.

Finally, to my sisters, Rosie and Lucy, for always boosting my confidence and letting me know I can do anything I put my mind to. Also to Josh and Marc, alongside my siblings, who have left me with an unending stream of videos and photos of the beautiful Betsy and Rupert, which have kept me smiling throughout the last six months. To my mum and dad, thank goodness you persuaded me to take all Sciences as A-levels and not Photography all those years ago. Where would I be otherwise? Thank you both for everything you do for me, from the little things to the big, they all make a difference to me. I am dedicating this thesis to you all, my family.

To Nat, you have looked after me over the last four years, and for longer even before that. I owe this PhD to you. You are the one who encouraged me to apply in the first place and the one who has helped me to get to the end. I cannot wait to become your wife!

(Also, I feel I must mention Stephen Fry and J. K. Rowling for being the voices inside my head for these past four years).

Table of Contents

A statement addressing the impact of the COVID-19 global pandemic upon this thesis iii
Abstract vii
Declaration of Authentication ix
Publication Note xi
Acknowledgements xiii
Table of Contents xv
List of Abbreviations xx
1 Introduction 1
1.1 Cancer and its treatment 1
1.1.1 General introduction 1
1.1.2 Traditional approaches to cancer treatment 2
1.2 Cancer immunotherapy 3
1.2.1 Cancer and the immune system 3
1.2.2 Tumour cell-intrinsic mechanisms of immune evasion 6
1.2.3 TME-mediated immune evasion 7
1.2.4 Immunotherapeutic strategies 10
1.3 Bispecific T cell engagers 16
1.3.1 Structure and mode of action 16
1.3.2 BiTE activation versus HLA-dependent activation 18
1.3.3 Benefits and challenges 20
1.4 Oncolytic viruses 21
1.4.1 The basis of OV selectivity 21
1.4.2 Route of delivery 23
1.4.3 Mode of action 25
1.4.4 ‘Arming’ OVs 27
1.4.5 RNA interference 30
1.5 Nutrient depletion in the TME 32
1.5.1 Amino acid metabolism in cancer 32
1.5.2 Impact of nutrients on oncolytic virus metabolism 35
1.5.3 Impact of nutrient depletion on immunometabolism 36
1.5.4 Models of TME-based nutrient levels 38
1.6 Acidification of the TME 40
1.6.1 Lactic acid in the TME 40
1.6.2 Further acidification of the TME 47
1.6.3 Current treatment targeting lactic acid and acidification 50
1.7 Thesis overview and aims 53
1.7.1 Overview 53

1.7.2 Thesis aims and hypotheses 54
2 Materials and Methods 55
2.1 Tissue culture 55
2.1.1 Cell line maintenance 55
2.1.2 Cryopreservation of cells 55
2.1.3 Cell seeding 56
2.1.4 Treatments and reagents for cell culture 56
2.1.5 RNA and DNA transfections 59
2.1.6 pH measurement of reagents and medium 60
2.1.7 Lactate measurements of conditioned medium 60
2.2 Molecular cloning 61
2.2.1 Bacterial transformation 61
2.2.2 Hairpin construction 61
2.2.3 DNA plasmid preparation and purification 62
2.2.4 DNA restriction digests 63
2.2.5 Polymerase chain reaction 63
2.2.6 Agarose gel electrophoresis 64
2.2.7 DNA purification from agarose gels 64
2.2.8 DNA quantification 64
2.2.9 DNA ligation and Gibson assembly 65
2.2.10 Sequencing 65
2.3 Molecular biology methods 66
2.3.1 BiTE preparation 66
2.3.2 Protein extraction, preparation and quantification 66
2.3.3 SDS-PAGE gel electrophoresis 67
2.3.4 Immunoblotting 67
2.3.5 Enzyme-linked immunosorbent assay to assess BiTE concentration 69
2.3.6 RNA extraction and complementary DNA synthesis 69
2.3.7 Reverse transcription PCR and reverse transcription quantitative PCR 69
2.4 Flow cytometry 71
2.4.1 Harvesting cells 71
2.4.2 Cell surface staining 71
2.4.3 Intracellular staining 72
2.4.4 Absolute cell counts 73
2.4.5 Assessment of BiTE binding 74
2.4.6 Data acquisition and analysis 75
2.5 Immune cell assays 77
2.5.1 General statement 77
2.5.2 Isolation of lymphocytes from human peripheral blood 77
2.5.3 CD3-positive T cell extraction 79
2.5.4 Co-culture experiments of T cells and target cells 79

2.5.5 Characterisation of T cell activation 80
2.5.6 Characterisation of T cell cytotoxicity 80
2.5.7 Characterisation of T cell degranulation 81
2.5.8 Expansion of a ST8.24 $CD8^+$ T cell clone 81
2.5.9 ST8.24 $CD8^+$ T cell clone co-culture with target cells 83
2.6 Target cell cytotoxicity assays 84
2.6.1 Lactate dehydrogenase release assay 84
2.6.2 MTS cell proliferation assay 85
2.6.3 PrestoBlue cell viability assay 86
2.6.4 $EGFR^+$ count viability assay using flow cytometry 86
2.6.5 Cell adhesion with the xCELLigence Real-Time Cell Analysis system 87
2.7 Ex vivo experiments with malignant clinical samples 88
2.7.1 General statement 88
2.7.2 Processing patient-derived peritoneal ascites fluids 88
2.7.3 Amino acid level determination by HPLC 88
2.7.4 Ascites-based nutrient stress models 91
2.8 Virology methods 92
2.8.1 Viral infections 92
2.8.2 Adenovirus cloning 93
2.8.3 Adenovirus rescue 94
2.8.4 Plaque purification 94
2.8.5 Adenovirus propagation 95
2.8.6 Adenovirus purification 96
2.8.7 Determination of adenovirus quantification using dsDNA measurements 98
2.8.8 Infectious viral particle assessment by $TCID_{50}$ 98
2.8.9 Infectious viral particle measurement by plaque-forming assay 99
2.8.10 Measuring adenovirus genome replication using qPCR 100
2.8.11 Quantification of infectious units using a luminescent reporter 101
2.8.12 Virus tracking and quantification of viral expression using reporter genes 103
2.9 Statistical analysis 104
3 Determining the effect of amino acid depletion on EpCAM BiTE-induced T cell activation and EnAd activity 105
3.1 Introduction and chapter aims 105
3.1.1 Introduction 105
3.1.2 Chapter aims 108
3.2 Results 108
3.2.1 SKOV-3 tumour cell viability when individual amino acids are absent from culture medium 108
3.2.2 The ability of EpCAM BiTE to activate T cells is impacted by amino acid deficiencies 110
3.2.3 Biomarkers of cytotoxicity potential are reduced when glutamine is absent after EpCAM BiTE activation of $CD3^+$ T cells 114

3.2.4 SKOV-3 cytotoxicity via the EpCAM BiTE is less affected by amino acid depletion and makes HLA-dependent killing more potent 117
3.2.5 Medium deficient in aspartic acid medium resulted in faster tumour cell apoptosis....122
3.2.6 EnAd viral replication is diminished through loss of amino acids 126
3.2.7 Decreases in cytolysis by EnAd reflect decreased levels of viral replication....129
3.2.8 Pathological nutrient levels of the TME can be mirrored using *ex vivo* ascites fluid....133
3.2.9 EpCAM BiTE-induced T cell activation is unhindered by ascites fluids devoid of cytokines and chemokines 136
3.2.10 Cytotoxicity potential of T cells after culture in EpCAM BiTE and exudate fluids is not changed compared to control medium....139
3.2.11 EpCAM BiTE-induced T cell dependent target cell lysis is not reduced in patient ascites fluids 140
3.2.12 EnAd potency is diminished in clinically relevant *ex vivo* models representing realistic nutrient levels 145
3.3 Conclusions....149
3.4 Discussion....149
4 Assessing BiTE-induced T cell function during lactic acid accumulation 154
4.1 Introduction and chapter aims....154
4.1.1 Introduction 154
4.1.2 Chapter aims....156
4.2 Results....156
4.2.1 Lactic acid concentrations of more than 20 mM (pH 6.2) cause tumour cell death in 2D culture 156
4.2.2 Lactic acid inhibits activation and the cytolytic potential of T cells induced by the EpCAM BiTE and CD3/CD28 beads 159
4.2.3 Activation and markers of cytolytic potential in T cells is reduced in both T cell subsets.164
4.2.4 EpCAM BiTE-induced and HLA-dependent cytotoxicity are incapacitated by lactic acid accumulation....167
4.2.5 Inhibition of BiTE-mediated T cell activation by lactic acid can be partially reversed with HEPES addition....171
4.2.6 Complete neutralisation of low pH caused by lactic acid accumulation fully restores BiTE activity 174
4.2.7 HCl-induced low pH diminished EpCAM BiTE-induced T cell activation 179
4.2.8 Binding of EpCAM BiTE constructs to $EpCAM^+$ tumour cells and $CD3^+$ T cells changes in acidic conditions....182
4.2.9 Multiple BiTE constructs are negatively influenced by low pH....185
4.2.10 Generation and production of PD-L1 targeting nanoBiTEs 190
4.2.11 T cell activation and biomarkers of T cell cytotoxicity potential induced by a PD-L1 nanoBiTE remains inhibited during lactic acidosis 195
4.3 Conclusions....198
4.4 Discussion....198
5 Assessing the potential of targeting acidosis using armed oncolytic adenoviruses....201
5.1 Introduction and chapter aims....201
5.1.1 Introduction 201

5.1.2 Chapter aims 202
5.2 Results 203
5.2.1 Conditioned medium from DLD-1 tumour cell cultures inhibits T cell activation by EpCAM BiTE 203
5.2.2 Culturing cells in high glucose increases the level of acidification, recreating the environment more likely observed in patient tumours 205
5.2.3 Conditioned medium from EnAd-infected tumour cells does not worsen inhibition of T cells in medium from uninfected tumour cells 207
5.2.4 Transfection of siRNA targeting LDHA and MCT-4 does not improve T cell activation in glucose-mediated acidosis 211
5.2.5 The activity of EnAd in an acidic cellular environment is affected more in glycolytic cells than cells that rely on oxidative phosphorylation 216
5.2.6 The cytolytic activity of EnAd decreased in accumulating lactic acid 221
5.2.7 Gene knockdown of LDHA and MCT-4 do not affect EnAd genome replication, cell permissiveness or infectious particle release 224
5.2.8 Design of hairpin siRNAs that target LDHA, LDHB and MCT-4 silence target proteins after DNA transfection 230
5.2.9 Cloning strategy to generate OVs containing hairpins against LDHA, LDHB and MCT-4 and a GFP reporter 233
5.2.10 Engineered EnAd viruses with hairpins knock down lactic acid pathway target proteins 239
5.2.11 Viral genome replication and oncolytic activities of hairpin-armed EnAd viruses is slightly reduced compared to parental EnAd 242
5.2.12 EnAd-expressing shRNA against LDHA successfully knocks down expression of LDHA after infection 245
5.3 Conclusions 247
5.4 Discussion 248
6 Final conclusions and discussion 251
6.1 Overview of the thesis 251
6.2 Final discussion 254
6.3 Concluding remarks 260
7 Appendices 261
Appendix I Materials 261
Appendix II DNA and amino acid sequences 263
Appendix III HPLC amino acid standard curves 266
8 References 267

List of Abbreviations

Ab	Antibody
Abs	Absorbance
ASCT	Alanine-serine-cysteine exchanger
ACT	Adoptive cell therapy
AdV	Adenovirus
Akt	Protein kinase B
AMPK	5’ AMP-activated protein kinase
ANOVA	Analysis of variance
APC	Antigen-presenting cell
Asc.	Peritoneal ascites
ATCC	American type culture collection
ATF	Activating transcription factor
ATP	Adenosine triphosphate
BCA	Bicinchoninic acid
BCAA	Branched chain amino acid
BiTE	Bispecific T cell engager
BSA	Bovine serum albumin
CA	Carbonic anhydrase
CAF	Cancer-associated fibroblast
CAR	Chimeric antigen receptor
CD	Cluster of differentiation
cDNA	Complementary DNA
CFSE	Carboxyfluorescein succinimidyl ester
CHC	α-cyano-4-hydroxycinnamate
CM	Conditioned medium
CMV	Cytomegalovirus
CTL	Cytotoxic T lymphocyte
CTLA-4	Cytotoxic T-lymphocyte-associated protein 4
CPE	Cytopathic effect
CsCl	Caesium chloride
DAMP	Danger-associated molecular patterns

DC	Dendritic cell
DMEM	Dulbecco's modified Eagle's medium
DMSO	Dimethyl sulfoxide
DPBS	Dulbecco's Phosphate buffered saline
EC_{50}	Half the maximal effective concentration
ECM	Extracellular matrix
EDTA	Ethylenediamine tetra-acetic acid
EGFR	Epidermal growth factor receptor
ELISA	Enzyme-linked immunosorbent assay
EnAd	Enadenotucirev
EpCAM	Epithelial cell adhesion molecule
E:T ratio	Effector:target ratio
FAP	Fibroblast-associated protein
FBS	Foetal bovine serum
Fc	Fragment crystallisable
FcR	Fc receptor
FDA	Food and Drug Administration
FMOC	9-fluorenyl-methyl chloroformate
FLuc	Firefly luciferase
g	Standard gravitational force
GCN2	General control non derepressable 2
gMFI	Geometric mean fluorescence intensity
GFP	Green fluorescent protein
GM-CSF	Granulocyte-macrophage colony-stimulating factor
GPR	G-protein coupled receptor
GrB	Granzyme B
GSH	Glutathione
GSK-3	Glycogen synthase kinase 3
HCl	Hydrochloric acid
HIF	Hypoxia inducible factor
HEPES	4-(2-hydroxyethyl)-1-piperazineethanesulfonic acid
HLA	Human leukocyte antigen
hpi	Hours post-infection
HPLC	High pressure liquid chromatography

HRP	Horseradish peroxidase
HSV	Herpes simplex virus
ICD	Immunogenic cell death
ICI	Immune checkpoint inhibitor
IDO	Indoleamine-2, 3-dioxygenase
IFN	Interferon
Ig	Immunoglobulin
IL	Interleukin
IR	Infrared
LAG-3	Lymphocyte-activation gene 3
LAT	L-type amino acid antiporters
LB	Lysogeny broth
LDH	Lactate dehydrogenase
LiTE	Bispecific light T-cell engager
mAb	Monoclonal antibody
MCT	Monocarboxylate transporter
MDSC	Myeloid-derived suppressor cell
MHC	Major histocompatibility complex
MLP	Major late promoter
mRNA	Messenger RNA
MOI	Multiplicity of infection
mTOR	Mammalian target of rapamycin
mTORC1	mTOR complex 1
MTS tetrazolium	3-(4,5-dimethylthiazol-2-yl)-5-(3-carboxymethoxyphenyl)-2-(4-sulfophenyl)-2H-
MWCO	Molecular weight cut-off
NaCl	Sodium chloride
NAD^+	Nicotinamide adenine dinucleotide
NADP	Nicotinamide adenine dinucleotide phosphate
NaL	Sodium lactate
NDV	Newcastle disease virus
NHE1	Sodium-hydrogen exchanger
NHSBT	NHS blood and transport service
NK	Natural killer

OAdV	Oncolytic adenovirus
OD	Optical density
OPA	Ortho-phthalaldehyde
OV	Oncolytic virus
OVT	Oncolytic virus therapy
OXPHOS	Oxidative phosphorylation
PAMP	Pathogen-associated molecular pattern
PBMC	Peripheral blood mononuclear cell
PBST	DPBS-Tween
PCR	Polymerase chain reaction
PDA	Photodiode array
PDH	Pyruvate dehydrogenase
PDK	Pyruvate dehydrogenase kinase
PD-1	Programmed cell death protein 1
PD-L1	Programmed death-ligand 1
PHA	Phytohaemagglutinin
pH_e	Extracellular pH
pH_i	Intracellular pH
PI3K	Phosphoinositide 3-kinase
PFU	Plague forming unit
P/S	Penicillin-streptomycin
PPI	Proton pump inhibitor
qPCR	Quantitative PCR
RBC	Red blood cell
RISC	RNA-induced silencing complex
RNAi	RNA interference
ROS	Reactive oxygen species
RPMI	Roswell Park Memorial Institute
RT	Room temperature
RTCA	Real-time cell analysis
RT-qPCR	Reverse transcription quantitative PCR
SA	Splice acceptor
scFv	Single-chain variable fragment
SD	Standard deviation

SDS	Sodium dodecyl sulphate
SDS-PAGE	SDS-polyacrylamide gel electrophoresis
siRNA	Small interfering RNA
shRNA	Short hairpin RNA
SOC	Super optimal broth with catabolite repression
TAA	Tumour-associated antigen
TCA	Tricarboxylic acid
TAM	Tumour-associated macrophage
$TCID_{50}$	Median tissue culture infectious dose
TCR	T cell receptor
TGF-β	Transforming growth factor beta
Th	T helper cell
TIL	Tumour-infiltrating lymphocyte
TME	Tumour microenvironment
TNF-α	Tumour necrosis factor alpha
Treg	Regulatory T cell
Tris	Trisaminomethane
TriTE	Trivalent T cell engager
T-Vec	Talimogene laherparepvec
v/v	volume/volume
VACV	Vaccinia virus
V-ATPase	Vacuolar-ATPase
VEGF	Vascular endothelial growth factor
vg	Viral genome
VH	Heavy chain variable
VHH	Heavy chain only domain, nanobody
VL	Light chain variable
vp	Virus particle
VSV	Vesicular stomatitis virus

1 Introduction

1.1 Cancer and its treatment

1.1.1 General introduction

Cancer is the generic term used for a group of diseases which can affect any part of the body. Cancer is characterised by a set of hallmarks, as described by Hanahan and Weinberg; including uncontrollable cell proliferation and tissue invasion (Hanahan and Weinberg 2011). Cancers arise as a result of the interaction between a person's genetic factors and external carcinogenic agents; both of which can cause mutations in the cell's DNA, resulting in the aberrant control of multiple cellular processes. These culminate in a progressive and complex disease capable of invading adjoining parts of the body in a process called metastasis. This metastasis from primary lesions to distal sites is the major cause of death in cancer patients and represents a big challenge for cancer treatment (Gupta and Massagué 2006).

Cancer is a prevalent disease worldwide, accounting for 9.6 million deaths in 2018 (World Health Organisation, 2020). In the UK alone there are 367,000 new cases of cancer every year and a reported 164,901 deaths (2015 – 2017), accounting for 28% of all deaths in the UK. Since the 1970s the overall incidence of mortality due to cancer has dropped, despite the lifetime risk of developing cancer increasing to 1 in 2 people born in the UK after 1960 (Cancer Research UK, 2020). This is largely due to continuous advances and breakthroughs in early diagnostics, traditional treatments, and more recently in immunotherapy. However, cancer remains incurable for the majority of patients and its incidence is expected to rise over the coming decades due to a growing and aging population (World Health organisation, 2020).

1.1.2 Traditional approaches to cancer treatment

The three most common treatment modalities available for cancer are chemotherapy, radiotherapy and surgery. While each therapy is effective, either as a monotherapy or in combination, they all have a limitation in treating metastatic disease. Surgery is effective and sometimes curative in removing primary tumours, yet only those tumours that are accessible can be removed (Arruebo et al. 2011). Radiotherapy may be able to target surgically-inaccessible tumours but this technique still struggles to target distal lesions without causing damage to healthy tissue (Vilalta, Rafat, and Graves 2016). Finally, although chemotherapy has the means to target all rapidly dividing cells throughout the body, thus broadly targeting proliferating cancer cells, it also affects proliferating normal tissues. This lack of specificity results in significant side effects, and the reduction of the patient's quality of life (E. K. Choi et al. 2014; Carelle et al. 2002). In the majority of cancers these traditional approaches produce only modest effects and in most cases disease relapse occurs.

After the 1970s, a deeper understanding of the molecular changes that occur in cancer cells led to the development of targeted therapies. These treatments inhibit specific molecular targets essential to cancer cells only (Sierra, Cepero, and Giordano 2010). This approach has come with incredible success in a subset of tumour types. Perhaps the best example being the revolutionary treatment of chronic myeloid leukaemia (CML) with Imatinib, a tyrosine kinase inhibitor (Iqbal and Iqbal 2014). Although targeted therapies have had success in single mutation cancers such as CML, most cancers possess genome plasticity and are phenotypically heterogeneous, making them challenging to target with a single agent. Furthermore the intrinsic genomic instability characterised by cancer cells facilitates their escape from targeted therapies and unfortunately resistance-related relapses are common (Engelman and Settleman 2008; Keefe and Bateman 2019).

1.2 Cancer immunotherapy

1.2.1 Cancer and the immune system

Despite William Coley reporting a link between bacterial infection and cancer regression, and Paul Ehrlich hypothesising the role of the immune system in protecting the host from cancer cells over a century ago (Decker et al. 2017; Coley 1909), the concept of the immune system's involvement in cancer since has been hotly debated and largely ignored. Ehrlich's hypothesis was revived in the 1950s by Burnet and Thomas, who coined the term "cancer immunosurveillance". However due to a lack of understanding of experimental models and direct evidence at the time, the hypothesis was abandoned (Dunn et al. 2002). Only recently has there been an accumulation of strong experimental evidence to support the concept including; the positive correlation between lymphocyte infiltration found in tumours and patient survival (Galon et al. 2006; Clemente et al. 1996; Z. Wei et al. 2020), the increased cancer incidence in immunodeficient mice and humans (Dunn et al. 2002), and the discovery of T cells specific for peptides from tumour-associated antigens (TAAs) (van der Bruggen et al. 1991).

Nonetheless, cancer still develops despite the presence of a supposedly functionally active immune system. It has now been established that the immune system does not just surveil but has a dual role in both host-protection and tumour-landscaping. Immunosurveillance results in the selection of less immunogenic variants, contributing towards cancer immune evasion and assisting tumour growth. This led Dunn and colleagues to refine the hypothesis to "cancer immunoediting", which consists of three sequential phases (Dunn et al. 2002).

Elimination

Tumour cell recognition and elimination is mediated initially by the innate immune response, whereby, during the early stages of cancer development, activated natural killer (NK) cells will

target transformed cells, and endogenously produce interferon-γ (IFNγ) (Marcus et al. 2014; Kim, Emi, and Tanabe 2007). Secondly, triggered by NK cell-triggered eradication, immunogenic tumours are then targeted by the adaptive immune response. This process is best described by the cancer-immunity cycle, shown in Figure 1.1. In brief, TAAs are released by tumour cells during cell death or phagocytosis of dead or dying cells (step 1). Antigens are captured by antigen presenting cells (APCs) such as dendritic cells (DCs) (step 2), which mature and migrate to lymph nodes where they present the antigens captured on the major histocompatibility complex class I and II molecules (MHC I/II), resulting in T cell selection and priming through the cognate T cell receptor (TCR) specific to the TAA presented in the context of MHC I or II (step 3). Activated T cells proliferate and then migrate to the tumour (step 4), and infiltrate (step 5). After infiltration, cancer cells are recognised via TCR-peptide/MHC interactions (step 6) and killed by the adaptive immune cells (step 7), thus starting the cycle over again (Kunimasa and Goto 2020; Huber et al. 2017).

Equilibrium

Tumour cells that are not successfully eradicated move to the equilibrium phase, or what is sometimes called the dormancy phase. This phase is the least understood, and is difficult to study due to the inability to identify preneoplastic or early lesions. This equilibrium phase represents a fine balance between tumour cells and immune cells whereby the immune system and the tumour cells coexist together. It is likely this phase lasts for the longest period in the cancer immunoediting process. It has been hypothesised that from here, one of two scenarios will occur; either all transformed cells will eventually be eradicated, thus returning the relationship to the elimination phase; or the constant interaction between tumour cells and immune cells results in the editing of the tumour cells phenotype. The latter scenario thereby

enables the selection of a tumour that is less immunogenic, and is less susceptible to attack from the immune system and thus leads to its progression (Teng et al. 2008).

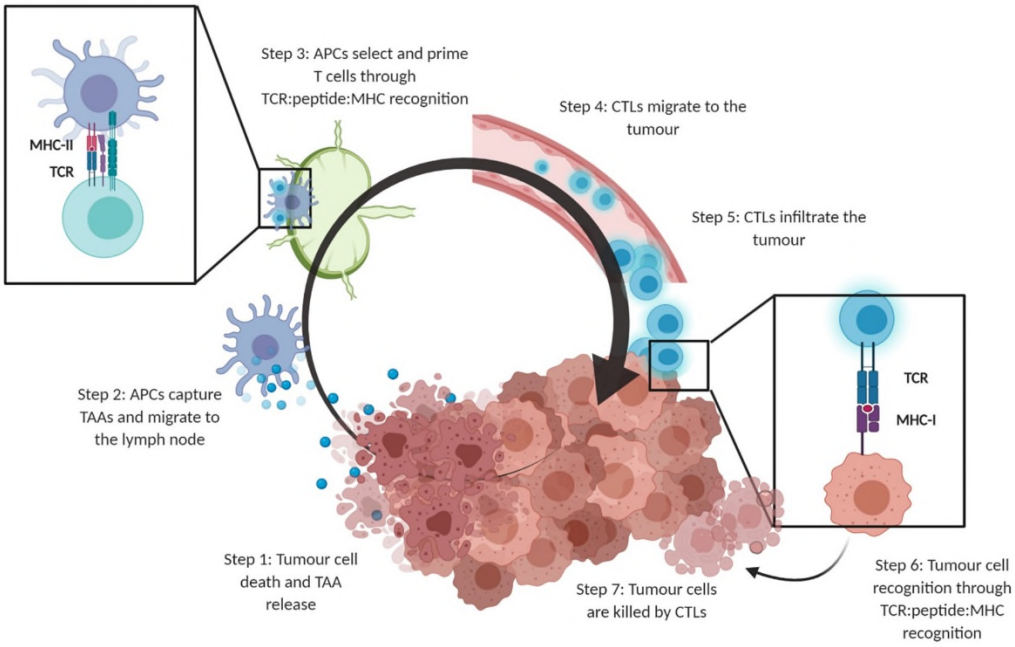


Figure 1.1 The cancer-immunity cycle. In order to eliminate cancer cells an anti-cancer response must be triggered and it must be successful. The cancer-immunity cycle is split into seven steps. TAAs are released at the beginning through tumour cell death, and the cycle ends with T cells infiltrating the tumour and killing more cancer cells. The steps required are as described. The image was adapted from (Kunimasa and Goto, 2020; Huber et al, 2017) and was created using BioRender.com.

Escape

Tumour variants that survive the equilibrium phase have acquired genetic or epigenetic changes, leading to an insensitivity to immunological detection and/or elimination (steps 2 and 6 of the cancer immunity cycle respectively) (Dunn et al. 2002). This is the escape phase of immunoediting, in which most clinically detectable tumours exist (Kunimasa and Goto 2020). Much of the research based around tumour immunology and the generation of immunotherapies lies in this phase. Numerous studies have demonstrated that tumours circumvent the immune system and instead use it to aid their growth, local progression and dissemination. Mechanisms

to avoid the immune system are detailed in the next sections (Teng et al. 2008; Rescigno, Avogadri, and Curigliano 2007).

1.2.2 Tumour cell-intrinsic mechanisms of immune evasion

Perhaps the best documented mechanism of immune evasion is the ability for tumour cells to avoid recognition all together. This can be achieved by circumvention of antigen presentation by the MHC class I. Garrido and colleagues showed the total percentage of the various types of human leukocyte antigen (HLA)-I molecule loss from various human cancers ranged from 65% to 90% depending on cancer type (Garrido et al. 2016). Meanwhile others have shown the down-regulation of antigen processing machinery aided immune evasion, including studies describing the defective expression of the transporter associated with antigen processing (TAP1) in brain metastases (Y. Liu et al. 2012) and in human pancreatic cancer (Pandha et al. 2007).

Alternatively, tumour cells can avoid immune destruction following their recognition by cytotoxic T cells. They may do so by exploiting the negative signalling pathways normally required to control immune responses, and/or by directly avoiding destruction through mediation of cell death pathways. It is well documented that tumour cells up-regulate the expression of immune inhibitory surface molecules (e.g. Cluster of Differentiation (CD)80 to interact with cytotoxic T-lymphocyte-associated protein 4 (CTLA-4) on T cells, programmed death ligand 1 (PD-L1), and lymphocyte-activation gene (LAG3)) (S. C. Wei, Duffy, and Allison 2018) and they secrete immunosuppressive cytokines (e.g. interleukin (IL)-10 and transforming growth factor (TGF)-β) which modulate the immune system toward tolerance (Mittal et al. 2014). Furthermore, tumour cells will directly avoid destruction by: inducing insensitivity to IFNγ; expressing Serpin B9, a serine protease inhibitor that inactivates granzyme B (GrB); or through defective death receptor signalling, for instance through the loss

of tumour necrosis factor (TNF)-related apoptosis-inducing ligand (TRAIL) (Medema et al. 2001; Gallmeier et al. 2013). While this list is not exhaustive, it gives an idea of how many potential routes of escape tumour cells possess in addition to those mediated by the tumour microenvironment (TME) outlined below.

1.2.3 TME-mediated immune evasion

The further progression of cancer is not solely reliant on intrinsic genetic mutations of the cancer cells themselves. The 'seed and soil' hypothesis was proposed by Paget in 1889, wherein he implied that fully neoplastic cells (seeds) were not absolute entities, but were dependent on their environment (soil) to express advantageous phenotypes. The TME is a complex, dynamic and heterogeneous network, depicted in Figure 1.2 and has roles in promoting cancer development, progression and metastasis, and for protection from the immune system. These features make it one of, if not the main, obstacle in treating solid tumours and a better understanding of the TME's biology will be instrumental in cancer management (Duan et al. 2020).

Solid malignant tumours comprise of active cellular and non-cellular components, the proportions and compositions of which are dependent on the location and developmental stage of the tumour (Reina-Campos, Moscat, and Diaz-Meco 2017). It is reported that more than 50% of the mass of primary tumours and their metastases are non-malignant cells (Balkwill, Capasso, and Hagemann 2012). These cells include: cancer stem cells, vascular endothelial cells, pericytes, cancer-associated fibroblasts (CAFs), and immune cells (Hanahan and Weinberg 2011). The latter category comprises of immunosuppressive cells including: regulatory T cells (Tregs), myeloid-derived suppressor cells (MDSCs), tumour-associated macrophages (TAMs) and tumour-associated neutrophils. All of these immunosuppressive cells

may aid in tolerising the immune response towards the malignant cells that have not yet escaped immunosurveillance (Duan et al. 2020).

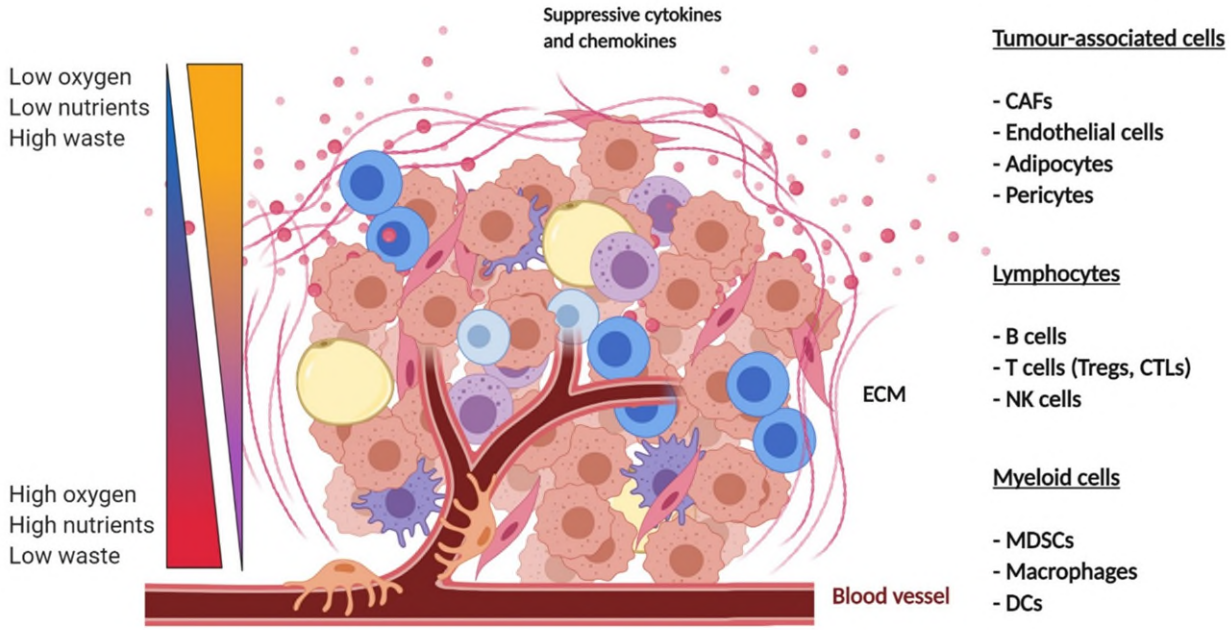


Figure 1.2 Schematic of the immunosuppressive TME. A tumour forms so that it doesn't only rely on its own cells but co-opts the functions of others as well as other aspects of the environment around it, including; the extracellular matrix, the vasculature, stromal cells, metabolites and immune cells. This forms a complex and dynamic environment that allows the tumour to grow, invade other tissues, metastasise, and resist therapy. Image created with BioRender.com and adapted from (Balkwill, Capasso and Hagemann, 2012). ECM, extracellular matrix; CAF, cancer-associated fibroblast; Treg, regulatory T cell; CTL, cytotoxic T lymphocyte; NK, natural killer; MDSC, myeloid-derived suppressor cell; DC, dendritic cell.

In most solid tumours, T cells are rarely in contact with tumour cells but are enriched in the stroma-surrounding microenvironment. Stroma-associated cells are known to control the motile behaviour of T cells; disfavouring trafficking of cytotoxic T lymphocytes (CTLs) through chemokines (Salmon and Donnadieu 2012). As well as producing extracellular matrix (ECM) which acts as a physical barrier to T cell penetration (Harlin et al. 2009; Feig et al. 2013). A further obstacle to an effective immune response is the aberrant cytokine profile in the TME. IL-10, TGF-β, and growth factors (vascular endothelial growth factor (VEGF) and fibroblast growth factor) released by tumour cells and tumour-associated cells are known to regulate

effector T cells both directly and indirectly via the suppression of DCs and TAMs (Rescigno, Avogadri, and Curigliano 2007; Mikhail Binnewies et al. 2018). TAMs are also reported to express IL-4 and IL-13 as well as programmed cell death protein 1 (PD-1) and CTLA-4 ligands, all of which act to depress T cell and NK cell function (Pollard and W. 2015; Lin and Yan 2018). Other regulatory immune cells contributing to the suppressive milieu are Tregs, an increase in their frequency is associated with poor outcomes in patients (Faget et al. 2011; Curiel et al. 2004). Their main modes of suppression are: to limit the amount of IL-2 available using constitutive expression of a high affinity IL-2 receptor α chain (CD25), to express CTLA-4 to bind and downregulate CD80/CD86 co-stimulatory molecules on APCs, to produce immunosuppressive factors; IL-10, TGF-β, adenosine, and to mediate direct killing of anti-tumour cells by secreting granzymes (Tanaka and Sakaguchi 2017).

Additionally the vascular system set by tumour development is aberrant and creates yet another barrier aiding immune evasion. A defining property of the unlimited and uncontrolled growth of malignant cells is the resulting deficit in an adequate blood supply leading to areas of hypoxia. This stimulates a number of tumour-benefiting characteristics via the hypoxia-inducible factor (HIF) pathway (Dehne et al. 2017). The role of HIF is to reverse the effects of hypoxia. However, often in tumours, the vessel structures that are produced are abnormal and circulation remains defective, resulting in temporal and regional fluctuations of hypoxia, nutrient depletion and the accumulation of waste (Renner et al. 2017). In addition to this, other target genes of HIF promote glycolysis, a well-documented altered phenotype of malignant cells identified by Otto Warburg and known to be a hallmark shared by multiple cancer types (Warburg 1956; Hanahan and Weinberg 2011). Supplementary to poor vasculature are active tumour and tumour-associated cell intrinsic mechanisms that further deplete the TME of nutrients and lower the pH; such as indoleamine-2,3-dioxygenase (IDO) and arginase expression (Munn and Mellor 2007; Molon, Calì, and Viola 2016). Changes in the metabolic

environment will be described further in later sections; namely nutrient depletion and acidification.

1.2.4 Immunotherapeutic strategies

Immunotherapy is an umbrella term that describes a range of strategies that all aim to energise the anti-tumour response that already exists but is being successfully evaded. A wide range of strategies are in development, ranging from stimulating effector mechanisms to counteracting suppressive ones. While these strategies have been profound for some patients, with life-changing results, the clinical outcome for others, who are resistant to such therapies, is still somewhat disappointing. The main reasons for this are believed to be: the induction of tolerance to cancer antigens, the contribution of the TME to evasion, and the extent of heterogeneity within a single tumour (Whiteside et al. 2016; Rescigno, Avogadri, and Curigliano 2007; Pilon-Thomas et al. 2016). Outlined briefly are just some of the immunotherapeutic strategies, focusing on T cell based therapies, that are currently in the field.

1.2.4.1 Cancer vaccines

Following the discovery that T cells specific for TAAs exist in patient tumour samples, there was an increased effort to hone the ability of a patient's immune system to mount a response against malignant cells using a vaccination approach (P. P. Lee et al. 1999). The strategies used to boost the cancer immunity cycle by stimulating the uptake and presentation of TAAs by APCs include: whole cell-based vaccines with polyvalent sources of TAAs, autologous DC-based vaccines loaded with TAAs, protein/peptide-based vaccines derived from TAAs and DNA/RNA based vaccines encoding TAAs (Kerr et al. 2020).

Vaccination is used successfully as a prophylactic against infectious diseases, including cancer-causing viruses such as hepatitis B virus and human papilloma virus. However, in contrast to

prophylactic vaccines which are against known agents, cancer vaccines must be designed against unpredictable TAAs, due to the mutational status and heterogeneity of antigen expression within a tumour bed. One of the two main obstacles is therefore the identification of a suitable antigen. The other is the requirement to overcome immune tolerance, cancer vaccines must overcome immune evasion mechanisms already well established by the tumour as discussed in sections 1.2.2 and 1.2.3, some of which may include loss of MHC, meaning vaccines would be truly limited (Farkona, Diamandis, and Blasutig 2016).

An autologous DC vaccine that has been approved by the Food and Drug Administration (FDA) is Sipuleucel-T (Provenge). A DC-vaccine against metastatic prostate cancer; based on a DC-loaded fusion protein consisting of prostatic acid phosphatase linked to granulocyte-stimulating factor (GM-CSF), a DC growth factor.

1.2.4.2 Adoptive T cell therapy

One strategy that avoids the issue of insufficient numbers of weak TAA-recognising T cells is to use adoptive T cell therapies (ACT). This approach involves extracting a patients T cells, then depleting the patient of remaining regulatory immune cells i.e. Tregs and MDSCs, then infusing the *ex vivo* expanded population of patient T cells back into the body after treatment with T cell activating cytokines (Topalian et al. 1987). ACT has become a viable approach over the last 20 years particularly with the inclusion of lymphodepletion. Rosenberg and colleagues, the pioneers of ACT treated 93 patients with metastatic melanoma with infused autologous tumour-infiltrating lymphocytes (TILs) and IL-2 following various lymphoconditioning regimens. They reported that the treatment lead to the durable complete regression in up to 40% of patients (Rosenberg et al. 2011). While the efficacy and toxicity profile of ACT therapy in melanoma has been extraordinary this therapy is costly and labour intensive (Farkona, Diamandis, and Blasutig 2016).

Advances in culturing techniques and genetic engineering has resulted in the advent of chimeric antigen receptor (CAR)-T cell therapy. Before reinfusion, autologous T cells are engineered into CAR-T cells before *ex vivo* expansion. The constant domain of the TCR of a CAR-T cell, intracellular CD3ζ, is fused to the extracellular binding domain of a cancer antigen (usually the single-chain variable fragment (scFv) derived from a TAA-targeting monoclonal antibody (mAb). This design omits the need for MHC presentation as T cells obtain the recognition properties of an antibody (Ab) against any surface antigen, thus enabling antigen-independent T cell activation. CAR-T cell therapy has had exceptional success in a number of haematological malignancies, including the FDA approval of tisagenlecleucel (Kymriah) which targets CD19 for the treatment of acute lymphoblastic leukaemia. Despite this ingenious feat of cellular engineering, there remains some challenges. For example; the cost and complexity, the safety and immune-related adverse effects, and the lack of long lasting responses (June and Sadelain 2018; Turtle et al. 2016).

1.2.4.3 Monoclonal antibodies against tumour-associated antigens

Better targeted therapies as discussed above in section 1.1.2 allow for the specific treatment of cancer cells and the reduced off-target effects on healthy tissues. Most targeted therapies are based on either small molecule drugs or mAbs that bind to specific surface targets. There are a number of mAbs now used in clinical practice for various cancer types and more than 30 have been approved by the FDA for treatment of both haematological and solid malignancies (reviewed in (Chiavenna, Jaworski, and Vendrell 2017)).

Tumour cell mediated killing using mAbs can occur through multiple mechanisms: those that are fragment crystallisable (Fc)-dependent, involving engagement of the Fc tail; or those that are Fc-independent; or a combination of both. Fc-dependent mechanisms of target cell killing are: antibody-dependent cellular cytotoxicity, mediated by NK cells, macrophages and

granulocytes; antibody-dependent cellular phagocytosis mediated by macrophages; and complement dependent cytotoxicity. Fc-independent mechanisms, on the other hand, are direct methods of killing including apoptosis induction and direct receptor antagonism. Rituximab (Rituxan), the first huge advance in mAb-based immunotherapies, binds $CD20^+$ B cells and stimulates NK cells to eradicate them (van Meerten et al. 2006). However, as is the case for many of the targeted therapies mentioned, the efficacy of mAbs is hindered by resistance due to antigen escape, a lack of penetration into solid tumours, and a lack of long lasting responses (Thurber, Zajic, and Wittrup 2007; Friedberg 2005).

1.2.4.4 Immune checkpoint inhibitors

Other therapies based on T cells aim to stimulate the activity of T cells *in vivo*. T cells *in situ* may be stimulated by using biologics such as bispecific antibodies, or by releasing the "brakes" that are negatively regulating T cells with administration of immune checkpoint inhibitors (ICIs). It is unequivocally accepted that T cells have multiple receptors; some resulting in positive signals for activation and some negative to induce regulation. The balancing of signalling through these inhibitory or activatory receptors allows for the tight control of T cell responses. Furthermore, these same mechanisms are exploited by the tumour to establish immune evasion, but also targeted by immunotherapies to reverse cancer-induced immune suppression.

The use of ICIs has gained much recognition in the last decade, and have sparked a revolution in cancer treatment, being the immunotherapeutic of choice in most immunotherapy combination treatments currently being tested (Melero et al. 2015). Perhaps the most well-known are the ICIs that block either the CTLA-4 pathway or the PD1-PDL1/2 axis. Ipilimumab (Yervoy), an anti-CTLA-4 mAb, was approved by the FDA in 2011 as the first line of treatment for metastatic melanoma. While nivolumab (Opdivo) and pembrolizumab (Keytruda), mAbs

targeting PD-1 were approved by the FDA in 2014 for advanced melanoma and non-small cell lung carcinoma, and have since been approved for more malignancies (U.S. Food & Drug Administration, 2020). Due to the relative success of CTLA-4 and PD-1 inhibitors, multiple other immune checkpoints are being researched, with several making their way into pre-clinical trials and/or clinical trials including: antibodies against T cell immunoglobulin and mucin-domain containing-3 (TIM3), and LAG3 (Qin et al. 2019). However despite good clinical responses and potent anti-tumour properties in a range of cancers, they have some safety issues, particularly with CTLA-4 blockade, and there is still a chance of resistance to ICIs through HLA downregulation or immunoevasion in the TME (Hodi et al. 2010; Kakavand et al. 2017).

1.2.4.5 Bispecific antibodies

Bispecific antibodies are able to recognise two different epitopes, as opposed to one which is recognised by a mAb. There are three main classes of bispecifics; with the most established class being cytotoxic effector cell redirectors (Dahlén, Veitonmäki, and Norlén 2018). Their bivalent nature allows them to engage a polyclonal population of T cells whilst specifically targeting antigens on tumour cells simultaneously, resulting in the activation of T cells and directing T cell killing towards the chosen target cells. This crucially allows them to activate T cell cytotoxic machinery irrespective of TCR specificity therefore negating the requirement of HLA: peptide recognition and antigen presentation, however they could still suffer from resistance if the TAA chosen to target is lost (Frankel and Baeuerle 2013; Wolf et al. 2005).

Bispecific antibodies consist of a panel of more than 100 different formats that have evolved over the last two decades. In an oncology context, most IgG-like (those with an Fc tail) bispecifics experience some sort of limitation; the requirement of co-stimulation or pre-activation of T cells and/or the need for a large excess of T cells over target tumour cells. Despite this there has been some success in trials, including those targeting epithelial cell

adhesion molecule (EpCAM), CD20, CD123, and CD276 (reviewed in (Dahlén, Veitonmäki, and Norlén 2018)). By far the most clinically advanced being the bispecific T cell engager (BiTE) format, discussed in detail in section 1.3.

1.2.4.6 Oncolytic viruses

Oncolytic viruses (OVs) offer a unique set of characteristics making them an attractive and novel form of cancer therapy; they act directly on cancer cells, induce a systemic immune response and offer themselves as a delivery vehicle for transgene expression directly to the tumour (Duffy, Fisher, and Seymour 2017). It has been known since the early 1900s that viruses have the capability to kill cancer cells, documented by George Dock (Dock 1904). In the 1950s clinicians began to use them to treat cancers with some success however some patients' lives were lost (Ledford 2015). During these early years wild-type viruses were used and since the advent of genetic engineering the next generation of oncolytic virotherapies began, with genetic alterations to reduce pathogenicity, and increase oncolytic properties (Alberts et al. 2018).

OVs work through two modes of action. They induce cancer death through cell entry, replication and eventual cell lysis to release progeny virions, a direct mode of action. Then indirectly, they induce a cancer-specific and virus-specific immune response via the release of danger-associated molecular patterns (DAMPs) and pathogen-associated molecular patterns (PAMPs) following infection-induced cell lysis. By 2018 there were three OVs registered for clinical use; ECHO-7 (Rigvir), a naturally non-pathogenic wild-type picornavirus used in Latvia; H101 (Oncorine), an engineered adenovirus (AdV) approved in China; and talimogene laherparepvec (T-Vec; Imlygic), an engineered herpes simplex virus 1 (HSV1) approved in Europe and the USA. Due to their distinct mechanisms of action and excellent safety profiles, there are a number of DNA and RNA-based viruses currently being tested including: coxsackievirus, Seneca Valley virus, reovirus, measles virus, and vaccinia virus (VACV)

(reviewed in (Kaufman, Kohlhapp, and Zloza 2015)). T-Vec, the most advanced agent to date, was approved for advanced metastatic melanoma in 2015 by the FDA. It has modifications in its HSV-1 genome (deleted for ICP47 and both copies of ICP34.7) to attenuate its viral activity, prevent latency and promote its therapeutic activity. Furthermore, it encodes GM-CSF, to favour APC recruitment following infection. In phase II and III clinical trials in patients with unresectable stage IIIc or stage IV melanoma it achieved a 26% objective response rate and superior survival compared to controls with only mild side effects such as fever and local injection site inflammation (Farkona, Diamandis, and Blasutig 2016). As of July 2019 there were 118 clinical trials testing OVs alone or in combination with other therapies, with 13 different viruses being tested (M. Zheng et al. 2019). OV's will be discussed in further detail in section 1.4.

1.3 Bispecific T cell engagers

1.3.1 Structure and mode of action

BiTEs are the most clinically advanced member of the class of bispecific antibodies used to redirect the cytotoxic effect of T cells. They typically consist of two scFvs joined by a flexible glycine-serine rich linker in a polypeptide chain. An scFv is the minimal amount of a monoclonal antibody required to achieve antigen binding, made up of the variable heavy (VH) and variable light (VL) domains (Figure 1.3A). By linking two separate scFvs together, these molecules become bivalent and able to recognise two different antigens (Ellerman 2019). The basic mechanism of BiTEs in cancer immunology is to bind T cells (most commonly via CD3ε) and target cells (via a surface TAA) simultaneously. This results in TCR crosslinking and clustering, which culminates in the formation of a pseudoimmune synapse, and the subsequent T cell-mediated killing of the target TAA^{+}-cancer cell (Figure 1.3B). Most importantly, BiTEs

will induce killing, regardless of that T cell's TCR specificity, its original effector function and without the requirement of co-stimulatory molecules (Brischwein et al. 2006; Wolf et al. 2005).

The mechanism by which BiTEs promote T cell killing is not fully understood; however, there are several features that are reported to be play a part in the process. One characteristic that has been confirmed by many, including Brischwein *et al* (Brischwein et al. 2007), is that the activation of T cells by BiTEs is strictly dependent upon target cell binding and that lack of prevents cytotoxicity and cytokine expression (IFNγ, IL-6, IL-10, TNF-α) (Huehls, Coupet, and Sentman 2015).

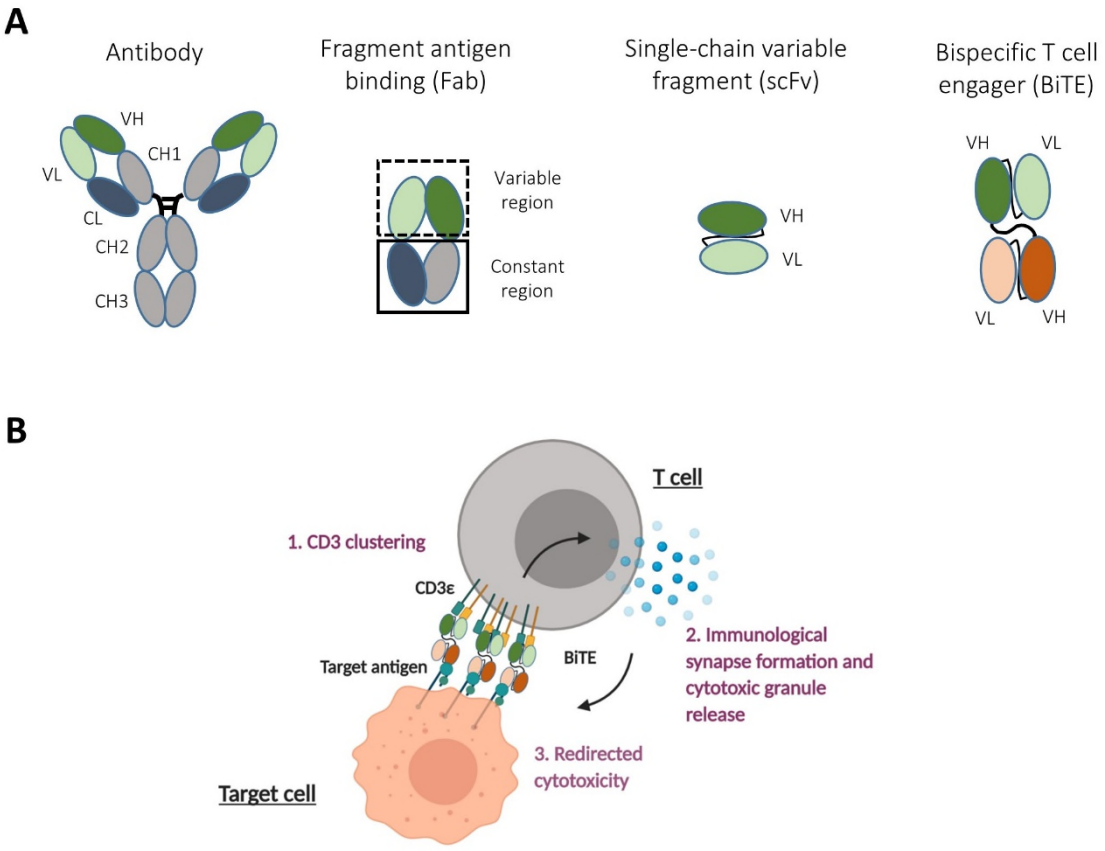


Figure 1.3 The structure of a BiTE and its mode of activation. (A) Depiction of the components a BiTE is constructed from, *i.e.* the scfv fragments and where they are located in parental antibodies. VH, variable heavy chain; VL, variable light chain; CL, constant light chain; CH, constant heavy chain. **(B)** Multiple points of binding between BiTEs, their antigen on a target cell's surface and CD3ε on a T cell's surface; results in CD3 clustering and triggered T cell activation which leads to redirected cytotoxicity of the target cell. Figure adapted from (Scott et al., 2018). Image created with BioRender.com.

The presence of a cytolytic immunological synapse containing perforin, protein kinase C (PKC(θ)), Lck and CD3 was confirmed by Offner *et al* using confocal microscopy (Offner et al. 2006). GrB, known to directly activate caspases, is delivered to target cells after BiTE activation (Browne et al. 1999).

Years of research and development in the area of genetic engineering and the discovery of new antibodies has allowed for the development of next generation BiTEs. Diego Ellerman (Ellerman 2019) reviewed the many different factors that can affect BiTE efficacy including: physical properties, such as size, valency, and geometry; but also target cell indicators, like number of antigen copies on a cell and the affinity of its binding. Furthermore, the discovery of nanobodies (heavy chain only (VHH) domains) from sharks and camelids has furthered the field of antibodies in many areas including in cancer therapy. The advent of nanobodies has allowed for the development of formats that have improved therapeutic properties including: reduced size, allowing for greater tissue penetration and improved pharmacokinetics; easily expressed, due to the smaller protein size; more specific binding; increased affinities; and more tolerance to extreme conditions, including temperature, pH, proteolytic degradation and chemical denaturation (reviewed in (Jovčevska and Muyldermans 2020)).

1.3.2 BiTE activation versus HLA-dependent activation

The shared feature between HLA-dependent and HLA-independent activation (via BiTEs), is that both require TCR clustering and formation of an immunological synapse (or cytolytic synapse) to carry out their effector functions. This suggests there are common signalling pathways that are required to activate cascades required to stabilise this supramolecular complex at the interface between the T cell and target cell. Currently, the exact signalling pathways required for BiTE activation of T cells are unknown, while those for conventional HLA-dependent CTL direct killing are still being further developed (Kabanova, Zurli, and

Baldari 2018). However, two important factors are apparent: BiTE activation will result in a higher density of TCR clusters at the cell-cell interface, compared to HLA-dependent activation; and BiTE-mediated activation of T cells can occur without co-stimulation.

BiTEs directly couple target surface antigens with CD3ε on T cells, as opposed to the HLA: peptide complex targeted by a TCR in physiological T cell activation. The number of events required in the latter scenario has been reported to be as few as 10 events per cell by Purbhoo *et al* (Purbhoo et al. 2004). However, they also reported that lower numbers of interactions meant a reliance on Fas-mediated apoptosis of target cells, whereas granzyme-mediated apoptosis requires a larger number of events for a more stable immunological synapse. In contrast, there are possibly up to 100,000 TCRs on a T cell (Schodin, Tsomides, and Kranz 1996), all of which, using the EpCAM BiTE as an example, could potentially interact with the 1×10^6 EpCAM receptors reported on cells from pleural effusion patient samples (X. Yao et al. 2013). Given this difference, it is acceptable to assume a much higher density of binding events per cell following BiTE activation which will lead to greater CD3 clustering, and consequently a higher rate of T cell response i.e. activation (C. Y. Ma et al. 2020). Richard *et al* (Richard et al. 2018) also suggested that stimulation strength does not dictate different activation routes but rather just how rapidly and simultaneously T cells are activated. This will consequently lead to the formation of a more stable synapse, and thus will result in more efficient cell death by lytic granule secretion, which is known to be involved in BiTE-induced T cell dependent cytolysis (Wolf et al. 2005).

In light of this, it is possible for BiTEs to cause T cells to become 'super-activated'. Additionally, BiTEs rely solely on CD3ε activation (Wolf et al. 2005), whereas HLA-dependent activation requires co-stimulation via CD28 for example (Smith-Garvin, Koretzky, and Jordan 2009). Reports (reviewed in (Appleman and Boussiotis 2003)) suggest that, in the absence of CD28 co-stimulation, T cells become anergic and represent an exhausted phenotype, linked

heavily with the metabolic state of a T cell. It is known that CD28 signalling enhances HLA-dependent TCR signalling, and is the dominant trigger for the phosphoinositide 3-kinase (PI3K)/protein kinase B (Akt)/ glycogen synthase kinase 3 (GSK-3) signalling pathway in primary human T cells. This pathway ultimately triggers mammalian target of rapamycin (mTOR), the main metabolic controller in cells. BiTE stimulation occurs without these co-stimulatory signals, activating T cells to the same extent or more so than physiological activation with CD3/CD28 beads (Freedman et al. 2017). It could be suggested therefore that activation occurs in a manner that may bypass the important metabolic checkpoints that would otherwise control T cell activation, although mTOR is now known to regulated independently from PI3K by other sensors such as 5' AMP-activated protein kinase (AMPK), cytoplasmic amino acids via Ras-related small GTPase Rag proteins and chemokine receptors (Waickman and Powell 2012; Gamper et al. 2012).

1.3.3 Benefits and challenges

The clinical results observed with an anti-CD19/anti-CD3 BiTE (blinatumomab, Blincyto) were so successful in treatment of acute lymphoblastic leukaemia (Kantarjian et al. 2017), that it confirmed proof-of-concept of BiTEs. This has led to a number of other T-cell engaging bispecific Abs being developed (Dahlén, Veitonmäki, and Norlén 2018). For example, nanobody-based bispecifics are making good progress. A bispecific light T-cell engager (LiTE) generated by Molgaard *et al* (Mølgaard et al. 2018), consisting of a CD3 scFv and an anti-epidermal growth factor receptor (EGFR) nanobody has shown great potential in *in vitro* studies.

The results in haematological indications for BiTE therapy have not yet been replicated in solid tumours. BiTEs are able to induce activation and killing with remarkable potency and at half-maximal effective concentrations typically in the picomolar range. However, the safety of

BiTEs, like all other antibody-based therapeutics, will depend on the selected target antigen and its specificity to cancer cells alone. Additionally, due to their small size compared to a mAb, they are rapidly cleared from circulation with a terminal half-life of 1.25 hours and therefore require continuous IV infusion (Brinkmann and Kontermann 2017). Another potential issue faced by BiTEs is that there may be insufficient numbers of T cells within the tumour tissue *in vivo.* Numerous studies have actually shown that nearly all human cancers contain TILs, however they are frequently immune suppressed (Frankel and Baeuerle 2013). The question therefore is whether BiTEs can reactivate enough TILs for an efficacious response, despite the immunosuppressive mechanisms at play?

1.4 Oncolytic viruses

1.4.1 The basis of OV selectivity

There are over 3000 species of viruses, but not all are suitable as OVs. They need to be non-pathogenic to humans, have cancer-selectivity and have the ability to be genetically engineered to attenuate them or arm them to improve their efficacy (Russell and Peng 2018). Cancer cell selectivity can be due to several factors including but not limited to: viral entry receptors, for example, herpes virus entry mediator (HVEM) for entry of HSV-1 is overexpressed in many cancers including glioblastoma, breast and gastric (Tsang et al. 2017; Lan et al. 2017; Han et al. 2019); aberrant intracellular signalling, for example, the prevalence of anti-apoptotic factors in cancer cells; or an inherent shut down of innate immune defences giving advantages to cancer cells and viruses alike, for example, the dysregulation of the type I IFN response (Kaufman, Kohlhapp, and Zloza 2015). Generally, there is a large amount of crossover between the hallmarks of cancer, as described by Hanahan and Weinberg (Hanahan and Weinberg 2011), and those hallmarks that represent successful viral replication. It is here that the mechanisms of

underlying cancer selectivity are found, reflecting the phenotype of cancer cells as active and proliferative (Seymour and Fisher 2016). Using criteria as above, rational design of OVs can allow for improved selectivity, mostly achieved with genetic engineering, however recently, the use of directed evolution to select for suitable OV candidates has shown great promise (Kuhn et al. 2008).

Targeting specific receptors is perhaps the most immediate method of improving cancer selectivity. An example of this reported by Hanni Uusi-Kerttula *et al* (Uusi-kerttula et al. 2018) showed that an Ad5 vector with mutations in all of its major capsid proteins ($Ad5_{null}$), thereby diminishing all natural tropism, could be retargeted to αvβ6 integrin, a protein overexpressed in a range of cancers but not detected in healthy tissue. They reported selective infection of $\alpha v\beta 6^{+}$ cell lines, in primary ascites-derived epithelial ovarian cancer samples *ex vivo* and in murine models *in vivo*. Alternatively, OVs are engineered so that certain viral genes will be under the control of tumour-associated promoters and tissue-specific transcriptional regulatory elements. An example of this is CV706, an Ad5 which uses the prostate specific antigen promoter-enhancer element to control E1A expression; an early gene in the AdV genome. Limiting infection to prostate tissue (cancer and normal) (Small et al. 2006). A further genetically engineered method of selectivity is to delete viral genes that are essential for successful infection and replication, but that will be complemented for by the aberrant pathways in the dysregulated tumour cell phenotype. A specific example of this is JX-594, an oncolytic VACV which is deleted for viral thymidine kinase, which only infect cancer cells with the over active enzyme (Russell and Peng 2018).

An approach which offers a route of selection that bypasses the requirement for rationally selecting for specific mechanisms of cancer, and instead results in selection of a cancer phenotype, is bioselection or “directed evolution”. A method developed by Irene Kuhn and colleagues which uses the complexity of human tumour cells to direct selection of highly potent

viruses (Kuhn et al. 2008). Briefly this involves the use of a diverse library of viruses which are repeatedly passaged in cancer cells under recombinant conditions. Each passage results in the selection of viruses with the best replicative or lytic capabilities for targeting the specific cells used. EnAdenotucirev (EnAd) is an oncolytic adenovirus (OAdV) that was developed by the same group, Kuhn *et al*, using this method of selection (Kuhn et al. 2008). Selection was based on HT29 colon cancer cells, and the resultant lead virus EnAd (originally named ColoAd1) is a chimera of group B AdVs, types 3 and 11p. EnAd is a promising OV candidate, which was shown to be able to be delivered systemically rather than intratumourally (Illingworth et al. 2017), and was proven to be safe in early phase clinical trials (NCT02028442, NCT02028117). It is now being investigated in combination with chemoradiation (NCT03916510) and with PD-1 checkpoint inhibitor, nivolumab (NCT02636036). A possible caveat of the use of EnAd as a therapy is it's preference of using CD46 as its cellular entry receptor as opposed to the coxsackie-adenovirus receptor (CAR) used by most Ad-serotypes. This receptor is expressed on all nucleated human cells and despite evidence of EnAd's selectivity for tumour cells, the ubiquitous nature of this receptor means all cells may act as viral sinks for EnAd-based therapies.

1.4.2 Route of delivery

Two major challenges for OV therapy (OVT) are: 1) the various anti-viral responses that clear viruses before they can take effect and 2) viral biodistribution, whereby certain cells will act as virus sinks and limit the number of virus particles reaching a tumour. Delivery to the tumour is therefore a key hurdle. Although intratumoural injection can avoid these issues, systemic intravenous delivery would be the preferred route of delivery. This would allow OVTs to target disseminated disease and inaccessible tumours. OV design must therefore take into account the various obstacles for viruses present in a patient. In the bloodstream, an OV needs to avoid

serum factors including complement, natural immunoglobulin (Ig)-M, anti-viral cytokines, blood coagulation factors, erythrocytes and neutralising Abs (M. Zheng et al. 2019). Meanwhile, throughout the body, OVs must avoid being sequestered by phagocytes present in multiple organs that act as viral particle sinks and reduce the effective availability of virus dose for the tumour itself (biodistribution) (Marelli et al. 2018). Furthermore, once they have overcome these systemic obstacles, OVs will then have to penetrate the tumour itself and efficiently spread. However, due to physical barriers like dense ECM and stroma resulting in high interstitial fluid pressure, this has led to a limited capacity for OVs to achieve consistent responses when given intravenously (Mckee et al. 2006; Maroun et al. 2017).

A few ways in which research groups are currently trying to overcome these issues include: blunting or eliminating anti-viral mediators; using cell carriers, such as mesenchymal stem cells to avoid recognition (Mader et al. 2009); expressing proteases to reduce ECM burden (ICOVIR17 expresses hyaluronidase) (Guedan et al. 2010); and taking advantage of OVs that can kill cancer-associated cells as well as tumour cells (for example, vesicular stomatitis virus (VSV) vectors are known to replicate and kill activated hepatic stellate cells that promote ECM remodelling in hepatocellular carcinoma) (Altomonte et al. 2013). Recognition by the immune system can be limited by using shielding methods such as polymer coatings (M. Zheng et al. 2019; J. W. Choi et al. 2015), chemically modifying envelope and capsid proteins, or using chimeric OVs (a chimeric Ad5 with the fiber protein from Ad35, which is a less seroprevalent AdV) (M. Yang et al. 2017). EnAd has shown remarkable strides in providing a proof-of-concept for systemic delivery. Pre-clinical investigations have shown immunohistochemical evidence of that intratumoural viral replication after the systemic delivery of EnAd (Illingworth et al. 2017). Furthermore EnAd has been shown to be stable in whole human blood and remain infectious, due to its protein coat being based on the Ad11p genome, a less seroprevalent AdV (Di, Seymour, and Fisher 2014).

1.4.3 Mode of action

As stated in section 1.2, the anti-tumour mechanisms of OVs are twofold: direct cell lysis, as a natural end to the viral life cycle after replication; and indirectly, via the release of DAMPs and PAMPs to activate the immune system through APCs (Figure 1.4). In summary, OVs can: activate cellular innate immune responses (NK cells and neutrophils); activate the anti-tumour adaptive immune response, via TAA release and presentation; overcome immunosuppression by depleting Tregs and MDSCs; increase tumour recognition, by increasing MHC class I and

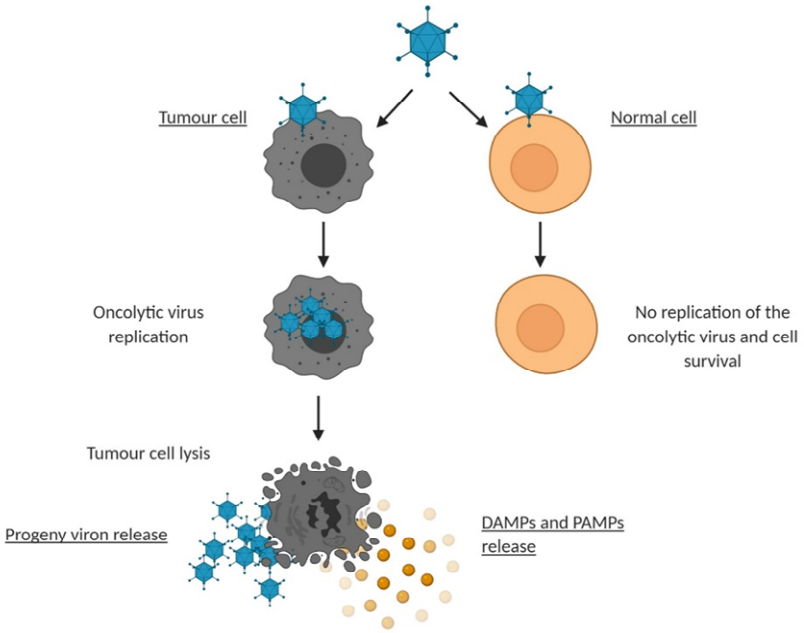


Figure 1.4 The dual mode of action of oncolytic viruses. OVs do not replicate in normal cells and only selectively infect and replicate in tumour cells. This leads to tumour cell lysis through the natural OV life cycle and the release of viral progeny. If immunogenic cell death is induced, DAMPs and PAMPs are released leading to an anti-tumour response indirectly. Figure adapted from (Scott et al., 2018). Image created with BioRender.com.

II expression on APCs and tumour cells; attack cancer-associated cells, like CAFs; attack the vascular endothelial system feeding the tumour; and trigger the release of pro-inflammatory cytokines (Achard et al. 2018).

To activate an immune response OVs must induce an immunogenic form of cell death (ICD), including pyroptosis, necroptosis, immunogenic apoptosis and autophagic cell death. ICD results in the exposure or release of DAMPs and PAMPs, as well as a broad range of TAAs, thought to help with antigen spread. As DAMPs are released, APCs are attracted and engulf the TAAs released, as well as receiving maturation signals. DCs will present TAAs to naïve T cells and produce pro-inflammatory cytokines, mediating an adaptive immune response (Davola and Mossman 2019). The initial release of pro-inflammatory factors after OV-mediated ICD results in the re-balancing of the immunosuppressed TME, mediating the recruitment of cytokine-releasing immune cells which will then escalate the pro-inflammatory state further, and help to accentuate the anti-tumour response. This process has been referred to by some as 'turning an immunologically cold tumour, hot'. There is some controversy as to whether it is the infection of tumour cells by viruses that first triggers the immune response with virus-specific antigens, before then subsequently triggering an anti-tumour response; or if the exposure of OVs to the immune response actually diminishes their anti-tumour activity, restricting OV efficacy by limiting replication and spread. This relationship was best described by Filley and Dey, who said that it is ever-changing, dependent on which phase of infection and tumour destruction is occurring (Filley and Dey 2017). *In vitro* studies found that EnAd infection leads to direct lysis of tumour cells via oncosis, a form of ICD. This then stimulated DCs, followed by the activation of $CD4^+$ T cells in a mixed tumour leukocyte reaction (Dyer et al. 2017). Clinical data also exemplified the recruitment of $CD8^+$ T cells to the site of viral infection in tumour biopsies of patients who received EnAd treatment systemically (Garcia-Carbonero et al. 2017). This is in contrast to studies of wild-type group B AdVs which show that CD46-interaction by virus

particles causes a downregulation of the innate and adaptive immune responses, however this was not shown specifically for Ad11p, the serotype EnAd is based on (Iacobelli-Martinez et al. 2005).

It is worth noting that although both modes of action are of importance, some OVs will rely on one more than the other for their anti-tumour activity, depending on the OV type and its genetic design (Sivanandam et al. 2019). Furthermore, some studies have suggested using a combination of two OVs has the potential to bring about a better response. For example, Bridle *et al* (Bridle et al. 2010) showed that pre-treatment with an adenoviral vector carrying a specific TAA acted as a cancer vaccine in mice with brain or lung tumours. Then upon re-infection, with an oncolytic VSV encoding the same antigen, boosts in CTL responses were observed, while avoiding viral attenuation due to anti-viral immune responses to the initial adenoviral vector. Genetic engineering enables the opportunity to enhance one or the other of these mechanisms, overcoming reduced sensitivity of tumour cells to be killed and augmenting more potent lysis and/or immune responses; in essence "arming" OVs to become better therapies.

1.4.4 'Arming' OVs

The clinical responses of many OVs have been disappointing thus far. Therefore, improving their efficacy using alterations to their genomes or using them in combination has been widely adopted in OVT research. Furthermore, this approach has allowed researchers to revisit therapies that once demonstrated toxicity to normal tissues; allowing for increased doses in a self-amplifying manner and higher specificity, with transgenes also being able to be controlled both spatially and temporally (Bauzon and Hermiston 2014). Many 'armed' viruses are in the preclinical phase of research, however 17 are currently in clinical trials as of May 2020 in various phases, some in combination with other therapies like ACT, ICIs and chemotherapy

(reviewed in (Chaurasiya, Fong, and Warner 2020)). Examples of transgenes that can be used and their specific function are in Table 1.1.

EnAd, a well-tolerated OAdV contains deletions in its genome. These alterations make it 2470 bp shorter than the parental Ad11p genome, and ideal for packaging transgenes (A. T. Baker et al. 2018; Garcia-Carbonero et al. 2017). The AdV genome is split into early and late genes. The major late promoter (MLP) in the genome drives the expression of late genes, only when cells have been successfully infected and the virus is replicating efficiently. This makes it an effective promoter to use for transgene expression, especially for those transgenes that can target normal tissues and cause on-target, off-tumour effects (Machiels et al. 2019). Freedman *et al* (Freedman et al. 2017, 2018) has shown this approach; they cloned EnAd-expressing BiTEs with transgene expression controlled by a splice acceptor (SA) site for the AdV MLP. They showed improved killing of tumour cells with their modified virus, EnAd-SA-EpCAMBiTE and showed EnAd-encoded fibroblast-associated protein (FAP) BiTEs are able to target CAFs and reverse immunosuppression markers in patient fluids.

Table 1.1 Transgenes incorporated into OV genomes to improve OV efficacy. Table to summarise the transgenes currently being encoded into OVs, adapted from (Chaurasiya, Fong, and Warner, 2020). GM-CSF, granulocyte-macrophage colony-stimulating factor; HSV, herpes simplex virus; VACV, vaccinia virus; AdV, adenovirus; IL, interleukin; VSV, vesicular stomatitis virus; IFN, interferon; NDV, Newcastle disease virus; CCL, chemokine (C-C motif) ligand; CXCL, C-X-C motif chemokine ligand; VEGF, vascular endothelial growth factor; PGE2, prostaglandin E2; TGF, transforming growth factor; PD-1, programmed cell death protein 1; PD-L1, programmed death ligand 1; CTLA-4, cytotoxic T-lymphocyte-associated protein 4; LAG-3, lymphocyte-activation gene 3; TIM-3, T-cell immunoglobulin and mucin domain-3; TAA, tumour-associated antigen; OV, oncolytic virus; BiTE, bispecific T cell engager; HLA, human leukocyte antigen; FAP, fibroblast activation protein; CAFs, cancer-associated fibroblasts; CAR-T, chimeric antigen receptor-T cells; HA, hyaluronidase; ECM, extracellular matrix; MMP, metalloproteinase; RFP, red fluorescent protein; GFP, green fluorescent protein; TK, thymidine kinase; PET, positron emission tomography; NIS, sodium iodide symporter; TRAIL, TNF-related apoptosis inducing ligand; shRNA, small hairpin RNA; hTERT, telomerase reverse transcriptase.

Transgene class	Transgene	Function of Transgene	OV	References
Cytokines	GM-CSF	Antigen presentation	Multiple OVs	(Conry et al. 2018; Parato et al. 2012; Hemminki et al. 2014)
	IL-2, IL-12, IL-15	T cell or NK cell activation and proliferation and anti-angiogenic effect	Multiple OVs	(Z. Liu et al. 2018; Ge et al. 2020; Kowalsky et al. 2018)
	IFNs (Type I and II)	Antigen presentation and proinflammatory, angiogenesis inhibition. Induce cancer cell apoptosis	VACV, VSV	(Kirn et al. 2007; Patel et al. 2015; Roy et al. 2016)
Chemokines	CCL-5 and CXCL11	Attracts immune cells	Poxvirus, VACV	(Z. Liu et al. 2016; J. Li et al. 2011)
Immunosuppressor inhibitors	Secretory immunosuppressive factors (VEGF, PGE2, TGF-B)	Reverse inhibition of T cells and decrease immunosuppressive cell proliferation and reverse antigen presentation interference	VACV, AdV	(Patil et al. 2012; Hou et al. 2016; Y. Yang et al. 2019)
	Cellular immunosuppressive factors (PD-1, CTLA-4, LAG-3, TIM-3)	Reversal of checkpoint blockade to induce T cell activation	VACV, myxoma virus	(Kleinpeter et al. 2016; Bartee, Dunlap, and Bartee 2017)
TAAs	TAAs	Boost adaptive immune response to specific TAAs	Multiple OVs	(Higgins, Bernstein, and Hodge 2009)
T cell activating therapies	BiTEs	HLA-independent T cell activation against TAA or cancer-associated cell (FAP on CAFs)	VACV, AdV	(Yu et al. 2014; Fajardo et al. 2017; Freedman et al. 2017, 2018)
	CAR-Ts	HLA-independent T cell activation against TAA	VACV	(Aalipour et al. 2020)

Stromal modifiers	HA	Proteolytic enzyme, decreases ECM	AdV	(Guedan et al. 2010)
	MMP 9	Degrades collagen IV	VACV	(Schäfer et al. 2012)
	Decorin	To modify stroma	AdV	(Xu et al. 2015)
Imaging	RFP, GFP or luciferase	Facilitates optical imaging	Multiple OVs	(Haddad and Fong 2015)
	TK	A pro-drug converting enzyme to trap radiolabelled drugs for example ganciclovir for PET imaging	VSV	(Muñoz-Alvarez et al. 2015)
	NIS	Allows uptake of radioisotopes for imaging	Poxvirus, VACV	(Jun et al. 2014; Warner et al. 2019)
Suicide genes	Pro-apoptotic proteins (TRAIL, IL-24)	Induces apoptosis in infected cells	AdV	(L. Chen et al. 2009; Zhao et al. 2006)
	Tumour suppressors (p53, p16)	Induces cell death through restored cell death pathways	AdV	(J. Ma et al. 2009; Beusechem et al. 2002)
	shRNAs targeting survival or proliferation factors (hTERT, survivin)	Inhibits survival and growth pathways enhanced in cells	AdV	(J.-N. Zheng et al. 2009; Shen et al. 2009)

1.4.5 RNA interference

RNA interference (RNAi) was discovered only recently in 1998 in *Caenorhabditis elegans* by Fire and Mello. Three years later, Elbashir *et al* (Elbashir et al. 2001) and Caplen *et al* (Caplen et al. 2001) confirmed the same pathway was conserved in mammalian cells. dsRNAs of 21-22 nucleotides in length were reported to silence genes without eliciting a nonspecific IFN response. From here, the field has rapidly evolved into the design of small-interfering RNAs (siRNAs) as universal tools in biological and therapeutic research (Svoboda 2014). The RNAi pathway is depicted in Figure 1.5.

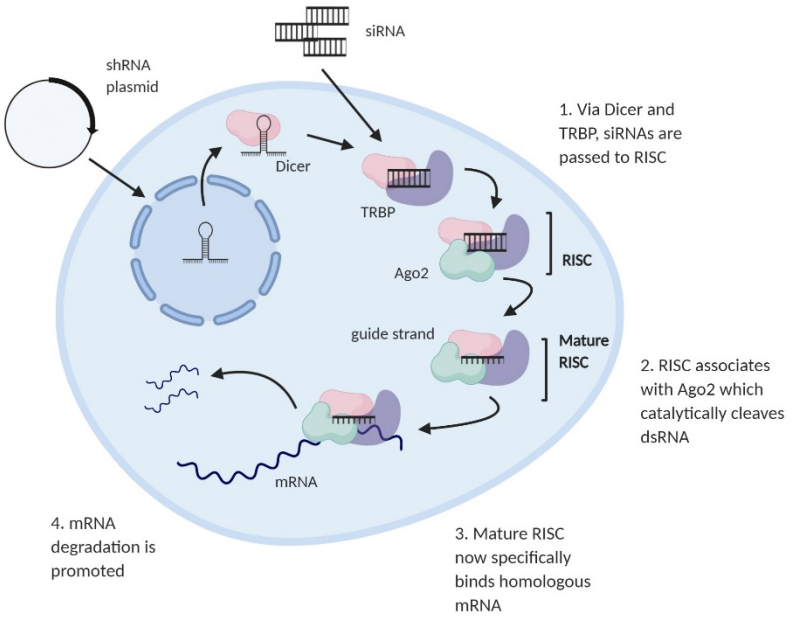


Figure 1.5 The RNAi pathway for siRNA and shRNA. Long dsRNA are cleaved into siRNAs by Dicer, or synthetic siRNAs are delivered exogenously by transfection. From Dicer, or in the case of shorter (less than 21 bp) siRNAs via TRBP, RNA duplexes are passed to the RISC loading complex, which is associated with Argonaute protein members. Ago2 catalytically cleaves the dsRNA duplex to select for the guide strand, whilst the passenger strand is discarded. Mature RISC now containing the guide strand will specifically pair with a sequence in an mRNA that is homologous leading to the regulation of gene expression. Image adapted from (Setten, Rossi, and Han, 2019; Kim and Rossi, 2008). Image created with Biorender.com. shRNA, short-hairpin RNA; siRNA, small-interfering RNA; TRBP, TAR RNA-binding protein; RISC, RNA-induced silencing complex; Ago, Argonaute.

As found with other therapies, RNAi as a cancer therapy has failed to meet expectations. It has limitations including off-target activities, varying degrees of silencing, as well as issues with reproducibility (Toniatti et al. 2014). As mentioned before, OVT offers a way to overcome these limitations and deliver RNAi constructs directly to tumour cells, as well as controlling their expression. OVs are armed with the ability to express siRNAs by encoding small hairpin RNAs (shRNAs) within their genome. The promoters commonly used in driving shRNA expression are U6 and H1. Both are easy to clone and package, produce high levels of

expression and have well-defined initiation and termination sites for accurate design of shRNAs (Giering et al. 2008).

Initially, it was thought RNAi and virus infection would be incompatible due to RNAi being involved in specific anti-viral defence mechanisms (reviewed in (Brachtlova and van Beusechem 2018)). However, Carette and colleagues (Carette et al. 2004) showed the potential of conditionally replicating (*i.e.* tumour specific) AdVs expressing shRNAs using a luciferase based model in 2004. Since the feasibility was demonstrated, multiple other shRNAs encoded into OAdVs have been tested. For example, the control of survival and proliferation proteins in cancer cells by shRNAs, mentioned in Table 1.1, are used to make OAdVs more effective in lysing tumour cells (Shen et al. 2009). Likewise, encoded shRNAs have been used to target mediators of immune suppression and tumour growth. For example, a shRNA silencing TGF-β2 was able to reverse the TGF-β2-mediated antagonism of GM-CSF, whilst preventing inhibition of antigen-specific T cell activation and reversing MDSC stimulation (Brachtlova and van Beusechem 2018).

1.5 Nutrient depletion in the TME

1.5.1 Amino acid metabolism in cancer

All mammalian cells, both normal and cancerous, require amino acids; essential amino acids are those that cannot be synthesised while non-essential can be synthesised endogenously. However, for those cells with high proliferation rates such as cancerous cells, even those amino acids that are non-essential become essential due to increased demand (Bhutia et al. 2015). Furthermore, some cancer cell types have lost their ability to synthesise specific amino acids all together, making them conditionally essential (Vettore, Westbrook, and Tennant 2020). Traditionally, studies of cancer cell metabolism have focused on glycolysis and the

tricarboxylic acid (TCA) cycle, however, more recently specific roles for amino acids have been reported. The primary function of amino acids is as building blocks of proteins, but in addition they have several other functions, such as fuels for metabolism, as precursors for hormones, and specialised metabolites such as polyamines, as anaplerotic metabolites for the TCA cycle and in redox homeostasis as the components of glutathione (GSH) (Vučetić et al. 2017).

Glutamine is the second most abundant amino acid in plasma (0.6-0.9 mM) after glucose and is the most well-studied in terms of its importance in cancer (Dereziński et al. 2017). It was recognised as early as the 1950s as a contributor that went far beyond the requirement for protein synthesis alone (H Eagle 1959). Many amino acid-based therapies focus on the uptake of glutamine and metabolism of glutamine to glutamate via glutaminases, mostly due to the glutamine-addicted phenotype associated with many cancer cell types induced by c-Myc expression (Wise et al. 2008). Glutamine is largely anaplerotic, generating α-ketoglutarate to support the TCA cycle or reductive carboxylation depending on oxygen availability (Hensley, Wasti, and DeBerardinis 2013). Other fuel sources that replenish the TCA cycle come from the branched chain amino acids ((BCAAs): isoleucine, leucine and valine); their catabolism supplies acetyl-CoA to the TCA cycle (Ananieva and Wilkinson 2018). As well as fuels, some amino acids act as precursors for the biosynthesis of other amino acids, or act as exchange factors. Asparagine, for example, requires glutamine for its *de novo* synthesis and, although not involved in biosynthesis itself, asparagine plays a role as an exchange factor and promotes uptake of serine and threonine. High rates of metabolism, including increased glycolytic activity in cancer cells, is associated with metabolic stress, caused by an accumulation in reactive oxygen species (ROS). Amino acids are involved in counteracting this oxidative stress by forming the antioxidant GSH from cysteine, glycine and glutamate. In order to maintain a reduced pool of GSH, NADPH is required, which is derived from the pentose phosphate

pathway via glycolysis, or from the folate cycle through serine (Vučetić et al. 2017). Finally, macromolecules like proteins, lipids and nucleic acids are required for DNA replication, cell division and therefore tumour growth. All require biosynthetic materials made from simple metabolites like sugars and amino acids. Glycine, glutamine and aspartate all contribute as either carbon or nitrogen donors to nucleotide synthesis, while methionine, glycine and serine act as carbon donors for nucleobases through the methionine-folate cycle.

Amino acid homeostasis is controlled by different factors, such as the entry and exit of amino acids through transporters, level-dependent biosynthesis or degradation of amino acids and the synthesis or degradation of proteins (reviewed in (Bröer and Bröer 2017)). Several amino acid transporters are upregulated in cancers to enhance amino acid uptake, including: sodium-coupled neutral amino acid co-transporters; alanine-serine-cysteine exchangers (ASCTs); L-type amino acid antiporters (LATs); and system x_c-light chain antiporters, which exchange glutamate for extracellular cystine (Bröer 2018). All work together to maintain the levels of 20 amino acids in the cytosol of a cell at higher concentrations than those found in blood (Bergstrom et al. 1974). In cancer cells, the signalling pathways for propagation of the tumour vary between types and due to this, it is likely that tumour cells will rely on different amino acid transporters to sustain their proliferative demands. As an example, LAT1 increases leucine uptake, a well-known activator of mTOR, one of two protein kinases responsible for controlling nutrient homeostasis alongside general control non derepressable 2 (GCN2), which senses uncharged tRNAs when amino acid levels are low (Bar-Peled and Sabatini 2014). Suppression of mTOR inhibits tumour growth, and this effect can be mediated through LAT1 and/or ASCT2 suppression and leucine or glutamine depletion, due to the coupling of these pathways to mediate mTOR activation (Lieu et al. 2020).

The physical restrictions of vasculature in tumours over 2 mm thick, and the overindulgence of nutrients by cancer cells, results in their limitation in the TME for use by other cell types, like

immune cells. In contrast to immune cells however, cancer cells will not be depleted, but rather undergo selection for those cells that can cope better with such conditions. Tumours are metabolically plastic and can adapt to limiting conditions using gene expression alterations, as well as interactions with neighbouring cells (metabolic symbiosis), to meet their energy requirements (Amend and Pienta 2015). Targeted therapies have tried to take advantage of conditionally essential amino acids by depleting them further, such as arginine, by using arginine-degrading enzymes such as PEGylated arginine deiminase (Phillips, Sheaff, and Szlosarek 2013). However, the plasticity of cancer cells and their ability to co-opt cancer-associated cells presents great challenges to this strategy (Z. Wang et al. 2014).

1.5.2 Impact of nutrients on oncolytic virus metabolism

OVs have an intrinsic selectivity for cancer cells. The mechanisms that underlie this are an active area of research with the aim of designing new and improved OVs. One such phenotypic hallmark that could be directing specific infection of cancer cells is their aberrant metabolism. The metabolic environment a tumour cell creates is one that would act favourably to viruses by providing excessive resources for production of infectious progeny (Seymour and Fisher 2016). In the case of EnAd, it has been suggested its preference for cancer cells over normal cells could be partly due to their metabolism. EnAd has a deletion in the E4ORF4 region (Dyer et al. 2017), this is known to improve viral replication by balancing early and late gene expression and inhibit host DNA damage responses. But most importantly here, it is known to activate mTOR and deregulate AMPK, both needed to create a resourceful cell environment for viral replication and are complemented for instead by the cancer cell phenotype (Kleinberger 2020). Improvements in metabolomics studies have allowed the identification of metabolic changes in tumour and virally-infected cells, specifically those that allow for successful OV replication. Likenesses between cancerous cells and those that are infected generally show increased uptake

and catabolism of nutrients (Dyer et al. 2020). Observations focusing on those viruses used as OVs show that some viral infections require glutamine and not glucose, whereas others require both. VSV can infect both normoxic and hypoxic cells and is inhibited when both glucose and glutamine are absent (Zhou et al. 2016), whereas Newcastle disease virus (NDV) decreases glycolysis to improve infection, and EnAd has been found to be most reliant on glutamine availability only (Al-Ziaydi et al. 2020; Dyer et al. 2019). These works and others clearly show that viruses and cancer cells have the same essential requirements of nutrients, like glucose and glutamine.

To date, however, only two studies by Esaki *et al* (Esaki et al. 2016) and Scheubeck *et al* (Scheubeck et al. 2019) are in medium that is more akin to those in the TME, *i.e.* low glucose or serum starved. They both showed that starvation of glucose can enhance OV effectiveness in the case of HSV and measles vaccine OVs respectively. While the majority of studies have shown requirements of OVs for glucose, fewer studies have focused on glutamine, and even fewer still on the effects of other amino acids. Additionally, no studies have investigated whether OV-infected cells could in fact make the characteristics of a TME worse in terms of nutrient competition and metabolic waste accumulation.

1.5.3 Impact of nutrient depletion on immunometabolism

Immune cells are used to moving across various environments each with its own community of different cells, ECM, nutrients and growth factors (Ganeshan and Chawla 2014; Buck et al. 2017). The concept of immunometabolism encompasses how immune cells respond to different environments, resource availability and how these factors translate to their functional responses. Compared to malignant cells, immune cells are much less metabolically plastic, relying heavily on the uptake of glucose, fatty acids and amino acids, making them vulnerable to changes implemented by the TME (Cohen, Danzaki, and MacIver 2017; Xiao, Locasale, and Dai 2020).

Amino acid availability in the TME has profound effects on the cells. In general, competition for glucose and most amino acids in the TME will bring about tolerised immune responses due to the activation of AMPK. For example, DCs become tolerant, while effector T cells become impaired and anergic following activation of AMPK by energy depletion, extracellular signals like adiponectin, and low amino acid availability. Specifically, in DCs this triggers fatty acid oxidation, glucose-fuelled electron transport chain use and autophagy, which are all reminiscent of a tolerant phenotype (Buck et al. 2017; Franchina, He, and Brenner 2018). Furthermore, MDSCs have many roles to evoke immunosuppression in the TME. One such role is to control amino acid availability by expressing arginase-1, IDO and sequestering cystine, which is usually reduced to cysteine by macrophages and DCs for the benefit of T cells, which cannot synthesise it themselves. Arginase-1 and IDO are both expressed in multiple pro-tumour cell types and deplete arginine and tryptophan respectively (Srivastava et al. 2010).

Amino acid depletion plays an important role for T cells. Activated T cells have shown an increased arginine metabolism, mediated through arginase-2, which is affected by low levels of arginine and results in impaired proliferation. However, when arginase-2 is deficient, intracellular arginine is increased, which in turn increases T cell survival after IL-2 withdrawal (Geiger et al. 2016). As well as arginine, extracellular serine and glycine also play an important role. Serine, a non-essential amino acid, is required for proliferation, and glycine is not enough to compensate for its requirement in the serine-glycine-one-carbon pathway. Furthermore, when serine is limited, secondary T cell responses are impacted in immunisation studies (E. H. Ma et al. 2017). Additionally, serine, alongside cysteine and glutamate, supplies glycine for GSH recycling, required to maintain T cell integrity during T cell activation (Franchina, He, and Brenner 2018). Moreover, depletion of tryptophan via IDO in tumour cells and other pro-tumour cells leads to an accumulation of kynurenine, a consequence of this is to inhibit T cell proliferation (increased kynurenine to tryptophan ratios are observed in Hodgkin lymphoma,

lung cancer and ovarian cancer (Lieu et al. 2020)). Most importantly during amino acid depletion is GCN2 activation in T cells, leading to GCN2 binding to uncharged tRNAs, which in turns aids with T cell survival when amino acid levels are low by limiting proliferation and inducing anergy. The latter is subject to more research, as even in GCN2-deficent T cells, proliferation is impaired when tryptophan, arginine, lysine, leucine or asparagine are low (Van de Velde et al. 2016).

1.5.4 Models of TME-based nutrient levels

Cell cultivation began in the early 1880's and since then, cell culture media has been developed and refined to such an extent, that we are now able to grow a vast number of different cells (T. Yao and Asayama 2017). In the past, culture media has been made up of natural biological fluids *i.e.* blood and lymph with undefined contents, but following the successes of cultivating cells for more than a few months, researchers sought to identify the pivotal components. This led to the wide range of media available today, both serum-containing and serum-free. In the early 1900s, Lillian Baker and Alexis Carrel were the first to demonstrate that amino acids and GSH were growth promoting in chick embryo fibroblasts (L. E. Baker and Carrel 1926; L. E. Baker 1928). The importance of amino acids was then further established by separate works from Fischer (A. Fischer 1948) and Eagle (H Eagle 1959), both independently demonstrating that the lower molecular weight fraction of medium was essential for proliferation. Eagle stated that thirteen amino acids and eight vitamins were the absolute minimum requirement for the proliferation of HeLa cells, one of the first immortal cell lines developed. The work resulted in the development of minimum essential medium (MEM) (H Eagle 1959).

As cell media has developed, those with excessive levels of certain nutrients have been selected for research to support cells with higher metabolic activity and proliferation rates (T. Yao and Asayama 2017). Dulbecco's modified Eagle medium (DMEM) (Dulbecco and Freeman 1959)

originally contained 5.6 mM glucose (as in blood), but the version more often used by researchers today contains 25 mM glucose. Furthermore, it contains four times the concentration of amino acids used in basal medium Eagle (BME) (Harry Eagle 1955) and two-fold higher concentrations than MEM prepared by Eagle 60 years ago (H Eagle 1959). Thus, most media used today contains wildly immoderate levels of certain nutrients, compared to the physiological concentrations found anywhere in the body, let alone in the nutrient-deprived TME. Glutamine, for example, of which medium contains 3-40 times more than has been reported in patients tumours, according to metabolic profiling studies (Goveia et al. 2016; Reznik et al. 2018). The importance of using relevant nutrient conditions to assess efficacy of cancer drugs is exemplified by a recent study by Jaeryun Lee *et al* (J. Lee, Park, and Lee 2017). They showed that reduced glucose actually enhanced the sensitivity of colorectal cancer cells to treatment with metformin. Furthermore, Pusapati *et al.* (Pusapati et al. 2016) showed that mTOR inhibitors were more effective when cells had been weaned off glucose, revealing a role for mTOR in metabolic reprogramming of tumour cells under these conditions.

There are now many groups trying to recapitulate the TME in order to properly assess various biopharmaceuticals, especially with developing 3D systems capable of mimicking zones of waste accumulation and nutrient depletion (Edmondson et al. 2014). These systems however, come with disadvantages such as ease of use, higher costs, variability in results and limitations with high-throughput methods. Another approach includes using tumour explants from biopsies, however, although more physiologically relevant, they are limited by their short life-span and their heterogeneity *ex vivo* (Burgos-Panadero et al. 2019). Animal models may also be used, whereby genetically engineered mice or xenograft models are often chosen. The disadvantages of animal models include high costs, untested relevance, time-commitment, intricacy and reproducibility (Burgos-Panadero et al. 2019).

It is appreciated that attempting to cover all variables in the TME is difficult whilst trying to maintain the integrity of an experiment, specifically whilst there are still current technical challenges with 3D culture techniques. For now, some groups have turned to the use of ascites fluids as a medium. This allows the ease of using well-characterised and cheap 2D culture systems, yet in a culture medium that is more physiologically reminiscent of the TME. Ascites is a fluid that accumulates in the peritoneal cavities of cancer patients. It contains tumours cells, non-cancerous cells, immune cells and soluble factors that form the TME, and is representative of fluctuating amino acid levels, proteins, cells, metabolites, and immunosuppressive factors that could hinder cancer therapies through multiple mechanisms (Scott et al. 2020). Studies by our lab have shown remarkable efficacy of BiTEs and virus-encoded BiTEs to infect, target and kill tumour and tumour-associated cells despite the immunosuppressive pressures known to be characteristic of malignant ascites (Freedman et al. 2017, 2018; Scott et al. 2019).

Altogether, it is vital that pre-clinical research in oncology moves more towards using models and/or conditions that closely resemble the conditions encountered in the TME, in order to more accurately assess and develop new therapeutics that can push past these barriers that are currently limiting efficacy and success. After all, if the hypothesis that cancer cell clonal selection occurs due to selective pressures from their environment is correct, then experimental conditions that mirror this selection should create the more aggressive and invasive phenotype that is currently the most difficult to target and treat (Laconi 2007; Talmadge 2007).

1.6 Acidification of the TME

1.6.1 Lactic acid in the TME

One of the emerging hallmarks reported in 2011 by Hanahan and Weinberg was the reprogramming of metabolism for rapid access to energy by tumour cells. In normal cells,

metabolism is well governed; dependent on neighbouring cells, environmental signals and on the cell itself. Under aerobic conditions, glucose is metabolised via glycolysis in the cytosol before being converted into carbon dioxide in the mitochondria (Hanahan and Weinberg 2011). Whereas under anaerobic conditions, glycolysis is uncoupled from oxidative phosphorylation (OXPHOS) via the TCA cycle, and thus glycolysis is favoured. Only a small amount of pyruvate is metabolised in the mitochondria, the rest is reduced to lactate, in order to replenish nicotinamide adenine dinucleotide (NAD^+) pools in the cell and allow glycolysis to continue. This metabolic switch has been adopted by cancer cells, even in the presence of oxygen, helping to provide material for macromolecules, intermediates of the TCA cycle and replenishing carbon skeletons (Romero-Garcia et al. 2011). Otto Warburg first observed this phenomenon of cancer cells, and multiple other cell types since have been identified to use the "Warburg effect" to support their energy demands too (Buck et al. 2017). One of the major by-products of this metabolic switch is lactic acid. Originally thought of as a waste product, it is now recognised as one of the foremost influencers of the TME, with control over the cancer cells, cancer-associated cells and immune cells present (Ippolito et al. 2018).

1.6.1.1 The production of lactic acid

The most significant populations that contribute to the elevation of lactate are glycolytic cancer cells and CAFs. Walenta *et al* measured lactate concentrations of various types of cancer and found that levels can vary greatly, but that higher levels were associated with higher incidences of metastasis. They classed those tumours with more than 8 μmol lactate per gram of tissue as high (average 7-13 μmol/g) and found that some tissues had up to 40 μmol/g (Walenta et al. 2000; Walenta and Mueller-Klieser 2004). This is compared to levels of less than 2 μmol/g found in serum (Aduen et al. 1994).

Lactic acid production and extrusion into the TME is mediated by lactate dehydrogenase (LDH) enzymes and monocarboxylate transporters (MCTs). There are five isoforms of LDH, each made up of monomer subunits that can either be encoded by the *LDHA* gene (muscle unit; M) or the *LDHB* gene (heart unit; H). The two types of monomer will combine to form either two homotetramers, LDH-1 and LDH-5, or three heterotetramers, LDH-2, -3, and -4, shown in Figure 1.6A. While LDH-5 (4x LDHA) is predominantly expressed in glycolytic tissues and skeletal muscle, LDH-1 (4x LDHB) is ubiquitously expressed but found largely in the heart (Doherty and Cleveland 2013). Due to differences in both their substrate affinity and their rates of reaction, LDH-5 is mostly associated with the reduction of pyruvate to lactate, while LDH-1 acts in the reverse to oxidise lactate back to pyruvate. (Draoui and Feron 2011). *LDHA* is most often associated with poor prognosis and was found to be highly expressed in several human cancers (Doherty and Cleveland 2013).

MCTs are lactate symporters that co-transport lactate anions and protons. They are capable of bidirectional transport, but the direction will depend on various environmental cues, as well as their cellular context. There are four MCTs associated with the transport of lactate specifically, out of a family of 14 members, MCT-1, -2, -3, and -4. Most often in the context of cancer cells, MCT-1 is induced by c-Myc expression and has been associated with the intake of lactate, while MCT-4 is responsible for lactate efflux and is induced by the HIF response. Both transporters are associated with poor prognosis in multiple aggressive malignancies (Counillon et al. 2016; Romero-Garcia et al. 2016). Studies by Le Floch *et al* showed that tumour cells expressing MCT-4 were more alkaline intracellularly and resulted in a lower extracellular pH (pH_e), more so than tumour cells expressing MCT-1/-2. Additionally they showed CD147/Basigin, a previously described pro-tumoural factor, is essential for MCT-1 and MCT-4 function (Le Floch et al. 2011).

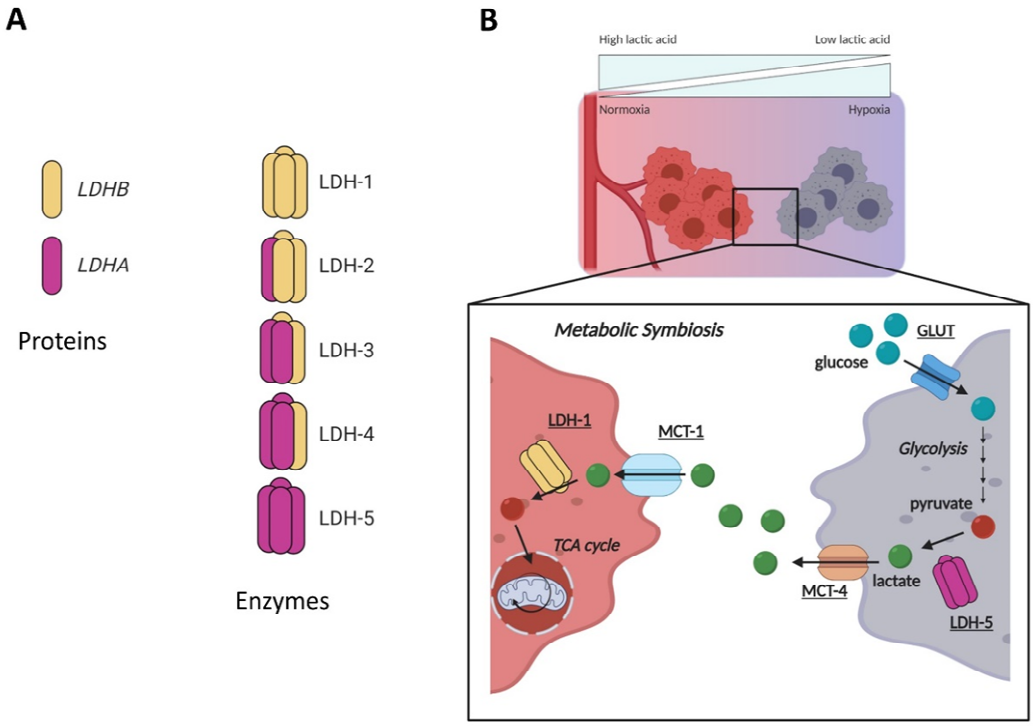


Figure 1.6 Lactic acid production and its role in metabolic symbiosis. (A) There are five isoforms of the LDH enzymes, each is a heterotetramer made up of four monomers. Monomers are proteins from either the LDHA gene or the LDHB gene. **(B)** The flux of lactate is driven by metabolic symbiosis in the TME. A gradient of oxygen develops from the functional blood vessels to the deeper cancer cells, while there is a reverse gradient of waste accumulation *i.e.* lactic acid. While aerobic tumour cells near to the blood supply take up lactate through MCT-1 and convert it to pyruvate by LDH-1 (LDHB) for use in mitochondrial OXPHOS. Hypoxic tumour cells take up the glucose that was spared by the oxidative tumour cells through GLUT transporters, metabolise it to pyruvate via glycolysis. Pyruvate is then reduced to lactate by LDH-5 (LDHA) and lactate is extruded via MCT-4. Once secreted its available for capture by the aerobic tumour cells. Figure A adapted from (J. Doherty and J. Cleveland, 2013). Figure B adapted from (O. Feron, 2009). Image created with BioRender.com.

1.6.1.2 Lactate as an energy source and signalling molecule

Extensive works and reviews by Brooks and Gladden (Brooks and Gladden 2003) have shown that lactate can be used as an alternative source of energy in metabolically-demanding tissues such as muscle and brain. This same mechanism has since been reported in tumours, which co-opt this lactate-shuttle hypothesis in order to remain metabolically plastic. The lactate-shuttle is a mechanism of metabolic symbiosis, in which lactate released by glycolytic cell types is used as fuel for TCA cycle in oxidative cells. Sonveaux *et al* (Sonveaux et al. 2008) showed in

mice that MCT-1 inhibition resulted in a shift from OXPHOS to glycolysis in oxidative tumour cells. This change in metabolic phenotype resulted in the death of distant cells in the hypoxic zone of tumours, showing that they were reliant on the originally oxidative cells using lactate instead of competing with them for glucose. In brief, symbiosis requires glucose transporters to uptake glucose in the glycolytic cells, then glucose is metabolised to pyruvate, and pyruvate reduced to lactate by LDH-5. The up-regulation of pyruvate dehydrogenase kinase (PDK) also aids in the generation of lactate as it inhibits pyruvate dehydrogenase (PDH), the enzyme that would catalyse pyruvate decarboxylation to acetyl-CoA for use in the TCA cycle. The lactate produced is then exported out of the cell by MCT-4 along with a proton (Ippolito et al. 2018). Both are then taken up by oxidative cells via MCT-1, oxidised back to pyruvate by LDH-1 and fed into the TCA cycle, while protons generated promote lysosomal acidification and autophagy dependent on V-ATPase (Brisson et al. 2016). A schematic of metabolic symbiosis is shown in Figure 1.6B. Tumour cells, CAFs and endothelial cells have all been shown to participate in lactate homeostasis in the TME (Vegran et al. 2011). CAFs act in accordance with the context of the tumour cells, donating lactate if tumour cells are oxidative or using it up if tumour cells are glycolytic (Bonuccelli et al. 2010; Koukourakis et al. 2006).

As well as being an alternative fuel, many other studies have elucidated roles for lactate as a signalling molecule. Vegran *et al* showed that in endothelial cells, lactate was imported by MCT-1 and triggered the phosphorylation and degradation of Iκβα, which stimulated the autocrine pathway NF-κβ/IL-8 and drove cell migration of endothelial cells and tube formation (Vegran et al. 2011). Furthermore, lactate may activate hyaluronan synthesis in CAFs through lactate-sensitive response elements (Stern et al. 2002), stimulate angiogenesis through the VEGF pathway, and stabilise HIF-1α by impairment of prolyl hydroxylases which mediates a number of other genes including further promotion of a malignant phenotype (reviewed in (Walenta and Mueller-Klieser 2004)). Moreover, as discussed in section 1.6.1.3, lactate also

acts as a signalling molecule to promote immune evasion particularly in the case of macrophages and DCs.

1.6.1.3 The role of lactic acid in immune evasion

Most activated immune cells with the potential to bring about an anti-tumour response require glucose as their main energy substrate, since glycolysis is the mainstay for most of these cells to activate and function at their full capacity. The list of such cells is extensive and includes M1 macrophages, N1 neutrophils, activated DCs, long-lived plasma cells, memory B cells, activated NK cells and effector T cells (CTLs, and Th1 and Th17 $CD4^+$ T cells) (Gatenby and Gillies 2004; Pearce and Pearce 2013). Therefore, these cells must compete for limited glucose and endure high concentrations of lactate, which acts to hinder anti-tumour responses in a negative feedback mechanism to stop excessive inflammation.

Indeed, this mechanism has been found naturally within humans in the colon, where lactate is known to reach high levels (10 mM) in the lumen, and this is sensed by colonic DCs through the lactate receptor, G-protein coupled receptor (GPR)81. This in turn induces regulatory factors, IL-10, IDO and retinoic acid, which tolerise DCs and inflammatory immune cells in the environment. GPR81 deletion in intestinal APCs in mice resulted in increased Th1/Th17 differentiation of T cells and reduced Treg differentiation (Ranganathan et al. 2018). Furthermore, in lung cancer cells, GPR81 sensing lactate has been shown to contribute to PD-L1/PD-1 immune checkpoint regulation of T cells (Feng et al. 2017). Additionally, macrophages are polarised to a pro-tumour (M2) phenotype by lactic acid, which uses oxidative metabolism as opposed to glycolysis for its effector functions. Zhang and Li showed that *LDHA* knockdown in gastric cancer cells suppressed the ability for conditioned medium from those cells to polarise macrophages to an M2 phenotype, shown through M2-related marker expression. Moreover, by using an MCT-1 inhibitor, α-cyano-4-hydroxycinnamate (CHC) or

HIF-1α knockdown in THP-1 cells, they abrogated expression of CD163 and arginase 1, common markers of an M2 phenotype. These findings together revealed that the lactate-MCT-1-HIF1α axis is a signalling cascade involved in macrophage polarisation in gastric cancer (Zhang and Li 2020).

While APCs become pro-tumour like due to lactate/lactic acid, effector T cells and NK cells are inactivated and become dysfunctional. Although helper T cells and CTLs are rendered inactive by lactic acid and struggle to buffer intracellular acidity, regulatory T cells thrive and exhibit the ability to adapt to low glucose, high lactate conditions. Adaptation is most likely enabled by the transcription factor FoxP3, as this is known to stimulate oxidation of lactate for use as fuel (Angelin et al. 2017).

There has been a great deal of research into the effects of pH and lactate on T cells. The main consensus is that acidosis impairs CTL activity, rather than lactate itself, as upon neutralisation or removal from the acidic milieu, functional ability can be regained (Mendler et al. 2012; Pilon-Thomas et al. 2016). A recent paper from 2020 by Hao Wu and colleagues verified that the inhibition of CTLs by lactic acid is in fact a natural phenomenon observed in lymph nodes, and is yet another mechanism exploited by tumours (Wu et al. 2020). The exact signalling cascade behind acidosis-induced inhibition of $CD8^+$ T cells has not yet been clarified. However, the reliance on mTOR for both $CD4^+$ and $CD8^+$ activation was shown by Pollizzi and Powell in 2015, and mTOR complex 1 (mTORC1) inhibition by acidosis has been shown by Walton *et al* in 2018 (Walton et al. 2018; Pollizzi and Powell 2015). Studies on both murine CTLs and human CTLs show susceptibility of T cells to acid, however, while all research groups reported diminished cytokine production and reduced cytolytic abilities, only some reported altered activation, survival and proliferation. This is most likely due to the setup of the experiments being different: some groups used hydrochloric (HCl) acid to acidify medium, while others used lactic acid; some used antigen-primed T cells to assess activity, while others used non-

specific forms of activation such as anti-CD3, anti-CD28 antibodies and high dose IL-2; and finally different groups measured different functional outputs, making it hard to come to any solid conclusions (reviewed in (Huber et al. 2017)). Conclusions that can be drawn include: 1) lactic acidosis disrupts $CD8^+$ T cell cytokine production and killing, 2) HCl-acidified medium was only able to exert these effects in part, 3) sodium lactate had no influence on $CD8^+$ T cell function at all, and 4) the effect is mediated by the inability for T cells to extrude lactic acid when levels are high extracellularly, most likely disrupting glycolysis (K. Fischer et al. 2007; Brand et al. 2016; Wu et al. 2020). While lactic acidosis rather than sodium lactate is responsible for defects in $CD8^+$ T cells, there have been reports that sodium lactate does influence $CD4^+$ helper cells. For instance, lactate regulates their motility, migration and chemotaxis through interference with glycolysis. The fact the same occurrence is not reported for $CD8^+$ T cells is put down to their differential expression of lactate transporters; $CD8^+$ expresses MCT1/SLC16A1, while $CD4^+$ expresses SLC4A12 (Haas et al. 2015). Furthermore Comito *et al* showed that lactate polarises $CD4^+$ T cells, reducing the frequency of Th1 cells and increasing regulatory T cells (Comito et al. 2019). The effects of lactic acidosis on immune cells and tumour-associated cells are summarised in Figure 1.7.

1.6.2 Further acidification of the TME

The price paid for the aberrant metabolic phenotype of tumour cells is the acidic burden in the TME, made worse by the chaotic vasculature, reminiscent of most tumours (Robert J Gillies et al. 2002). The main mechanism behind acidity is lactic acid build up, but due to the need for tumour cells to regulate their intracellular pH (pH_i), homeostasis is maintained by membrane transporters exporting protons, contributing further to TME acidification. Stabilising their pH_i allows tumour cells to continue using glycolysis, to produce ATP, to survive, to proliferate and to migrate despite their hostile environment (Chiche, Ricci, and Pouysségur 2013).

Cancer cells retain pH homeostasis by extruding excess protons and CO_2 using specialised proteins. Those described in the literature include: carbonic anhydrases (CAs) IX and XII, anion exchangers (SLC4A1, 2 and 3), proton transporter vacuolar ATPases (V-ATPase), sodium ion based chloride/bicarbonate exchangers (SLC4A8), and Na^+/H^+ exchanger 1 (NHE1; SLC9A1) and sodium-bicarbonate cotransporters (SLC4A7). Between them, they import weak bases while pumping out weak acids and manage to maintain the mildly alkaline pH balance inside of the tumour cells. CA IX and XII, are not actually transporters but are instead surface-associated enzymes that accumulate excess protons in the TME by catalysing the hydration of CO_2 to form carbonic acid, which is also released during metabolism of glycolytic intermediates via the pentose phosphate pathway. This mechanism contributes to the acidic TME in its own

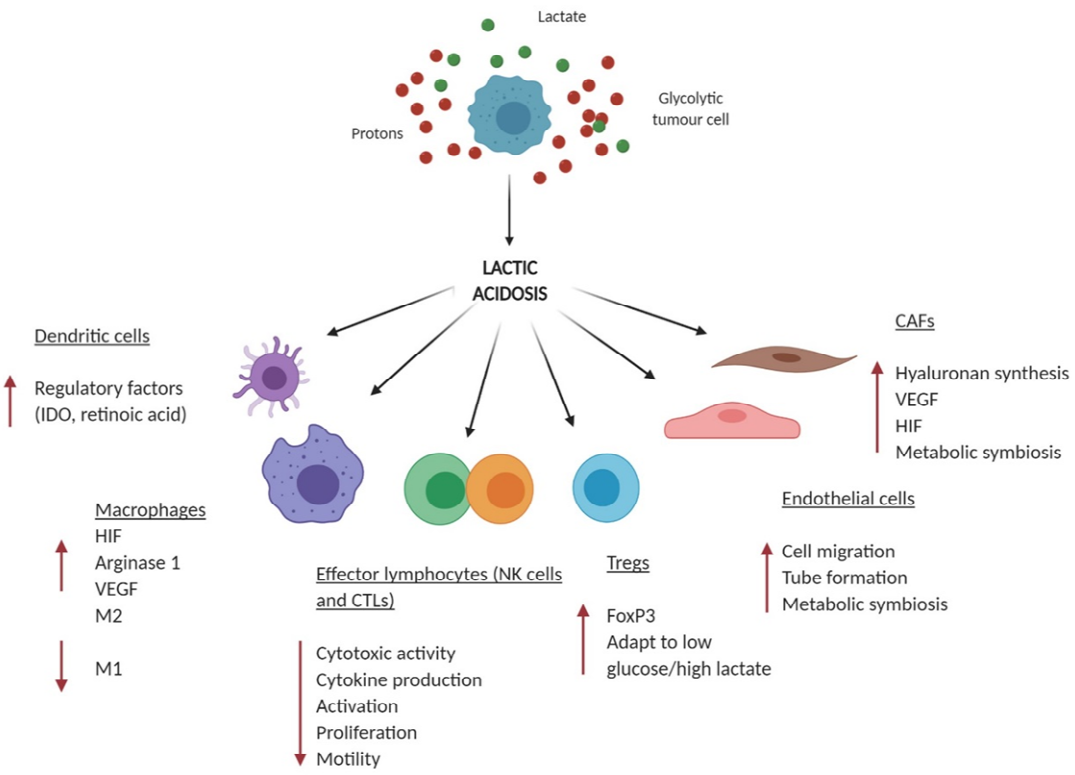


Figure 1.7 The role of lactic acidosis in immune evasion and tumour progression. Glycolytic tumour cells extrude lactic acid as a waste product to allow for the self-sufficiency of glycolysis (regenerating NAD^+ pools). Lactic acid, however, also has many roles in the TME to allow for tumour progression (in immune evasion, metastasis, and invasion). Depicted here are some of the reported phenotypes that develop when these cell types are subject to lactic acidosis. Image created with BioRender.com.

right, observed in glycolytically impaired mice where CO_2 is the main source of acid (Kato et al. 2013).

Methods to measure both the pH_e and pH_i, summarised in Table 1.2, have been improving over the last 70 years, yet various techniques are still met with challenges, with most still being tested pre-clinically (Ramamonjisoa and Ackerstaff 2017). Most recorded values of the pH_e for different tumour types are from animal models with xenografts of human tumour cell lines, or measured from cancer cells lines that have formed spheroids. Multiple studies report values between 6.4 and 6.8 using various techniques (Martin and Jain 1994; Va et al. 2009; L. Q. Chen and Pagel 2015; Sluis et al. 1999; R J Gillies and Bhujwalla 1994).

Table 1.2 Methods to measure the extracellular pH of a tumour. Adapted from (LQ Chen and Pagel, 2015 and Hao, Xu and Li, 2018).

Technology	Advantage	Limitation	Reference/s
pH-sensitive electrodes	Easily read and directly controlled	Surface accessible tumours and invasive	(Vaupel, Kallinowski, and Okunieff 1989)
Optical imaging	Sensitive and low cost, used to guide in surgery	Surface-accessible tumours, issues with deeper regions of tumour	(L. Q. Chen and Pagel 2015)
Positron emission tomography	Fast and able to image the whole body	Requires a radioactive isotope and has limited accuracy	(Weerakkody et al. 2013; Vavere et al. 2009)
Magnetic resonance imaging (MRI) spectroscopy	^{1}H ^{31}P ^{19}F MRS are all available ^{1}H measures metabolites and pH_e, while ^{31}P can measure both pH_i and pH_e simultaneously and ^{19}F is fast and sensitive	^{1}H has poor sensitivity and agents used can alter the pH, ^{31}P and ^{19}F require specific equipment	(Sluis et al. 1999; R J Gillies and Bhujwalla 1994; Oishi, Sumitani, and Nagasaki 2007)
Chemical exchange saturation transfer (CEST)-MRI	Good specificity and no special equipment as with MRI spectroscopy methods and non-invasive	Has poor sensitivity	(Ray et al. 2019; Randtke et al. 2017)

A specific study from Anderson *et al* used a pH-sensitive dye conjugated to pH-low insertion peptide (pHLIP) and reported pH_e values of 6.1-6.4 malignant and 6.7-6.9 for non-metastatic

cancer cells (Anderson et al. 2016). Those recorded for human patient samples were measured in 1985 by Thistlethwaite *et al* (Thistlethwaite et al. 1985), who reported the pH_e values from 14 human tumours spanning melanoma, squamous cell carcinoma, adenocarcinoma and sarcomas in a range from 5.55 to 7.69 with an average of 6.81.

Acidosis in the TME has been shown to have multiple effects, as well as those already mentioned in terms of lactic acid and its role in immune evasion. For the past 30 years, accumulating evidence has shown that low pH affects both the progression of a tumour and resistance to treatments, including radiation and chemotherapy. An acidic environment will encourage invasion through ECM degradation, promote evasion of apoptosis in specific clones resulting in resistant phenotypes, inhibit DNA repair resulting in high mutation rates, and induce VEGF (reviewed in (Romero-Garcia et al. 2011)). Additionally, several studies have reported a particular role for low pH in metastasis. In 2006 Rofstad *et al* showed that melanoma cells cultured in acidic medium (pH 6.8) formed four-fold more metastases after inoculation into mice than control mice inoculated with melanoma cells cultured in neutral medium (pH 7.4). They proposed this was due to the up-regulation of matrix metalloproteinases 2 and 9, cathepsin B, cathepsin L, and the up-regulation of pro-angiogenic factors including VEGF and IL-8 (Rofstad et al. 2006). These findings have consolidated the idea that a proton concentration gradient results in a periphery of apoptotic normal cells surrounding a tumour enabling malignant cells to then invade (Le Floch et al. 2011).

1.6.3 Current treatment targeting lactic acid and acidification

Despite the encouraging results from multiple anti-tumour immunotherapies over many years, clinical benefits have not always been as promising, specifically in solid tumours. Since the metabolic phenotype of cancer cells and acidity could render both chemotherapeutics and immunotherapies indolent, many research groups are now strategising ways to eliminate acidity

as a barrier. Some have shown the efficacy of their methods in combination with immunotherapies such as ICIs, as well as additional benefits to traditional cancer treatment (Ganapathy-Kanniappan 2017). Multiple methods are being employed to target TME acidity including neutralisation buffers, proton pump inhibitors (PPIs), sodium-hydrogen exchange inhibitors, antibodies against CAs, as well as small molecule inhibitors against MCTs and LDH. Those currently at various stages of development are in Table 1.3, although this is not an exhaustive list.

There are some challenges to overcome in order to successfully address tumour acidity in the clinic. Most important of which is that targeting metabolic pathways in tumours is difficult, given that tumour cells are so well-equipped to adapt to different metabolic pressures, with multiple pathways being capable of over-activation. For example, studies have found that tumours can compensate for MCT-1 inhibition with MCT-4, therefore inhibitors that are pan-MCT or MCT-4 specific are sorely needed. Furthermore, the metabolic pathways used by tumour cells are also used by normal cells, especially exemplified by the shared dependency on glycolysis by both tumour cells and active immune cells. Therefore, any general inhibitors of these metabolic pathways may result in off-tumour effects, causing adverse reactions or limiting the potential of the anti-cancer immune response. The best way to combat these resistance mechanisms and limit off-tumour effects will be to use multi-modal therapies that are highly specific, to target a number of pathways or hallmarks at once.

Table 1.3 Current agents used to target acidity in tumours. Adapted from (Martinez-Outschoorn et al, 2016).

Target	Agent	Observations	Reference/s
General acidity	Sodium bicarbonate	Oral doses reduced spontaneous metastases in mice models with breast cancer Hydrogel loaded sodium bicarbonate neutralises TME in mouse model and worked in combination with anti-PD-1	(Robey et al. 2009; Silva et al. 2009; Jin et al. 2019)
V-ATPase	Esomeprazole, omeprazole, pantoprazole, lansoprazole, rabeprazole	Highly selective for TME, due to preference for low pH	(B. Y. Wang et al. 2015)
Na^+/H^+ antiporter (NHE1)	Cariporide	Inhibited tumour growth *in vitro* and selectively at low pH Able to sensitise breast cancer cells to doxorubicin both *in vitro* and *in vivo*	(Wong, Kleemann, and Tannock 2002; Q. Chen et al. 2019)
Carbonic anhydrases (IX and XII)	Monoclonal antibodies, (cG250), sulphonamide compounds (Indisulam, SLC-0111)	Multiple antibodies being tested both pre-clinically and in Phase II/III trials	(Kazokaitė et al. 2017)
MCT1	AZD3965, CHC (non-specific), SR13800, AR-C155858, RNAi	AZD3965 is in clinical development	(Le Floch et al. 2011; Doherty and Cleveland 2013; Polanski et al. 2014)
MCT4	AZD0095, RNAi, CHC (non-specific)	Highly selective for MCT4 and potent, increases TILs in combination with anti-PD-1	(S. Choi et al. 2016; Critchlow et al. 2019)
LDHA	GNE-140, Gossypol, FX-11, galloflavin, RNAi	Most compounds are specific to LDHA however Gossypol also targets LDHB, none of these compounds are yet in clinical trials	(Martinez-Outschoorn et al. 2016)

1.7 Thesis overview and aims

1.7.1 Overview

Immunotherapies are now in a revolutionary era, showing promise in being a successful and powerful string in the fight against cancer's bow. However, their effectiveness is not as significant as had been hoped in solid tumours, mainly due to the heavily immunosuppressive TME. Burgeoning evidence implicates nutrient depletion and lactic accumulation in the development of an immune-suppressive and pro-tumoural TME (Kouidhi, Ayed, and Elgaaied 2018). While most immunotherapeutics, including BiTEs and OVs, show promise in pre-clinical experiments, these studies generally employ culture conditions or animal models that do not fully recapitulate the metabolic nature of advanced tumours. Treatments that are currently hampered by metabolic stress could be improved if specific barriers to their efficacies were to be identified.

Aberrant metabolism has been known as a characteristic of cancer now for 70 years (Warburg 1956); however, only in 2011 was it named a hallmark of cancer in its own right (Hanahan and Weinberg 2011). Since then, there has been gathering interest in targeting components of metabolism as anti-cancer therapies. Such attempts have been hampered thus far by poor tumour-selectivity, leading to on-target, off-tumour effects, and by unfavourable pharmacokinetics. OVs offer a unique platform in which inherent anti-cancer activity is combined with the possibility to encode therapeutic transgenes. These transgenes can be expressed in a tumour-restricted manner and go on to selectively target a whole host of processes in the infected cells. Among several OVs in clinical development, EnAd is a particularly promising candidate, with high selectivity, an excellent safety profile, blood

stability and good biodistribution, as well as a proven track record of maintaining viral activity despite an altered genome to include transgenes, including reporter genes and BiTEs.

The primary aim of this thesis is to characterise the functionality of two immunotherapies, BiTEs and OVs, in the presence of known obstacles reported in the TME, namely nutrient depletion and lactic acid accumulation. Part of this aim will include the use of relevant models to realistically represent the conditions being tested. This work will be performed primarily using a BiTE targeting EpCAM and using the group B OAdV, EnAd. Recent work published in our laboratory has shown that, in combination, they are efficacious even in immunosuppressive liquid biopsies from patients (Freedman et al. 2017); however they have not yet been tested under specific conditions of nutrient stress and waste accumulation. The result of these studies will inform the second overarching aim of this thesis: to explore strategies aimed at improving the efficacy of these therapies in conditions of metabolic stress. Importantly, this approach may help to find ways in which the metabolic functions of TILs in the TME can be restored and their anti-cancer activity reinvigorated.

1.7.2 Thesis aims and hypotheses

1. EpCAM BiTE and EnAd immunotherapies will induce killing of cancer cell lines during amino acid depletion (Chapter 3).
2. Clinically-relevant *ex vivo* models of human cancer (malignant ascites) represent realistic amino acid stress experienced in the TME (Chapter 3).
3. The EpCAM BiTE will remain functionally active and activate T cells despite the presence of immunosuppressive lactic acid (Chapter 4).

In the final chapter, based on the findings of chapter 4, a new hypothesis is proposed:

4. EnAd is a suitable platform with which to modulate the pH of the tumour microenvironment to improve therapies based on T cell activation *e.g.* BiTE-induced T cell activation (Chapter 5).

2 Materials and Methods

2.1 Tissue culture

2.1.1 Cell line maintenance

Adherent cell lines used and the culture medium they require are summarised in Table 2.1, all cell lines were sourced from the American Type Culture Collection (ATCC) and cultured in an incubator at 37 ˚C and 5% CO_2. To subculture cells, monolayers were washed with Dulbecco's phosphate-buffered saline (1x DPBS; #14190250, Gibco) and then treated with an enzymatic solution consisting of 0.25% trypsin and 0.02% ethylenediaminetetraacetic acid (EDTA) (#T4049, Sigma-Aldrich) until cells dissociated. Cells were then resuspended in medium at 10x the volume of trypsin used to neutralise the trypsin and split at a ratio of 1:10. Cell lines were routinely tested for mycoplasma using the MycoAlert Mycoplasma Detection Kit (#LT07-318, Lonza).

2.1.2 Cryopreservation of cells

For cryopreservation cells were resuspended in freezing medium consisting of FBS with 10% volume/volume (v/v) dimethyl sulfoxide (DMSO; #D2650, Sigma-Aldrich), aliquoted into 1.8 mL cryogenic vials and frozen at 1 ˚C per minute in a freezing container (CoolCell, Corning) at -80 ˚C.

To thaw cells, vials were incubated at 37 ˚C until thawed, then 30 mL of pre-warmed medium was added dropwise and cells were pelleted by centrifugation (400 x g, 5 mins). Cells were resuspended in fresh medium and left to adhere for 24 hours before medium was aspirated and replaced.

2.1.3 Cell seeding

If experiments required cells to be seeded in plasma-treated culture grade plastic plates (Greiner Bio-One), cells were dissociated with trypsin and the concentration of cells was determined by counting using a haemocytometer, viability was assessed by trypan blue exclusion (#15250061, Gibco). The cell number was adjusted to the required seeding density for each cell line as required in each experiment.

Table 2.1 Tumour cell lines used and their required culture conditions. DMEM, Dulbecco's modified eagles medium (#D5796, Sigma Aldrich); FBS, heat-inactivated foetal bovine serum (#10500064, Gibco); RPMI, Roswell park memorial institute 1640 medium (#R8758, Sigma Aldrich).

Cell Line	Description	Culture Medium and Supplement	Time before passage requirement (days)
293Ad	Human embryonic kidney cells with a stably integrated copy of the adenovirus E1 gene	DMEM + 10% FBS	2
A549	Human carcinoma cells derived from the lung	DMEM + 10% FBS	3
Colo205	Human colorectal adenocarcinoma cells, semi-adherent cell line	RPMI + 10% FBS	3
DLD-1	Human colorectal adenocarcinoma cell line	DMEM + 10% FBS	3
HCT116	Human colorectal carcinoma cells	DMEM + 10% FBS	2
HT29	Human adenocarcinoma cells derived from the colon	DMEM + 10% FBS	3
SKOV-3	Human ovarian adenocarcinoma cell line	DMEM + 10% FBS	5

2.1.4 Treatments and reagents for cell culture

All reagents used in cell culture medium are listed in Table 7.1 in Appendix I. To formulate media containing all but one amino acid, RPMI 1640 without amino acids (#RPL22, Caisson Labs) was used as a basal media, and relevant concentrations of amino acids were added individually using concentrated stocks of the amino acid reagents detailed in Table 2.2. Dialysed FBS containing no amino acids was also used (#26400044, Gibco) to supplement the medium to 2%. For experiments requiring media containing variable concentrations of tryptophan, appropriate amounts of tryptophan were added to tryptophan free RPMI 1640

(#P04-17598, Pan-Biotech). Media containing no glucose (DMEM; #11966025, Gibco, RPMI; #11879020, Gibco) was used as a basal medium for testing various concentrations of glucose, and medium containing no glutamine (DMEM; #11960044, Gibco) was used as a basal medium for testing glutamine concentrations.

Table 2.2 Formulation for RPMI 1640 and RPMI without amino acids media.

Component	1x R8758 (g/L)	1x RPL22 (g/L)	Amino acid stock volume added to 10 mL medium made (µL)	Amino acid stock concentration (g/L)
Inorganic salts				
Calcium nitrate	0.1	0.1		
Magnesium sulphate (anhydrous)	0.04884	0.04884		
Potassium chloride	0.4	0.4		
Sodium bicarbonate	2.0	2.0		
Sodium chloride	6.0	6.0		
Sodium phosphate dibasic (anhydrous)	0.8	0.8		
Vitamins				
D-Biotin	0.0002	0.0002		
Choline chloride	0.003	0.003		
Folic acid	0.001	0.001		
Myo-Inositol	0.035	0.035		
Niacinamide	0.001	0.001		
p-Amino benzoic acid	0.001	0.001		
D-Pantothenic acid·½Ca	0.00025	0.00025		
Pyridoxine·HCl	0.001	0.001		
Riboflavin	0.0002	0.0002		
Thiamine·HCl	0.001	0.001		
Vitamin B·12	0.000005	0.000005		
Other				
D-Glucose	2.0	2.0		
Glutathione (reduced)	0.001	0.001		
Phenol red·Na	0.0053	0.005		
Amino acids				
L-Arginine (free base)	0.2		100	20
L-Asparagine (anhydrous)	0.05		100	5
L-Aspartic acid	0.02		100	2
*L-Cysteine·2HCl	0.0652		100	6.52
L-Glutamic acid	0.02		100	2
L-Glutamine	0.3		100	30
Glycine	0.01		100	1
L-Histidine (free base)	0.015		100	1.5
Hydroxy-L-proline	0.02		100	2
L-Isoleucine	0.05		100	5
L-Leucine	0.05		100	5
L-Lysine·HCl	0.04		100	4
L-Methionine	0.015		100	1.5
L-Phenylalanine	0.015		100	1.5
L-Proline	0.02		100	2
L-Serine	0.03		100	3
L-Threonine	0.02		100	2
L-Tryptophan	0.005		50	1
L-Tyrosine·2Na·2H_2O	0.02883		640.7	0.45
L-Valine	0.02		100	2

2.1.5 RNA and DNA transfections

RNA and DNA transfections of cells were performed according to the manufacturer's instructions using Lipofectamine™ 2000 (#11668019, Invitrogen). RNA or plasmid DNA and Lipofectamine 2000 were both diluted in Opti-MEM (#31985062, Gibco), quantities used were dependent on cell culture vessel and are described in Table 2.3. Dilutions were incubated for 5 minutes at room temperature (RT) before mixing the solutions together and incubating at RT for a further 20 minutes. The DNA:Lipofectamine complexes were then added dropwise to target cells seeded 24 hours previously. After four hours of incubation, transfection medium was replaced by fresh 2% medium. RNA transfections were carried out in RNA interference (RNAi) experiments, the siRNAs (validated Silencer™ Select grade, Invitrogen) transfected are detailed in Table 2.4.

Table 2.3 Quantities and volumes of DNA and RNA added alongside Lipofectamine to transfect cells in different culture dishes.

Culture dish	Seeding volume (mL)	OptiMEM volume for dilution (µL)	Plasmid DNA (µg)	Lipofectamine 2000 (µL)	RNA (pmol)	Lipofectamine 2000 (µL)
96 well	0.10	25	0.2	0.5	5	0.25
48 well	0.25	40	0.4	1.0	10	0.5
24 well	0.50	50	0.8	2.0	20	1.0
12 well	1.0	100	1.6	4.0	40	2.0
6 well	2.0	250	4.0	10	100	5.0
T25	5.0	50	5.0	20	-	-
T75	7.6	1200	20	80	-	-

2.1.6 pH measurement of reagents and medium

A Jenway pH meter, model 3510, and long reach life science pH electrode (6.0 mm stem, #924049, Cole Palmer) were used to measure pH in medium made for experimental use in tissue culture or in culture medium following experimentation. Calibration was performed with standard buffer solutions of known pH values.

Table 2.4 A list of siRNAs used for RNA interference of lactic acid pathway targets.

Target gene	siRNA	Sense	Antisense
LDHA	A: s229665	CUUGCAUUUUGGGACAGAAtt	UUCUGUCCCAAAAUGCAAGga
	B: s350	CCAGCGUAACGUGAACAUAtt	UAUGUUCACGUUACGCUGGac
	C: s351	CAGUGGAUAUCUUGACCUAtt	UAGGUCAAGAUAUCCACUGga
LDHB	A: s8124	AAACAAUAAGAUCACUGUAtt	UACAGUGAUCUUAUUGUUUgg
	B: s8125	GUAUGUUACCUGGAAACUAtt	UAGUUUCCAGGUAACAUACgt
	C: s8126	CAGUCCUGAUUGCAUCAUAtt	UAUGAUGCAAUCAGGACUGta
MCT4	A: s17416	UCAAGGAGCUCAUACAGGAtt	UCCUGUAUGAGCUCCUUGAag
	B: s17417	CCGUCUACCUCUUCAGCUUtt	AAGCUGAAGAGGUAGACGGag
	C: s17418	GCAUUAGGAAGAAGCCCAAtt	UUGGGCUUCUUCCUAAUGCag
Negative Control	No. 2	N/A	N/A

2.1.7 Lactate measurements of conditioned medium

To measure the concentration of lactate in medium the Lactate-Glo assay kit (#J5021, Promega) was used according to manufacturer's instructions. Briefly samples were centrifuged (450 x g, 5 mins) to clear supernatants of cells then 2 µL was added to 98 µL of DPBS. A standard curve was produced of known lactate concentrations. Then a lactate detection reagent was prepared and 50 µL was added to 50 µL of diluted supernatants or standards before incubation for 60 minutes at RT. Then luminescence was measured using a Wallac 1420 Victor^2 plate reader (Perkin Elmer).

2.2 Molecular cloning

2.2.1 Bacterial transformation

Bacterial transformation was performed using the heat-shock method. An aliquot of DH10β cells was thawed on ice, approximately 10-100 ng plasmid DNA was mixed with the thawed cells and incubated on ice for 20 minutes before being transferred to a water bath at 42 ˚C for 45 seconds (heat-shocked) and then transferred back to ice for 5 minutes. 100 µL of super optimal broth with catabolite repression medium (SOC; #15544034, Invitrogen) was added before incubation at 37 ˚C in a shaker (SI-300R, Fisher Scientific) at 180 rpm for 1 hour. Transformation mixtures were spread on to pre-warmed lysogeny broth (LB) agar plates (#L2897, Sigma Aldrich) with the relevant antibiotic for selection (ampicillin or kanamycin, 100 ng/mL) and incubated overnight at 37 ˚C (Gallenkamp).

2.2.2 Hairpin construction

The shRNAs were designed following validation of target sequences by transfection of synthetic siRNA and verification of target knockdown. A forward strand oligonucleotide encoding both the sense and antisense strands of the siRNA candidate was designed and synthesised. The forward oligonucleotide contained a loop sequence in between the sense and antisense strands, and the appropriate 5’ and 3’ anchors either side to allow for plasmid insertion. A reverse oligo with sequence complementarity to the forward oligo was also designed to allow for annealing of the two strands, and for their successful insertion into a dsDNA plasmid. Oligomers were commercially synthesised (Integrated DNA Technologies (IDT)) and the scramble shRNA sequence was a gift from David Sabatini (Addgene #1864; http://n2t.net/addgene:1864 ; RRID:Addgene_1864) (Sarbassov et al. 2005). For annealing, 5

µL of each of the forward and the reverse oligomers (stock 10 µM) were combined with 4 µL 5x T4 DNA Ligase reaction buffer (#46300018, Invitrogen) and 8 µL dH_2O. Annealing reactions were incubated for 3 minutes at 95 ˚C in a water bath (Type T100, Grant Instruments), then the water bath was switched off and reactions were allowed to cool to RT whilst remaining in the water bath. Annealed oligo's were stored at 4 ˚C.

2.2.3 DNA plasmid preparation and purification

Clonal populations of bacteria transformed with the relevant plasmid were picked and used to inoculate mini-prep cultures of 3 mL LB broth (#L3022, Sigma Aldrich) supplemented with the relevant antibiotic. Maxi-prep cultures were inoculated by addition of 200 µL of the mini-prep culture into 200 mL LB broth with relevant antibiotic. Cultures were incubated overnight at 37 ˚C in a shaker at 180 rpm. Plasmid DNA was extracted from mini-prep cultures using the Monarch® plasmid miniprep kit (#T1010L, New England Biolabs (NEB)) following the manufacturer's instructions, and from maxi-prep cultures using the Qiagen Plasmid-Plus maxi-prep kit (#12945, Qiagen) following the manufacturer's instructions.

EnAd 2.4 vectors, parental or modified, were purified using an isopropanol precipitation method, as commercial kits are not suitable for purification of this size of fragment (> 20 kb). DNA was mixed with 0.6 volumes of cold isopropanol and incubated for 60 minutes at -80 ˚ C before centrifugation (12,000 x g, 30 mins) at 4 ˚C. Isopropanol was carefully removed and discarded, the remaining pellet was washed with 70% ethanol and centrifuged (12,000 x g, 5 mins) at RT. Ethanol was carefully removed and the pellet was air-dried at 60 ˚C before being resuspended in distilled nuclease-free water, ddH_2O (#AM9906, Invitrogen).

2.2.4 DNA restriction digests

Restriction digests were performed: to prepare vector backbones for molecular engineering, as a diagnostic tool to assess transgene insertion into plasmids and in order to linearise EnAd vectors before transfection. Digests were performed according to the chosen restriction enzyme's manufacturer's instructions with the relevant enzyme buffer (NEB). Typically, 1 μg of DNA was digested in a 50 μL reaction using 0.4 units/μL restriction enzyme. To digest or linearise a larger vector (> 20 kb), 25 μg of DNA was digested in a 110 μL reaction with 0.9 units/μL restriction enzyme. Reactions were incubated at 37 ˚C for 2 hours or overnight for larger vectors. If vector backbones were being prepared for further engineering, 1 unit alkaline phosphatase (#M0290S, NEB) was added to the mixture for the final 1 hour to prevent re-ligation of the backbone.

2.2.5 Polymerase chain reaction

Polymerase chain reactions (PCRs) were performed using 0.5 μM forward and reverse custom synthesised primers (IDT), 1 ng of the relevant DNA template and 10 μL Phusion® high-fidelity DNA polymerase master mix (#M0531S, NEB) in a 20 μL reaction. Reactions were performed using a PTC-225 Peltier Thermal Cycler DNA engine Tetrad (MJ Research) with the following conditions:

1. Initial denaturation: 98 ˚C for 30 sec
2. Denaturation: 98 ˚C for 10 sec
3. Annealing: Primer specific annealing temperature for 30 sec
4. Extension: 72 ˚C for 60 sec
5. Repeat cycles: to step 2, repeat 34x
6. Final extension: 72 ˚C for 10 mins
7. Storage: 4 ˚C forever

For a primer list see Table 7.3 Appendix II.

2.2.6 Agarose gel electrophoresis

Agarose gel electrophoresis was used to resolve DNA from purified plasmid preps, restriction digest fragments and PCR reactions. Agarose (#A4718, Sigma Aldrich) gels were prepared using 1x Tris-Acetate-EDTA buffer (TAE; recipe Table 7.2 in Appendix I) containing GelRed nucleic acid gel stain (#BT41003, Biotium) for visualisation. 0.8% agarose gels were used to resolve larger plasmids (> 20 kb) and 1% agarose gels for smaller plasmids (5-10 kb) and PCR products. Samples were prepared with 6x loading dye (#B7025S, NEB) and ran alongside a DNA ladder (#N0468S, NEB) for estimation of DNA molecule size unless otherwise specified. Gels were run in 1x TAE buffer at 120 V for 1 hour and were visualised and imaged using the ChemiDoc MP imaging system (BioRad).

2.2.7 DNA purification from agarose gels

For purification of specific DNA bands after resolution on agarose gels, bands were visualised using the ChemiDoc MP imaging system (BioRad) or under blue light using a Dark Reader trans-illuminator (GRI). These bands were then excised using a scalpel, and DNA extracted and purified using the Monarch DNA gel extraction kit (#T1020L, NEB) according to manufacturer's instructions.

2.2.8 DNA quantification

DNA quantity was determined using a NanoDrop™ One spectrophotometer (ThermoFisher Scientific), the instrument was blanked first using the diluent the DNA to be tested was suspended in.

2.2.9 DNA ligation and Gibson assembly

Sticky end ligation reactions were carried out using a molar ratio of 3:1 (insert:vector). 50 ng of digested plasmid backbone was used and the ligation calculator (NEBioCalculator) was used to calculate the amount of insert required. The ligation reactions contained 50 ng of plasmid backbone, the relevant concentration of insert, 1 μL T4 DNA Ligase (#46300018, Invitrogen) and 4 μL 5x T4 DNA Ligase buffer. Reactions were made up to 20 μL with dH_2O. Ligations were performed overnight at 16 ˚C and T4 DNA Ligase was heat inactivated for 10 minutes at 65 ˚C before storing mixtures at 4 ˚C until further use.

Gibson assembly allows for the combination of multiple DNA fragments in a single reaction. It relies on 20-40 bp overlapping regions between adjacent fragments, generated through PCR amplification of fragment inserts, restriction digests of vector backbones or commercially synthesised oligos (IDT) (Gibson et al. 2009). Reactions were performed using NEBuilder® HiFi DNA assembly master mix (#E2621L, NEB) following the manufacturer's instructions with purified DNA fragments. Briefly, 50 ng digested plasmid DNA was used at a vector:insert molar ratio of 1:2 for plasmids of 5-10 kb and a molar ratio of 1:15 for plasmids of > 20 kb. Reactions were incubated in a thermocycler (MJ research) for 1 hour at 50 ˚C and used immediately for bacterial transformation or stored at 4 ˚C until further use.

2.2.10 Sequencing

Plasmids with transgene insertions that showed the correct diagnostic digest patterns were sequenced by Sanger sequencing using GATC services according to their protocol (Eurofins Genomics) and aligned using *in silico* predicted sequences with Geneious® prime software (Geneious Biologics).

2.3 Molecular biology methods

2.3.1 BiTE preparation

T75 flasks were seeded with 1.5 x 10^6 293Ad cells 24 hours before DNA transfection with a BiTE-encoded plasmid, Opti-MEM was used as the complete medium for the length of the transfection. Supernatant was collected from the 293Ad cells 48 hours post-transfection and clarified by centrifugation (400 x g, 10 mins) before being concentrated 40-fold with Amicon® Ultra-15 10 kDa MWCO centrifugal filter units (#UFC901024, Merck), aliquoted and stored at -80 ˚C.

The EpCAM L2K BiTE was prepared as above using the pSF-CMV-EpCAM BiTE expression plasmid engineered and kindly provided by Dr. Joshua Freedman (Seymour Lab, Department of Oncology, University of Oxford). Other constructs used in chapter 4 of this thesis; EpCAM OKT3, PD-L1 OKT3, and PD-L1 LiTE were kindly provided by Dr. Hena Khalique (Seymour Lab, Department of Oncology, University of Oxford) who engineered, expressed and characterised them.

2.3.2 Protein extraction, preparation and quantification

Cells were placed on ice and washed with cold 1x DPBS. Depending on the culture vessel, treated cells were either scraped in 1x DPBS and transferred to a microcentrifuge tube before being centrifuged (300 x g, 4 mins) and the pellet lysed with Pierce™ RIPA buffer (#89900, ThermoFisher Scientific) containing Halt™ protease and phosphatase inhibitors (#78442, ThermoFisher Scientific) or culture vessels were treated directly with the RIPA buffer mix after 1x DPBS was aspirated off and cells were scraped and lysed directly in the wells.

Protein concentration in cell lysates was determined using the QuantiPro™ BCA assay kit (#QPBCA, Sigma Aldrich) following manufacturer's instructions using a standard curve of bovine serum albumin with known protein concentration (#P0914, Sigma Aldrich).

2.3.3 SDS-PAGE gel electrophoresis

Proteins were separated by their molecular weight using 4-20% gradient Mini-PROTEAN® TGX™ precast polyacrylamide gels (#4561096, BioRad) loaded with 15-50 μg protein. Samples were mixed with 6x Laemmli buffer (#J61337, Alfa Aesar) and dH_2O to reach the required concentration for loading, aliquoted and stored at -20 ˚C until required. Samples were thawed on ice and denatured for 5 minutes at 95 ˚C before being loaded alongside PageRuler™ Plus prestained protein ladder (#26619, ThermoFisher Scientific) and ran at 80 V for the first 20 minutes and 120 V for a further 1 hour in sodium dodecyl sulfate (SDS) running buffer (recipe in Table 7.2, Appendix I) in a BioRad TGX system (BioRad).

2.3.4 Immunoblotting

For western blot analysis resolved proteins were transferred to 0.2 μm nitrocellulose membranes (#77012, ThermoFisher Scientific) using a wet-tank technique with 1x Transfer buffer (recipe in Table 7.2, in Appendix I) at 4 ˚C for 90 minutes at 300 mA or using a transfer pack (#1704158, BioRad) and Trans-Blot® turbo transfer system (#1704150, BioRad) following the manufacturer's instructions. Membranes were stained with Ponceau S solution (#22001, Biotium) to determine transfer efficiency before being washed with dH_2O to remove the stain and with a final wash of PBS-Tween buffer (PBST; recipe in Table 7.2, Appendix I).

Membranes were blocked with blocking buffer (5% skim milk powder (#70166, Sigma Aldrich) diluted in PBST buffer) for 1 hour at RT before being incubated with the appropriate primary antibody overnight at 4 ˚C in blocking buffer on a shaking platform. Membranes were washed

3x with PBST buffer and incubated with the appropriate horseradish peroxidase (HRP)-conjugated secondary antibody for 1 hour at RT in blocking buffer and membranes washed again 3x with PBST buffer. SuperSignal™ west dura extended duration substrate solution (#34075, ThermoFisher Scientific) was applied and chemiluminescence was visualised using X-ray films by exposing them to the membrane and developing them in an automatic film processor (Agfa, CP1000) or the ChemiDoc MP imaging system (BioRad). The antibodies and their dilutions used throughout are listed in Table 2.5.

Dot blot analysis was used to quantify BiTE proteins secreted into supernatants from 293Ad cell cultures, 1.5 µL of supernatant was spotted onto a dry 0.2 µm nitrocellulose membrane. A deca-His tagged standard protein A (#NBP2-34965, Novus Bio) of known concentration was serially diluted and spotted alongside unknown supernatants, to make a standard curve. The membrane was allowed to air-dry for 30 minutes before analysing using the same procedure as in western blot analysis from the blocking step onwards.

Table 2.5 Antibodies and their dilutions and conditions required for western blot analysis.

Antibody target	Conjugate	Host	Dilution factor	Manufacturer	Catalogue number
ATF4	-	rabbit	1000	Cell Signalling Technology (CST)	#11815
His-Tag	-	mouse	5000	Invitrogen	46-0693
LDHA	-	rabbit	1000	CST	#3582
LDHB	-	rabbit	50000	Abcam	Ab53292
MCT4 (F-10)	-	mouse	1000	Santa Cruz biotechnology	sc-376101
GAPDH	-	mouse	5000	CST	#97166
β-actin	HRP	mouse	10000	Sigma Aldrich	A3854
Anti-mouse	HRP	goat	3000	CST	#9309
Anti-rabbit	HRP	goat	3000	CST	#7074

2.3.5 Enzyme-linked immunosorbent assay to assess BiTE concentration

Quantification of BiTEs was determined using a His Tag enzyme-linked immunosorbent assay (ELISA) detection kit (#L00437, GenScript) following the manufacturer's instructions. Samples were prepared by diluting BiTE supernatants 1 in 10 in the assay diluent provided and incubated alongside a serially diluted His Tag standard supplied with the kit, final concentrations were calculated based on the standard curve using graph pad prism.

2.3.6 RNA extraction and complementary DNA synthesis

For RNA extraction, 10^5-10^6 cells seeded in plates were washed on ice with cold 1x DPBS. DPBS was aspirated and RNA was extracted by lysing cells with addition of a cell resuspension solution (#E3030, NEB) and incubating for 10 minutes at 37 ˚C. Then adding a stop solution and incubating at RT for 5 minutes before cell lysates were stored at -80 ˚C for further use. Alternatively RNA was extracted using the RNAeasy Plus Mini Kit™ (#74143, Qiagen) according to manufacturer's instructions. Complementary DNA (cDNA) was synthesised from cell lysates containing RNA using the LunaScript® RT Supermix kit (#E3010, NEB) following the manufacturer's instructions after using cell resuspension solution. Alternatively RNA samples were directly quantified by Nanodrop and 800 ng RNA per sample was reverse transcribed using the Quantitect kit (#205311, Qiagen) following manufacturer's instructions after using the RNAeasy plus mini kit.

2.3.7 Reverse transcription PCR and reverse transcription quantitative PCR

To visualise changes in mRNA expression, 1 ng template cDNA was used in a PCR reaction with the relevant forward and reverse primers. The *OneTaq*® Quick-Load 2x master mix with

standard buffer (#M0486, NewEngland Biolabs) was used in a 25 µL PCR reaction according to section 2.2.5 before being resolved on an agarose gel as described in section 2.2.6.

To quantify mRNA expression cDNA produced using the method in section 2.3.6 was used as a template in a quantitative PCR (qPCR) reaction. qPCR reactions were prepared using 25 ng cDNA template, 2x qPCRBIO SyGreen Blue Mix Hi-ROX kit (#PB20.16-05, PCRBiosystems), and relevant primer sets for target genes (final concentration 400 nM). qPCR reactions were performed according to the manufacturer's instructions, on a regularly calibrated StepOnePlus instrument (Applied Biosystems). For relative quantification of SYBRgreen assays, the relative standard curve method was used. Known total amounts of RNA in control samples were used to calculate relative expression of target genes and an endogenous control, β-actin. Target primers used in both the reverse transcription (RT)-PCR and RT-qPCR assays are listed in Table 2.6.

Table 2.6 Primers for relative RT-qPCR analysis of cDNA targets.

Primer ID	Target gene	Primer	Annealing (˚C)	Efficiency (%)
42 β-actin Fwd RT	β-actin	GACAGGATGCAGAAGGAGATTACT	54	73.0
43 β-actin Rev RT		TGATCCACATCTGCTGGAAGGT	54	73.0
44 LDHA Fwd RT 2	LDHA	GACGTGCATTCCCGATTCC	52	73.0
45 LDHA Rev RT 2		TTCGATGACATCAACAAGAGCAA	52	73.0
46 LDHB Fwd RT 2	LDHB	GCTCAGCGGAGAGACTTGTT	53	N/A
47 LDHB Rev RT 2		TCAGCCAGAGACTTTCCCA	53	N/A
48 MCT4 Fwd RT 2	MCT4	CCTTCGGGAGGCAAACTC	52	102
49 MCT4 Rev RT 2		GCTCTTTGGGCTTCTTCCTAAT	52	102

2.4 Flow cytometry

2.4.1 Harvesting cells

To assess the activation of T cells, surface marker expression was measured by flow cytometry. T cells were harvested at 24 hours after their addition to target cells. Culture medium containing T cells was pooled and placed into 96V bottom plates (#M9686, Greiner CELLSTAR) and centrifuged (450 x g, 5 mins). Resulting supernatant was either transferred to a 96F bottom plate, covered with a seal (#15036, ThermoFisher Scientific) and stored at -20 ˚C until further analysis (LDH release assay, section 2.6.1) or discarded. The culture plate containing the adherent target cells was washed with 1x DPBS to remove any remaining T cells, and this wash solution was then used to wash the pellet formed in the 96V plates before a further centrifugation step.

If adherent cells were to be analysed for surface expression markers, they were detached at this stage using 100 µL enzyme-free dissociation buffer (#13151014, Gibco) and left for 10 minutes at 37 ˚C to allow the cells to lift. Cells were washed with 1x DPBS and collected with T cells, if in a co-culture, in the 96V plate before continuing to a further centrifugation step.

2.4.2 Cell surface staining

For consistency during staining protocols, total cell pellets were blocked by resuspending them in FcR blocking reagent (#130-059-901, Miltenyi Biotec) diluted 1/100 in MACs buffer (recipe in Table 7.2, in Appendix I) for 10 minutes at RT. During the blocking step, a well of cells to be analysed was taken out to be used as a Live/Dead positive control. Half of this cell suspension was heated at 95 ˚C for 5 minutes and then cooled for a further 5 minutes at 37 ˚C before being added back to the well, creating a 1:1 ratio of live and dead cells. The whole

blocked plate was then centrifuged (450 x g, 5 mins). Cells were then stained with a 1:5000 dilution of LIVE/DEAD™ Fixable Near-IR dead cell stain (#L10119, ThermoFisher Scientific) or with a 1:100 dilution of Viobility™ 488/520 Fixable dye (#130-110-207, Miltenyi Biotec) to determine viability, and stained for surface markers using fluorophore-conjugated antibodies at the dilutions indicated in Table 2.7. Antibodies and viability stains were diluted in MACs buffer (50 µL/well), and incubated with resuspended cells for 15 minutes at RT whilst the plate was in constant motion on a shaking platform protected from light.

To measure active apoptosis of cells, CellEvent™ Caspase 3/7 Detection Reagent (#C10423, Invitrogen) was used according to the manufacturer's instructions at a final concentration of 5 µM. CellEvent dye was added alongside Live/Dead stains as above and staining was continued as normal.

Following staining, cells were washed twice with 1x DPBS, and fixed for 15 minutes at RT by resuspending in 4% paraformaldehyde (100 µL/well) (#420801, BioLegend). Fixed cells were washed once with 1x DPBS and resuspended in 200 µL MACS buffer/well. Plates were stored protected from light at 4 ˚C for a maximum of 24 hours until required for data acquisition or intracellular staining.

2.4.3 Intracellular staining

Following surface staining as described in section 2.4.2, fixed cells stored in MACS buffer were centrifuged (450 x g, 5 mins), then resuspended in 150 µL intracellular staining permeabilisation wash buffer (Perm/Wash; #421002, BioLegend) diluted 1/10 in dH_2O. Cells were then resuspended again in 150 µL Perm/Wash buffer/well and centrifuged (450 x g, 5 mins). Following permeabilisation, cells were stained for intracellular markers by incubating with fluorophore-conjugated antibodies diluted in MACS buffer (50µL/well), a list of which is in Table 2.7. Cells were incubated with antibodies for 15 minutes at RT whilst the plate was in

constant motion on a shaking platform protected from light. Before being washed twice with 1x DPBS and resuspended in 200 µL MACs buffer/well. Plates were protected from light and stored at 4 ˚C. Data was acquired within two hours of this staining protocol.

Table 2.7 Antibodies and their dilutions used in flow cytometry analysis.

Antibody target	Clone	Isotype	Fluorophore (s)	Dilution	Company	Catalogue number (s)
CD3	OKT3	Ms, IgG2a, κ	APC, Pacific Blue	1:200	BioLegend	#300312, #300418
CD4	OKT4	Ms, IgG2b, κ	APC, FITC, PE	1:200	BioLegend	#317416, #317408, #317410
CD8a	HIT8a	Ms, IgG1, κ	APC	1:200	BioLegend	#300912
CD25	BC96	Ms, IgG1, κ	FITC, PE	1:200	BioLegend	#302604, #302606
CD69	FN50	Ms, IgG1, κ	FITC	1:200	BioLegend	#310904
GrB	GB11	Ms, IgG1, κ	Pacific Blue	1:100	BioLegend	#515408
IFNγ	4SB3	Ms, IgG1, κ	FITC	1:100	BioLegend	#502506
EGFR	9C4	Ms, IgG2b, κ	PE	1:200	BioLegend	#324206
CD107α	H4A3	Ms, IgG1, κ	PE	1:100	BioLegend	#328608
αHis-Tag	J095G46	Ms, IgG2a, κ	PE	1:100	BioLegend	#362603
Species	**Clone**	**Isotype**	**Fluorophore (s)**	**Dilution**	**Company**	**Catalogue number (s)**
Mouse (Ms)	IgG1, κ	MOPC-21	APC, FITC, Pacific Blue, PE	As above	BioLegend	#400120, #400108, #400151, #981804
Mouse	IgG2b, κ	MPC-11	APC, FITC, PE	As above	BioLegend	#400322, #400310, #400314

2.4.4 Absolute cell counts

To acquire absolute cell numbers, Precision Count Beads™ (#424902, BioLegend) were added to MACs buffer to reach a final concentration of 5000 beads in 200 µL buffer/well. Precision Count Beads™ are fluorescent particles and can be identified across a broad range of wavelengths on a flow cytometer. Comparison of the bead count and cell count is used to determine absolute cell numbers as shown below;

$$\%\ of\ volume\ passed\ through\ cytometer = \frac{bead\ count}{5000} * 100$$

$$Absolute\ cell\ number = \frac{cell\ count}{\%\ of\ volume\ passed\ through\ cytometer} * 100$$

2.4.5 Assessment of BiTE binding

To measure BiTE binding to the relevant cell type, a flow cytometry-based binding assay was used. Unstained cells were compared to cells stained with an Ab against a histidine (His)-Tag conjugated to R-phycoerythrin (R-PE; His-Tag-PE). αHis-Tag-PE will not bind unless a protein that has more than six His in a row is present on the cell's surface. When a BiTE (tagged with a 10 x His tail) is cultured with cells, it binds to the cell surface and thus provides an epitope on the cell's surface to which the αHis-Tag antibody can now bind, the mechanism for this assay is shown in Figure 2.1.

Target tumour cells or $CD3^+$ T cells extracted from lymphocytes were harvested as in section 2.4.1 but directly from culture flasks. Cell counts were set to 1 x 10^6/mL for effector cells and 2.5 x 10^5/mL for target cells. Cells were suspended in a 96V plate at 150 µL/well then centrifuged (450 x g, 5 mins). The pellets were resuspended in 100 µL relevant medium in three groups; unstained, stained without BiTE and stained with BiTE. BiTE was then added to the specified group of cell pellets in 50 µL relevant medium (1:3000 dilution) and cells were incubated for 1 hour unless otherwise specified at 4 ˚C. Plates were centrifuged (450 x g, 5 mins) then cell pellets were stained in 50 µL MACs buffer/well containing Viobility 488/520 Fixable dye only (unstained) or containing the αHis-Tag-PE antibody (Table 2.7) and Viobility 488/520 Fixable dye (stained without BiTE and stained with BiTE). Cells were stained for 15 minutes at RT before being topped with 1x DPBS and centrifuged (450 x g, 5 mins) then

resuspended in 200 µL MACs buffer/well. Plates were stored protected from light at 4 ˚C for a maximum of 24 hours until required for data acquisition.

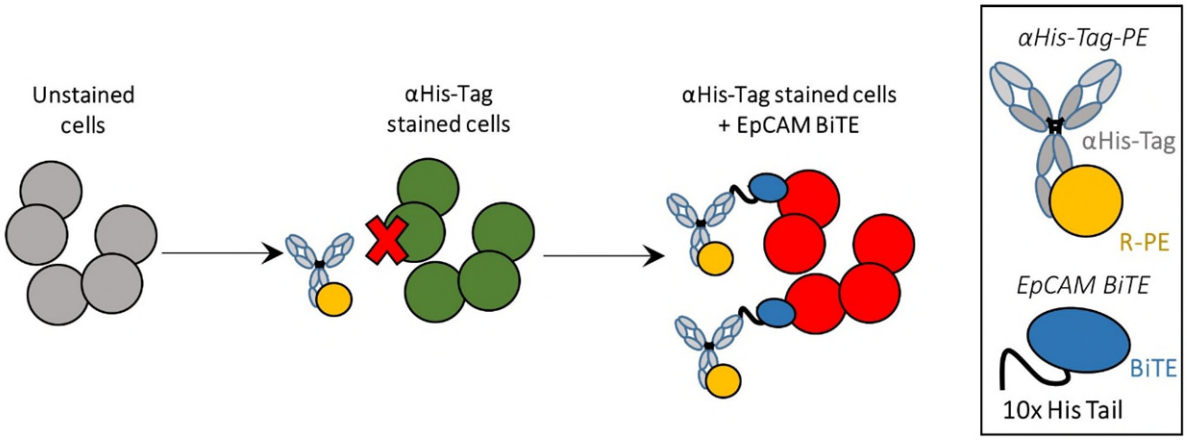


Figure 2.1 The principles behind the analysis of EpCAM BiTE binding to EpCAM-expressing target cells or CD3⁺ T cells. A schematic of the assay used to assess binding of the EpCAM BiTE to single cells, the BiTE's His-Tag tail is then used to identify those cells using a αHis-Tag Ab conjugated to a fluorophore, R-PE, which will be detected by flow cytometry.

2.4.6 Data acquisition and analysis

To acquire data for flow cytometry, an Attune™ NxT Flow Cytometer (ThermoFisher Scientific) was used to detect fluorescence during single cell flow. For each sample, at least 10,000 events were acquired at a flow rate of no more than 500 µL/min, and data was analysed using FlowJo™ v10.7 software (BD Biosciences). An example of a typical gating strategy for data processing is shown in Figure 2.2, including the identification of fluorescent beads. For all experiments only single cell populations were considered using a doublet discrimination strategy, followed by selection for live cells using viability stains.

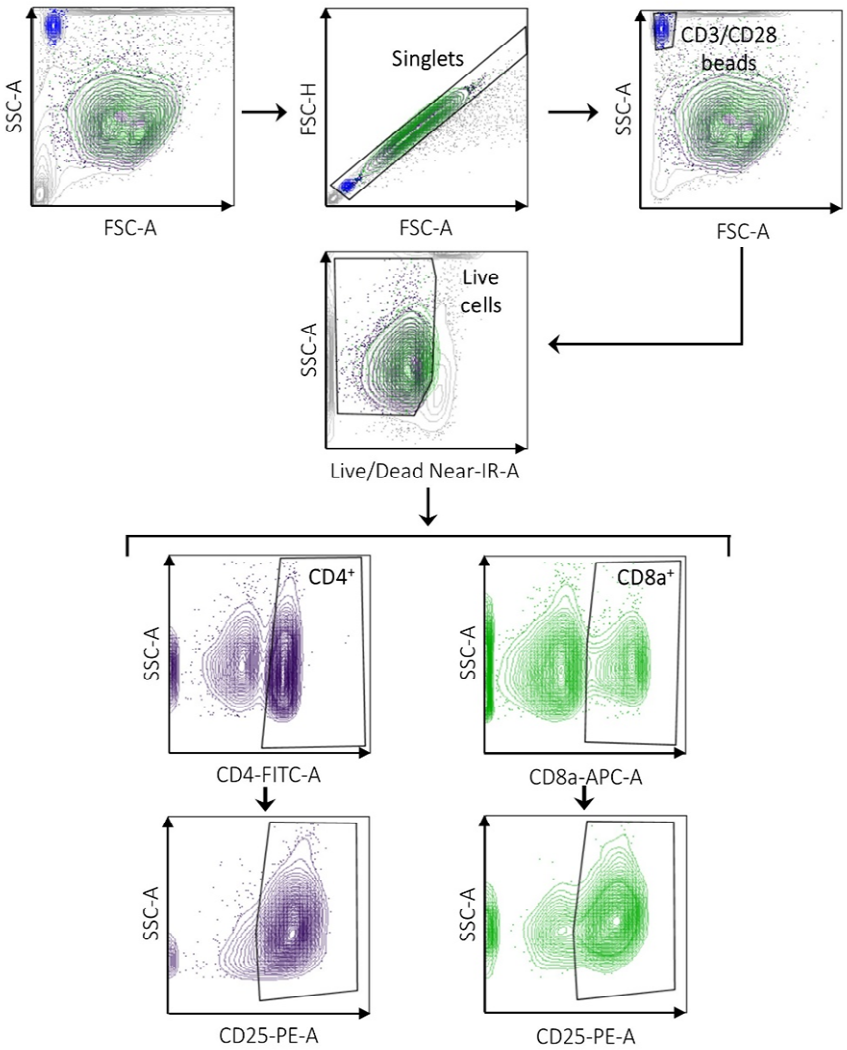


Figure 2.2 An example of a gating strategy used for flow cytometric analysis of T cell activation.. $CD3^+$ T cells were co-cultured with SKOV-3 cells and CD3/CD28 beads for 24 hours. T cells were harvested and stained with a LIVE/DEAD Near-IR stain alongside, anti-CD4 (FITC), anti-CD8a (APC) and anti-CD25 (PE) antibodies. Data was acquired with an Attune NxT flow cytometer then processed with FlowJo software. Doublet discrimination was first performed by plotting FSC-area (A) against FSC-height (H) (top middle panel), then CD3/CD28 beads were excluded when used (top right panel), and live cells were identified (centre panel). Within the live gate, CD4- and CD8- positive cells were selected (second from bottom left and right panels respectively) and analysed for expression of CD25 (bottom left and right panels).

2.5 Immune cell assays

2.5.1 General statement

Leukocyte cones and buffy coat residue bags used throughout this thesis were acquired from the NHS Blood and Transplant Service (NHSBT; Oxford, UK). Informed consent was obtained at the time of donation by the NHSBT. Ethical approval for the study was obtained from the Health Research Authority (REC reference 19/LO/1848; IRAS ID 253836).

2.5.2 Isolation of lymphocytes from human peripheral blood

Lymphocytes were obtained by double-density gradient centrifugation from whole blood leukocytes cones obtained from the NHSBT. Leukocyte cones contained a small volume of packed leukocytes from platelet donation by apheresis.

First, peripheral blood mononuclear cells (PBMCs) were isolated by diluting the 10 mL of blood from the leukocyte cone in 130 mL 1x DPBS. 35 mL of diluted blood was then carefully overlaid onto 4 x 50 mL falcon tubes each containing 15 mL Ficoll® Paque Plus (#GE17-1440-02, GE Healthcare) and centrifuged (settings in step 1 in Table 2.8). Four layers can be observed after centrifugation as seen in Figure 2.3A; from top to bottom, plasma, a PBMC interphase,

Table 2.8 Density gradient centrifugation and wash steps to isolate lymphocytes from human peripheral blood.

Step	Speed (x g)	Time (mins)	Acceleration	Deceleration
1	950	30	Half maximal	Off
2	950	10	Maximal	Half maximal
3	450	10	Maximal	Maximal
4	200	10	Maximal	Maximal

Ficoll and a granulocyte and red blood cell (RBC) pellet. The PBMC layer was collected and washed 3x in 1x DPBS according to steps 2-4 in Table 2.8.

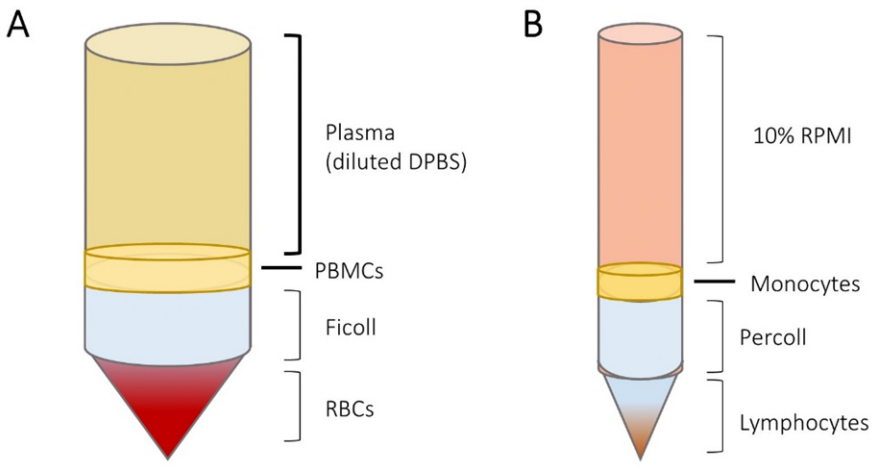


Figure 2.3 Ficoll and Percoll double-density gradient centrifugation to isolate lymphocytes from human peripheral blood. (A) The resultant layering of 1x DPBS diluted blood following separation with Ficoll. PBMCs are enriched in the interphase between the Ficoll layer and plasma while the red blood cells (RBCs) and granulocytes are pelleted. **(B)** Diluted PBMCs in 10% RPMI are separated further following centrifugation with 46% Percoll. Lymphocytes are pelleted while monocytes are at the interphase between the Percoll layer and RPMI.

Washed PBMCs were resuspended in 20 mL RPMI 1640 containing 10% FBS (10% RPMI), 5 mL of the suspension was overlaid onto 4 x 15 mL falcon tubes each containing 6 mL of a Percoll® PLUS solution (46%, 285 mOsm; #GE17-5445-01, GE Healthcare) and centrifuged as in step 1 of Table 2.8. Four layers can be observed after centrifugation as seen in Figure 2.3B; from top to bottom, 10% RPMI, a monocyte interphase, Percoll and a lymphocyte pellet. Both the monocyte interphase and lymphocyte fractions were collected separately and washed as before with 1x DPBS according to steps 2-4 in Table 2.8. Lymphocytes were cryopreserved and stored at -80 ˚C until needed (20 x 10^6 cells/mL freezing medium) unless otherwise specified.

2.5.3 CD3-positive T cell extraction

Lymphocytes were thawed and incubated to rest in 10% RPMI for at least 12 hours at 37 ˚C, 5% CO_2 at a concentration of 5 x 10^6 cells/mL. $CD3^+$ cells were directly separated using the Pan T cell isolation kit (#130-096-535, Miltenyi Biotec) following manufacturer's instructions. In this process non-T cells are magnetically labelled with biotinylated antibodies and then bound by anti-biotin microbeads. Bound cells are retained in an LS column when using a MACS® magnetic separator whilst the $CD3^+$ T cells pass through and can be collected.

2.5.4 Co-culture experiments of T cells and target cells

All experiments requiring co-culture of T cells and target tumour cells were performed as described below unless otherwise stated. Target cells were seeded in flat bottom 96-well plates in 150 µL of 10% RPMI at a concentration suitable for the experiment and tumour cell line chosen. Lymphocytes derived from a leukocyte cone were thawed and allowed to rest on the same day as target cells were seeded. $CD3^+$ T cells were extracted 24 hours later and seeded at an effector T cell: target cell (E:T) ratio of 5:1 alongside the adherent target cells in 2% RPMI. Any activating or inhibitory treatments of T cells to be tested were added at this stage alongside T cells at the relevant concentration in a final volume of 150 µL. Human T-activator CD3/CD28 beads (Dynabeads™; #11131D, Gibco) were added at 2 µL/well as a positive control for T cell activation. If the EpCAM BiTE was used in a co-culture for activation supernatant of BiTEs were added at a 1 in 3000 dilution, equivalent to a concentration of 1.52 ng/mL. If virus infection was required for T cell activation, target cells were seeded 24 hours prior to infection with 100 vp/cell of virus in 30 µL 2% RPMI. The infection was left for 2 hours before T cells were added at an E:T ratio of 5:1 in a final volume of 150 µL medium. Plates were incubated at 37 ˚C, 5% CO_2 for specified timepoints before non-adherent cells and/or adherent cells were harvested to be analysed depending on the experiment.

In studies investigating starvation in amino acid-absent medium, lymphocytes were left as a whole fraction without extracting $CD3^+$ T cells as they survived better overnight in starved media. Lymphocytes were thawed in 10% RPMI then left overnight in 10% RPMI (acute starvation) or in culture medium prepared with amino acids missing (chronic starvation). A portion of lymphocytes were expected to die during starvation therefore effector cell numbers needed to be corrected when setting up co-culture experiments to a 5:1 E:T ratio. To do this, a portion of lymphocytes were taken from each starved condition and harvested, then stained for CD4 and CD8 surface markers and viability with a LIVE/DEAD Near-IR stain as in sections 2.4.1 and 2.4.2. Cell counts of lymphocytes were analysed by flow cytometry as in section 2.4.6. Lymphocytes from each condition were then added to target cells based on the cell counts of live and CD4-/CD8-positive T cells.

2.5.5 Characterisation of T cell activation

To assess activation of T cells, surface marker expression was measured by flow cytometry as described in section 2.4. T cells were harvested 24 hours after addition of T cells to target cells. Cells were stained for CD25 and/or CD69 as surface markers for activation.

2.5.6 Characterisation of T cell cytotoxicity

To measure T cell cytotoxicity, the expression of inflammatory cytokine, IFNγ and GrB were used (Wolf et al. 2005; Freedman et al. 2017). To stain for IFNγ, T cells and target cells were cultured for 1 hour in normal conditions (37 ˚C, 5% CO_2) before GolgiStop (Monensin, #554724, BD Biosciences) and GolgiPlug (Brefeldin A, #555029, BD Biosciences) were added according to the manufacturer's instructions to all wells. Cells were left for a further 5 hours before being harvested and intracellularly stained for flow cytometry as described in section 2.4.3. The GolgiStop and GolgiPlug reagents, which are added to stimulated T cells, cause the

blockage of their intracellular protein transport processes. Cytokines that would usually be secreted accumulate in the Golgi complex allowing for detection (Prussin and Metcalfe 1995).

To stain for GrB, T cells and target cells were cultured for 18 hours in normal conditions as described in section 2.5.4 before GolgiStop and GolgiPlug were added according to the manufacturer's instructions to all wells. Cells were then left for 5 hours before being harvested and intracellularly stained as described in section 2.4.3.

2.5.7 Characterisation of T cell degranulation

To assess degranulation of T cells, cell surface CD107α was quantified using flow cytometry. T cells and target cells were cultured and stimulated in the presence of the CD107α fluorophore-conjugated antibody. Cells were left for 1 hour in normal culture conditions before GolgiStop and GolgiPlug were added according to the manufacturer's instructions. In this context the GolgiStop and GolgiPlug reagents inhibit the shuttling of CD107α between the cell surface and its intracellular compartments. Cells were incubated for a further 5 hours before being harvested and surface stained for flow cytometry as in section 2.4.

2.5.8 Expansion of a ST8.24 $CD8^+$ T cell clone

The ST8.24 $CD8^+$ T cell clone ($CD8^+$ T cell clone) and protocols describing how to expand the clone were kindly provided by Dr. Garry Dolton (Sewell Lab, School of Medicine, Cardiff University, UK). Details on how the lab created their library of T cell clones including their detection and isolation has been published (Theaker et al. 2016).

To expand the $CD8^+$ T cell clone for experimental use, cells were defrosted in the same way as tumour cell lines, as described in section 2.1.2 and incubated at a density of 2.0×10^6 cells/well in 1 mL T cell media (recipe in Table 7.2 in Appendix I) overnight at 37 ˚C. Subsequently, the

$CD8^+$ T cell clones were removed by lightly scraping the bottom of the plate and washing with 10% RPMI supplemented with 1% penicillin – streptomycin (1% P/S; #15140122, Gibco) and 2 mM L-glutamine. Cells were counted and then centrifuged (350 x g, 5 mins) and resuspended in 14 mL T cell media supplemented with 20 IU/mL human IL-2 IS, research grade (#130-097-743, Miltenyi Biotec) and 25 ng/mL human IL-15, research grade (#130-095-760, Miltenyi Biotec) at a density of 4.0 x 10^5 cells/14 mL.

To provide the $CD8^+$ T cell clone with feeder cells, PBMCs from three donors were prepared and irradiated. PBMCs were obtained from different donors, using a buffy coat residue bag purchased from the NHSBT. These bags contain the residue of buffy coats left over from four different donations following platelet pooling. Density gradient centrifugation was employed to isolate PBMCs as described in section 2.5.2 with Ficoll Paque Plus. Washed PBMCs were counted as in section 2.1.3 before their final centrifugation (step 4 in Table 2.8) and following centrifugation, PBMCs were resuspended at a density of 15 x 10^6 cells/mL in 10% RPMI. 10 mL of this suspension was placed into a T75 flask and irradiated at 3 Gy using a caesium-137 irradiator then left on ice (irradiated PBMCs now are feeder cells). All irradiation was performed by Dr. Tzveta Pokrovska (Seymour Lab, Department of Oncology, University of Oxford, UK). Feeder cells were centrifuged (400 x g, 5 mins) then resuspended in 10 mL T cell media supplemented with 20 IU/mL IL-2 and 25 ng/mL IL-15. A 1 mL aliquot of the feeder suspension was taken per T25 flask, containing prepared $CD8^+$ T cell clone to be fed. Phytohaemagglutinin (PHA; #11 249 738 001, Sigma Aldrich) was added to each aliquot of feeder suspension at a concentration of 15 μg/mL. The feeder:PHA mix was then added to a T25 flask containing the $CD8^+$ T cell clone. T25 flasks were left to incubate for eight days in an upright position at a 45˚ angle as shown in Figure 2.4. On the fifth day of incubation, 50% of the media was removed from the T25 flask, taking care not to disrupt the cell pellet which

had formed, and was replaced with the same volume of fresh T cell media supplemented as above.

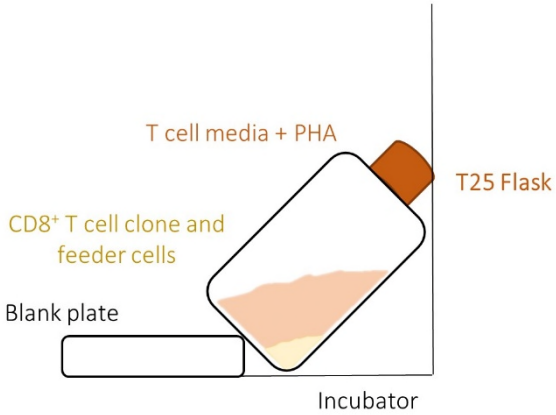


Figure 2.4 T25 flasks containing ST8.24 CD8$^+$ T cell clone with feeder cells and PHA must be kept at a 45˚ angle. T25 flasks are stored at an angle in an upright position against a spare plate in a 37 ˚C, 5% CO_2 incubator for eight days of culture from the point of feeding with irradiated PBMCs.

Following incubation, CD8$^+$ T cell clones were collected and counted using trypan blue exclusion as described in section 2.1.3 (assuming feeder cells would appear blue). Cells were washed in 10% RPMI and then resuspended in T cell media now supplemented with 200 IU/mL IL-2 and 25 ng/mL IL-15 at a density of 4.0 x 10^6 cell/well in 2 mL medium in a 24-well plate. CD8$^+$ T cell clones were then incubated in this state for two weeks in a tissue culture incubator, changing 50% of the media for fresh T cell media supplemented with 200 IU/mL IL-2 and 25 ng/mL IL-15 every 3 days. Following two weeks of incubation, CD8$^+$ T cell clones were ready to be frozen and stored as in section 2.1.2 for future expansion or used in an experiment.

2.5.9 ST8.24 CD8$^+$ T cell clone co-culture with target cells

All experiments requiring co-culture of CD8$^+$ T cell clone and target tumour cells were performed as described below unless otherwise stated. The ST8.24 CD8$^+$ human T cell clone expanded in this thesis has been shown to be cross-reactive and able to recognise multiple tumour-associated peptides. The clone was isolated from TILs from a (HLA)-A*0201$^+$ (HLA-

$A2^+$) melanoma patient donor and has been shown to recognise and kill HLA-$A2^+$ tumour cell lines including Colo205 and HCT116 (Bianchi 2016; Galloway et al. 2019).

Target cells were seeded in flat bottom 96-well plates in 150 µL 10% RPMI at a density of 1.5 x 10^4 cells/well. Target cells were left for 24 hours before addition of the $CD8^+$ T cell clone (+/- 1.56 ng/mL EpCAM BiTE or control BiTE) at an E:T ratio of 5:1 unless otherwise specified. Cultures were performed in 2% RPMI unless otherwise specified and incubated for 72 hours in a humidified incubator at 37 ˚C. Target cells were then analysed for signs of cytotoxicity using the methods set out below in sections 2.6.3 and 2.6.4.

In studies investigating starvation in amino acid absent medium, aliquots of the $CD8^+$ T cell clone were left overnight in 10% RPMI (acute starvation) or in 2% (dialysed FBS) culture medium prepared with amino acids missing (chronic starvation). A portion of the $CD8^+$ T cell clone was expected to die during starvation therefore effector cell numbers needed to be corrected to reach a 5:1 ratio. To do this an aliquot of the $CD8^+$ T cell clone was taken for each condition and harvested, then stained for the CD8 surface marker and for viability as in sections 2.4.1 and 2.4.2. Counts were quantified by flow cytometry as in section 2.4.6 then added to target cells based on the live, CD8-positive T cells.

2.6 Target cell cytotoxicity assays

2.6.1 Lactate dehydrogenase release assay

LDH is released from the cytosol of cells upon cell lysis, and therefore its accumulation in the supernatant can be used to quantify levels of cell lysis. To measure LDH in the supernatant, a CytoTox96® Non-Radioactive Cytotoxicity Assay kit (#G1780, Promega) was used according to the manufacturer's instructions. This kit includes a reagent containing tetrazolium salt that is

converted into a red formazan product in an enzymatic reaction coupled with LDH, resulting in the conversion of lactate to pyruvate. Target cells were seeded at a density of 2.0 x 10^4 and incubated for 24 hours before the addition of the relevant effector (activated T cells or virus). After the specified time in culture, 50 µL supernatant from each well was collected and cleared of any floating cells by centrifugation, supernatants were then transferred to a 96F plate. Supernatants were tested immediately or stored at -20 ˚C for future use. In brief, 50 µL assay reagent was added to each well and plates incubated for 30 minutes at RT protected from light. To stop the reaction, 50 µL Stop solution was added and the absorbance measured at 490 nm using a Wallac 1420 Victor^2 plate reader (Perkin Elmer).

LDH release was reported as either absorbance or cytotoxicity. Percentage cytotoxicity was calculated using the following formula:

$$\%\ cytotoxicity = \frac{Experimental - effector\ spontaneous - target\ spontaneous}{Target\ maximum - target\ spontaneous}\ x\ 100$$

2.6.2 MTS cell proliferation assay

MTS is a tetrazolium compound that is bioreduced by viable cells into a coloured formazan product that can be measured. To measure cell viability, the CellTiter 96® AQ_{ueous} One Solution Cell Proliferation Assay (MTS) kit (#G3582, Promega) was used according to the manufacturer's instructions. The kit's reagent contains MTS (3-(4,5-dimethylthiazol-2-yl)-5-(3-carboxymethoxyphenyl)-2-(4-sulfophenyl)-2H-tetrazolium, inner salt) and an electron coupling agent (phenazine ethosulphate; PES). Target cells were seeded at a density of 2.0 x 10^4 and incubated for 24 hours before the addition of the effector (activated T cells or virus). After a specified time in culture, supernatant was removed from wells, wells were washed with 150 µL 1x DPBS, and 100 µL of MTS reagent at working concentration (5-fold dilution in 1x DPBS) was added to each well. Plates were incubated at 37 ˚C in a humidified incubator for 1

– 4 hours and the absorbance was measured at 490 nm using a Wallac 1420 Victor^2 plate reader (Perkin Elmer).

2.6.3 PrestoBlue cell viability assay

PrestoBlue® is a cell permeable resazurin-based solution. PrestoBlue can be used to assess cell viability due to the reducing power of viable cells that modify the assay reagent causing it to become fluorescent. This fluorescence can then be quantified as a measure of cell viability. Resazurin undergoes colorimetric changes in response to oxidation-reduction (REDOX) reactions. Resazurin is a weakly fluorescent blue, however upon its reduction to resorufin it becomes pink and highly fluorescent, and the intensity of this product is proportional to the number of cells undergoing respiration. To measure cell viability, the PrestoBlue Cell Viability reagent (#A13261, Invitrogen) was used according to the manufacturer's instructions. Target cells were seeded at a density of 2.0 x 10^4 cells/well and incubated for 24 hours before the addition of the effector (activated T cells or virus). After a specified time in culture, medium was removed from wells to remove the effector cells. Wells were washed twice with 150 µL of 1x DPBS. PrestoBlue reagent was diluted 1/10 in 1x DPBS and 100 µL was added to each well. Plates were incubated at 37 ˚C in a humidified incubator for 1 – 6 hours depending on target cell type and fluorescence was measured at 544/590 nm (excitation/emission) using a POLARstar® Omega (BMG LabTech).

2.6.4 EGFR$^+$ count viability assay using flow cytometry

Another approach to assess cell viability following treatments is to count the number of residual target cells remaining. Target cells were harvested as described in section 2.4.1 and stained as described in section 2.4.2 for the surface marker epidermal growth factor receptor (EGFR$^+$) and with the LIVE/DEAD™ Fixable Near-IR dead cell stain kit (#L10119, ThermoFisher

Scientific). Absolute cell numbers were quantified as described in sections 2.4.4 and 2.4.6. EGFR is a transmembrane protein present on the surface of normal cells and cancer cells and can be used to track cancer cells during single cell analysis and distinguish them from T cells and feeder cells that don't express any or as much EGFR. In T cell (clone or isolated $CD3^+$ T cells) co-culture experiments, target cell cytotoxicity was assessed after 72 hours unless otherwise specified, and in virus infection studies cytotoxicity was assessed at a timepoint dependent on the infected cell line which is specified for each experiment.

2.6.5 Cell adhesion with the xCELLigence Real-Time Cell Analysis system

Target cell viability can be monitored in real-time using xCELLigence Real-Time Cell Analysis (RTCA) technology (ACEA Biosciences Inc.). This system uses specialised E-plates (ACEA Biosciences Inc.) with microelectrodes embedded at the base of each well. In the presence of conductive solutions, an electric potential is placed across the electrodes which causes electrons to pass from the negative terminal, through the bulk solution and deposit to a positive terminal to complete a circuit. If adherent cells are bound to the bottom of the well, and therefore present at the electrode-solution interface, the electron flow between electrodes is impeded. The magnitude of electrical impedance is therefore correlated to cell adherence and morphology, and can be used to calculate a cell index value which relates to cell viability.

xCELLigence assays were performed according to the manufacturer's instructions albeit with slight variations. Sealed E-plates were incubated at 37 ˚C in a humidified incubator, along with 1x DPBS and 2% RPMI for 1 hour to equilibrate their temperature. Target cells were seeded in the E-plates at 1.5 x 10^4 target cells/well in 150 µL warmed 2% RPMI medium, whilst the spaces between wells were filled with warm 1x DPBS to minimize loss of well media through evaporation. E-plates were incubated for 20 hours to allow cells to adhere before medium was aspirated. Culture medium was replaced with control medium or experimental media containing

virus particles or T cells and their relevant activator. If both virus infections and T cell co-cultures were required, target cells were infected in 100 μL medium containing virus particles for two hours before isolated $CD3^+$ T cells were added to wells in 50 μL medium. Cell index values were measured every 15 minutes for the duration of the experiment.

2.7 Ex vivo experiments with malignant clinical samples

2.7.1 General statement

Ascites samples used in chapter 3 of this thesis were acquired with informed consent from cancer patients at the Churchill Hospital, Oxford, UK using a routine therapeutic paracentesis procedure. Ethical approval for the study was gained from the institutional review board and research ethics committee of the Oxford Centre for Histopathology Research (Reference 09/H0606/5+5) in accordance with the UK Human Tissue Act 2004 and Declaration of Helsinki.

2.7.2 Processing patient-derived peritoneal ascites fluids

Using aseptic techniques ascites fluids were collected into 50 mL falcon tubes and centrifuged (400 x g, 10 mins) at RT to separate the fluid components from the cellular fraction. The fluid component was centrifuged for a second time (400 x g, 10 mins) before being stored at -20 ˚C until required.

2.7.3 Amino acid level determination by HPLC

To determine amino acid levels in ascites fluids, they were first thawed for 1 hour at 37 ˚C in a humidified incubator. Fluids were then poured through sterile 70 μm cell strainers (#CLS431751-50EA, Corning) to remove any remaining cellular components. Next, the protein

component of the fluids was removed using Amicon Ultra-0.5 mL 3.0 kDa MWCO centrifugal filter units (#UFC500396, Merck). Filter units were filled with 400 µL of ascites fluid and centrifuged (13,400 x g, 30 mins) at RT, if serum or other protein containing fluids were to be used as controls these were also filtered in the same way as the ascites fluids. Filtered fluids were then subjected to HPLC analysis alongside RPMI 1640 medium (containing no serum) acting as a control for amino acid concentrations, as well as Amino Acid Standards (#AAS18-10X1ML, Sigma Aldrich).

HPLC analysis was performed following a method developed by Agilent (Henderson and Brooks 2010). The method uses ortho-phthalaldehyde reagent (OPA; #5061-3335, Agilent) and 9-fluorenyl-methyl chloroformate reagent (FMOC; #5061-3337, Agilent) to derivatise amino acids. The pre-column derivatisation is shown in Table 2.9. Separation was achieved using an Agilent ZORBAX Eclipse Plus C18 stationary phase column, 4.6 x 250 mm, 5 µm (#95999-902, Agilent) at 40 ˚C. An Agilent 1100 HPLC system (Agilent Technologies) controlled using ChemStation software (Agilent) and equipped with a photodiode array (PDA) detector. Amino acids were detected at 338 nm, 10 nm bandwidth and 262 nm, 16 nm bandwidth. Recipes for buffers used; Mobile phase A, Mobile Phase B and injection diluent are detailed in Table 7.2 in Appendix I and borate buffer was supplied (#5061-3339, Agilent). The flow rate was set to 1.5 mL/min and the gradient used is shown in Table 2.10. HPLC was performed in collaboration with Dr. Brian Lyons (postdoctoral researcher, Department of Oncology, University of Oxford).

Table 2.9 Steps for derivatisation of amino acids prior to running through an Agilent ZORBAX Eclipse Plus C18 column. Steps were taken directly from the Agilent devised programme (Henderson and Brooks 2010).

Step	Action/Setting
1	Draw 2.5 µL from borate vial
2	Draw 1.0 µL from sample vial
3	Mix 3.5 µL in air, default speed x5
4	Wait 0.2 min
5	Draw 0.5 µL from OPA vial
6	Mix 4.0 µL in air, default speed x10
7	Draw 0.4 µL from FMOC vial
8	Mix 4.4 µL, default speed x10
9	Draw 32 µL from injection diluent vial
10	Mix 20 µL in air, default speed x8
11	Inject
12	Wait 0.1 min
13	Valve bypass

Table 2.10 High resolution gradient method for HPLC.

Time (min)	% Mobile Phase B
0	2
0.84	2
33.4	57
33.5	100
39.3	100
39.4	2
40	end

2.7.4 Ascites-based nutrient stress models

Ascites fluids were thawed as described in section 2.7.3 and ran through a 70 μm cell strainer before being placed in an Amicon Ultra-15 mL 3.0 kDa MWCO centrifugal filter unit (#UFC900324, Merck). Filtered fluids were mixed with amino acid-free RPMI 1640 (#RPL22) at a 1:1 ratio. As controls, RPMI supplemented with 2% FBS (2% RPMI) was used as complete medium or it was mixed in a 1:1 solution with amino acid-free RPMI 1640 medium as above. These controls represent complete medium (with supra-physiological amino acid concentrations) and medium with half the concentration of amino acids (physiological).

For experiments involving T cell activation, target cells were seeded at a density of 1.5 x 10^4 cells/well 24 hours before the addition of T cells at a density of 7.5 x 10^4 cells/well (5:1). T cells were resuspended in the medium conditions described above either alone, with CD3/CD28 beads, or with EpCAM BiTE-containing supernatant (1.56 ng/mL). T cells and/or target cells were harvested as described in section 2.4.1 at the indicated timepoint for activation or cytotoxicity assessment.

For experiments regarding EnAd infection and cell lysis, target cells were seeded at a density of 2.5 x 10^4 cells/well in 96 well plates. For unstarved conditions, target cells were seeded in 2% RPMI; whilst for starved conditions, target cells were seeded in the ascites fluid medium conditions described above. Target cells were left for 24 hours before the addition of virus, unstarved plates had the medium removed and replaced with ascites fluid medium whilst the starved plates retained their medium. Cells were infected with 20 μL virus-containing medium (RPMI 1640 w/o amino acids). Cells were incubated until the indicated timepoint and then harvested as described in section 2.4.1.

2.8 Virology methods

2.8.1 Viral infections

Generally, infection dosages were performed based on seeding cell density of target cells unless otherwise stated, and in medium containing 2% FBS. The viruses used during this thesis are listed in Table 2.11. Inoculum volumes were calculated using the plaque assay titres (plaque forming units (PFU)/mL) for each virus stock and is described in experiments as the multiplicity of infection (MOI). The MOI is defined as the ratio of infectious viral particles to infection target, i.e. an MOI 10 would mean infecting each target cell with 10 infectious particles, or PFU.

Table 2.11 Virus stocks used throughout this thesis with their titres, tissue culture infectious doses and plaque forming units determined by dsDNA Picogreen assay, serial titration on A549 cells and by plaque assay respectively. vp, virus particle; FFU, focus-forming unit; PFU, plaque-forming unit. ** Virus stocks made and quantified by Dr Joshua Freedman, (Seymour laboratory, Department of Oncology, University of Oxford).

Virus	Promoter	Transgene	Picogreen (vp/mL)	TCID50 (FFU/mL)	Plaque assay (PFU/mL)
Enadenotucirev (EnAd)	N/A	N/A	1.79×10^{12}	N/A	9.50×10^{10}
EnAd-CMV-GFP	CMV	GFP	9.44×10^{11}	7.67×10^{10}	5.75×10^{10}
EnAd-SA-GFP	MLP-SA	GFP	$4.83x\ 10^{11}$	9.91×10^{09}	1.80×10^{10}
EnAd-SA-FLuc	MLP-SA	Firefly luciferase	2.50×10^{11}	5.03×10^{09}	1.08×10^{10}
EnAd-Scramble	CMV, U6	GFP, shScramble	N/A	N/A	1.25×10^{04}
EnAd-LDHA	CMV, U6	GFP, shLDHA (s350)	N/A	N/A	1.03×10^{06}
EnAd-LDHA	CMV, U6	GFP, shLDHA (s351)	N/A	N/A	1.38×10^{06}
EnAd-MCT4	CMV, U6	GFP, shMCT4 (s17416)	N/A	N/A	1.13×10^{07}
EnAd-LDHB	CMV, U6	GFP, shLDHB (s8125)	N/A	N/A	5.00×10^{03}
*EnAd-CMV-EpCAMBiTE	CMV	EpCAM BiTE	$1.00 \text{ X } 10^{12}$	$2.51 \text{ X } 10^{10}$	N/A
*EnAd-SA-EpCAMBiTE	MLP-SA	EpCAM BiTE	$1.22 \text{ X } 10^{12}$	$3.16 \text{ X } 10^{10}$	N/A

2.8.2 Adenovirus cloning

Transgene cassettes were engineered to encode GFP downstream of an exogenous cytomegalovirus (CMV) promoter alongside hairpins downstream of a U6 promoter. They were inserted into the parental EnAd plasmid backbone (pEnAd2.4) linearised with SbfI using Gibson assembly as described in section 2.2.9. The pEnAd2.4 backbone (Figure 2.5) containing the EnAd genome was kindly provided by PsiOxus Therapeutics Ltd. Transgenes were encoded downstream of the fiber gene. Insertion success was confirmed by restriction digest and Sanger sequencing as described in sections 2.2.4 and 2.2.10.

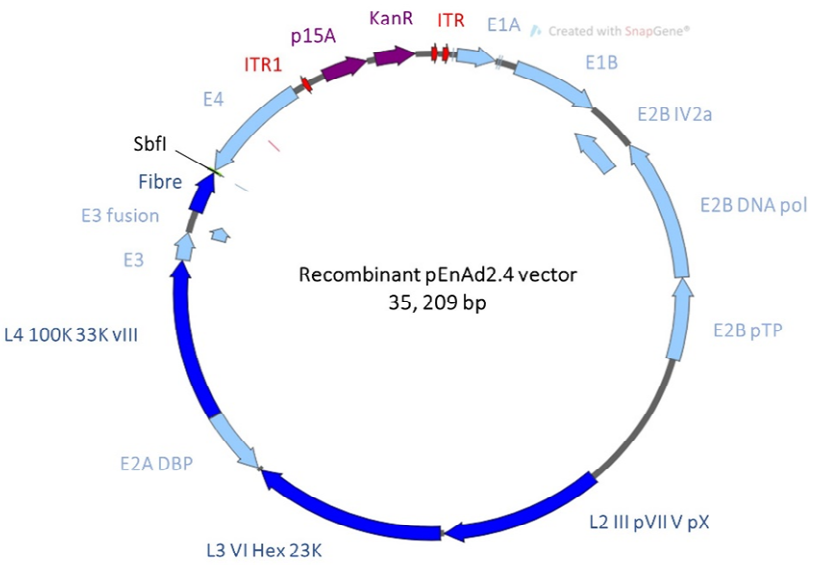


Figure 2.5 The plasmid map of pEnAd2.4 vector. The vector contains the EnAd genome and is used for engineering recombinant viruses. SbfI cleavage of the vector is used to insert transgene cassettes downstream of the fibre gene. All genes in the plasmid are necessary for plasmid propagation in bacteria and for production of the virus in 293Ad cells. ITR, inverted terminal repeat; E, early; L, late; Hex, hexon; p15A, origin of replication; KanR, kanamycin resistance. Plasmid map made using SnapGene.

2.8.3 Adenovirus rescue

Engineered pEnAd2.4 backbones were linearised by restriction digest as described in section 2.2.4 using restriction enzyme AscI (#R0558L, NEB). Linearisation was confirmed by running a small sample on a 0.8% agarose gel and the remainder was purified as described in section 2.2.3 using isopropanol precipitation.

To rescue modified EnAd virus, 1.0 x 10^6 293Ad cells were seeded into a T25 flask to reach 80% confluency 24 hours later. For each T25 flask, 5 μg linearised backbone was complexed with 20 μL Lipofectamine 2000 (#11668019, Invitrogen) and 293Ad cells were transfected as described in section 2.1.5. The transfected T25 flasks were incubated at 37 ˚C in a humidified incubator at 5% CO_2 and the cell monolayer was monitored over the course of 2 weeks for signs of the cytopathic effect (CPE). Once CPE was observed viruses were harvested from cells by the following procedure:

1. Cells and medium were collected
2. Three freeze-thaw cycles were carried out by alternating samples between liquid nitrogen and a 37 ˚C water bath incubation
3. Samples were centrifuged to separate cells from supernatant (450 x g, 15 mins)
4. The supernatant was then filtered by passing it through a 0.22 μm syringe filter (#GSWP04700, Merck Millipore)

Clarified supernatants were subsequently used for plaque purification.

2.8.4 Plaque purification

Two rounds of plaque purification were used to select for single virus clones. A549 cells were seeded to confluency in 6 well plates at a density of 1.0 x 10^6 cells/well 24 hours prior to infection. Clarified supernatants were 10-fold serially diluted and 400 μL of virus inoculum

was used to infect each well for two hours. Plates were incubated at 37 ˚C in a humidified chamber, rocking plates every 15 minutes.

Infection medium was then removed and monolayers overlaid with 2.5 mL of an agarose-DMEM mixture (recipe in Table 7.2 in Appendix I). Plates were incubated at RT for 40 minutes to allow the agarose to solidify before being moved to a 37 ˚C humidified incubator for seven days. One well was chosen for plaque selection, plaques were picked by scraping the monolayer of cells through the layer of agarose with a pipette tip and aspirating it into 5 mL of 2% RPMI. To amplify the virus from picked plaques, the 5 mL of infected medium was vortexed and applied to A549 cells in a T25 flask at 80% confluency. A549 cells were harvested upon extensive CPE.

Three plaques were picked and assessed for transgene expression as described in section 5.2.10. The virus plaque which showed the highest levels of transgene expression was selected for a second round of plaque purification in the same way as just described. After two iterations of plaque purification, cells and supernatants from the final T25 flask were harvested as described in section 2.8.3 and virus was titred by plaque assay for small scale studies.

2.8.5 Adenovirus propagation

To propagate higher concentration virus stocks large scale adenovirus particle production was performed using a Corning™ HYPERFlask® (#CLS10020, Corning). 293Ad cells were grown to 90% confluency in a T175 flask, they were then detached by trypsinisation and used to seed one HYPERFlask in 500 mL 10% DMEM with 1% P/S. After 72 hours, culture medium was removed and replaced with infection medium supplemented with 2% FBS and containing virus at a dose of 100 virus particles per cell, assuming 200 x 10^6 cells per HYPERFlask. Flasks were monitored closely after 48 hours until CPE was observed around flask edges, infected cells were not lysed.

To harvest virus-containing cells, HYPERFlasks were knocked gently from side to side to detach cells, both cells and medium were centrifuged in 250 mL conical tubes (#CLS430776, Corning) at 300 x g for 10 minutes at RT. Most of the supernatant was discarded, but 5 mL was kept for resuspension of the cell pellet. The HYPERFlask was washed once with 1x DPBS and the cell pellet resuspended with the wash and centrifuged again (300 x g, 10 mins). The final cell pellet was resuspended in 5 mL retained infectious supernatant and stored at -80 ˚C until purification using a caesium chloride (CsCl) gradient described in the following section.

2.8.6 Adenovirus purification

To obtain virus from frozen cell suspensions from section 2.8.5, they were subjected to three freeze-thaw cycles as described in section 2.8.3. After the final freeze-thaw step, 0.01x volumes of water-saturated n-Butanol (recipe in Table 7.2 in Appendix I) was added to the thawed lysate. The lysates were left to incubate for 1 hour rotating at 4 ˚C. Lysates were centrifuged (500 x g, 10 mins) at 4 ˚C and virus-containing supernatants were transferred to a new tube.

Adenoviruses can be purified by ultracentrifugation over two discontinuous CsCl density gradients, this results in the purification of mature virus particles based on their size and density. Briefly, gradients were constructed in 14 mL Open-Top Thinwall Ultra-Clear™ centrifuge tubes (#344060, Beckman Coulter). A layer of 3 mL 1:32 ρ CsCl was underlaid with 2 mL 1:45 ρ CsCl using a 21-gauge long needle (#AN*2150R1, Terumo) and a 2.5 mL syringe (Greiner-Bioone) and overlaid with 2 mL 40% glycerol (recipes for gradient layers in Table 7.2 in Appendix I). A volume of 4.5 mL – 5 mL virus-containing supernatant was overlaid on top of the gradient and tubes were centrifuged using a Beckman Coulter Optima L-80 XP Ultracentrifuge with a SW40Ti rotor (78,925 x g, 90 mins) at 10 ˚C.

Following centrifugation two discrete bands can be observed below a layer of cell debris, Figure 2.6A. To collect intact virus particles, the centrifuge tube was carefully punctured 1 cm below

the lower band with a 21-gauge short needle (#AN*2138R1, Terumo) and the band was aspirated into a 5 mL syringe (Greiner-Bioone). CsCl was removed from the viral suspension by injecting into a 3-12 mL 10,000 MWCO Cut-off Slide-A-Lyzer dialysis cassette (#66810, ThermoFisher Scientific) which was then subjected to two 20 minute dialysis steps and a final overnight dialysis, all in 500 mL 1x DPBS at 4 ˚C.

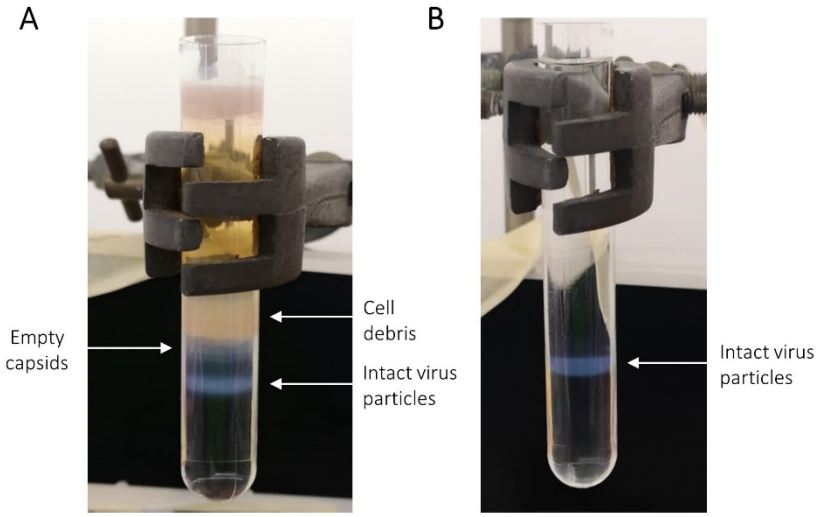


Figure 2.6 Bands observed following double CsCl density gradient ultracentrifugation to purify adenovirus. (A) Representative image following ultracentrifugation after the first round of CsCl banding. Two bands are observed below cellular debris; the top band consists of empty capsids, the bottom band is intact virus particles. **(B)** Representative image after the second round of CsCl banding only one band is observed, intact virus particles.

Following dialysis, the DPBS-virus solution was recovered from the cassette and treated with 2 mM magnesium chloride (#M8266, Sigma Aldrich) and 1 µL/mL Benzonase® Nuclease ultrapure (#E8263-5KU, Sigma Aldrich) for 1 hour rotating at RT. A second round of CsCl banding was then performed using the method just described, layering new gradients of CsCl and glycerol, the resulting band of purified virus can be seen in Figure 2.6B. The same steps were followed until the final round of dialysis, in which the 500 mL of 1x DPBS was supplemented with 5 mM HEPES (#H0887-20ML, Sigma Aldrich). The virus solution was removed from the dialysis cassette and glycerol was added to a final concentration of 20% to

act as a cryoprotectant. Viruses were aliquoted, snap-frozen in liquid nitrogen and stored at -80 ˚C until further use.

2.8.7 Determination of adenovirus quantification using dsDNA measurements

Purified adenovirus stock DNA concentrations (viral genomes/mL) were quantified using the Quant-iT™ Picogreen™ dsDNA Assay kit (#P7589, Invitrogen). This kit contains a PicoGreen probe that selectively binds dsDNA and fluoresces upon binding. Stocks of adenovirus were diluted 1/10, 1/250, 1/500 and 1/1000 in 1x TE buffer (recipe in Table 7.2 in Appendix I) supplemented with 0.05% SDS (1x TES buffer) and heat treated (56 ˚C, 30 mins) to disrupt virus particle capsids. A standard curve was prepared by serially diluting bacteriophage λ-DNA in two fold steps in 1x TES buffer, starting from a stock of 0.5 µg/mL. For each standard or sample, 50 µL was mixed with 50 µL PicoGreen reagent (1/200 dilution in 1x TE buffer) in solid black 96-well assay plates (#3925, Corning). Fluorescence was measured using a Wallac 1420 Victor^2 plate reader (Perkin Elmer) at 485/535 nm (excitation/emission). Virus genome concentration was then calculated assuming 1 µg dsDNA equates to 2.7 x 10^{10} adenovirus particles. This assumption was based on the mass of an adenovirus particle consisting of 13% DNA and 87% viral protein (Murakami and McCaman 1999).

2.8.8 Infectious viral particle assessment by $TCID_{50}$

The number of infectious viral particles in purified virus stocks or virally-infected cultures were measured using a $TCID_{50}$ (tissue culture infectious dose that will infect 50% of cells) technique. One day prior to infection, A549 cells were seeded at a density of 1.0 x 10^4 cells/well. Virus stocks to be tested were serially diluted 10-fold in 2% DMEM medium with an initial dilution of 10^{-1} to 10^{-14}, ten replicate wells were infected for each dilution. A549 cells were infected

with 200 µL/well of each dilution with 10 wells receiving virus-free medium as a control. Plates were incubated for 7 days in a 37 ˚C, 5% CO_2 humidified incubator, and subsequently wells were scored for the presence of plaques (or significant CPE) using a Zeiss Axiovert 25 microscope. $TCID_{50}$/mL was calculated using the KARBER statistical method:

$$Titer\left(\frac{TCID50}{mL}\right) = 10^{1+D\,(S-0.5)}$$

D = log (d); d = dilution factor

S = sum of the ratios of wells with CPE to CPE-free wells

2.8.9 Infectious viral particle measurement by plaque-forming assay

Monolayers were created by seeding 6 well plates with 1.0 x 10^6 A549 cells/well and leaving plates in a humidified incubator for 24 - 48 hours until 100% confluency was reached. Cells were infected with 10-fold serially diluted virus preparations starting from a 10^{-3} dilution. Infections were performed with 400 µL of infection media for two hours at 37 ˚C with gentle rocking every 15 minutes.

Virus-containing medium was then removed and monolayers were overlaid with 2.5 mL of a low-melting point agarose-DMEM mixture (recipe in Table 7.2 in Appendix I). Plates were left at RT for 40 minutes to allow for the agarose to solidify before being moved to 37 ˚C, 5% CO_2 incubators for seven days. Infected wells were then fixed with an acetic acid:methanol mix (1:3, v/v) for 30 minutes on a rocker, fixative and agarose layers were removed and wells gently washed with H_2O. Plates were left for 5 minutes at 64 ˚C to air-dry before wells were stained with 1% crystal violet in a water:methanol mix (1:5, v/v) for 1 minute. The staining solution was removed and wells were washed again with H_2O before being air-dried at 64 ˚C. Plaques were manually counted in each well and the titre of the virus stock (PFU per mL) was calculated

based on the dilution factor of the well where the plaque count lay between 10 and 100 to minimise error;

$$Titer\left(\frac{PFU}{mL}\right) = \frac{Number\ of\ plaques}{volume\ of\ inoculum\ x\ dilution\ factor}$$

Example EnAd-SA-GFP:

$$\frac{72}{0.4\ mL\ x\ 10^{-8}} = 1.80\ x\ 10^{10}\ PFU/mL$$

2.8.10 Measuring adenovirus genome replication using qPCR

Adenoviral genomes can be quantified by qPCR in order to assess the virus replication. Cells were seeded in 24-well plates at a density of 1.0 x 10^5 cells/well, 24 hours later culture medium was removed and cells were infected with the viruses to be assessed under varying culture conditions, generally at an MOI of 1 unless otherwise specified. After the appropriate amount of time, cells and medium from wells were harvested by scraping and then frozen at -20 ˚C for future use. Samples were thawed and total genomic DNA was extracted using a PureLink™ Genomic DNA Mini Kit (#K182002, Invitrogen) according to manufacturer's instructions.

Total viral genomes were quantified by qPCR using primers and a probe (Sigma Aldrich) against the EnAd hexon gene, listed in Table 2.12. Briefly, primers (400 nM) and probe (200 nM) were mixed in a reaction with 5 µL 1/1000 diluted total DNA in dH_2O and 2x qPCRBIO Probe Mix Hi-ROX (#PB20.22, PCRBiosystems) and made up to 20 µL with ddH_2O (#AM9906, Invitrogen).

Reactions were run on an ABI PRISM 7000 system (Applied Biosystems) with the following steps;

1. **Polymerase activation:** 95 ˚C for 2 mins
2. **Denaturation:** 95 ˚C for 5 secs
3. **Annealing/extension:** 60 ˚C for 30 secs
4. **Extension:** 72 ˚C for 1 min/kb
5. **Repeated cycles:** Return to step 2 and repeat 39x

Samples were run alongside standards constructed by serial dilution of purified virus stocks of known concentration (vp/mL) which had previously been calculated using the PicoGreen assay.

Table 2.12 Primers and probes used for qPCR against the EnAd hexon gene.

Primer ID	Target gene	Primer/Probe
EnAd/Ad11p forward	Hexon	5′ – TACATGCACATCGCCGGA – 3′
EnAd/Ad11p reverse		5′ - CGGGCGAACTGCACCA – 3′
EnAd/Ad11p probe		5′ - [6FAM] - CCGGACTCAGGTACTCCGAAGCATCCT - [TAM] - 3′

2.8.11 Quantification of infectious units using a luminescent reporter

An alternative method for measuring infectious particles in experimental samples was developed by Dr. Egon Jacobus (Seymour Lab, Department of Oncology, University of Oxford, UK) of our lab. This method uses a modified adenovirus, EnAd-SA-FLuc also created by Dr. Jacobus, and enables higher throughput quantification of infectious particles in samples without requiring time-consuming plaque assays. The method was developed based on a method used to titre other viruses (Garcia et al. 2014).

To analyse supernatants of unknown concentrations of EnAd-SA-FLuc, samples were aliquoted into 96V plates before being stored at -80 ˚C until use. A549 cells were seeded in solid black 96-well plates at a density of 1.5 x 10^4 cells/well in 10% DMEM. After 24 hours a standard

curve was prepared by diluting a purified stock of EnAd-SA-FLuc with known PFU/mL, dilutions made are shown in Table 2.13. Samples were thawed and 25 µL samples or standard dilutions were added to cells in triplicate before centrifuging the plates (600 x g, 10 mins) to maximize virus to cell binding. The infection medium was left for 2 hours then replaced with 90 µL 10% RPMI. Plates were left for 22 hours at 37 ˚C, 5% CO_2 in a humidified incubator.

Table 2.13 The preparation of dilutions of EnAd-SA-FLuc to create a standard curve for the luminescence based infectivity assay using ONE-Glo.

Virus volume (µL)	2% RPMI (µL)	Dilution factor	PFU in 25 µL
1	485	485	5.57×10^5
500	500	2	2.79×10^5
250	750	4	6.96×10^4
250	750	4	1.74×10^4
250	750	4	4.35×10^3
250	750	4	1.09×10^3
250	750	4	2.72×10^2
0	1000		0

To measure luciferase activity, the ONE-Glo™ Luciferase Assay System (#E6110, Promega) was used following the manufacturer's instructions. Briefly, ONE-Glo reagents were allowed to equilibrate to RT before the ONE-Glo Luciferase Assay Buffer was added to the ONE-Glo Luciferase Assay substrate and plates were removed from the incubator. Lysis solution (#G1780, Promega) was added to each experimental well at a 1x concentration (10 µL) and incubated at 37 ˚C for 30 minutes to ensure release of luciferase from the infected A549 cells. The same volume of ONE-Glo reagent was mixed with lysed samples and luminescence was quantified after 3 minutes using a POLARstar Omega plate reader (BMG LabTech). Plaque-forming units/25 µL for supernatants with unknown concentrations were interpolated from the standard curve formed from serial dilution of a known EnAd-SA-FLuc stock.

2.8.12 Virus tracking and quantification of viral expression using reporter genes

EnAd-CMV-GFP and EnAd-SA-GFP are modified adenoviruses used as reporter viruses originally engineered and kindly provided by PsiOxus Therapeutics Ltd. In these viruses GFP is placed under the control of the exogenous CMV immediate early promoter, or alternatively under the control of the endogenous adenovirus MLP via alternative splicing to an inserted 5' short SA sequence (Carette et al. 2005).

Viral gene expression can be quantified by infecting cells with modified GFP EnAd viruses and tracking virus infection and replication using flow cytometry. Cells were seeded in 24-well plates at a density of 1.0 x 10^5 cells/well, 24 hours later culture medium was removed and cells were infected with the modified viruses at an MOI of 1 unless otherwise specified in the relevant culture conditions being assessed. After the indicated amount of time, virus-containing medium was removed. The cells left on the plate were harvested by washing them once with 150 µL 1x DPBS. The wash was placed into 96V plates and pelleted by centrifugation (400 x g, 5 mins) to preserve any cells that may have been removed from the plate during the wash. 50 µL of trypsin:EDTA solution was added to each well and the plate incubated for 10 minutes at 37 ˚C until all cells had detached. The enzymatic solution was then quenched with addition of 150 µL 10% RPMI and the suspension was added to the corresponding pellets in the 96V plate. Plates were centrifuged (400 x g, 5 mins) and wells in the culture plates washed once more with 1x DPBS. This final wash was added to the cell pellets in the 96V bottom plate and centrifuged (400 x g, 5 mins) then cells were fixed as in section 2.4.2. The resulting cell pellet was resuspended in 200 µL MACs buffer and analysed for GFP expression using an Attune NxT Flow Cytometer (ThermoFisher Scientific) as described in section 2.4.6. If the cells were also to be analysed for cytotoxicity the cell pellet was stained with LIVE/DEAD™ Fixable Near-IR

dead cell stain kit (#L10119, ThermoFisher Scientific) in 50 µL MACs buffer for ten minutes at RT before 150 µL 1x DPBS was added to the wells and the plate was centrifuged (400 x g, 5 mins). The cell pellet was fixed then resuspended in 200 µL MACs buffer and analysed as above.

2.9 Statistical analysis

Charts, plots and statistical analyses were performed using GraphPad Prism 8.3.1. Where more than two variables were being compared, a one-way analysis of variance (ANOVA) test was used with Tukey's *post hoc* analysis or Dunnett's *post hoc* analysis if one mock condition was compared. For grouped datasets with multiple variables, a two-way ANOVA test was used with Tukey's *post hoc* analysis or Dunnett's *post hoc* analysis. All data are presented alongside error bars indicating standard deviation (±SD) unless otherwise specified. The significance levels used were *; $0.01 < p \leq 0.05$, **; $0.001 < p \leq 0.01$, ***; $0.0001 < p \leq 0.001$, ****; $p \leq 0.0001$. All *in vitro* experiments were performed in biological triplicate unless otherwise stated.

3 Determining the effect of amino acid depletion on EpCAM BiTE-induced T cell activation and EnAd activity

3.1 Introduction and chapter aims

3.1.1 Introduction

Proliferating cells require vast amounts of amino acids to fulfil multiple roles in addition to their primary function as the biosynthetic material that make up proteins. Cancers cells are known to use amino acids as an alternative source of energy to feed into the TCA cycle, like glutamine and BCAAs, to aid in redox homeostasis (cysteine, glutamate and glycine), as precursors for various types of metabolites; polyamines and spermidines, and as substrates for epigenetic modifications, acetylation and methylation (Vettore, Westbrook, and Tennant 2020). Their excessive use by tumour cells, the numerous mechanisms at play to deplete nutrient availability to other anti-tumour cells, and the general physical limitation of reduced blood supply due to poor vasculature all result in a nutrient poor environment (Vaupel, Kallinowski, and Okunieff 1989). While cancer cells are equipped to handle this, due to their metabolic plasticity, other cells which would otherwise act to defend against the tumour, such as effector T cells, unfortunately suffer, with many even differentiating into regulatory T cells that instead aid the tumour's growth.

There is a literature precedent to suggest T cells rely on serine, tryptophan and arginine for their proper proliferation and activation (J. Wei et al. 2017). Many immunotherapeutic strategies will rely either directly or indirectly on effector T cells to activate and induce tumour cell lysis,

thereby promoting elimination of the tumour. Due to the significant metabolic stress that T cells would be exposed to in the TME, it is important to consider the influence nutrient depletion may have on the efficacy of the T cell-promoting activity being tested. BiTEs can activate T cells independently of HLA recognition in a manner that is both excessive and without co-stimulation. We hypothesise that BiTEs will "super-activate" T cells due to the high density of target antigens available on a cancer cells surface to interact with a number of CD3 receptors available on a T cell. This is compared to HLA:peptide:TCR complexes, which can stimulate T cell activation even at low frequencies, but only under physiological conditions (X. Yao et al. 2013; Purbhoo et al. 2006). Furthermore, BiTEs could potentially bypass certain metabolic checkpoints usually triggered during physiological activation. BiTEs do not require any influence from CD28, which acts as the dominant trigger for the PI3K-Akt-GSK signalling pathway in activated T cells (Appleman and Boussiotis 2003) and results in the adaptation of the T cell metabolic profile to meet energy demands. We also suspect that BiTEs may be able to activate despite the lack of CD28 stimulation, regardless of the state of metabolic stress.

OVs can be used as genetic carriers to directly deliver BiTEs to a tumour site, avoiding on-target, off-tumour effects and issues with dose toxicity (Dahlén, Veitonmäki, and Norlén 2018). Examples of this technology have been demonstrated by our group using EnAd encoding either an EpCAM BiTE, a BiTE targeting FAP, or tri-valent T cell engagers (TriTEs) as well as many others (Freedman et al. 2017, 2018; Scott et al. 2019; Shi et al. 2020). While most OVs are engineered with intentional deletions or insertions, EnAd was produced via directed evolution. Its selectivity for cancer cells is not yet fully understood, though recent publications suggest that the specific metabolic phenotype of a cancer cell is attractive for EnAd replication due to the extensive available resources and unhampered activation of mTOR (Dyer et al. 2017; Kleinberger 2020). Several groups, including ours, have shown some OVs have a preference for available exogenous glutamine, even over available glucose, and that inhibition of

glycolysis could improve the potency of OVs, including NDV (Deng et al. 2014), VACV (Fontaine, Camarda, and Lagunoff 2014) and adenoviruses (Dyer et al. 2019; Thai et al. 2015). We must therefore consider that viral infection of tumour cells by EnAd may be affected by the loss of other amino acids that have defined roles in cancer cells, as with glutamine. This may, in turn, affect the ability of EnAd to effectively express encoded transgenes.

To date, most studies performed *in vitro* use cell culture medium supplemented with high levels of nutrients, with very little waste accumulation and in conditions of high oxygen. Both RPMI 1640 and DMEM media contain supra-physiological levels of amino acids compared to physiological levels measured in the plasma of a healthy individual. For example, serum has been reported to contain 0.1-0.6 mM glutamine (Bergstrom et al. 1974; Watanabe et al. 1984), whereas DMEM contains 4.0 mM glutamine (D5796; (Morton 1970; Rutzky and Pumper 1974)) and RPMI-1640, 2.0 mM (R8758; (G. E. Moore, Gerner, and Franklin 1967)). As such, traditional cell culture media is not a true representation of the metabolic environment in the TME, where a heterogeneous tumour will experience fluctuations of normoxia/hypoxia, nutrients levels and waste accumulation. An understanding of the interactions between cancer therapies, particularly immunotherapies, and the heterogenous TME will be instrumental in improving drug design and treatment of cancers.

Therefore, in this chapter, we established whether treatment of solid tumours with virotherapy expressing EpCAM BiTE was hindered in an environment suffering nutrient deprivation. We first identified the amino acids that were essential for T cell cytotoxicity of target cells after activation by the EpCAM BiTE. In addition, we assessed the effect of nutrient depletion on the ability of EnAd to express reporter proteins as a surrogate for transgenes like BiTEs and as an indication of viral replication, and to induce viral-mediated lysis of tumour cells. To expand on this we performed further assay development using an alternative medium that better represents the true levels of amino acids found in the TME. Consequently we chose to use a range of *ex*

vivo malignant ascites fluids from patients, evaluated their amino acid contents using HPLC and selected those with varied levels of key amino acids identified above. EpCAM BiTE and EnAd function were reassessed using this new model.

3.1.2 Chapter aims

The aims of this chapter were to:

1. Characterise EpCAM BiTE-directed activation of T cells and compare their cytotoxic effect with physiological killing by a $CD8^+$ T cell clone in medium depleted of amino acids,
2. Quantify EnAd-induced viral protein expression and tumour cell death in medium depleted of amino acids,
3. Establish human malignant ascites fluids as an *ex vivo* model to reflect amino acid levels in the TME.

3.2 Results

3.2.1 SKOV-3 tumour cell viability when individual amino acids are absent from culture medium

In vivo, tumour cells appear to survive and even prosper despite a lack of typical nutrients. This is proposed to be the result of a complex network purposely built by tumour cells as a survival mechanism (Vettore, Westbrook, and Tennant 2020). Most assays *in vitro* are performed in 2D cell culture, limiting the extent to which such survival features of the TME can be modelled. We therefore must investigate which cell lines are most vulnerable or resilient to amino acid deficiencies.

We assessed the viability of HCT116, A549 and SKOV-3 cells after 24 hours of exposure to medium depleted of individual amino acids. Amino acid-depleted medium was prepared as detailed in section 2.1.4 and viability assays were performed as described in section 2.6.3. We found that SKOV-3 ovarian cells remained as viable in all mediums compared to RPMI-1640 supplemented with 2% of dialysed serum, used as a control. The viability of HCT116 colon cells and A549 lung cells, however, was reduced by 50% when medium with no amino acids was used and varied depending on the missing amino acid (Figure 3.1). We confirmed SKOV-3 cells maintained their viability even after 72 hours, confirming their suitability for subsequent analysis with amino acid-deprived culture conditions (Figure 3.1C).

Our data concludes that SKOV-3 cells represent a suitable model to investigate the effects of amino acid depletion on the activity of EpCAM BiTE and EnAd. SKOV-3 cells are resistant to amino acid depletion and, as EnAd replicates more slowly in this cell line, they offer a larger window of time to examine the effects of nutrient loss on EnAd infection (Dyer et al. 2019).

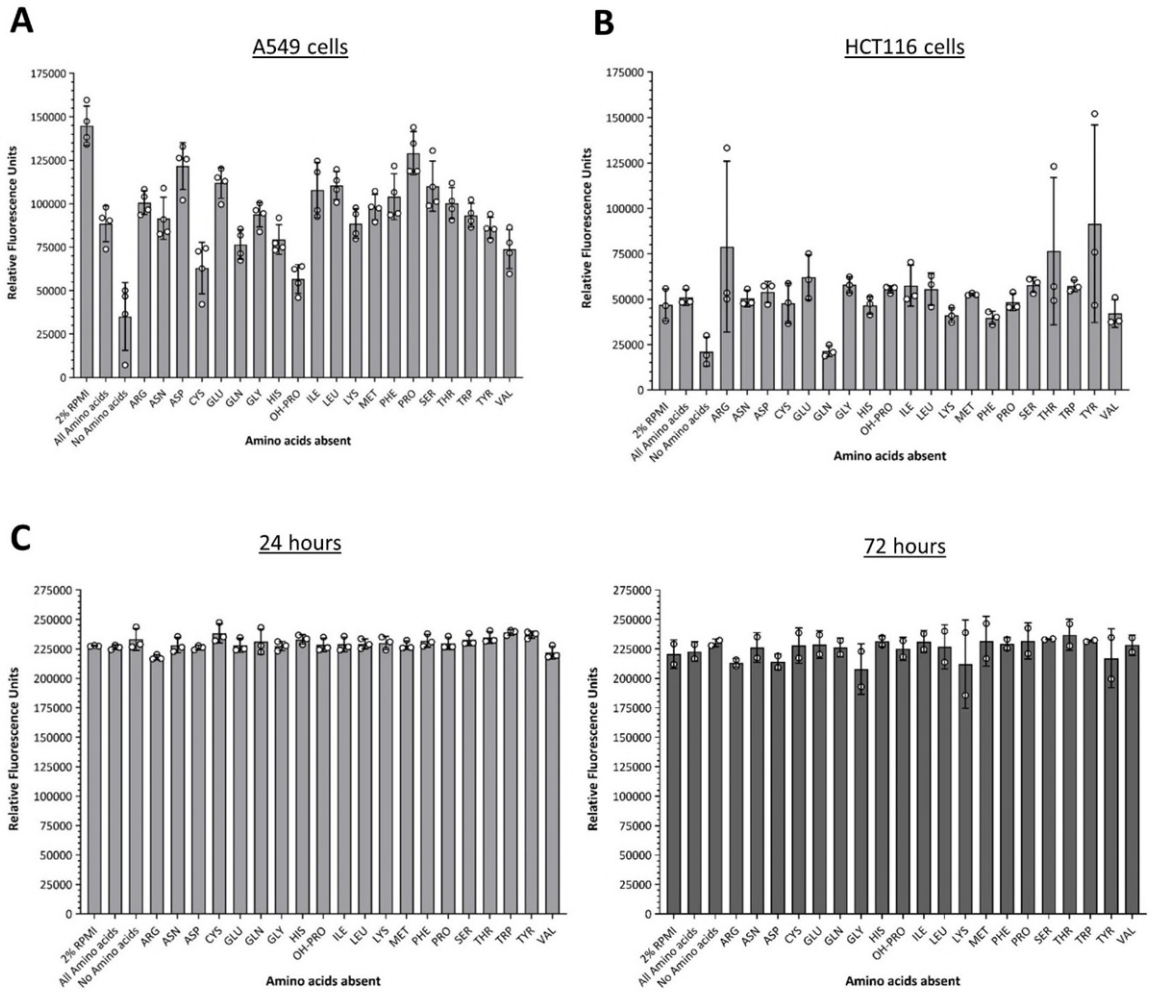


Figure 3.1 SKOV-3 viability is sustained in amino acid depleted medium. 2.0 x 10^4 A549 cells **(A)** or HCT116 cells **(B)** were cultured in medium without individual amino acids. After 24 hours medium was removed and cell viability was determined using PrestoBlue cell viability reagent. Relative fluorescence as a representative of viability was measured. **(C)** 1.5 x 10^4 SKOV-3 cells were cultured in medium without individual amino acids over 72 hours. At 24 hours and at 72 hours, cell viability was determined. Data show mean ± SD of biological triplicates.

3.2.2 The ability of EpCAM BiTE to activate T cells is impacted by amino acid deficiencies

We first sought to identify which amino acids, if any, were essential for T cell activation following their stimulation with EpCAM BiTE cultured with SKOV-3 cells. To achieve this,

we isolated T cells as described in section 2.5.3 then cultured them with SKOV-3 cells at an E:T of 5:1 in the presence or absence of EpCAM BiTE. T cells cultured alone were used as a control. T cell activation was then quantified using flow cytometry to measure CD69 and CD25 on the surface of single T cells as markers of early and late activation, respectively.

Prior to analysis, the concentration of EpCAM BiTE was established using a dot blot (Figure 3.2A) and its ability to activate T cells to lyse tumour cells was measured by an LDH release assay, as described in section 2.6.1 (Figure 3.2B). In cultures of T cells alone or T cells cultured with SKOV-3 cells, no elevation of CD25 nor CD69 was observed in any media tested. In the presence of EpCAM BiTE in 2% RPMI control medium, a significant increase in both markers was observed, as expected. In amino acid-depleted media, the percentage of CD25-positive T cells dropped for some conditions (Figure 3.3.A), while the percentage of CD69, the earlier activation marker, remained high, above 90% in all media tested, even medium without any amino acids (Figure 3.3B). The percentage of CD25-positive T cells decreased by half in medium containing no amino acids, no glutamine or no tryptophan (Figure 3.3A).

While early activation, represented by CD69 surface expression, remained unchanged in medium depleted of amino acids, later activation, represented by CD25, was reduced by the absence of most amino acids. This was particularly noticeable in the absence of glutamine or tryptophan. These findings suggest that T cells cultured in medium without any amino acids would not be activated to their potential maximum observed in control medium. This effect would likely be a consequence of the absence of glutamine and tryptophan, in particular.

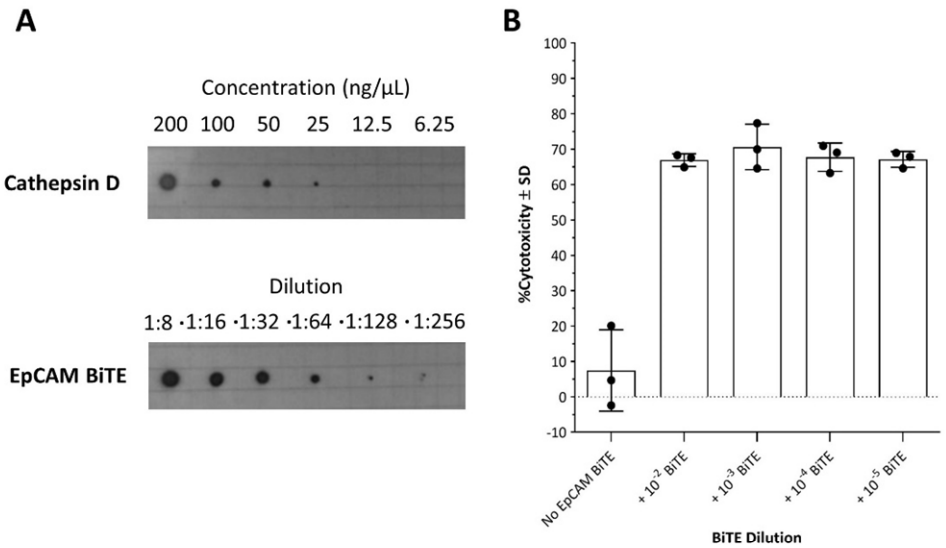


Figure 3.2 Quantification and functional validation of EpCAM BiTE. (A) EpCAM BiTE was quantified using a dot blot to estimate the quantity following expression from 293Ad cells against a C-terminal decahistidine-tagged protein standard, Cathepsin D. **(B)** $EpCAM^+$ tumour cells, Colo205 cells, co-cultured with $CD3^+$ T cells incubated with no EpCAM BiTE or increasing EpCAM BiTE dilutions starting from 1/100. Lysis was determined by LDH release into the supernatant and the percentage of cytotoxicity was calculated against spontaneous LDH release from Colo205 cells alone and T cells alone. Each condition is measured in biological triplicate and represented as mean ± SD.

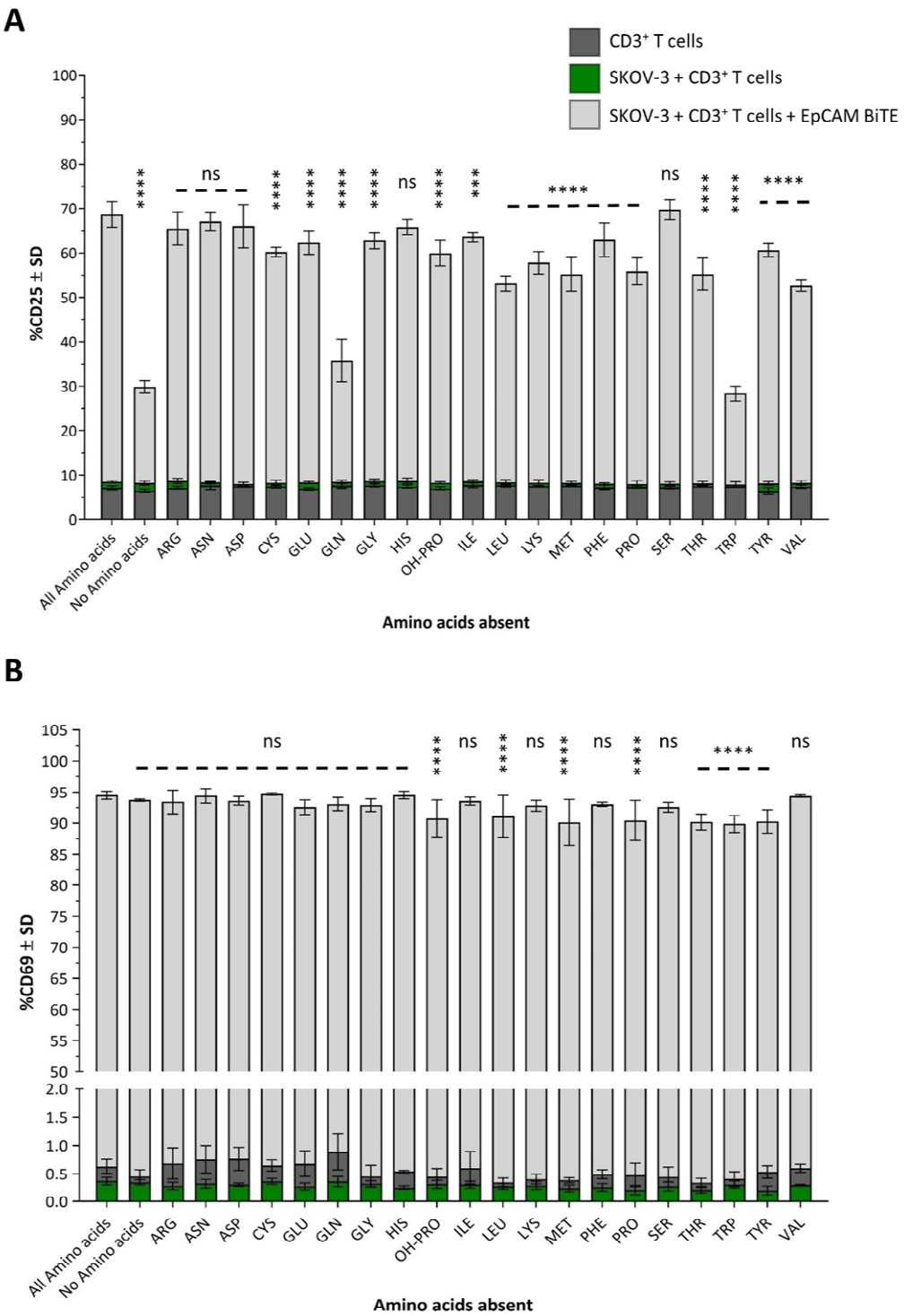


Figure 3.3 EpCAM-BiTE induced activation of T cells in co-culture with SKOV-3 cells under conditions without individual amino acids. BiTE-containing supernatant was added to a co-culture of $CD3^+$ T cells and SKOV-3 cells (5:1) and after 24 hours activation was measured by the surface expression of CD25 **(A)** and CD69 **(B)** analysed by flow cytometry. Each condition was measured in biological quadruplicate and data is represented as the mean ± SD. Significance was assessed by a two-way ANOVA test with Dunnett's post-hoc analysis comparing with the "All Amino acids" control condition (*, $p < 0.05$; **, $p < 0.01$; ***, $p < 0.001$; ****, $p < 0.0001$; ns, non-significant).

3.2.3 Biomarkers of cytotoxicity potential are reduced when glutamine is absent after EpCAM BiTE activation of $CD3^+$ T cells

Following the reduction in activation observed in the absence of glutamine and tryptophan, we assessed the cytotoxic potential and terminal effector functions of T cells in killing target tumour cells. The EpCAM BiTE is capable of activating both T cell subsets, $CD4^+$ and $CD8a^+$, to kill target cells. Flow cytometry was used to analyse intracellular expression of GrB and IFNγ in $CD4^+$ and $CD8a^+$ T cells above levels observed in cultures of T cells and SKOV-3 cells alone.

Our data revealed that the most essential amino acids for GrB expression in either T cell subset after treatment with EpCAM BiTE were cysteine, glutamine, threonine, tryptophan and valine (Figure 3.4). Surprisingly, the complete absence of amino acids did not impact GrB expression levels as strongly as the absence of individual amino acids.

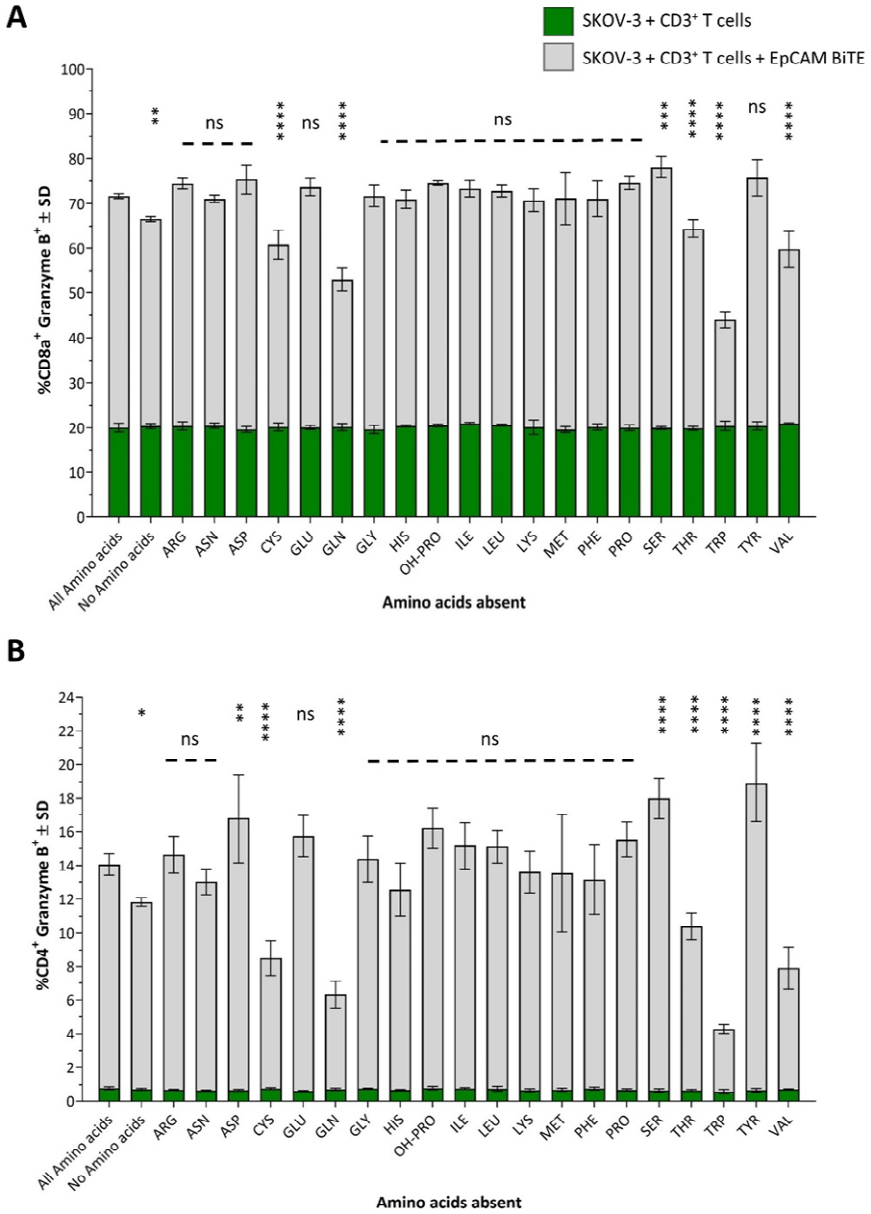


Figure 3.4 EpCAM-BiTE induced GrB expression measured in CD8a$^+$ and CD4$^+$ T cell subsets in co-culture with SKOV-3 cells under conditions without individual amino acids. BiTE-containing supernatant was added to a co-culture of CD3$^+$ T cells and SKOV-3 cells (5:1) and after 24 hours GrB expression was measured by intracellular staining and analysis by flow cytometry. **(A)** Surface expression of CD8a$^+$ alongside expression of GrB. **(B)** Surface expression of CD4$^+$ alongside expression of GrB. Each condition was measured in biological quadruplicate and data is represented as the mean ± SD. Significance was assessed by a two-way ANOVA test with Dunnett's post-hoc analysis comparing with the "All Amino acids" control condition (*, $p < 0.05$; **, $p < 0.01$; ***, $p < 0.001$; ****, $p < 0.0001$; ns, non-significant).

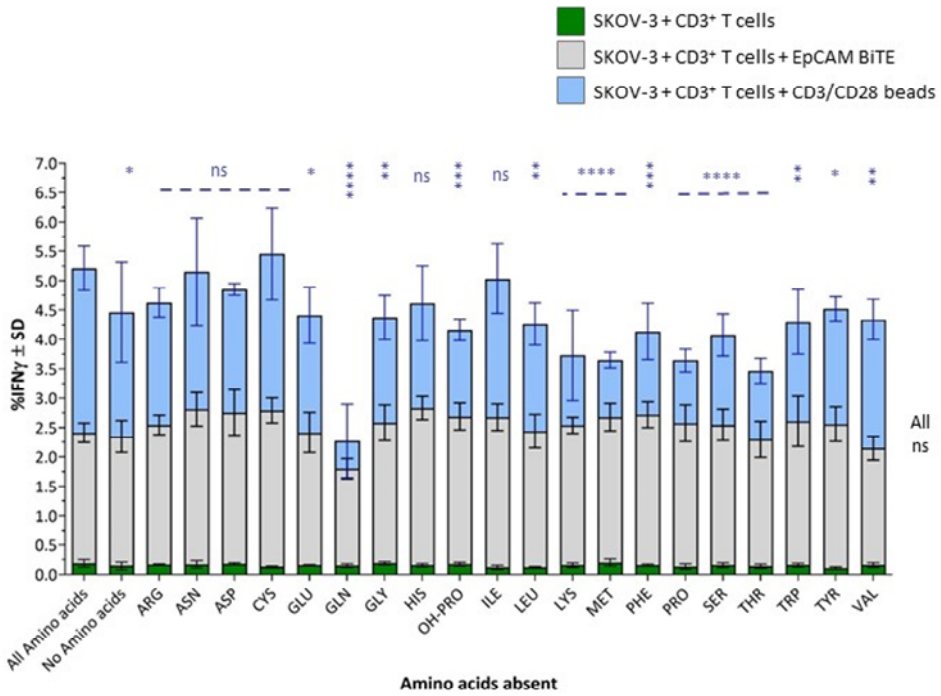


Figure 3.5 EpCAM-BiTE induced IFNγ expression was unhindered by amino acid loss. CD3/CD28 bead activation, however, was diminished. BiTE-containing supernatant or 2 µL CD3/CD28 beads were added to a co-culture of $CD3^+$ T cells and SKOV-3 cells (5:1) with various culture mediums containing one less amino acid. After 6 hours T cells were harvested and intracellularly stained for IFNγ. Each condition was measured in biological quadruplicate and data is represented as the mean ± SD. Significance was assessed by a two-way ANOVA test with Dunnett's post-hoc analysis comparing with the "All Amino acids" control condition (*, $p < 0.05$; **, $p < 0.01$; ***, $p < 0.001$; ****, $p < 0.0001$; ns, non-significant).

We also characterised *de novo* IFNγ expression (which is an indication of those T cells with cytolytic potential) in $CD3^+$ T cells incubated in amino acid-depleted medium (Tau et al. 2001; Freedman et al. 2017). The EpCAM BiTE induced a 20-fold increase in the percentage of IFNγ-positive T cells compared to T cells cultured with SKOV-3 alone. There was no significant decrease from this level of expression in the absence of individual amino acids, though the absence of glutamine resulted in the lowest level of expression (Figure 3.5). In contrast, in T cells activated with CD3/CD28 beads, a more physiological means of T cell activation (Trickett and Kwan 2003), IFNγ expression decreased by 50% following activation in medium depleted of glutamine. Slight decreases in the percentage of IFNγ were observed in the other test media compared to a 40-fold increase in the presence of all amino acids.

Although the absence of cysteine, threonine, tryptophan and valine resulted in decreased expression of GrB in T cells, glutamine had the biggest influence on expression of both GrB and IFNγ following BiTE activation of T cells. Our results show that glutamine is an essential amino acid for both T cell activation (CD25) and cytotoxicity (GrB, IFNγ) when stimulated by EpCAM BiTE.

3.2.4 SKOV-3 cytotoxicity via the EpCAM BiTE is less affected by amino acid depletion and makes HLA-dependent killing more potent

Next, we examined whether a lack of glutamine, which results in reduced CD25 activation on T cells and reduced IFNγ and GrB expression, would translate into reduced killing of $EpCAM^+$ target cells by EpCAM BiTE-activated T cells. We quantified tumour cell viability as described in section 2.6.3 and assessed EpCAM BiTE-induced cytolytic activity compared to an activated cytotoxic $CD8^+$ T cell clone recognising the same tumour cell line, SKOV-3, via MHC-I. We assessed killing capacity for both modes of killing over 72 hours in amino acid-depleted medium.

The $CD8^+$ T cell clone used here was originally reported to kill Colo205 and HCT116 tumour cells. As shown in section 3.2.1, HCT116 cells did not cope well when subjected to amino acid depletion, even for 24 hours in medium depleted of single amino acids (Figure 3.6A). The $CD8^+$ T cell clone was reported to have broad peptide specificity and the ability to kill multiple tumour cell lines. Here, we confirmed that the clone could kill SKOV-3 cells by measuring live $EGFR^+$ cells after incubation with increasing numbers of the $CD8^+$ T cell clone (Figure 3.6B). We also confirmed using a dye indicating caspase 3/7 activation, CellEvent Caspase 3/7, that BiTEs triggered apoptosis via caspases 8x faster than HLA-dependent apoptosis via the $CD8^+$ T cell clone alone and required an E:T ratio of only 1:3 to achieve maximal killing (between 6-12h as opposed to 96h) (Figure 3.6C)

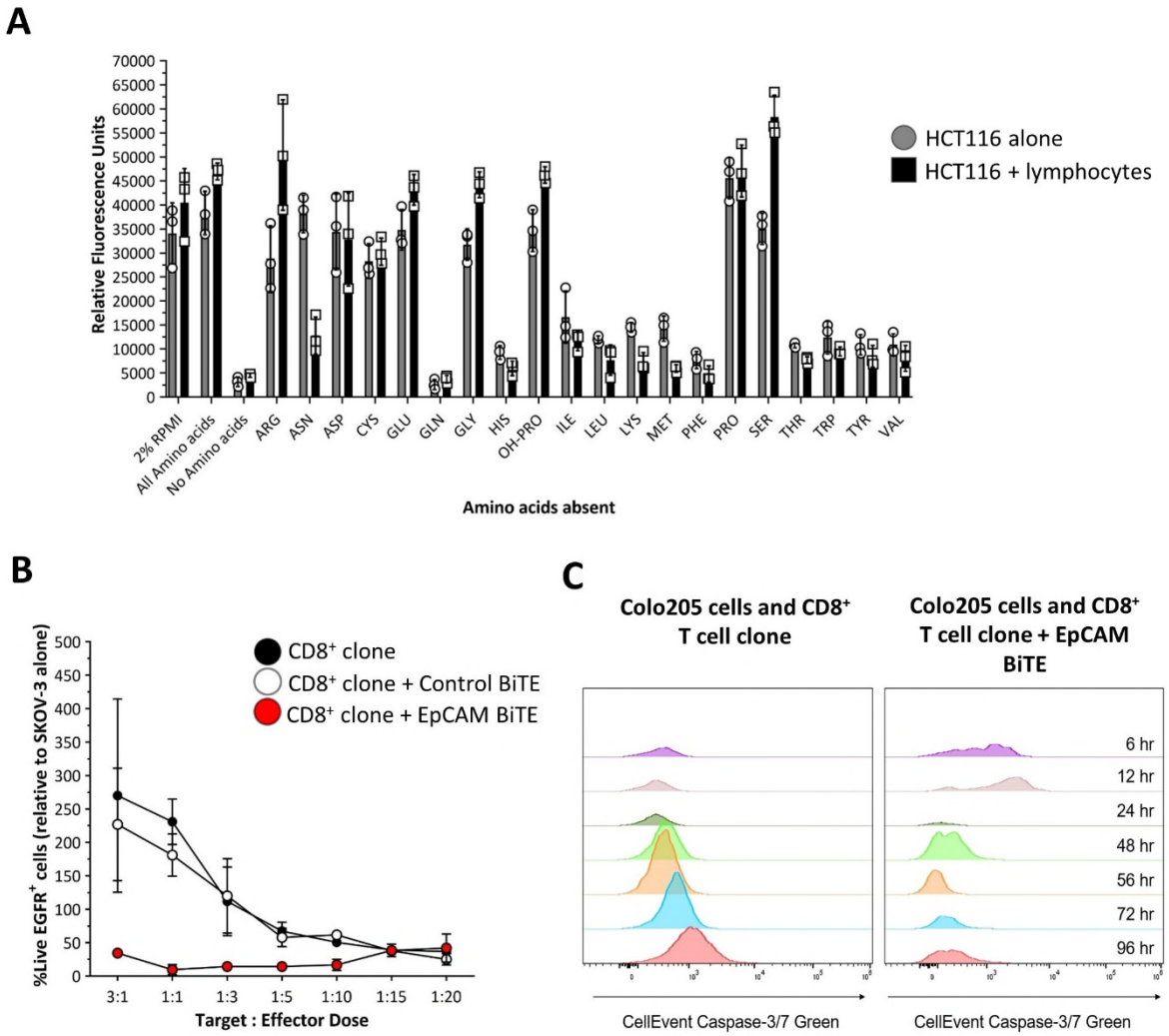


Figure 3.6 SKOV-3 and CD3$^+$ T cell viability is more stable when cultured in amino acid absent medium and SKOV-3 cells are targeted for lysis by the ST8.24 CD8$^+$ T cell clone. (A) HCT116 cells were cultured with and without lymphocytes (5:1) in culture medium lacking one amino acid alongside three controls; 2% RPMI 1640, all amino acids medium and no amino acids medium. After 72 hours cells were measured for viability using PrestoBlue. **(B)** SKOV-3 cells were cultured alone or with the ST8.24 CD8$^+$ T cell clone for 72 hours at the indicated effector to target cell ratios. Wells were left untreated or treated with control BiTE or EpCAM BiTE. The percentage of live cells were calculated by staining with EGFR and analysing with flow cytometry. For all experiments each condition was measured in biological triplicate and data is represented as the mean ± SD. **(C)** 3.0 x 10^4 Colo205 cells were co-cultured with CD8$^+$ T cell clone (1:10, E:T) incubated with or without EpCAM BiTE. T cells and adherent cells were harvested at 6, 12, 24, 48, 56, 72, and 96h and at each point were stained with EGFR and CD8 fluorophore-conjugated antibodies, Live/Dead near IR viability stain and CellEvent Caspase 3/7 reagent then fixed before each timepoint was analysed by flow cytometry on the same day.

After acute starvation of SKOV-3 and T cells in deprived media for 72 hours, SKOV-3 viability decreased by 53% when SKOV-3 cells and lymphocytes were treated with EpCAM BiTE in control medium containing all amino acids. Unexpectedly, amino acid-free medium resulted in higher EpCAM BiTE-mediated T cell killing of SKOV-3, whilst depletion of lysine and serine from medium decreased killing (Figure 3.7A). HLA-dependent cytolysis of tumour cells with the $CD8^+$ T cell clone resulted in the death of more than 80% of SKOV-3 cells after 72 hours. This activity decreased in the absence of arginine, cysteine, glutamine or lysine. Addition of the EpCAM BiTE to cultures containing the $CD8^+$ T cell clone and SKOV-3 cells potentiated killing, with death of more than 95% of cells. A reduction in death was observed with depletion of the aforementioned amino acids (Figure 3.7B).

Due to the unexpected finding that medium with no amino acids resulted in better killing of SKOV-3 cells by T cells activated with the EpCAM BiTE, we reasoned that high cancer cell stress due to starvation could actually improve killing by T cells. To further investigate these findings, we modified the assay by starving the T cells, either lymphocytes derived from PBMCs or the $CD8^+$ T cell clone, in amino acid-depleted media for 24 hours before addition to the tumour cells. SKOV-3 viability decreased by 65% in medium containing all amino acids compared to only 53% with acutely-starved lymphocytes (Figure 3.8A vs Figure 3.7A). Serine depletion slightly hampered cytolytic activity, but this was not as significant as previously observed in acutely starved T cell assays. Chronic starvation of T cells in medium without amino acids, glutamine-free medium and tryptophan-free medium resulted in improved EpCAM-induced T cell cytotoxicity (Figure 3.8A). This observation was not restricted to apoptosis induced by the EpCAM BiTE, as chronic starvation of the $CD8^+$ T cell clone also resulted in improved HLA-dependent T cell killing of SKOV-3 cells (Figure 3.8B).

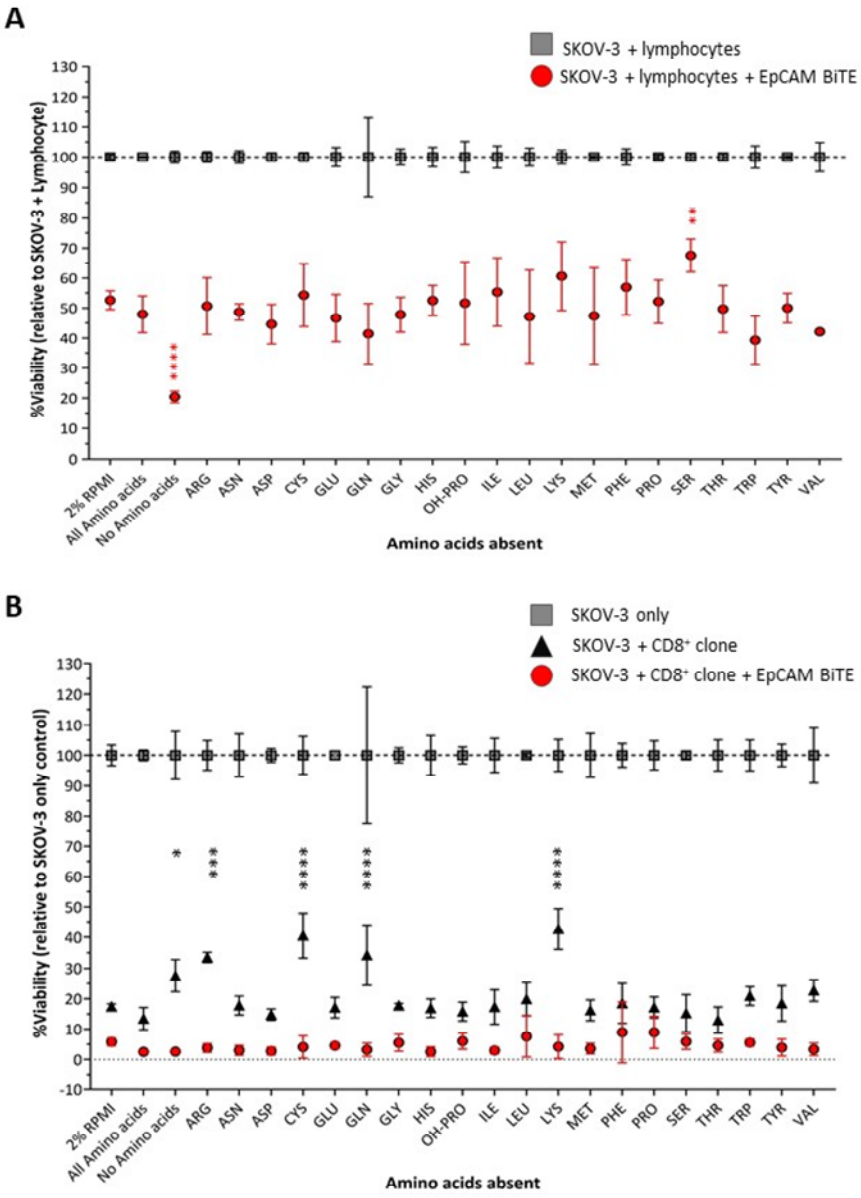


Figure 3.7 HLA-dependent T cell killing is reduced by the absence of arginine, cysteine, glutamine and lysine, whilst EpCAM-BiTE induced killing is only affected by serine loss. (A) PrestoBlue was used to determine SKOV-3 viability after co-culture with acutely starved lymphocytes (E:T, 5:1) for 72 hours. Those co-cultures treated with BiTE-containing supernatant were quantified relative to co-cultures accounting for non-specific SKOV-3 cell death in co-culture with lymphocytes to account for sticky effector cells that may have become adherent. In **(B)** the co-culture is with acutely starved $CD8^+$ T cell clone (E:T, 5:1) for 72 hours. Viability is quantified relative to SKOV-3 cells alone accounting for non-specific SKOV-3 cell death due to absent amino acids. Data shows the mean ± SD of biological triplicates. Statistical significance was assessed by two-way ANOVA followed by Dunnett's post-hoc analysis, each treatment was compared to the relevant "All Amino acids" culture condition (*, $p < 0.05$; **, $p < 0.01$; ***, $p < 0.001$; ****, $p < 0.0001$; ns, non-significant).

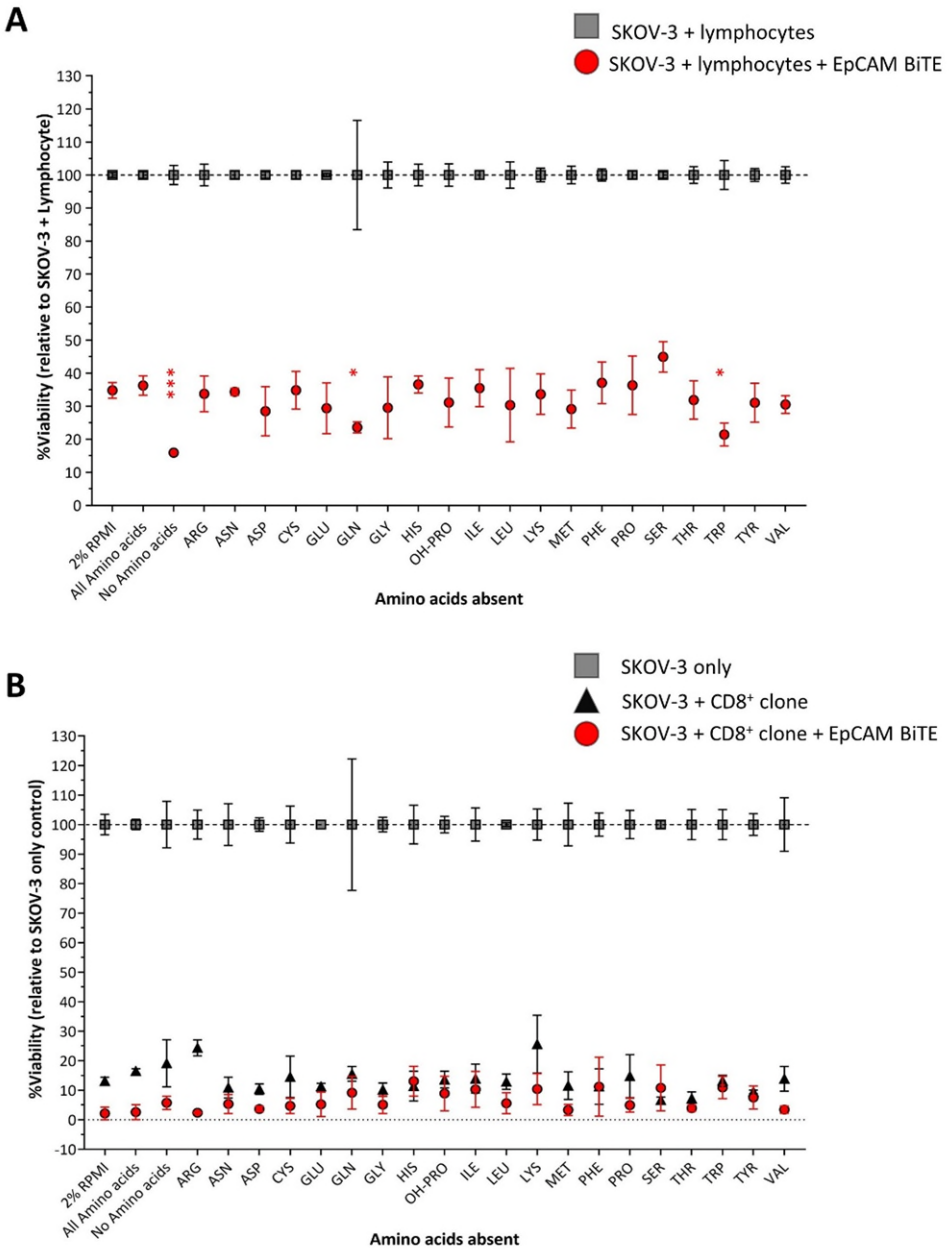


Figure 3.8 T cell starvation before addition to SKOV-3 cells results in more potent T cell-directed killing. (A) Lymphocytes were starved for 24 hours in amino acid depleted mediums before addition to SKOV-3 cells with or without BiTE-containing supernatant. SKOV-3 viability was assessed 72 hours later using the PrestoBlue reagent and relative fluorescence was measured. In **(B)** the ST8.24 $CD8^+$ T cell clone was starved for 24 hours before addition to SKOV-3 cells (5:1) with or without BiTE. Data shows the mean ± SD of biological triplicates. Statistical significance was assessed by two-way ANOVA followed by Dunnett's post-hoc analysis, each treatment was compared to the relevant "All Amino acids" culture condition (*, $p < 0.05$; **, $p < 0.01$; ***, $p < 0.001$; ****, $p < 0.0001$; ns, non-significant).

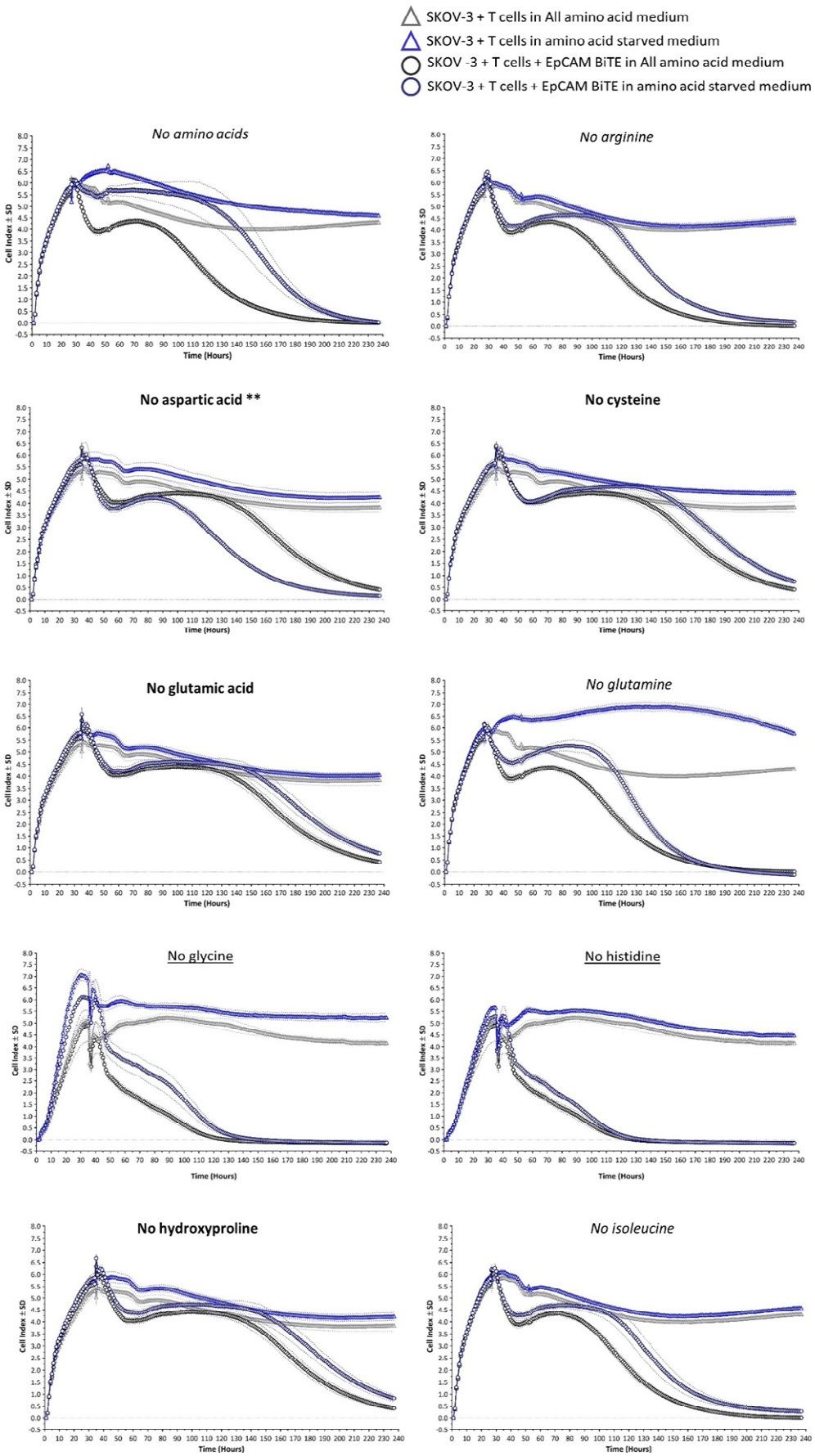
Together, these data suggest the EpCAM BiTE remains active despite being cultured in amino acid-free medium or medium depleted of glutamine. Depletion of glutamine and tryptophan, the amino acids that appeared to play the most important role expression of CD25 and GrB, resulted in the highest improvement of cytolytic ability. Furthermore, nutrient starvation improved tumour cell killing in both a HLA-dependent manner by the $CD8^+$ T cell clone and in an HLA-independent manner by the EpCAM BiTE. These findings are, however, based on a single timepoint and do not capture the kinetics of killing in nutrient-depleted medium.

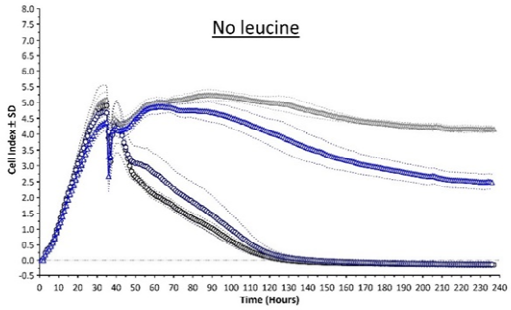
3.2.5 Medium deficient in aspartic acid medium resulted in faster tumour cell apoptosis

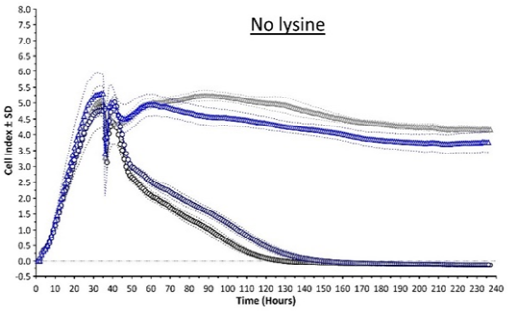
To monitor tumour cell killing by BiTE-activated T cells in real-time an xCELLigence assay was performed as described in section 2.6.5. The goal of this assay was to reveal whether any of the amino acids cause a delay in killing that was not captured in the static assay performed above.

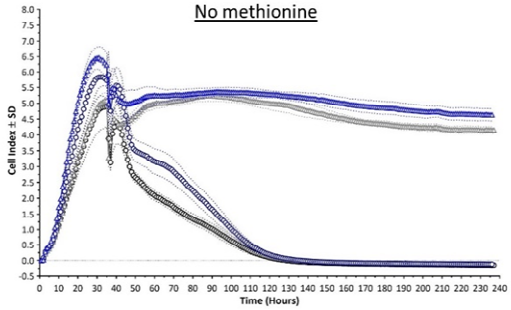
Cytolysis of SKOV-3 cells was observed in the presence of the EpCAM BiTE when cultured in medium with all tested amino acids missing (Figure 3.9). Each plot represents an assay undertaken in medium devoid of a particular amino acid compared with culture medium containing all amino acids at concentrations found in the standard formulation of RPMI-1640 medium (R8758). Amino acid-free medium and medium depleted of serine and valine resulted in a delay of more than 24 hours for SKOV-3 cytotoxicity. Half of the media tested with depleted amino acids resulted in slower killing kinetics, though these media all killed more than 75% of tumour cells within 15 hours of the same percentage of killing in the control medium. Medium with no aspartic acid resulted in faster killing kinetics of SKOV-3 cells with the EpCAM BiTE.

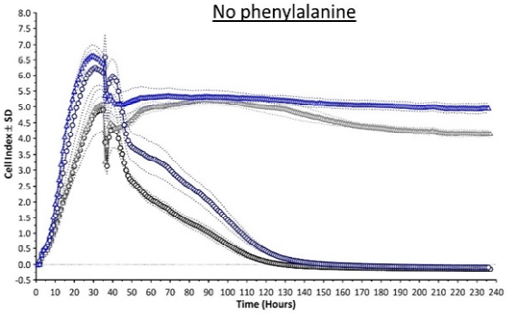
Taken together, these data suggest the EpCAM BiTE activated T cells to kill tumour cells despite being starved of essential nutrients for activation and cytolytic potential. The kinetics of killing was slower but most, if not all tumour cells, were killed to the same extent as in the presence of supra-physiological levels of nutrients, as in RPMI-1640 medium. Interestingly, we found that aspartic acid may play a role in inhibiting or delaying killing potential, and that serine and valine were most important for cytolytic ability, despite earlier results on activation and cytolytic expression profiles suggesting that glutamine depletion would have the strongest effect (Figures 3.3 - 3.5).

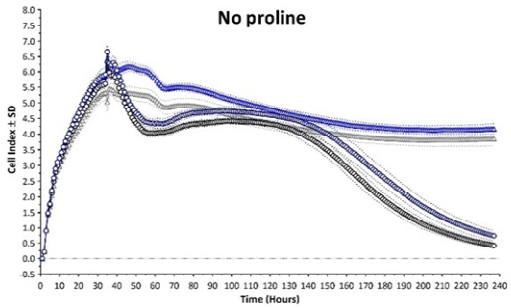

SKOV-3 + T cells in All amino acid medium
SKOV-3 + T cells in amino acid starved medium
SKOV -3 + T cells + EpCAM BiTE in All amino acid medium
SKOV-3 + T cells + EpCAM BiTE in amino acid starved medium
No amino acids
No arginine
No aspartic acid **
No cysteine
No glutamic acid
No glutamine
No glycine
No histidine
No hydroxyproline
No isoleucine
Cell Index ± SD
Time (Hours)

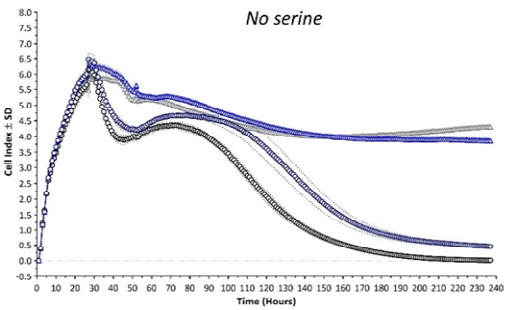

No leucine
Cell Index ± SD
Time (Hours)

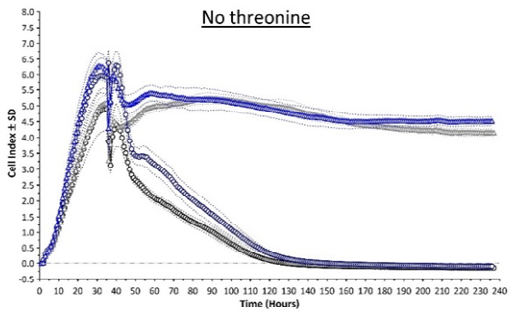

No lysine
Cell Index ± SD
Time (Hours)

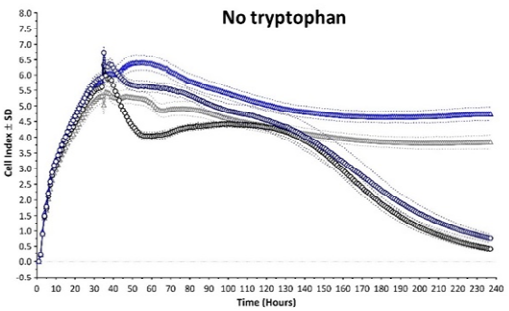

No methionine
Cell Index ± SD
Time (Hours)

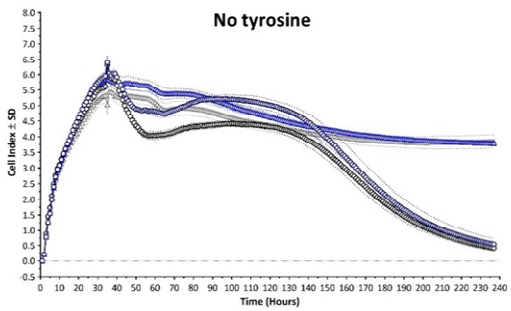

No phenylalanine
Cell Index ± SD
Time (Hours)


No proline
Cell Index ± SD
Time (Hours)


No serine
Cell Index ± SD
Time (Hours)


No threonine
Cell Index ± SD
Time (Hours)


No tryptophan
Cell Index ± SD
Time (Hours)


No tyrosine
Cell Index ± SD
Time (Hours)

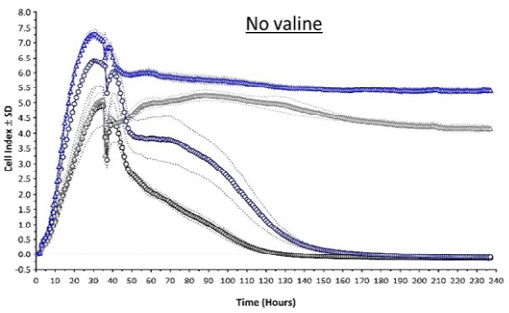

No valine
Cell Index ± SD
Time (Hours)

Figure 3.9 Real-time monitoring shows EpCAM-targeted BiTE induces T cell-dependent cytotoxicity faster in medium without aspartic acid. The viability of 1.5 x 10^4 SKOV-3 cells was monitored in real time over 240 hours by an xCELLigence based cytotoxicity assay. Data presented is SKOV-3 cells and $CD3^+$ T cells with and without EpCAM BiTE cultured in medium without named amino acids (blue) compared to an all amino acid control (black). Titles in italics represent one experimental plate, titles underlined represent a second and titles that are bold represent a third each used a different batch of EpCAM BiTE and a different donor of T cells. Electrical impedance was measured at 15 minute intervals. Each condition was measured in biological quadruplicate and represented as the mean ± SD (dashed lines).

3.2.6 EnAd viral replication is diminished through loss of amino acids

The replication of EnAd, used as a delivery vehicle to express BiTEs at the site of a tumour, may also suffer from nutrient deprivation in the tumour microenvironment. To assess this, we used the same medium depleted of individual amino acids to quantify GFP expression following infection with EnAd-SA-GFP, where GFP expression is driven by the MLP, a surrogate for viral replication and indicative of cell permissivity to the virus. As the virus relies on the host cell's machinery for successful viral replication, we first assessed if there were differences in nutrient sensing between uninfected and infected tumour cells, as this could account for differences in response to depleted amino acids. We chose to analyse the expression of ATF4, a transcription factor induced by the phosphorylation activity of GCN2 and activated when low amino acid levels are sensed.

We confirmed that EnAd infection strongly inhibits ATF4 expression in response to glutamine starvation (Figure 3.10). A reduction was observed after 24 hours in A549 cells, suggesting inhibition occurred during the early phase of the virus life cycle and was most likely mediated by early proteins; knockdown of ATF4 persisted throughout the infection (up to three days shown).

The percentage of A549 cells positive for GFP expression reached 85% in medium containing all amino acids, falling to 10% of cells when infection occurred in amino acid-free medium

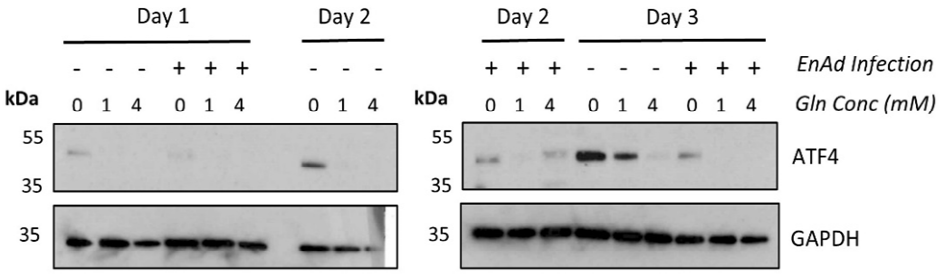
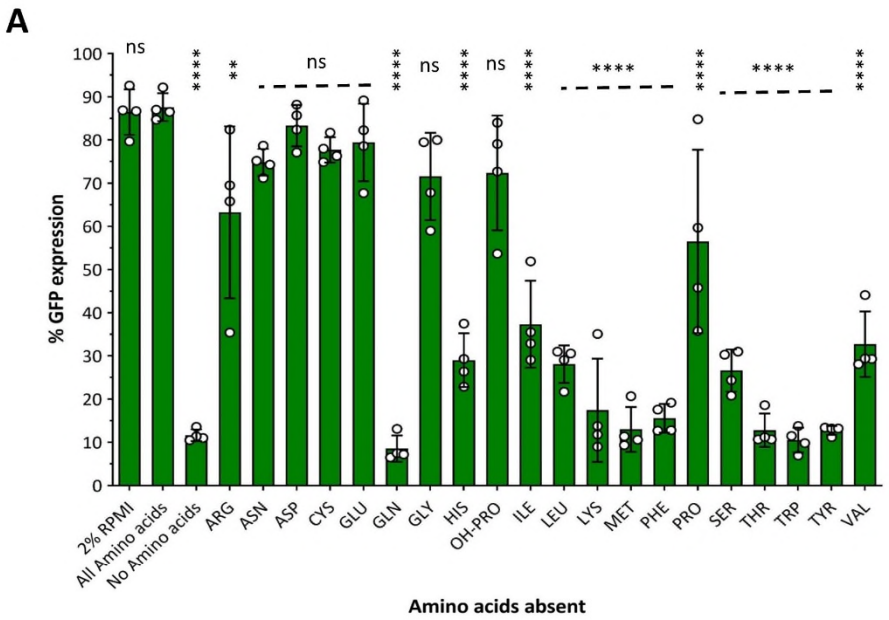
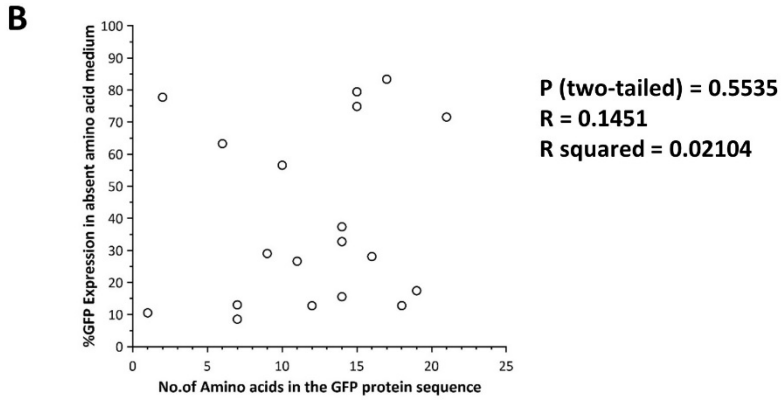


Figure 3.10 EnAd infection switches off the nutrient starvation response and viral replication is affected by amino acid loss. A549 cells cultured in 0, 1 or 4 mM glutamine were infected with EnAd at MOI 1. Lysates were harvested after either, 24 hpi, 48 hpi or 72 hpi and subject to ATF4 (38 kDa) detection by western blot. α-GAPDH (34 kDa) was used as a loading control.

(Figure 3.11A). In twelve of the twenty media conditions tested that were depleted of one amino acid, 35% of cells were positive for GFP after infection. A Pearson's correlation analysis did not suggest any correlation between media starved of an amino acid which caused a reduction in GFP expression and the frequency of the same amino acid in the GFP amino acid sequence, suggesting inhibition of replication was not due to a lack of amino acids for GFP translation (Figure 3.11B).

As uninfected A549 cells struggled to proliferate in amino acid-depleted medium, virus replication may be inhibited due to a lack of viable cells. In a similar assay as above using SKOV-3 cells, a higher proportion of the tested media depleted of single amino acids resulted in a significant reduction of GFP-positive SKOV-3 cells (Figure 3.11C). Only the absence of asparagine appeared to have no effect on viral replication in either cell line tested. Glutamine, methionine and tyrosine-depleted media had the largest impact on GFP expression in both cell lines in addition to amino acid-free medium.


A
% GFP expression
Amino acids absent
2% RPMI
All Amino acids
No Amino acids
ARG
ASN
ASP
CYS
GLU
GLN
GLY
HIS
OH-PRO
ILE
LEU
LYS
MET
PHE
PRO
SER
THR
TRP
TYR
VAL


B
%GFP Expression in absent amino acid medium
No.of Amino acids in the GFP protein sequence
P (two-tailed) = 0.5535
R = 0.1451
R squared = 0.02104

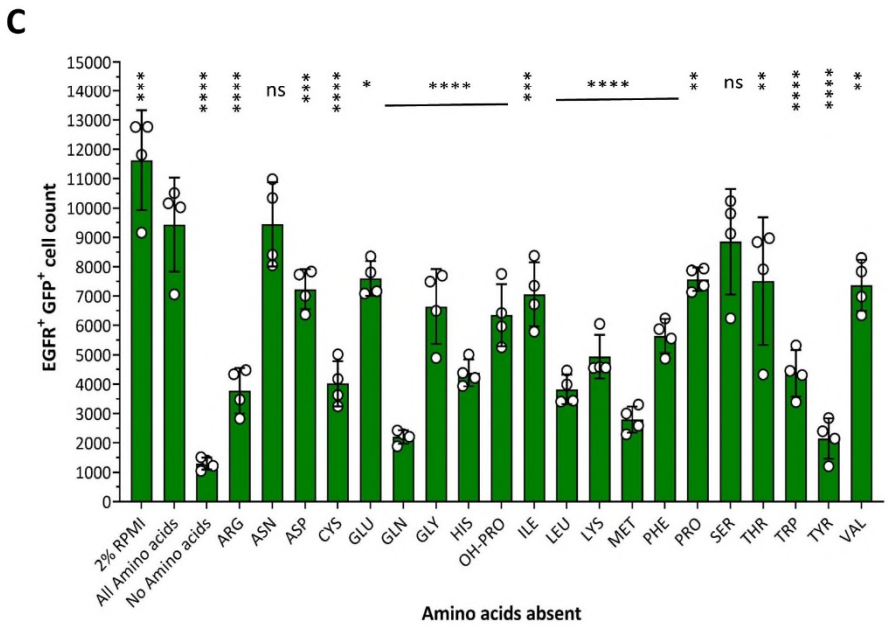

C
EGFR+ GFP+ cell count
Amino acids absent
2% RPMI
All Amino acids
No Amino acids
ARG
ASN
ASP
CYS
GLU
GLN
GLY
HIS
OH-PRO
ILE
LEU
LYS
MET
PHE
PRO
SER
THR
TRP
TYR
VAL

Figure 3.11 EnAd infection switches off the nutrient starvation response and viral replication is affected by amino acid loss. (A) Percentage of cells expressing GFP were measured by flow cytometry five days after infection of A549 cells with EnAd-SA-GFP at an MOI 1. Data shows the mean ± SD of biological quadruplicates. Statistical significance was assessed using a one-way ANOVA test with Dunnett's post-hoc analysis with each condition compared to the "All Amino acids" control, (*, $p < 0.05$; **, $p < 0.01$; ***, $p < 0.001$; ****, $p < 0.0001$; ns, non-significant). **(B)** Percentage of cells expressing GFP was plotted against the frequency of the amino acid appearing in the GFP amino acid sequence and missing from the medium and statistical analysis was performed by Pearson's correlation test. **(C)** GFP expressing EGFR-positive cells were measured by flow cytometry eight days after infection of SKOV-3 cells with EnAd-SA-GFP at an MOI 10 in culture mediums with amino acids absent. Data shows the mean ± SD of biological quadruplicates. Statistical significance was assessed using a one-way ANOVA test with Dunnett's post-hoc analysis with each condition compared to the "All Amino acids" control, (*, $p < 0.05$; **, $p < 0.01$; ***, $p < 0.001$; ****, $p < 0.0001$; ns, non-significant).

Our data revealed that the vast majority of amino acids in complete medium appeared to be important for viral replication in tumour cell lines representing either a glycolytic phenotype, such as A549 cells, or those that use both glycolysis and OXPHOS, such as SKOV-3 cells. ATF4 expression patterns in uninfected and infected cells confirmed that the starvation response in host cells was switched off during infection, most likely to hinder early apoptosis of cells before virus propagation is complete.

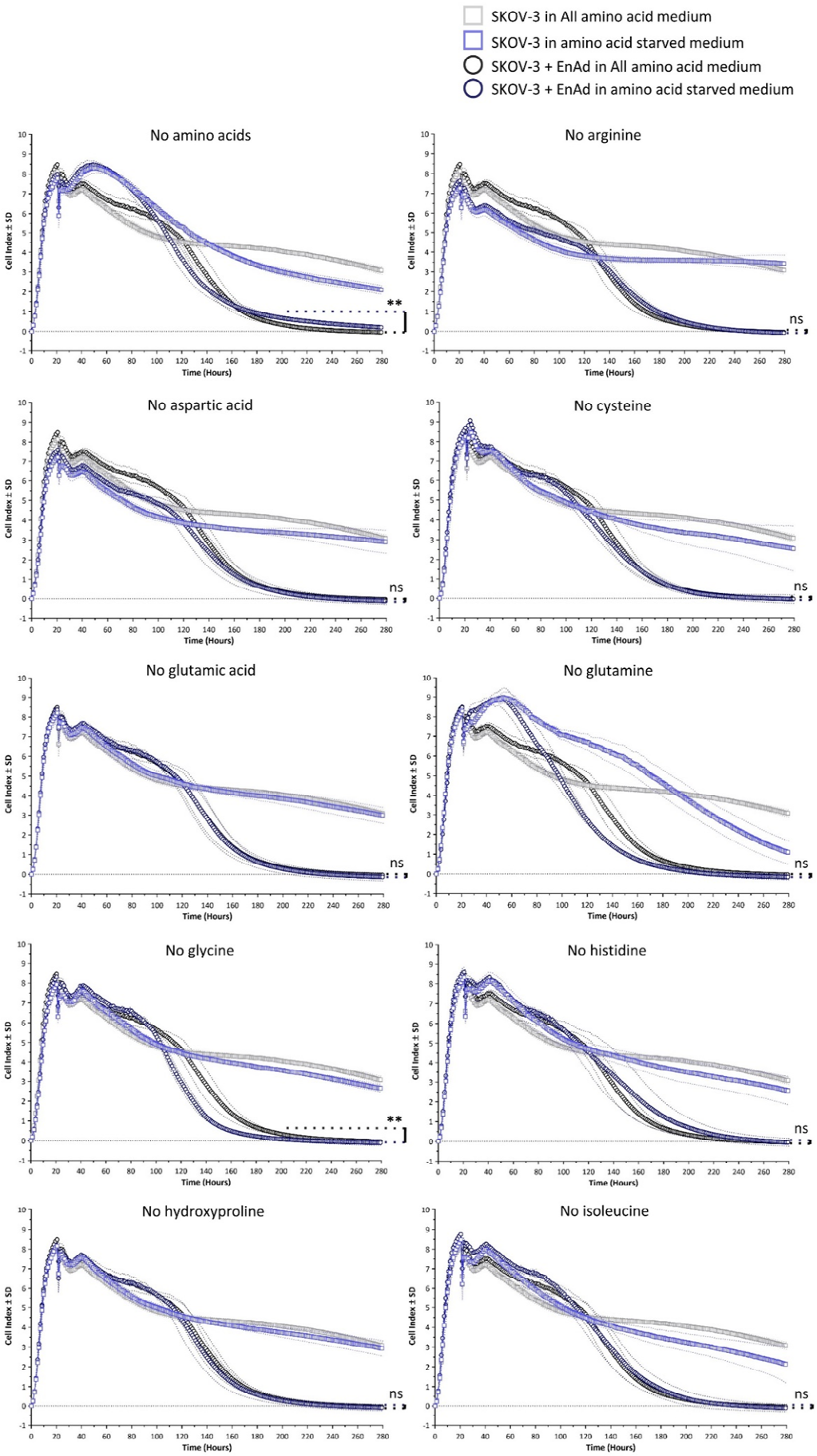
3.2.7 Decreases in cytolysis by EnAd reflect decreased levels of viral replication

The ultimate therapeutic aim of EnAd is to lyse cells and release viral progeny to infect and spread to other tumour cells. We next assessed if the impact on viral replication, as indicated by GFP expression, translated into reduced cytolytic ability of EnAd in the same media depleted of amino acids. We used xCELLigence to monitor viability of SKOV-3 cells over 12 days, allowing us to precisely monitor killing kinetics.

Each plot shown in Figure 3.12 represents infection of SKOV-3 cells in medium depleted of single amino acids compared with medium containing all amino acids. Viability was compared in the same conditions with uninfected SKOV-3 cells. Significance was assessed at 200 hours,

representing the timepoint at which more than 99% of cells were lysed in the control wells containing medium with all amino acids. A reduction in lysis was observed in media depleted of all amino acids, methionine, threonine, tryptophan or tyrosine. Surprisingly, an absence of glutamine did not result in significantly reduced lysis. The absence of either glycine or serine resulted in faster lysis of SKOV-3 cells.

These data suggest that although viral replication is severely affected by the depletion of single amino acids, subsequent cytolysis remains active. Though methionine, tryptophan and tyrosine appear to be most important factors for lysis, cell killing still occurs in the absence of these amino acids, albeit with a delay of more than 40 hours. The absence of glutamine did not reduce lysis, as expected from previous findings in our lab (Dyer et al. 2019), though uninfected SKOV-3 cells died in glutamine-free medium. Our explanation for this is that fewer cells were available for EnAd infection in glutamine-depleted wells and, given that the same number of virus particles were added for all conditions, the kinetics of viral lysis may have occurred faster due to a higher multiplicity of infection compared to control wells containing all amino acids.


SKOV-3 in All amino acid medium
SKOV-3 in amino acid starved medium
SKOV-3 + EnAd in All amino acid medium
SKOV-3 + EnAd in amino acid starved medium
No amino acids
No arginine
No aspartic acid
No cysteine
No glutamic acid
No glutamine
No glycine
No histidine
No hydroxyproline
No isoleucine
Cell Index ± SD
Time (Hours)
**
ns

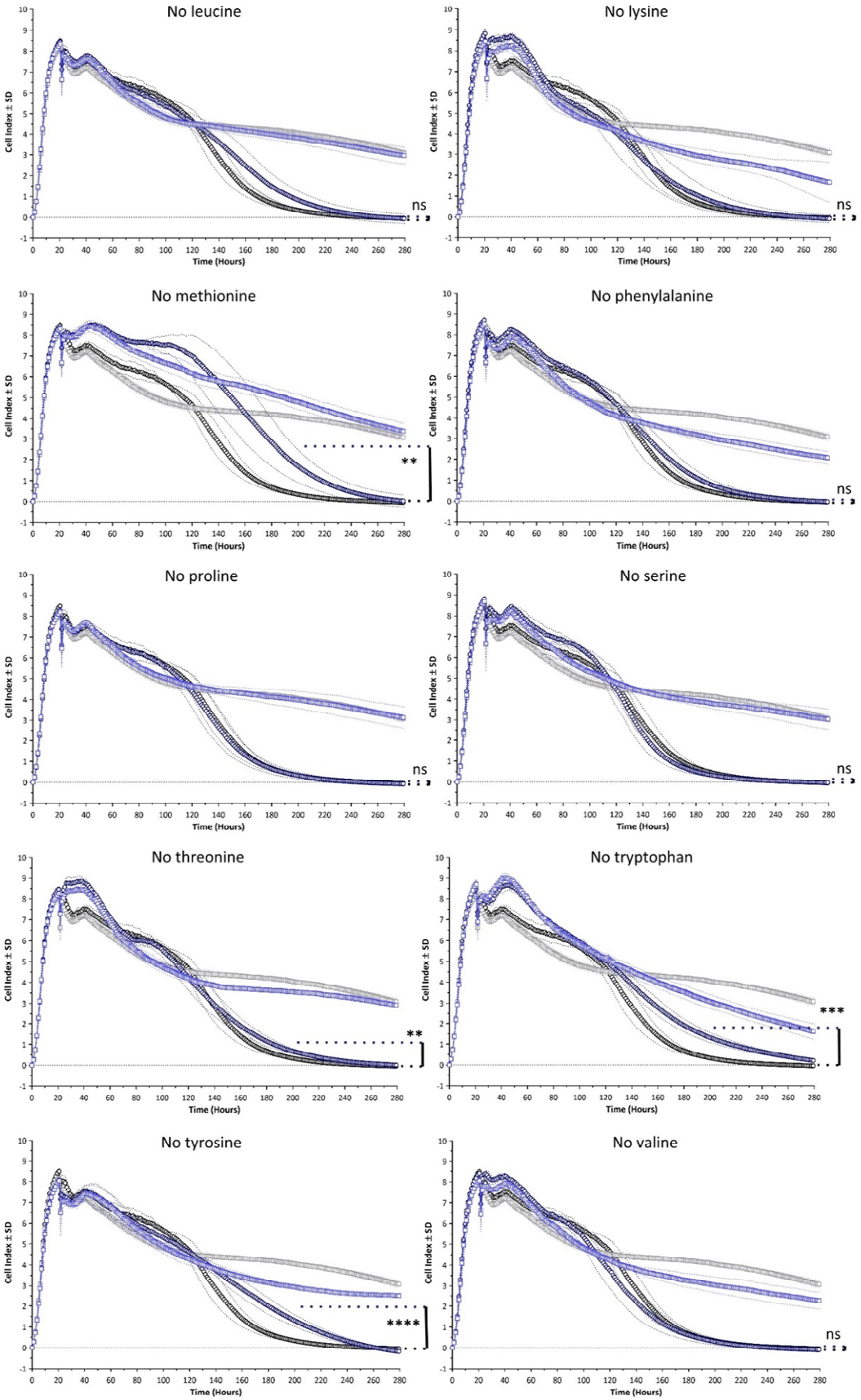

No leucine
No lysine
No methionine
No phenylalanine
No proline
No serine
No threonine
No tryptophan
No tyrosine
No valine
Cell Index ± SD
Time (Hours)
ns
**
***
****

Figure 3.12 Real-time monitoring shows EnAd-induced tumour cell lysis is slower when methionine, threonine, tryptophan and tyrosine are absent. SKOV-3 cell viability was monitored over 280 hours, 1.0 x 10^4 cells were infected at an MOI 15 with EnAd. Data presented is SKOV-3 cells +/- EnAd infection in medium without named amino acids (blue) compared to an all amino acids control (black). Electrical impedance was measured at 15 minute intervals, each condition was measured in biological quadruplicate and represented as the mean ± SD (dashed lines). Statistical significance was assessed using a one-way ANOVA test with Tukey's post-hoc analysis. Significance presented was the experimental medium with EnAd compared to the "All Amino acids + EnAd" control at the timepoint 200 hours where the control had killed > 95% cells, (*, $p < 0.05$; **, $p < 0.01$; ***, $p < 0.001$; ****, $p < 0.0001$; ns, non-significant).

3.2.8 Pathological nutrient levels of the TME can be mirrored using *ex vivo* ascites fluid

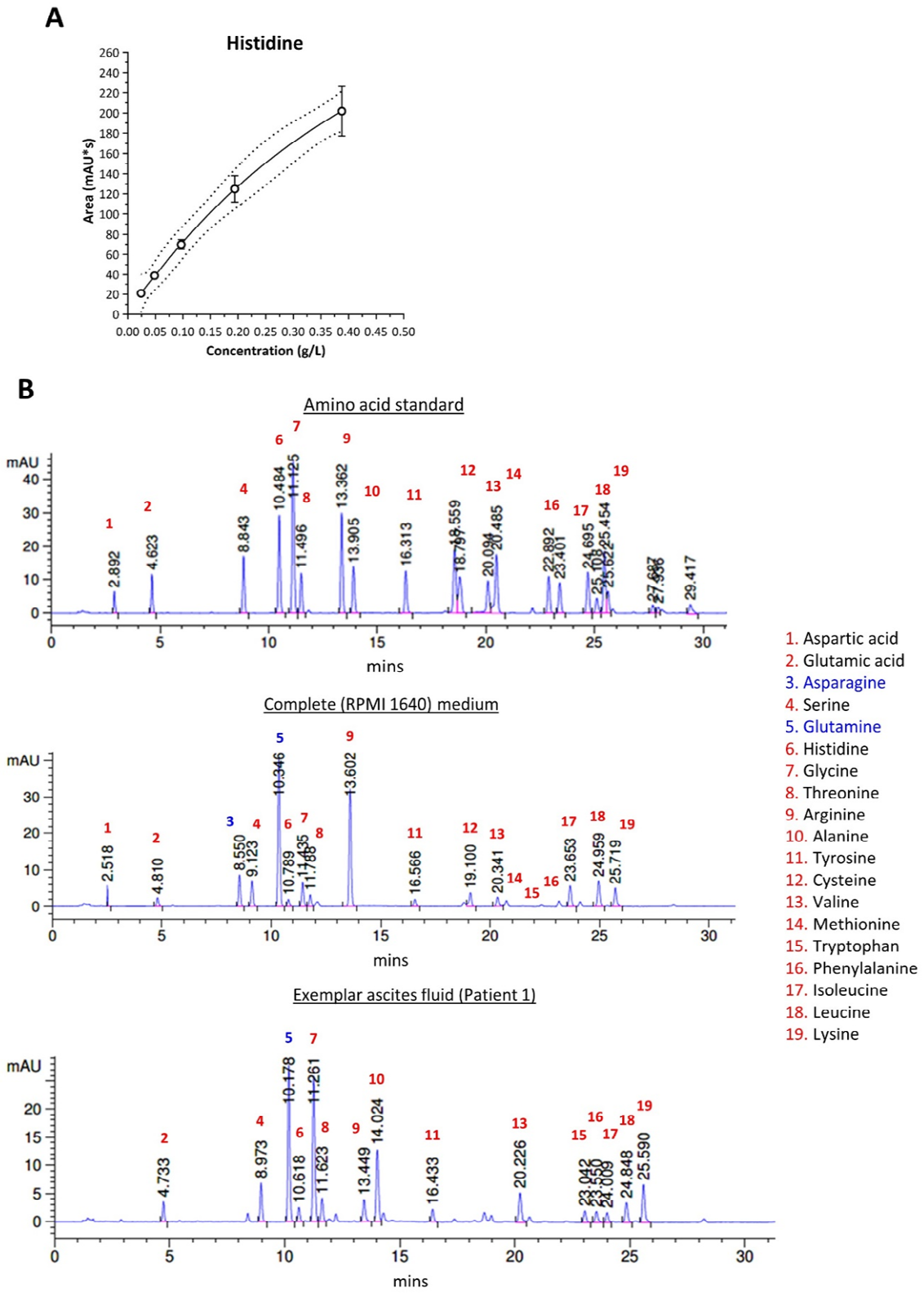
In the first part of this chapter, we identified individual amino acids that were essential for EnAd viral replication and cytolysis, and the functional response of EpCAM BiTE-induced T cell killing. However, medium containing supra-physiological levels of amino acids depleted of a single amino acid does not accurately represent the microenvironment of a tumour mass. In reality, the TME contains fluctuating levels of nutrients, which is influenced by many variables. These include patient-related environmental factors, such as diet or time of day, and the characteristics of the tumour, such as vasculature and stromal cell network. To properly assess how our proposed therapeutics will perform in an environment with realistic levels of amino acids, we used acellular malignant patient ascites fluids as clinically relevant *ex vivo* models.

In 1948, Fischer developed a method to separate low and high molecular weight fractions of blood plasma to identify the constituents aiding cell growth during the early development of cell culture media (A. Fischer 1948). Here, we have adapted Fischer's method to isolate the low molecular weight fraction of ascites fluids containing amino acids by filtering the fluid through a 3 kDa molecular weight cut-off centrifugal unit. This separation allowed us to simplify the assay and focus on key experimental criteria, removing other components that could otherwise impact BiTE activity or EnAd replication. For example, ascites fluids contain

immunosuppressive factors including IL-6 (21 kDa), IL-10 (18 kDa) and TGF-β (13 kDa) (Freedman et al. 2017; Scott et al. 2020).

We quantified the amount of each identifiable amino acid present in 21 different filtered patient ascites samples using HPLC as described in section 2.7.3. The concentration of amino acids found in fluids were compared with the concentration in complete medium. Amino acid concentrations in fluids were determined using standard curves of each amino acid prepared by serially diluting amino acid standards of known concentration (Figure 3.13A, all standard curves are in Figure 7.1, Appendix III). Examples of HPLC chromatograms for an amino acid standard solution (2.5 μmol/mL), complete medium (RPMI 1640) and an example of a patient ascites fluid (Patient 1) are shown in Figure 3.13B. Figure 3.13C shows the concentration of each amino acid identified relative to the concentration measured in complete medium. Noticeably, glutamine levels in all ascites fluids were three-fold lower than in complete medium, whilst arginine levels were six-fold lower. Glutamic acid, glycine, and valine levels are higher in most fluids than in complete medium. Valine levels were too low to measure in complete medium by this method.

Six ascites fluids (Asc1-6) were chosen as *ex vivo* models to represent the TME. Fluids were chosen based on their variability in glutamine concentration, with three high- and three low-glutamine fluids compared to other fluids. In addition, the fluids chosen had variable levels of arginine, serine, lysine, and valine. Low levels of arginine (Asc4) reduced HLA-dependent T cell cytolysis. Low levels of serine (Asc5 and Asc6) reduced cytotoxicity driven by EpCAM BiTE-activated T cells but increased EnAd cytolytic activity. Low levels of valine (Asc4) reduced EpCAM BiTE-induced cytolysis. Low levels of lysine (Asc3 and Asc4) reduced both HLA-dependent and HLA-independent cytolysis.


A
Histidine
Area (mAU*s)
Concentration (g/L)
B
Amino acid standard
mAU
mins
Complete (RPMI 1640) medium
mAU
mins
Exemplar ascites fluid (Patient 1)
mAU
mins
1. Aspartic acid
2. Glutamic acid
3. Asparagine
4. Serine
5. Glutamine
6. Histidine
7. Glycine
8. Threonine
9. Arginine
10. Alanine
11. Tyrosine
12. Cysteine
13. Valine
14. Methionine
15. Tryptophan
16. Phenylalanine
17. Isoleucine
18. Leucine
19. Lysine

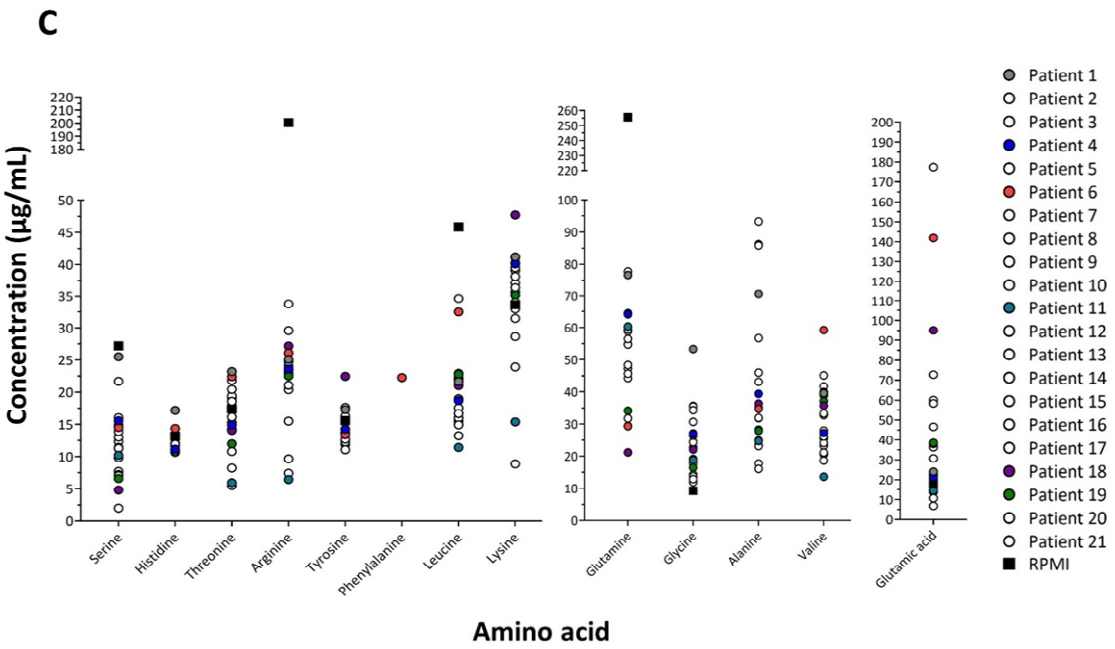


Figure 3.13 Characterisation of amino acid levels in filtered acellular ascites fluids. (A) An example of a standard curve of a series of dilutions of known concentration of histidine against the area measured for each following HPLC analysis of amino acids. Performed using a 250 mm, Agilent ZORBAX Eclipse Plus C18 5 µm column with OPA and FMOC reagents over a 30 minute method using a borate buffer gradient. **(B)** HPLC traces produced from analysing an amino acid standard solution of known concentration, complete RPMI 1640 medium and an exemplar filtered patient ascites fluid (patient 1). The key indicates the amino acids identified in each trace. **(C)** Amino acid concentrations in 21 ascites fluids were calculated based on standard curves of each amino acid using standards with known concentrations. Ascites fluids 1-6 are highlighted as coloured dots (patient 1, Asc1, grey; patient 4, Asc2, blue; patient 6, Asc3, red; patient 11, Asc4, turquoise; patient 18, Asc5, purple; patient 19, Asc6, green) and RPMI 1640 medium amino acid concentrations are highlighted as a black square if applicable, the rest of the ascites fluids tested are white dots.

3.2.9 EpCAM BiTE-induced T cell activation is unhindered by ascites fluids devoid of cytokines and chemokines

To characterise EpCAM BiTE activity in *ex vivo* ascites fluids, we quantified T cell activation after incubation with either the EpCAM BiTE or CD3/CD28 beads. Using 100% ascites fluids in experiments of co-cultures of tumour cells with T cells induced cell death, as reported previously by Dr Joshua Freedman (unpublished). Based on these recommendations, ascites fluids were mixed at a ratio of 1:1 (v/v) with amino acid-free medium for each assay. Hence the reason for two controls used in the remaining studies of this chapter. 2% RPMI is normal

complete medium (RPMI-1640), and 1:1 No AA and 2% RPMI is complete medium mixed at a ratio of 1:1 (v/v) with amino acid-free medium to control for the ascites mixes. Additionally, DLD-1 colorectal tumour cells were used as the target cell line for activity assays for EnAd or the EpCAM BiTE in exudate fluids. This cell line was chosen due to its higher levels of EpCAM expression and increased permissivity to EnAd compared to SKOV-3 cells.

A significant increase in T cell counts was observed when complete medium was at 50% v/v as a control, a surprising result given RPMI 1640 medium was developed for lymphocyte culture (T. Yao and Asayama 2017) (Figure 3.14A). The percentage of T cells expressing CD25 reached 75% for $CD4^+$ T cells and 85% for $CD8a^+$ T cells after incubation with the EpCAM BiTE in 50% complete medium (v/v). In four out of the six ascites samples, we observed a significant reduction in the percentage of $CD4^+$ T cells expressing CD25, though the percentage was above 60% in all samples. In $CD8^+$ T cells, the same fluids - Asc2, Asc3 and Asc4 - resulted in a reduction in the percentage of cells expressing CD25 but none dropped below 80% (Figure 3.14B).

Although ascites fluids were observed to inhibit T cell activation by the EpCAM BiTE, the levels reached in the cytotoxic T cell subset $CD8^+$ remained higher than those induced by CD3/CD28 beads in complete medium. This suggests BiTE-induced activation in patient fluids can mediate tumour cell killing, as CD3/CD28 beads can activate T cell cytotoxicity at this level observed in complete medium. The low levels of glutamine in Asc3, Asc5 and Asc6 were still high enough to induce T cell activation.

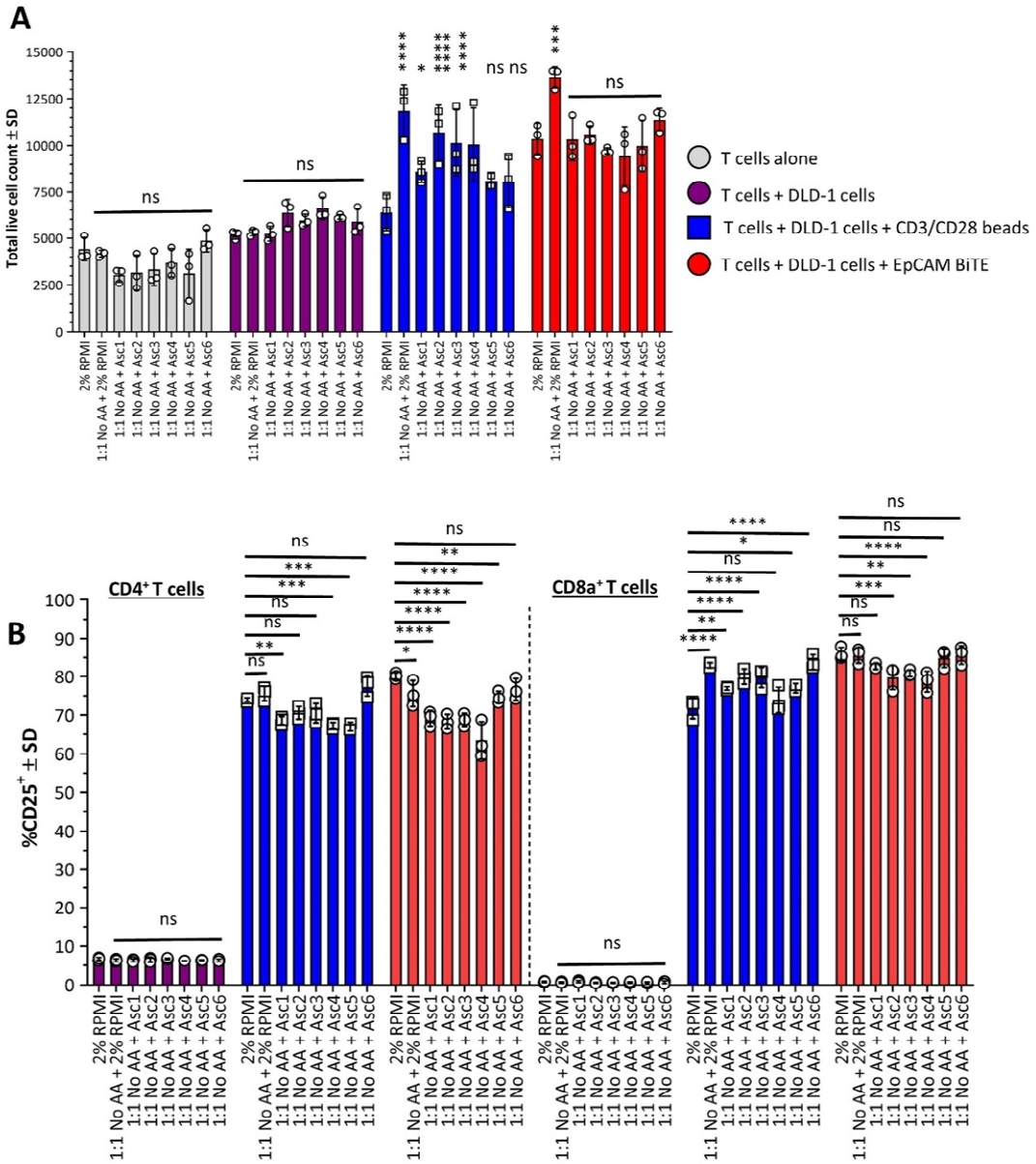


Figure 3.14 T cell activation induced by the EpCAM BiTE and CD3/CD28 beads is slightly reduced in patient ascites medium. $CD3^+$ T cells were co-cultured with DLD-1 cells (5:1) and T cells were activated by CD3/CD28 beads (blue) or the EpCAM BiTE (red). T cell viability and activation were assessed by flow cytometry after 24 hours of culture in six different patient ascites fluids (1:1 v/v in RPMI without amino acids) compared with complete medium (RPMI with 2% FBS) and 50% RPMI (1:1 v/v in RPMI without amino acids). The percentage of live T cells **(A)** were measured in addition to the percentage of CD25-positive T cells **(B)** in both $CD4^+$ and $CD8^+$ T cell subsets. Each condition was measured in biological triplicate and data is represented as the mean ± SD. Significance was assessed by a two-way ANOVA test with Dunnett's post-hoc analysis comparing with the "2% RPMI" complete medium condition (*, $p < 0.05$; **, $p < 0.01$; ***, $p < 0.001$; ****, $p < 0.0001$; ns, non-significant).

3.2.10 Cytotoxicity potential of T cells after culture in EpCAM BiTE and exudate fluids is not changed compared to control medium

We characterised the cytotoxic potential of activated T cells after incubation with the EpCAM BiTE in ascites fluids as a model for the TME.

There was no significant change in the percentage of IFNγ expressed from either T cell subset after treatment with the EpCAM BiTE. The average percentage measured was 5%, increasing to 7.5% and 10% for Asc1 and Asc2, respectively, in $CD4^+$ T cells. In $CD8a^+$ T cells, Asc2 was observed to increase from an average of 10% to 13% (Figure 3.15A). These fluids did not have the same effect following activation with CD3/CD28 beads. Complete medium at 50% v/v resulted in a 10% increase in the percentage of IFNγ-positive $CD4^+$ cells. In the same figure, the same trend was apparent for the $CD8a^+$ T cell subset at slightly higher levels of expression following activation with CD3/CD28 beads.

Together, these data suggest that the cytolytic potential induced by BiTE activation of T cells is not impeded by ascites fluids used as clinically relevant models for amino acid levels found in the TME.

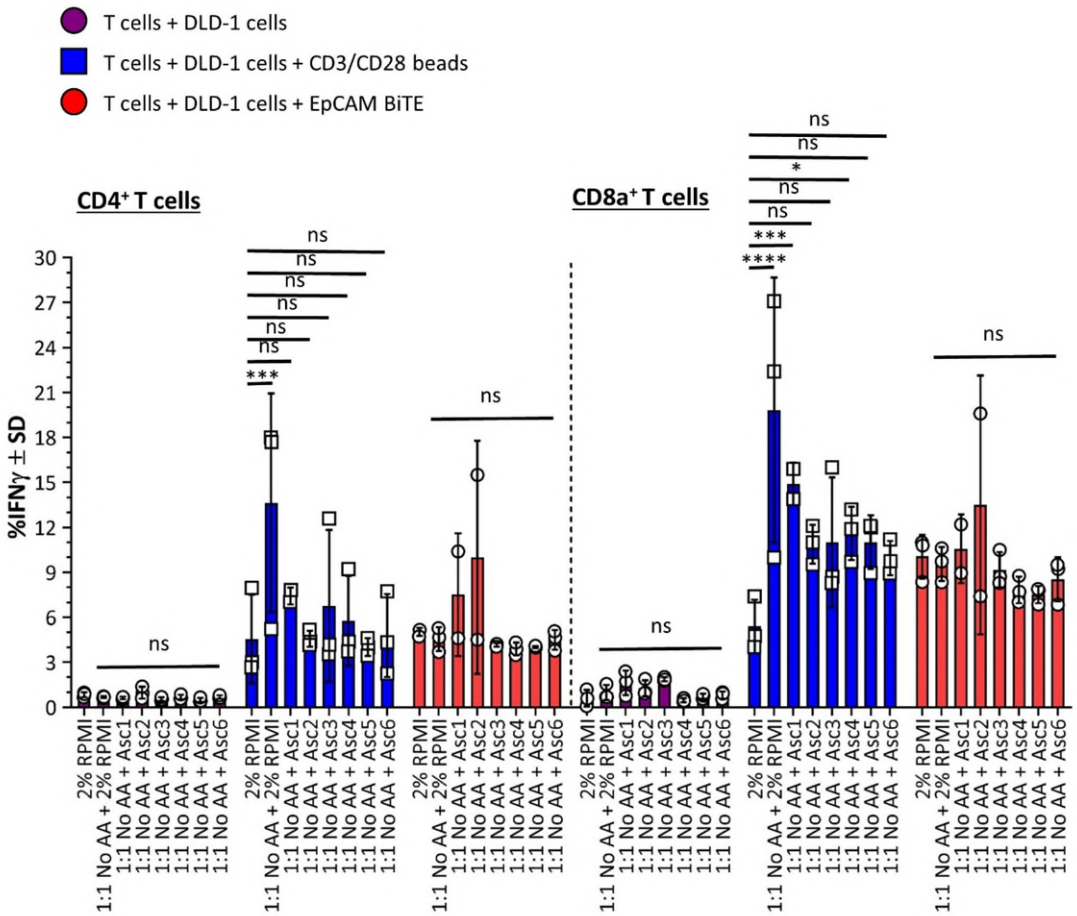


Figure 3.15 T cell cytotoxicity induced by the EpCAM BiTE and CD3/CD28 beads remains high in patient ascites medium. $CD3^+$ T cells were co-cultured with DLD-1 cells (5:1) and T cells activated by CD3/CD28 beads (blue) or the EpCAM BiTE (red). The percentage of IFNγ-positive T cells in both T cell subsets to represent T cell cytotoxicity potential was assessed by flow cytometry after 6 hours of culture in six different patient ascites fluids (1:1 v/v in RPMI without amino acids) compared with complete medium (RPMI with 2% FBS) and 50% RPMI (1:1 v/v in RPMI without amino acids).

3.2.11 EpCAM BiTE-induced T cell dependent target cell lysis is not reduced in patient ascites fluids

Following confirmation that IFNγ expression in T cells after BiTE activation was not affected by incubation in malignant ascites fluids, we assessed the cytolysis of DLD-1 colorectal tumour cells by EpCAM BiTE-activated T cells using xCELLigence, as described in section 2.6.5. We

compared killing via the EpCAM BiTE to that induced by the $CD8^+$ T cell clone in HCT116 colon carcinoma cells in culture with the same patient fluids.

Figure 3.16 shows cytolysis of DLD-1 tumour cells cultured in control media or six different filtered ascites fluids, either alone, with T cells, or T cells and EpCAM BiTE. In all tested media, the BiTE induced significant death of DLD-1 cells, to the same extent as in the control media (both 2% RPMI and RPMI at 50% amino acid concentration at 1:1 with RPMI with no amino acids).

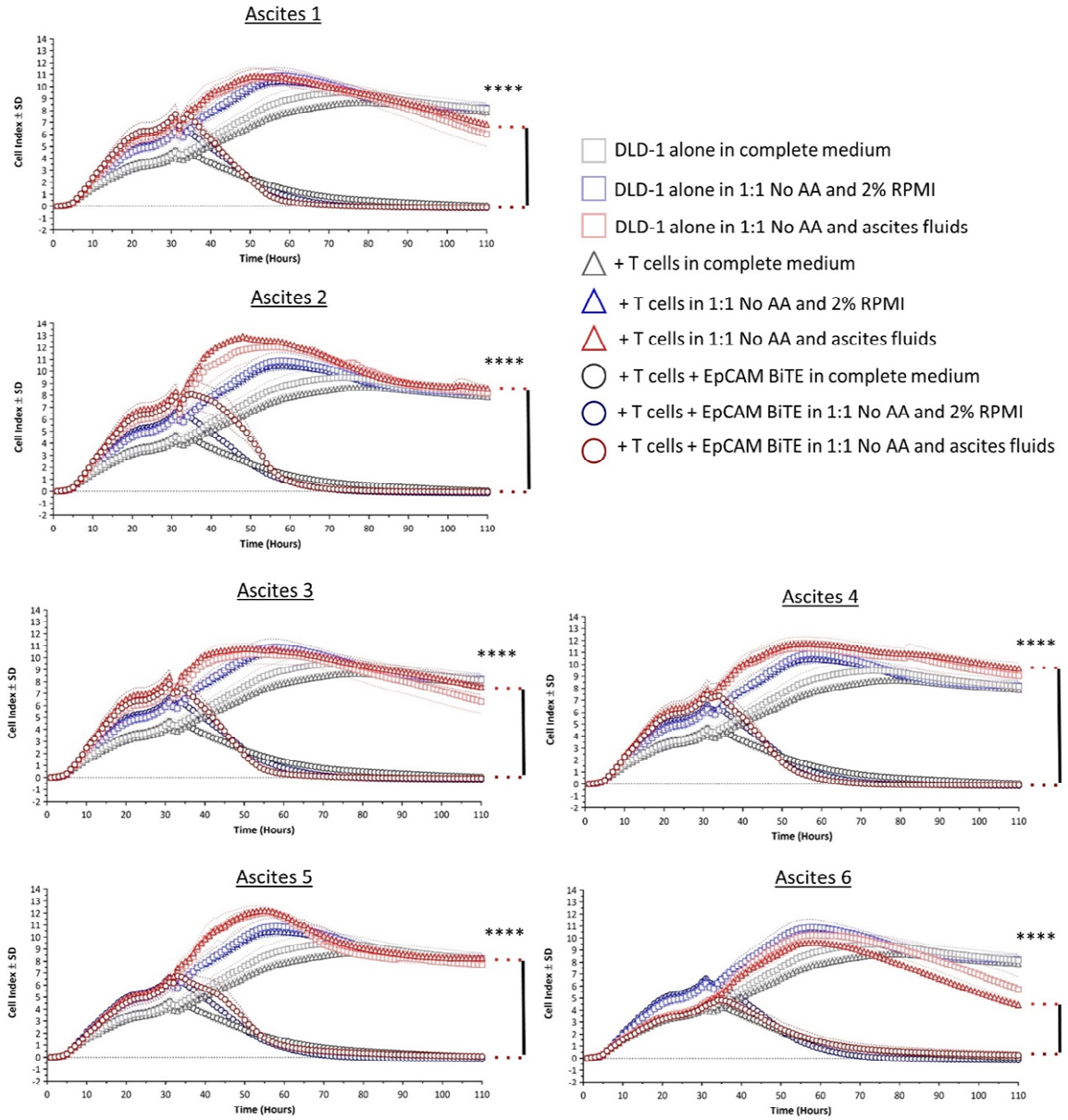


Figure 3.16 Culture in patient ascites medium does not change T cell mediated lysis by EpCAM BiTE of DLD-1 cells compared to culture in complete medium. Viability of DLD-1 cancer cells was monitored over 110 hours in real-time by an xCELLigence based assay. DLD-1 cells were seeded at 1.5 x 10^4 cells/well for 16 hours before $CD3^+$ T cells (5:1) with or without EpCAM BiTE were added in culture mediums; complete medium (RPMI with 2% FBS) (black), 50% RPMI (1:1 v/v in RPMI w/o amino acids) (blue) and six different patient ascites fluids (1:1 v/v in RPMI w/o amino acids) (red). Electrical impedance was measured at 15 minute intervals, each condition was measured in biological quadruplicate and represented as the mean ± SD (dashed lines). Statistical significance was assessed using a one-way ANOVA test with Tukey's post-hoc analysis. Significance presented was the experimental condition with EpCAM BiTE compared to the "DLD-1 + T cell control" at the timepoint 110 hours where the control had killed more than 99% of cells (*, $p < 0.05$; **, $p < 0.01$; ***, $p < 0.001$; ****, $p < 0.0001$; ns, non-significant).

The activation status of the $CD8^+$ T cell clone was measured by analysing CD25 expression in addition to its capacity to kill HCT116 cells. In wells containing the $CD8^+$ T cell clone alone, 50% of the cells were positive for CD25 expression. This increased to over 90% when the clone was cultured with HCT116 cells in complete medium. The percentage of cells expressing CD25 was reduced in ascites fluids Asc3, Asc4, Asc5 and Asc6 (Figure 3.17B). This reduction in activation status for Asc3, Asc5 and Asc6 translated into reduced cytolytic ability by the $CD8^+$ T cell clone, as measured by xCELLigence (Figure 3.17C). When EpCAM BiTE was added to the culture of the $CD8^+$ T cell clone and HCT116 cells, the BiTE induced more potent activation of the clone (Figure 3.17B), abrogating any inhibitory effects observed in the presence of ascites fluids.

Despite the varied levels of amino acids in the chosen ascites fluids, there was no indication of a reduction in EpCAM BiTE-mediated T cell activation or IFNγ expression. Maximal lysis of DLD-1 cells was achieved by T cells induced with EpCAM BiTE, despite culture in *ex vivo* malignant ascites fluids. Furthermore, the EpCAM BiTE was able to rescue activation of a $CD8^+$ T cell clone, which was inhibited by 4 of the 6 tested ascites fluids (Figure 3.17B).

Strikingly, the ascites fluids with the lowest levels of glutamine (Asc3, Asc5, Asc6) had the strongest inhibitory effect on activation and HLA-dependent killing by the $CD8^+$ T cell clone. Though this experiment was only repeated once, this data is in agreement with Figure 3.7B above, which showed that medium depleted of all glutamine hindered HLA-dependent killing of SKOV-3 cells by the clone.

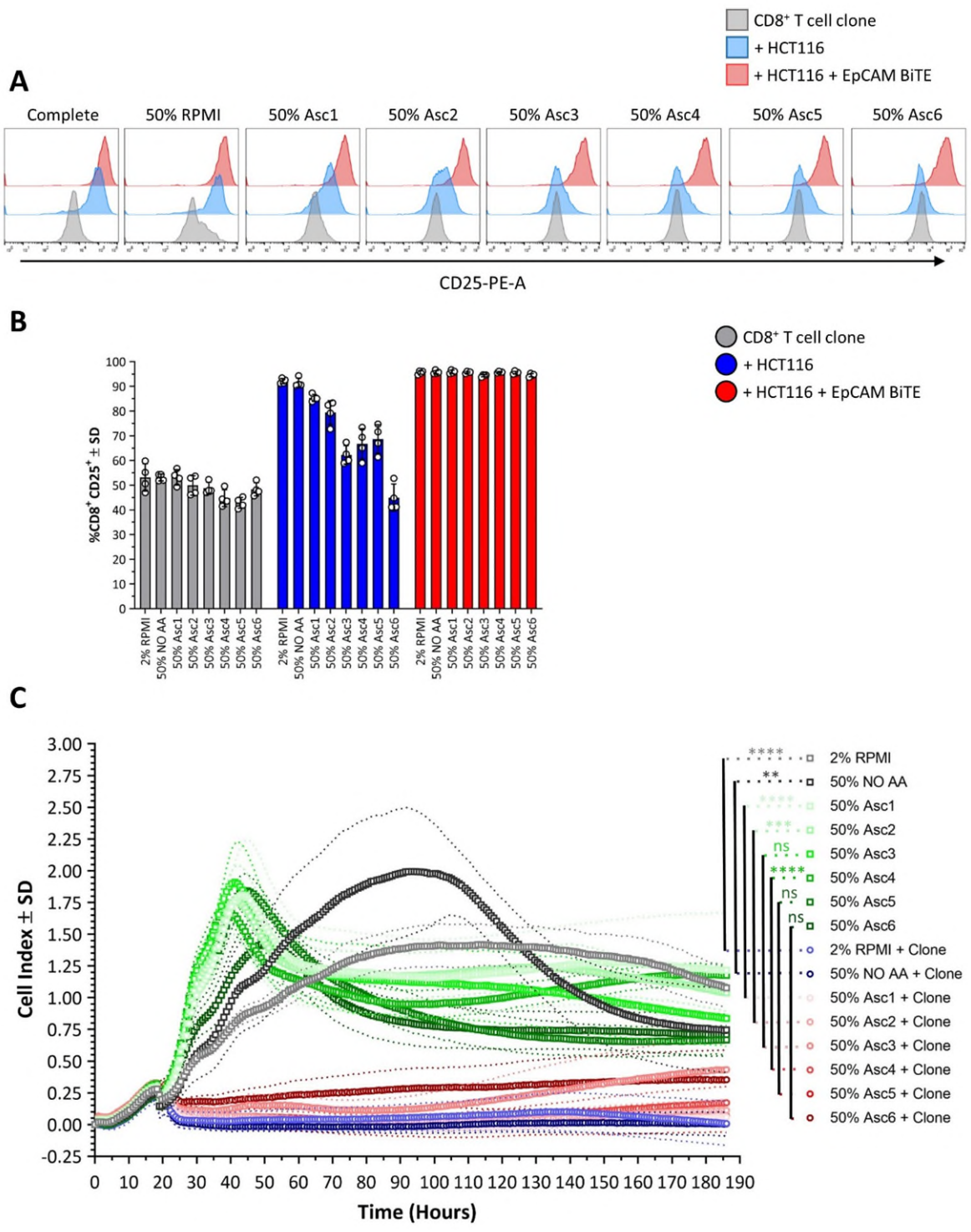

A
CD8+ T cell clone
+ HCT116
+ HCT116 + EpCAM BiTE
Complete
50% RPMI
50% Asc1
50% Asc2
50% Asc3
50% Asc4
50% Asc5
50% Asc6
CD25-PE-A
B
CD8+ T cell clone
+ HCT116
+ HCT116 + EpCAM BiTE
%CD8+ CD25+ ± SD
2% RPMI
50% NO AA
50% Asc1
50% Asc2
50% Asc3
50% Asc4
50% Asc5
50% Asc6
C
Cell Index ± SD
Time (Hours)
2% RPMI
50% NO AA
50% Asc1
50% Asc2
50% Asc3
50% Asc4
50% Asc5
50% Asc6
2% RPMI + Clone
50% NO AA + Clone
50% Asc1 + Clone
50% Asc2 + Clone
50% Asc3 + Clone
50% Asc4 + Clone
50% Asc5 + Clone
50% Asc6 + Clone

Figure 3.17 HLA-dependent T cell mediated lysis of HCT116 cells is impaired in three ascites fluids. The $CD8^+$ T cell clone was co-cultured with HLA-$A2^+$ HCT116 cells (5:1). The percentage of CD25-positive T cells were measured by flow cytometry after 24 hours in culture in complete medium (RPMI with 2% FBS), 50% RPMI (1:1 v/v in RPMI w/o amino acids) and six patient ascites fluids (1:1 in RPMI w/o amino acids). Histogram plots of the change in gMFI of CD25 in each culture medium when the clone is cultured alone or with HCT116 cells with or without BiTE are shown in **(A)** whilst the percentage of CD25-positive CD8-positive T cells (clone) are plotted in **(B)**. **(C)** Viability of HCT116 cells was monitored over 190 hours in real-time by xCELLigence. HCT116 cells were seeded at 1.0 x 10^4 cells/well for 16 hours before $CD8^+$ T cell clone (5:1) was added in appropriate culture mediums to half the wells. Electrical impedance was measured at 15 minute intervals, each condition was measured in biological triplicate and represented as the mean ± SD (dashed lines). Statistical significance was assessed using a one-way ANOVA test with Tukey's post-hoc analysis. Significance presented was the experimental condition with the T cell clone (blue/red) compared to the "HCT116 alone control" (grey/green) at the timepoint 185 hours where the clone in control medium had lysed more than 99% cells (*, $p < 0.05$; **, $p < 0.01$; ***, $p < 0.001$; ****, $p < 0.0001$; ns, non-significant).

3.2.12 EnAd potency is diminished in clinically relevant *ex vivo* models representing realistic nutrient levels

Using the same ascites fluids for which we have characterised for amino acid content in section 3.2.8, we examined whether the potency of EnAd would be inhibited compared to infection in complete medium. After infection with EnAd-SA-GFP, GFP expression, cell viability and viral progeny release were quantified. Tumour cells were subject to 24 hours of pre-culture in the fluids before infection (starved cells) or fluids were added at the point of infection (unstarved cells), as described in section 2.7.4.

The percentage of DLD-1 cells expressing GFP was measured after seven days. Expression was significantly reduced when cells were infected in any of the tested ascites fluids compared to controls in the unstarved group. The highest percentage of GFP expression in any of the ascites fluids was achieved in Asc6, with 35%; this was two times lower than the controls in complete medium, and 1:1 complete medium to amino acid-free medium (Figure 3.18). In starved conditions, we observed unexpected changes in the percentage of cells expressing GFP. In four of the six ascites fluids tested, GFP expression levels were lower than those measured in

unstarved conditions (< 10%) as expected. In Asc4, GFP expression levels were the same as in the unstarved group. In Asc2, the percentage of GFP expression unexpectedly increased to 91%.

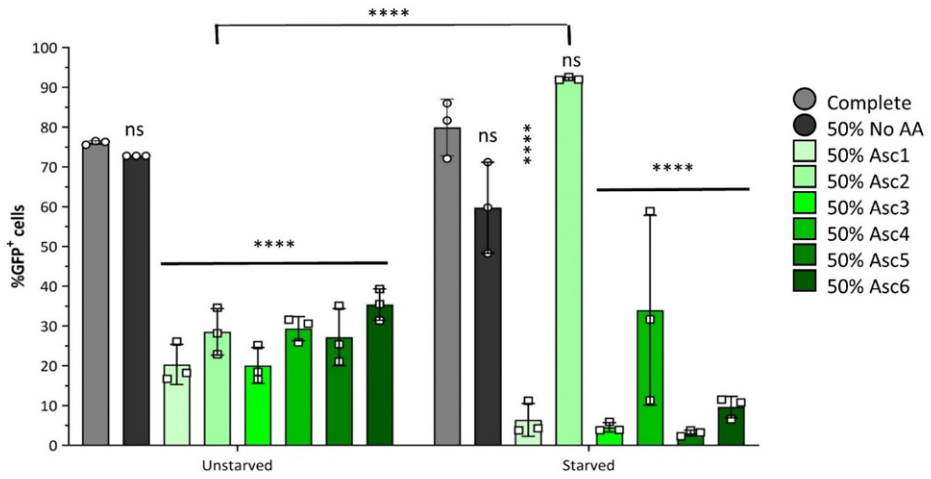


Figure 3.18 Viral protein expression after infection with EnAd in patient ascites fluids decreases in unstarved conditions. However, when cells are starved in Asc 2, protein expression increases. DLD-1 cells were exposed to complete medium (RPMI with 2% FBS) (grey) or 50% RPMI (1:1 v/v in RPMI w/o amino acids) (black) or one of six different patient ascites fluids (1:1 v/v in RPMI w/o amino acids) (green) for 24 hours. Medium was then changed in "unstarved cells" to the mediums indicated or left in the same medium "starved cells" and DLD-1 cells were infected with MOI 5 of EnAd-SA-GFP. Seven days later the percentage of GFP-positive cells indicating cell permissivity to infection was measured by flow cytometry. Each condition was measured in biological triplicate and represented as mean ± SD. Statistical significance within each group was assessed using a two-way ANOVA test with Tukey's post-hoc analysis with each condition compared to the "2% RPMI" control. Statistical significance between unstarved and starved groups was assessed by two-way ANOVA with Sidak's post-hoc analysis, (*, $p < 0.05$; **, $p < 0.01$; ***, $p < 0.001$; ****, $p < 0.0001$; ns, non-significant).

To further investigate this unexpected result, the viability of unstarved and starved DLD-1 cells following infection was assessed using a viability stain and flow cytometry, as described in section 2.4. In Figure 3.19A, we show that, by day 7, EnAd infection resulted in the lysis of 90% of DLD-1 tumour cells. A difference in the level of tumour cell death was observed in complete medium compared with 1:1 complete medium to amino acid-free medium (v/v). In all wells where tumour cells were cultured in ascites fluids, a significant proportion of tumour cells remained viable, almost 70% of cells. We sought to compare the viability of DLD-1 tumour cells in unstarved and starved conditions and found that Asc2 starvation resulted in a

significant increase in the ability for EnAd infection to induce cell lysis. A partial increase in cell killing was also observed after starvation in Asc4 (Figure 3.19B). Culture in these media potentiated EnAd lysis activity compared to complete medium.

Culture medium was taken from the viability studies in Figure 3.19B and titred to determine the number of infectious progeny released during the course of infection using $TCID_{50}$, as described in section 2.8.8. Infectious progeny numbers supported data seen with GFP expression and viability assays. All six ascites fluids in the unstarved experimental group reduced the number of plaque-forming units per mL compared to complete medium (around 10^6 lower) (Figure 3.19C). Starvation of tumour cells in Asc2 increased the viral titre compared to the unstarved condition, bringing the titre to within 10 PFU/mL of that in the control medium.

Simultaneous EnAd-SA-GFP infection and treatment of cells with ascites fluids to model amino acid levels found in the TME, resulted in significant impairment of all aspects of EnAd infection, from replication to viability to progeny release. The sudden drop in amino acid levels likely caused sudden changes in the cell, triggering stress responses to a factor present in ascites fluids or the sudden decline in amino acids. To our surprise, pre-exposure to Asc2 and, to a lesser extent, Asc4 resulted in an extreme increase in GFP expression, cytolysis and number of infectious viral particles released after lysis. This suggests DLD-1 tumour cells adapted to the conditions presented in those fluids, and that this adaptation improved EnAd activity.

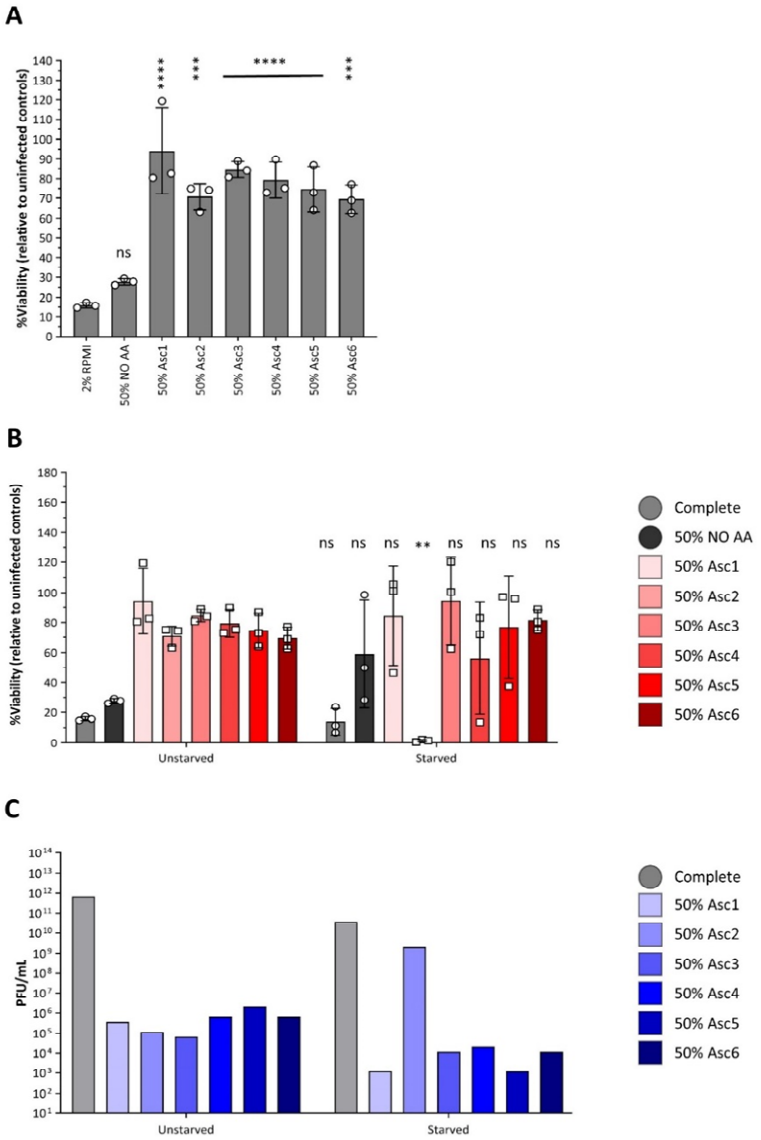


Figure 3.19 DLD-1 cells were more viable following EnAd infection in patient ascites medium but the same trend of ascites 2 potentiating EnAd infection was observed. DLD-1 cells were exposed to complete medium (grey) or 50% NO AA RPMI (1:1 v/v in RPMI w/o amino acids) (black) or one of six different patient ascites fluids (1:1 v/v in RPMI w/o amino acids) (red) for 24 hours. Medium was then changed in "unstarved cells" to the relevant mediums or left in the same medium "starved cells" and DLD-1 cells were infected with MOI 5 of EnAd-SA-GFP. **(A)** Cells were harvested after seven days and viability was assessed by flow cytometry using a LIVE/DEAD near-IR stain. The percentage of viable cells presented is relative to the uninfected cell control to account for tumour cell proliferation in ascites fluids. Each condition was measured in biological triplicate and represented as mean ± SD. Statistical significance within each group was assessed using a one-way ANOVA test with Tukey's post-hoc analysis with each condition reported compared to the "2% RPMI" control. **(B)** Cells harvested after seven days and viability measured by flow cytometry as above. The percentage of viable cells presented is relative to uninfected cells. Each condition was measured in biological triplicate and represented as mean ± SD. Statistical significance between unstarved and starved groups was assessed by two-way ANOVA with Sidak's post-hoc analysis. **(C)** Supernatants harvested after seven days from the same cultures in (A) and (B) were titered using a $TCID_{50}$ method to quantify the number of infectious progeny released, based on one biological replicate (*, $p < 0.05$; **, $p < 0.01$; ***, $p < 0.001$; ****, $p < 0.0001$; ns, non-significant).

3.3 Conclusions

The conclusions of this chapter were:

1. EpCAM BiTE remains functionally active despite nutrient depletion, both when individual amino acids are artificially depleted and in ascites fluids with low concentrations of amino acids,
2. EnAd infection depends greatly on amino acid concentrations, with amino acid depletion leading to significantly slower infection kinetics,
3. Malignant ascites fluids sampled from cancer patients are a suitable model to mirror the amino acid levels present in the TME,
4. Ascites fluids could potentiate EnAd activity by altering the phenotype of cancer cells.

3.4 Discussion

OV-encoded BiTEs hold promise as one of the next powerful therapeutic agents in cancer therapy. However, as with other therapeutics of this nature, the effects of the TME need to be considered to achieve a long and durable response against cancer. In this chapter, we assessed the impact of nutrient depletion on the activity of a BiTE targeting EpCAM and on the replication of EnAd, an oncolytic adenovirus. Due to the strength of T cell signalling triggered by binding of the BiTE and the lack of co-stimulation required, we hypothesised that the usual checkpoints performed during T cell activation to assess the availability of resources for a complete effector response are bypassed during BiTE-mediated activation.

We found that glutamine and tryptophan depletion impaired BiTE-mediated T cell activation. GrB and IFNγ expression were also impaired in the absence of glutamine. While no changes in expression of the early T cell activation marker CD69 were observed after BiTE stimulation,

even in medium depleted of all amino acids, expression of the late activation marker CD25 was affected (Figure 3.3). CD69 is thought to act as a metabolic gatekeeper for T cells, and associates with the LAT1-CD98 complex, an amino acid transporter, on the T cell surface. This association occurs before the determination of nutrient sufficiency to support energy-demanding activation and may explain why CD69, but not CD25 expression, remains unhindered (Cibrián and Sánchez-madrid 2017).

Glutamine and leucine are the main regulators of mTOR. While leucine is sensed directly by mTOR, glutamine is required in excess intracellularly to exchange for extracellular leucine by the amino acid transporter LAT1. A reduction in activation and cytokine expression is therefore unsurprising in the absence of glutamine (Figures 3.3A, 3.4, and 3.5). mTOR, the main regulator of metabolism, in turn regulates the differentiation and functional status of T cells (Gamper et al. 2012). Surprisingly, depletion of glutamine, tryptophan or all amino acids leads to higher BiTE-induced cytotoxicity. Furthermore, this effect is accentuated when T cells were starved in these conditions for 24 hours before addition to the co-culture and BiTE (Figures 3.7 and 3.8), the opposite of the expected effect. A recent study by Gropper *et al* (Gropper et al. 2017) reported that CTLs under hypoxia are capable of enhanced cytolysis. Hypoxia induces the inclusion of more GrB molecules per cytotoxic granule, which in turn results in more potent lysis. Although we have confirmed that this is not the mechanism involved here, as GrB levels are lower in our studies (Figure 3.4), we speculate that the sudden drop in amino acids in acute starvation or starvation for 24 hours in depleted medium, allows for T cells to adapt in ways that may improve their lytic ability in stressed conditions. Further work is needed to explore this hypothesis and elucidate the relevant adaptations. It is important to note that for this set of experiments and for those using T cells isolated from healthy PBMC donors throughout this thesis variability is introduced due to different donors being used.

EpCAM BiTE was able to increase the lytic activity of an antigen-specific T cell clone despite nutrient depletion to an even higher extent than in PBMC-derived T cells from healthy donors (Figures 3.7 and 3.8). This mirrors a report by Dreier *et al* (Dreier et al. 2002), who showed the most potent killing by a CD19-specific BiTE was achieved by an immortalised T cell clone, not non-specific T cells. BiTE potency varies and may even require co-stimulation to reach maximal potency, though this is not the case with the EpCAM BiTE. This may be due to either the BiTE format or EpCAM antigen density, which allows for stronger stimulation of the TCR and therefore much faster rate of activation (Figure 3.6) (Ellerman 2019; Richard et al. 2018). Optimal activation could potentially be achieved through a sufficiently strong stimulus to the TCR via CD3ε without CD28 (Wolf et al. 2005), activating mTOR. However, the mechanism by which BiTE-activated T cells avoid metabolic checkpoints that act independently of PI3K, such as AMPK and cytoplasmic amino acid associated GTPases (Rag), is unknown.

Elucidating the mechanisms behind EpCAM BiTE-mediated evasion of metabolic stress to evoke maximal killing could be important for the development and design of more efficacious T cell-based therapies. Identification of the key pathways and players would allow therapies to support T cell activity in the face of nutrient deficiencies. Examples of this have already been shown in the literature. Rivadeneira *et al* (Rivadeneira et al. 2019) used an OV to express leptin, which has been shown to improve metabolic function of T cells and increase their expression of IFNγ, possibly via mTOR activation (Waickman and Powell 2012). Alternatively, inhibition of GCN2 has been shown to dampen the response to starvation and increase expression of IFNγ and GrB. The latter technology is currently being developed by FLX Bio in San Francisco (Ravishankar et al. 2019).

In reporter gene, GFP, expression studies, the loss of amino acids caused a significant reduction in the ability for the virus to express proteins. This did not correlate with whether amino acids were essential or non-essential (Figure 3.11). Expecting poor cytolysis due to the drastic

changes in protein expression, we were surprised to find that, in most media depleted of a single amino acid, EnAd was still able to induce cell death, with only marked differences in medium without methionine, tryptophan and tyrosine (Figure 3.12). EnAd-induced lysis was only consistently inhibited in medium depleted of methionine across multiple cell lines (data not shown). Further experimental evaluation would be required to elucidate its exact role in the viral replication cycle. Of note, EnAd infection resulted in the decreased expression of ATF4, a transcription factor upregulated to regulate amino acid levels when starvation is sensed by GCN2 (Figure 3.10). We propose that EnAd interrupts the nutrient sensing pathway to keep mTOR active. Early studies have shown a similar mechanism whereby adenoviruses encode RNA to compete with dsRNA to prevent activation of dsRNA-activated protein kinase (PKR) which would phosphorylate eIF2α in order to shutdown general translation (Weitzman and Ornelles 2005).

A caveat of the work above, as with other studies involving cell culture, is that all media used, even those depleted of a single amino acid, contained excessive amounts of the remaining amino acids and high levels of glucose; RPMI 1640, for example, contains 300 μg/mL glutamine (around 2 mM) (G. E. Moore, Gerner, and Franklin 1967). In reality, the glutamine concentration in the serum of healthy individuals is around 73 μg/mL (around 0.5 mM). This value, derives from a study by Derezinski *et al* (Dereziński et al. 2017) who quantified free amino acid levels in the serum of healthy donors compared to prostate cancer patients.

To correct for the limitation of common culture media, we employed ascites fluid as a more accurate model for amino acid profiles in the TME. The concentration of amino acids in 21 different patient fluids was measured by HPLC (Figure 3.13D). We then focused on 6 samples with varying levels of glutamine, an essential amino acid to both EpCAM BiTE activation and EnAd replication (Figures 3.3-5 and 3.11). In line with our result using depleted media, we found the EpCAM BiTE was able to induce cell death of tumour cells despite culture in low

amino acid-containing ascites fluids (Figure 3.16). In contrast, activation and cytotoxicity of an HLA-dependent T cell clone was inhibited in the *ex vivo* models (Figure 3.17). EpCAM BiTE was able to rescue activation by the T cell clone, as seen previously in assays using artificial amino acid depletion (Figures 3.17B, 3.7B and 3.8B). While viral replication was inhibited in all ascites fluids when infection and ascites fluid addition occurred simultaneously, pre-starvation of the tumour cells in Asc2 for 24 h before infection improved EnAd potency. More tumour cells were infected and expressed GFP (Figure 3.18), and greater lysis was observed (Figure 3.19B) compared to infection in the complete medium control. Greater release of infectious progeny was also achieved (Figure 3.19C). The composition of Asc2 will need to be further defined to identify the factor leading to the observed improvement in viral activity and enable the design and development of a more potent oncolytic virus. Additionally as whole ascites contains many factors that could otherwise impact the efficacy of OVTs, for instance complement proteins, clotting factors and neutralising Abs, it would be important to consider whether including the higher molecular weight fraction of these ascites fluid, particularly Asc2, would reverse the improvement to viral infection observed in these studies.

4 Assessing BiTE-induced T cell function during lactic acid accumulation

4.1 Introduction and chapter aims

4.1.1 Introduction

The TME is known to be acidic in nature, as yet few studies have investigated what implications this may have for targeted T cell immunotherapies such as BiTEs. In this chapter, we assessed the activity of multiple BiTE constructs and formats to activate T cells against target cells under lactic acid stress.

The main source of acidity in the TME is the accumulation of lactic acid as a by-product of the up-regulation of glycolysis, known as the Warburg effect, which is characterised in many tumour types. Literature suggests that tumour cells can produce up to forty times more lactic acid than normal cells due to this reprogramming hallmark (Tannock and Rotin 1989; Holm et al. 1995). Not only malignant cells but other tumour-associated non-malignant cells upregulate their production of lactic acid, contributing further to acidification and signalling processes that aid tumour survival and progression, including immune evasion (Romero-Garcia et al. 2016). Lactic acid is not only a by-product but an effective pro-tumour molecule that has a role in metabolic symbiosis, proangiogenic signalling, metastasis and, most importantly here, immunosuppression (Wu, Ying, and Hu 2016).

A multitude of studies have demonstrated the effects of acidic pH induced by both HCl and lactic acid on T cells specific to both humans and mice. Each investigation used a different mode of activation in combination with a different acidic medium, making it difficult to

conclude key mechanisms at play. The results agree that a low pH reversibly inhibits cytokine production. However, the studies present differing effects on proliferation and activation marker expression, potential of CD28 co-stimulation to reverse inhibition, influence of lactic acid alone compared to HCl on inhibition of cytolytic ability, relevant signalling pathway components, and the potential of an additive role for sodium lactate in dysregulation, specifically in T cell motility (reviewed in (Huber et al. 2017; Howie and Degauque 2018)).

Most immunotherapeutic strategies rely on T cell activation and cytotoxicity to promote elimination of cancer cells and, possibly due to the difficulties of accurately modelling the TME, the ability of such therapies has not been extensively studied in acidic conditions. Our hypothesis is that BiTEs may be able to overcome the T cell suppression by lactic acid observed to hinder HLA-dependent activation of T cells (Howie and Degauque 2018) via two potential mechanisms. Firstly, BiTEs can trigger T cell 'super-activation' due to the high density of target antigens on the cell surface compared to the HLA:peptide complex, resulting in a stronger signal and faster rate of T cell activation (C. Y. Ma et al. 2020). Secondly, BiTEs negate the need for CD28 co-stimulation, activating T cells in a manner that could bypass metabolic checkpoint mechanisms observed in physiological activation, co-ordinated by CD28 via the PI3K/Akt/GSK-3 pathway (Freedman et al. 2017; Appleman and Boussiotis 2003).

Therefore, in this chapter we examined whether 'super-activation' of T cells by the EpCAM BiTE could overcome inhibition mediated by lactic acid. We explored the mediator behind this inhibition to clarify whether it was low pH or high lactate. We assessed binding of the BiTE to its relevant targets to determine whether lack of activity is induced by target binding disruption. Finally, we measured activation of T cells following their exposure to target cells and multiple BiTE constructs with different target receptors. We reasoned that next-generation BiTE constructs could potentially cope better with extreme conditions, and engineered and characterised nanoBiTEs to assess their function in low pH conditions.

4.1.2 Chapter aims

The aims of this chapter were to:

1. Optimise the lactic acid concentration for clinically-relevant functional testing of the EpCAM BiTE,
2. Characterise EpCAM BiTE-directed activation of T cell subsets and functional cytotoxicity towards $EpCAM^+$ tumour cells in lactic acid,
3. Determine the extent of inhibition of lactic acid on T cell activation induced by EpCAM BiTE and other BiTE constructs,
4. Engineer PD-L1-targeting nanobody BiTEs (nanoBiTE),
5. Compare T cell activation induced by the PD-L1 nanoBiTE and PD-L1 scFv BiTE in acidic conditions.

4.2 Results

4.2.1 Lactic acid concentrations of more than 20 mM (pH 6.2) cause tumour cell death in 2D culture

To determine the limit of tumour monolayer plasticity in lactic acid and the appropriate therapeutic window for subsequent EpCAM BiTE functionality tests, we measured the point at which culture medium is too acidic to maintain tumour cell viability.

The viability of SKOV-3 human ovarian carcinoma cells, DLD-1 human colon adenocarcinoma cells, and $CD3^+$ T cells isolated from healthy human peripheral blood was determined by flow cytometry, PrestoBlue and the xCELLigence cytotoxicity as described in section 2.6. Medium containing lactic acid was added to adherent cell monolayers or a suspension of T cells and

their viability was measured 24 hours later (Figure 4.1) or in real-time over seven days in the case of the xCELLigence assay (tumour cells only, Figure 4.2). The concentration of lactic acid used (0 – 25 mM) corresponded to an approximate pH range of 7.5 – 5.3, respectively (Figure 4.1A). This range encompassed the pH values reported for tumour cells *in situ* (Hao, Xu, and Li 2018). We observed that 25 mM lactic acid (pH 5.3) resulted in the death of all cell types tested, whilst marked cytotoxicity was observed in only DLD-1 cells at 20 mM lactic acid (pH 6.1), suggesting T cells are more resistant to lactic acid than DLD-1 cells.

The pH values and the corresponding lactic acid concentrations required to reach them are disparate between cells growing *in vitro* in a monolayer and those in a tumour *in vivo*. While the lactic acid concentration is reported to peak at 40 mM in some tumour types, with a range of reported pH values above 6.4, the pH values we observed in our assay were far lower, even at less than half the concentration of lactic acid (Romero-Garcia et al. 2016). However, the TME *in vivo* includes pro-tumour support cells, considerable ECM and connective tissue that can provide a buffering effect to lessen the falling pH. As monolayers of tumour cells in 2D culture lack this extracellular matrix, we employed a range of 0 – 20 mM lactic acid for all future experiments to model reported pH values, as opposed to reported lactic acid values.

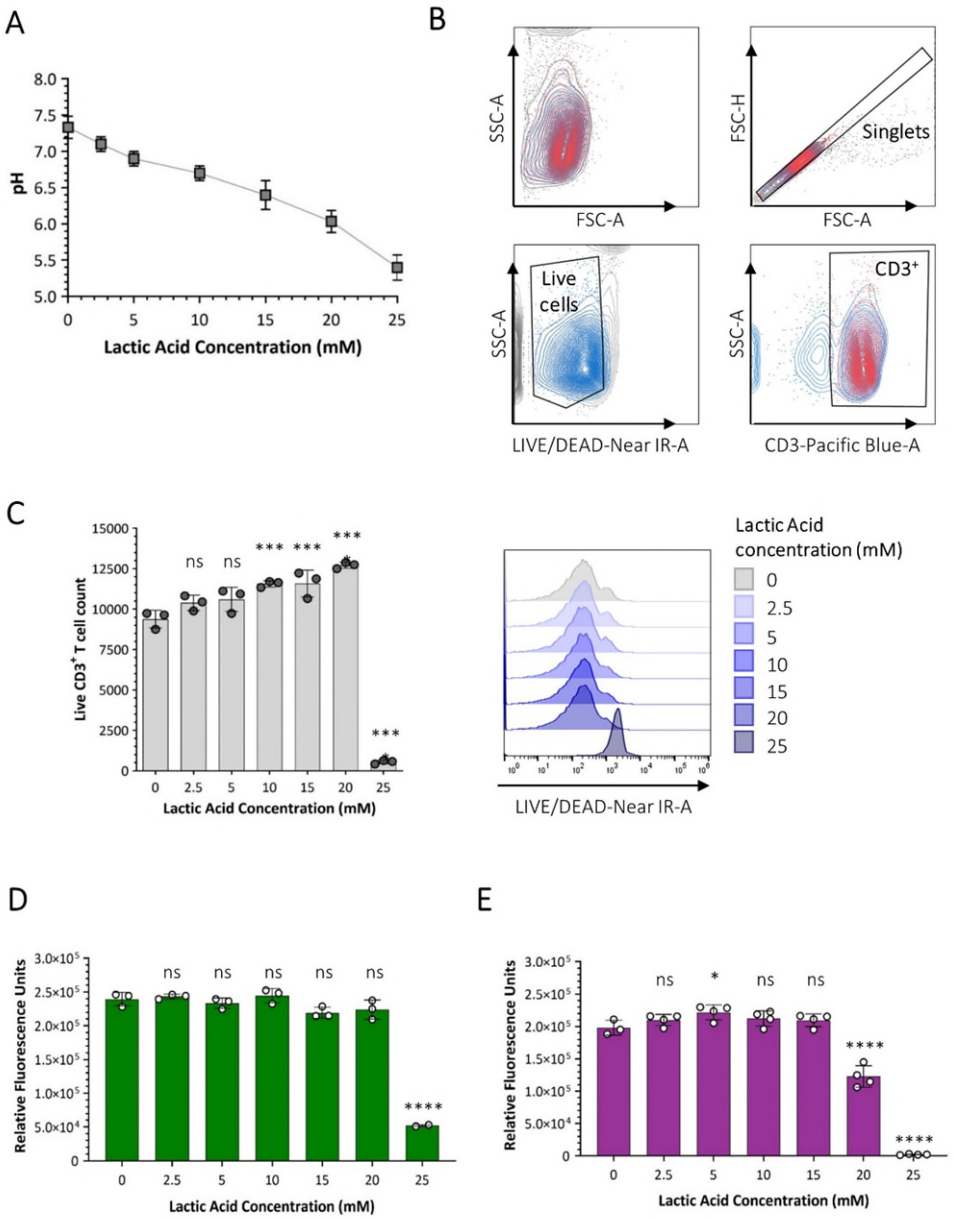


Figure 4.1 SKOV-3 and DLD-1 cell viability is reduced in medium containing 20-25 mM lactic acid. (A) RPMI 1640 medium was prepared with incremental amounts of 0 – 25 mM lactic acid from a 1 M lactic acid stock in RPMI 1640 medium. A pH probe and meter was used to determine pH values of the medium prepared. **(B)** Flow cytometry plots showing the gating strategy used to identify live $CD3^+$ T cells **(C)** Live $CD3^+$ T cells were analysed by flow cytometry after 24 hours in culture with lactic acid medium. Data show mean ± SD of biological triplicates. (**D, E**) SKOV-3 ovarian cancer cells, 1.5 x 10^4 (green) (D) or DLD-1 colon cancer cells, 2.0 x 10^4 (purple) (E) were cultured in lactic acid medium over 24 hours and viability was measured using the PrestoBlue cell viability reagent. Relative fluorescence as a representative of viability was used. (C-E) Statistical significance was assessed by a one-way ANOVA test with Dunnett's post-hoc analysis, each treatment being compared to the "0 mM" control condition (*, $p < 0.05$; **, $p < 0.01$; ***, $p < 0.001$; ****, $p < 0.0001$; ns, non-significant).

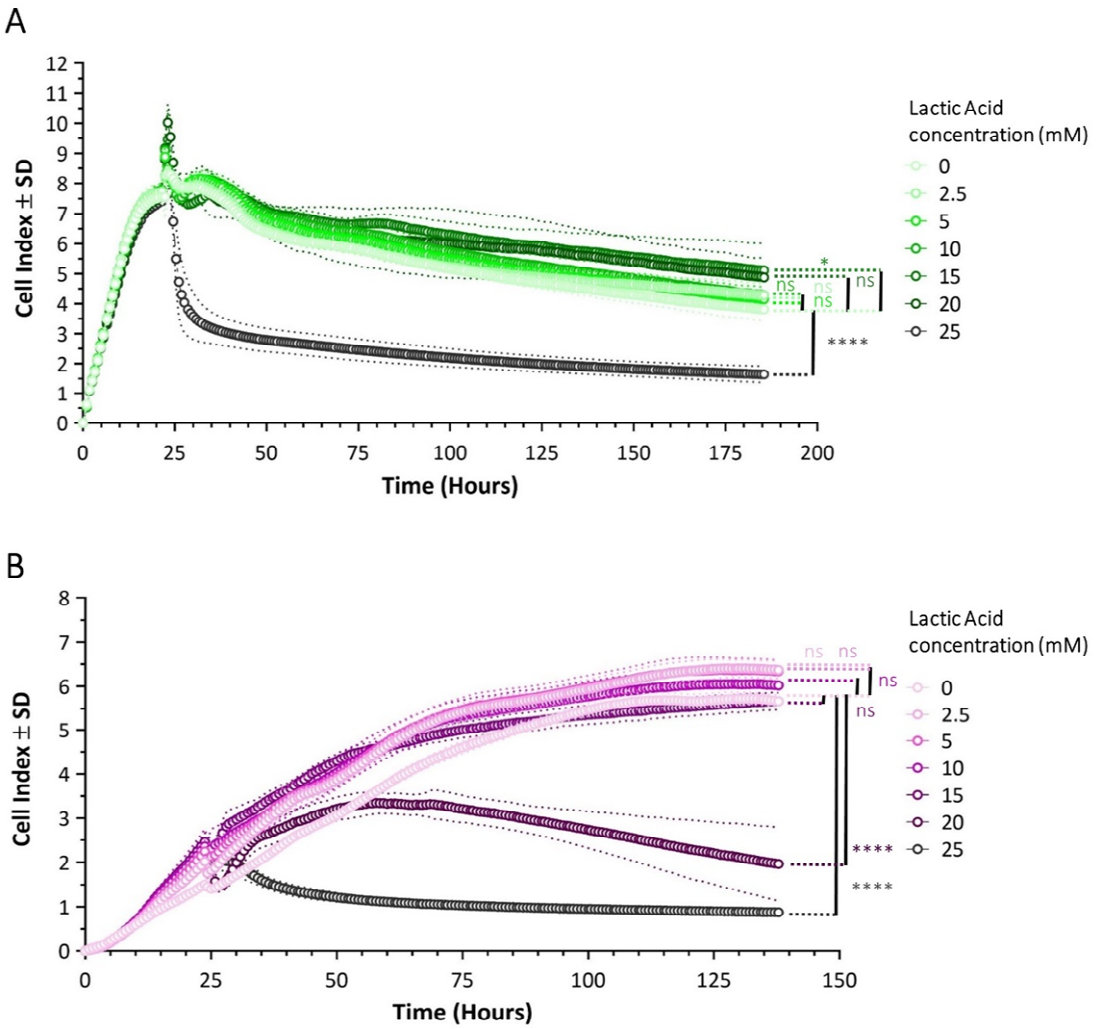


Figure 4.2 SKOV-3 and DLD-1 cell viability is reduced in medium containing 20-25 mM lactic acid. To monitor viability in real-time over a number of days an xCELLigence cytotoxicity assay was used for SKOV-3 cells **(A)** and DLD-1 cells **(B)**. Data show mean ± SD of biological quadruplicates. Statistical significance was assessed by a one-way ANOVA test with Dunnett's post-hoc analysis, each treatment being compared to the "0 mM" control condition at 185 hours in (A) and 140 hours in (B) (*, $p < 0.05$; **, $p < 0.01$; ***, $p < 0.001$; ****, $p < 0.0001$; ns, non-significant).

4.2.2 Lactic acid inhibits activation and the cytolytic potential of T cells induced by the EpCAM BiTE and CD3/CD28 beads

HLA-dependent T cell activation relies on signals from both CD3 and the co-stimulatory receptor CD28, whereas the EpCAM BiTE mediates activation through CD3 alone. To assess if this difference in signalling could distinguish the two modes of activation in the presence of

lactic acid, we cultured T cells with target tumour cells in the presence of either the BiTE or CD3/CD28 beads. We then analysed T cells to characterise BiTE and CD3/CD28 bead functionality using activation markers (CD25 and CD69), a degranulation marker (CD107α /LAMP-1), and an inflammatory cytokine (IFNγ) by flow cytometry as described in section 2.5. IFNγ is associated with the activation of Th1 type $CD4^+$ T cells and cytotoxic $CD8^+$ T cells (Freedman et al. 2017, 2018; Scott et al. 2019) and is required for the cytotoxic activity of $CD8^+$ T cells (Tau et al. 2001).

The ability of EpCAM BiTE to stimulate T cell expression of CD25 and CD69 was assessed in the presence of 15 and 20 mM lactic acid (pH 6.4 and 6.1, respectively), compared to complete medium (2% RPMI without lactic acid) (Figures 4.3A and B). The manufacturers of CD3/CD28 beads claim that activation with the beads is reflective of the physiological process, which includes co-stimulation via CD28, hence these were included in parallel studies as a model for the physiological activation pathway (Trickett and Kwan 2003). Representative flow cytometry histograms are shown in Figure 4.4A. Following treatment with EpCAM BiTE the percentage of CD25-expressing T cells after 24h was only 1.7-fold and 3.5-fold lower for medium with 15 mM and 20 mM lactic acid, respectively. Interestingly 15 mM lactic acid had no deleterious effect on the ability of CD3/CD28 beads to stimulate CD25 expression, although 20 mM gave 1.3-fold lower expression than the control (Figure 4.4B). The percentage of CD69 expression, around 88% for both modes of activation after 24h in control medium, was also inhibited in the presence of 15 and 20 mM lactic acid following activation with EpCAM BiTE (66% and 40%, respectively) but was largely unaffected for the CD3/CD28 beads (91% and 84%, respectively) (Figure 4.4C).

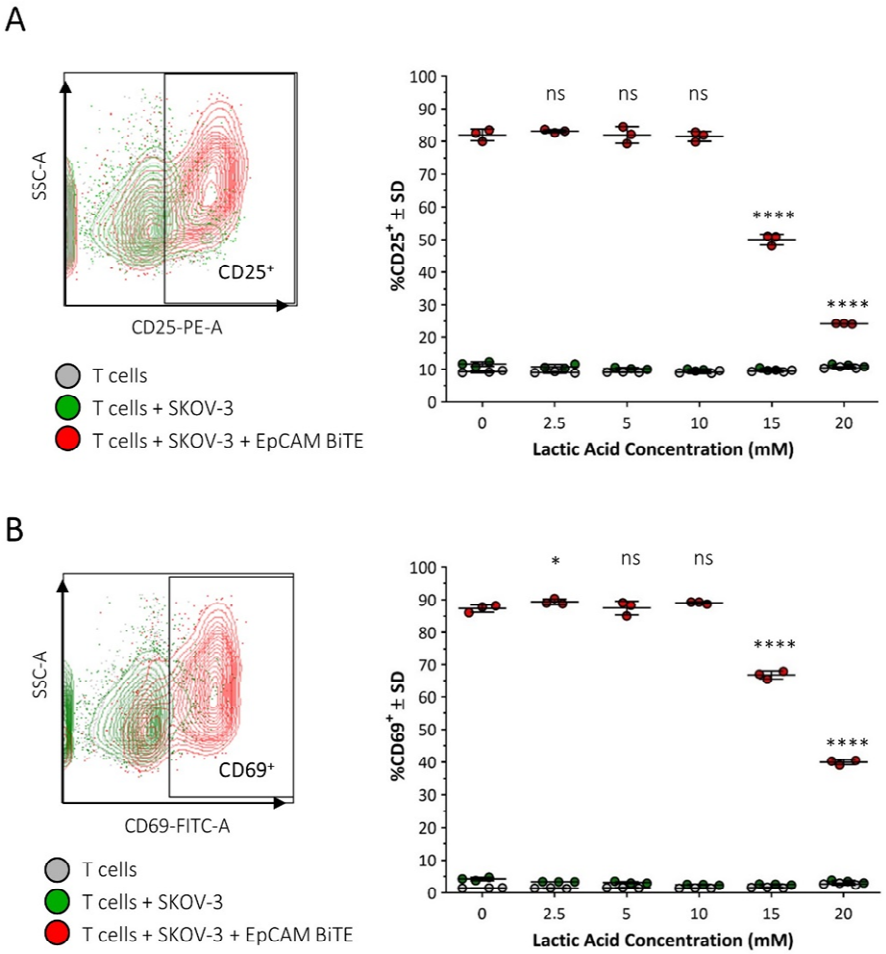


Figure 4.3 EpCAM-BiTE induced activation of T cells in co-culture with SKOV-3 cells decreases in 15 and 20 mM lactic acid. (A) BiTE-containing supernatant was added to a co-culture of $CD3^+$ T cells and SKOV-3 cells (5:1) and after 24 hours activation was measured by the surface expression of CD25 **(A)** and CD69 **(B)** analysed by flow cytometry. A representative flow cytometry plot of CD25 activation in complete medium with the T cell control in grey, the T cell and SKOV-3 control in green and SKOV-3 cells and T cells activated with EpCAM BiTE in red **(A)** and the same plot for CD69 activation is in **(B)**. Each condition was measured in biological triplicate and data is represented as the mean ± SD. Significance was assessed by a two-way ANOVA test with Dunnett's post-hoc analysis comparing with the "0 mM" control condition (A-B) (*, $p < 0.05$; **, $p < 0.01$; ***, $p < 0.001$; ****, $p < 0.0001$; ns, non-significant).

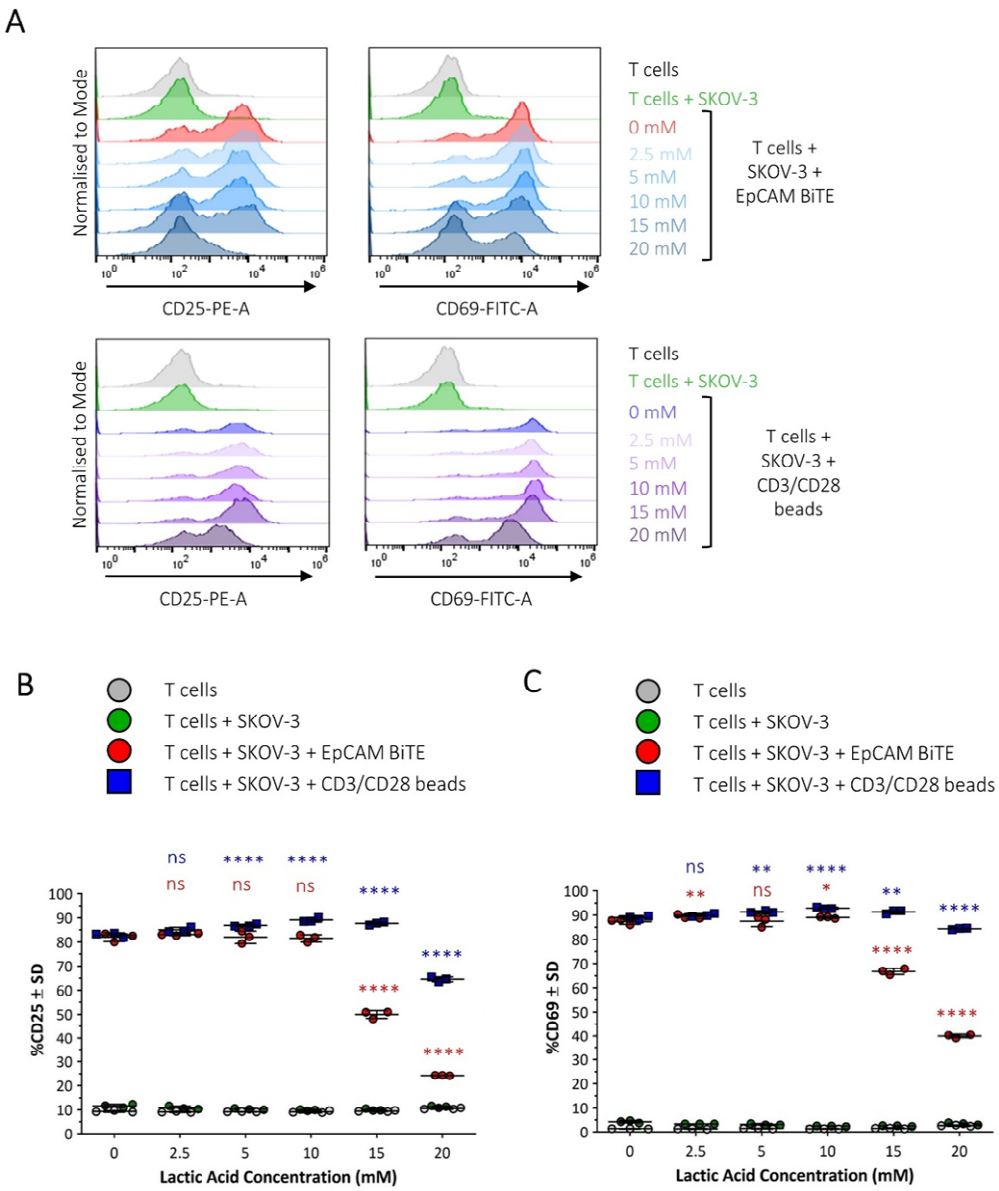


Figure 4.4 CD3/CD28 bead activation of T cells in co-culture with SKOV-3 cells decreases in medium with 20 mM lactic acid. (A) Representative flow cytometric histograms of CD25 and CD69 on the surface of T cells activated by either the EpCAM BiTE or 2 µL CD3/CD28 beads in medium with increasing lactic acid concentrations. Activators were added to a co-culture of $CD3^+$ T cells and SKOV-3 cells (5:1) and after 24 hours, activation was measured by the surface expression of CD25 **(B)** and CD69 **(C)** analysed by flow cytometry. Each condition was measured in biological triplicate and data is represented as the mean ± SD. Significance was assessed by a two-way ANOVA test with Dunnett's post-hoc analysis comparing with the "0 mM" control condition (B-C) (*, $p < 0.05$; **, $p < 0.01$; ***, $p < 0.001$; ****, $p < 0.0001$; ns, non-significant).

Surface expression of CD107α is a marker of degranulation and occurs early, around 30 minutes after stimulation, in cytotoxic T cell subsets. This is followed by IFNγ synthesis from 2 hours after stimulation (Wolint et al. 2004). Both markers were used to assess the cytolytic activity of T cells 6h after stimulation in increasing lactic acid concentrations. Lactic acid appeared not to inhibit the percentage of T cells expressing CD107α on their surface for either mode of activation (Figure 4.5A). However, 15 mM lactic acid caused a fall in the percentage of *de novo* expression of IFNγ (1.7-fold lower for both the EpCAM BiTE and CD3/CD28 beads). In 20 mM acid, there was a 6-fold decrease following activation using beads and a 4-fold decrease following BiTE activation, both reaching background levels observed for the controls containing no activators (Figure 4.5B).

Taken together, we conclude that EpCAM BiTE activation of T cells cannot overcome the inhibitory action of lactic acid known to affect the physiological activation of T cells. Furthermore, this data suggests EpCAM BiTE-induced activation is more severely inhibited than physiological activation with CD3/CD28 beads in lactic acid, potentially implying that CD3 activation is disrupted more than CD28 stimulation. It is possible that the addition of CD28 activation (positive) signals counteracts inhibitory (negative) signals of lactic acid in stimulation involving the CD3/CD28 beads.

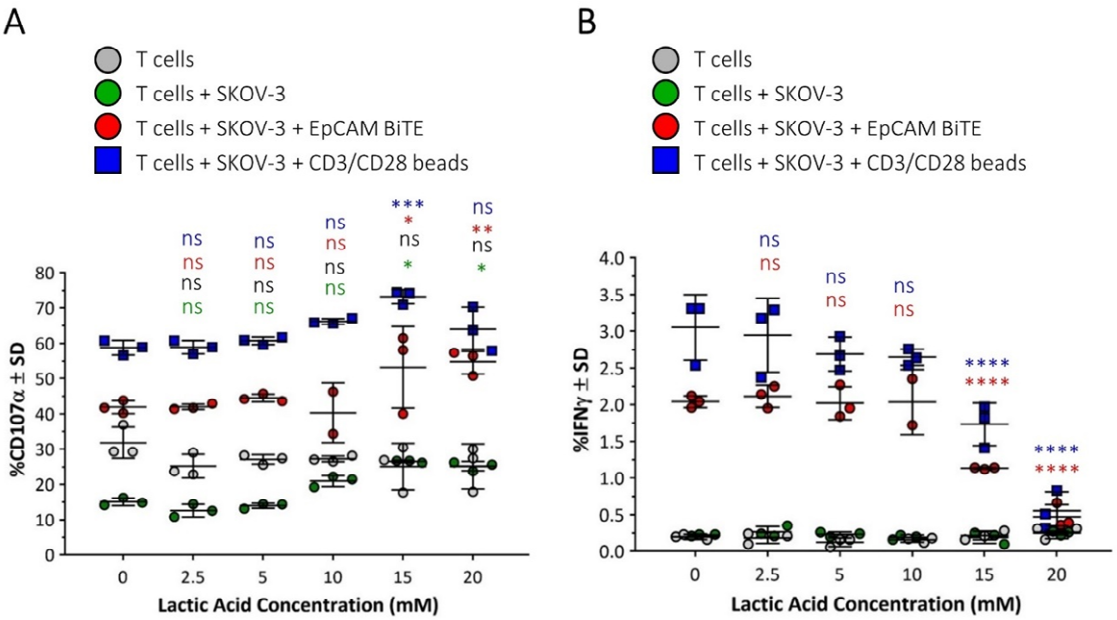


Figure 4.5 Degranulation in T cells is increased in lactic acid containing medium and cytokine expression decreased. (A) EpCAM BiTE containing supernatant or 2 µL CD3/CD28 beads were added to a co-culture of $CD3^+$ T cells and SKOV-3 cells (5:1). After 6 hours degranulation, measured by surface expression of CD107α isolated at the surface using Golgi reagents **(A)** or *de novo* IFNγ expression, trapped intracellularly with Golgi reagents **(B)**, were analysed by flow cytometry. Data show the mean ± SD of biological triplicates. Statistical significance was assessed by a two-way ANOVA test with Dunnett's post-hoc analysis, each treatment being compared to the "0 mM" control condition (A-B) (*, $p < 0.05$; **, $p < 0.01$; ***, $p < 0.001$; ****, $p < 0.0001$; ns, non-significant).

4.2.3 Activation and markers of cytolytic potential in T cells are reduced in both T cell subsets

As EpCAM BiTE has been previously shown to activate and induce cytotoxic activity in both $CD4^+$ and $CD8^+$ T cells, we next assessed whether activation in the two subsets was inhibited to the same extent by lactic acid. An example of the gating strategy used to identify individual T cell subsets after flow cytometry is shown in Figure 2.2.

Representative contour plots and histograms of each T cell subset expressing CD25 after BiTE activation in lactic acid medium are shown in Figure 4.6A. The percentage of surface CD25 after activation with EpCAM BiTE was significantly lower in medium containing 15 mM and

20 mM lactic acid compared to control medium. As observed previously, activation by CD3/CD28 beads was less susceptible to the effects of lactic acid than the BiTE (Figure 4.6B). The percentage of IFNγ expression by $CD8^+$ T cells activated with BiTE decreased by 2.1% in 10 mM lactic acid (pH 6.8) compared to medium without lactic acid. Separation by T cell subtype after CD3/CD28 bead activation clearly showed that IFNγ expression diminished in lactic acid concentrations as low as 2.5 mM acid in both T cell subsets (pH 7.1), falling as much as 50% in $CD8^+$ T cells in medium with 10 mM acid (Figure 4.6C).

Both T cell subsets exhibited reduction in both activation and cytolytic potential in medium containing lactic acid. Due to the low levels of IFNγ in $CD4^+$ T cells, the true impact of lactic acid on $CD8a^+$ T cells by both the EpCAM BiTE and physiological CD3/CD28 beads was concealed.

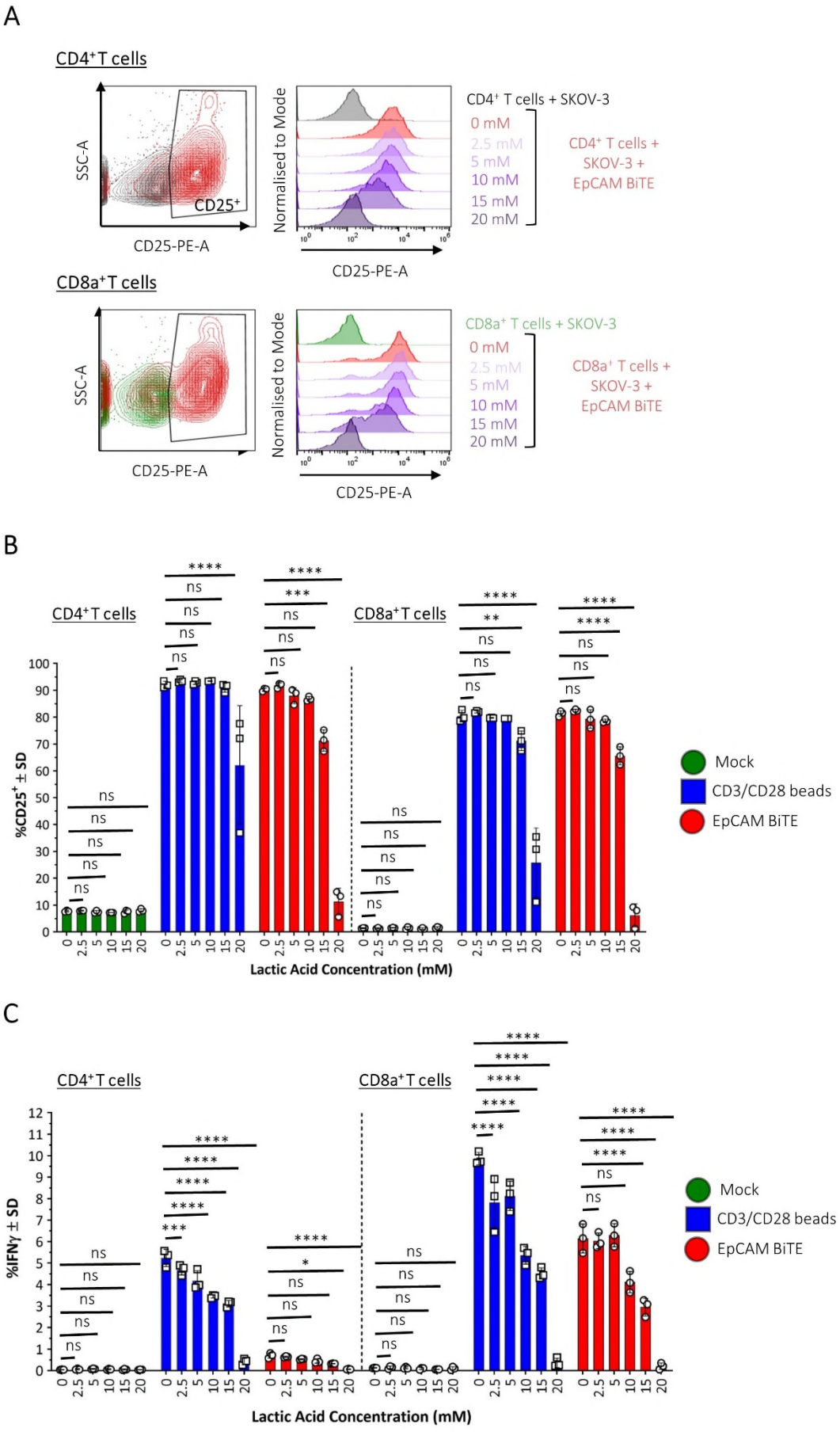

A
CD4⁺T cells
SSC-A
CD25⁺
CD25-PE-A
Normalised to Mode
CD25-PE-A
CD4⁺ T cells + SKOV-3
0 mM
2.5 mM
5 mM
10 mM
15 mM
20 mM
CD4⁺ T cells + SKOV-3 + EpCAM BiTE
CD8a⁺T cells
SSC-A
CD25-PE-A
Normalised to Mode
CD25-PE-A
CD8a⁺ T cells + SKOV-3
0 mM
2.5 mM
5 mM
10 mM
15 mM
20 mM
CD8a⁺ T cells + SKOV-3 + EpCAM BiTE
B
CD4⁺T cells
CD8a⁺T cells
%CD25⁺ ± SD
Lactic Acid Concentration (mM)
Mock
CD3/CD28 beads
EpCAM BiTE
C
CD4⁺T cells
CD8a⁺T cells
%IFNγ ± SD
Lactic Acid Concentration (mM)
Mock
CD3/CD28 beads
EpCAM BiTE

Figure 4.6 Analysis of individual T cell subsets activated in lactic acid medium show both subsets have reduced activation and cytotoxicity potential. SKOV-3 cells in co-culture with T cells were treated with CD3/CD28 beads, EpCAM BiTE or were left untreated (mock). **(A)** Representative flow cytometry plots showing the gates used to analyse each T cell subset, CD4 (grey) and CD8a (green), for their surface expression of CD25 (red) after activation. Representative histograms of CD25 expression on live T cells 24 hours after BiTE addition in increasing amounts of lactic acid medium. The percentage of CD25 **(B)** and IFNγ **(C)** of $CD4^+$ and $CD8a^+$ T cell subsets was measured after 24 hours and 6 hours respectively. Data is represented as the mean ± SD of biological triplicates. Significance was assessed by a two-way ANOVA test with Dunnett's post-hoc analysis, each treatment was compared to the "0 mM" control condition (B-C) (*, $p < 0.05$; **, $p < 0.01$; ***, $p < 0.001$; ****, $p < 0.0001$; ns, non-significant).

4.2.4 EpCAM BiTE-induced and HLA-dependent cytotoxicity are incapacitated by lactic acid accumulation

To establish whether the lactic acid-dependent inhibition of activation and cytolytic potential translates to reduced tumour cell lysis by T cells activated with EpCAM BiTE, cytotoxicity of SKOV-3 and DLD-1 tumour cells was assessed using PrestoBlue and xCELLigence as described in sections 2.6.3 and 2.6.5, respectively.

Lysis of SKOV-3 cells by EpCAM-BiTE-activated T cells was significantly inhibited in 10 mM lactic acid compared to controls, in agreement with the observed low level of IFNγ expression in T cells in the same medium (Figure 4.7A). Complete inhibition of BiTE-induced cytotoxicity by T cells was observed in DLD-1 cells in medium with 15 mM and 20 mM acid using xCELLigence (Figure 4.7B).

When measuring DLD-1 cell viability with PrestoBlue (Figure 4.7C), a two-fold change in cytotoxicity was seen in medium with 5 mM lactic acid (pH 6.9). Cytotoxicity decreased in a dose-dependent manner until 15 mM lactic acid, where no difference in cytotoxicity in cultures with or without EpCAM BiTE was observed.

HCT116 cell viability was assessed 72h following treatment with T cells extracted from peripheral blood with CD3/CD28 beads and EpCAM BiTE or when treated with a $CD8^+$ T cell

clone specific for HCT116 cells at either a 3:1 (E:T) ratio or 10:1, and compared to control wells containing HCT116 cells only (100% viability) (Figure 4.7D). Significance was assessed compared to the level of cytotoxicity in complete medium without lactic acid for each treatment. In control medium, without lactic acid, all of the HCT116 cells were killed by all treatments and relative viability was close to zero. However, cytotoxicity was inhibited in the presence of lactic acid for each, leading to increased relative viability. In the case of T cells activated with CD3/CD28 beads, not only did this lead to a complete loss of cytotoxicity (and restoration of 100% relative viability) at 5mM lactic acid, but at higher lactic acid levels the viability increased even beyond controls. As a decrease in cell viability was seen for the HCT116 cells alone as acid accumulated, this suggested that T cells and CD3/CD28 beads actually aid in keeping HCT116 cells alive when acid begins to accumulate.

The cytotoxicity of T cells activated with EpCAM BiTE-against HCT116 cells steadily decreased with increasing lactic acid concentrations, with the viability observed in 20 mM lactic acid medium significantly elevated over controls. HLA-dependent killing of HCT116 cells also decreased in the presence of lactic acid, with 100% viability restored in the presence of 5 mM lactic acid and up to 200% in 10 mM and above. These data also suggest that medium containing lactic acid was actually inducing HCT116 cell proliferation. Although the use of a higher effector-to-target ratio resulted in more potent HCT116 killing, overcoming inhibition in 5 mM acid, culturing in 10 mM lactic acid still resulted in increased viability of HCT116 cells.

Together, these results show that reduced cytolytic potential of T cells translates into a reduced ability to kill target tumour cells in medium containing lactic acid. Not only was EpCAM BiTE functionality affected by lactic acid, but also killing induced by either treatment with CD3/CD28 beads or an HLA-matched antigen-specific T cell clone (NLSALGIFST, from protein insulin-like growth factor 2 mRNA binding protein 2 (IF2B2)). The effect of lactic acid does not appear to be specific for any single activator but does affect CD3/CD28 bead-mediated

activation to a greater extent than BiTE-mediated activation (Figure 4.7D), corresponding to data for IFNγ (Figure 4.6C) but not CD25 expression on T cells (Figure 4.6B).

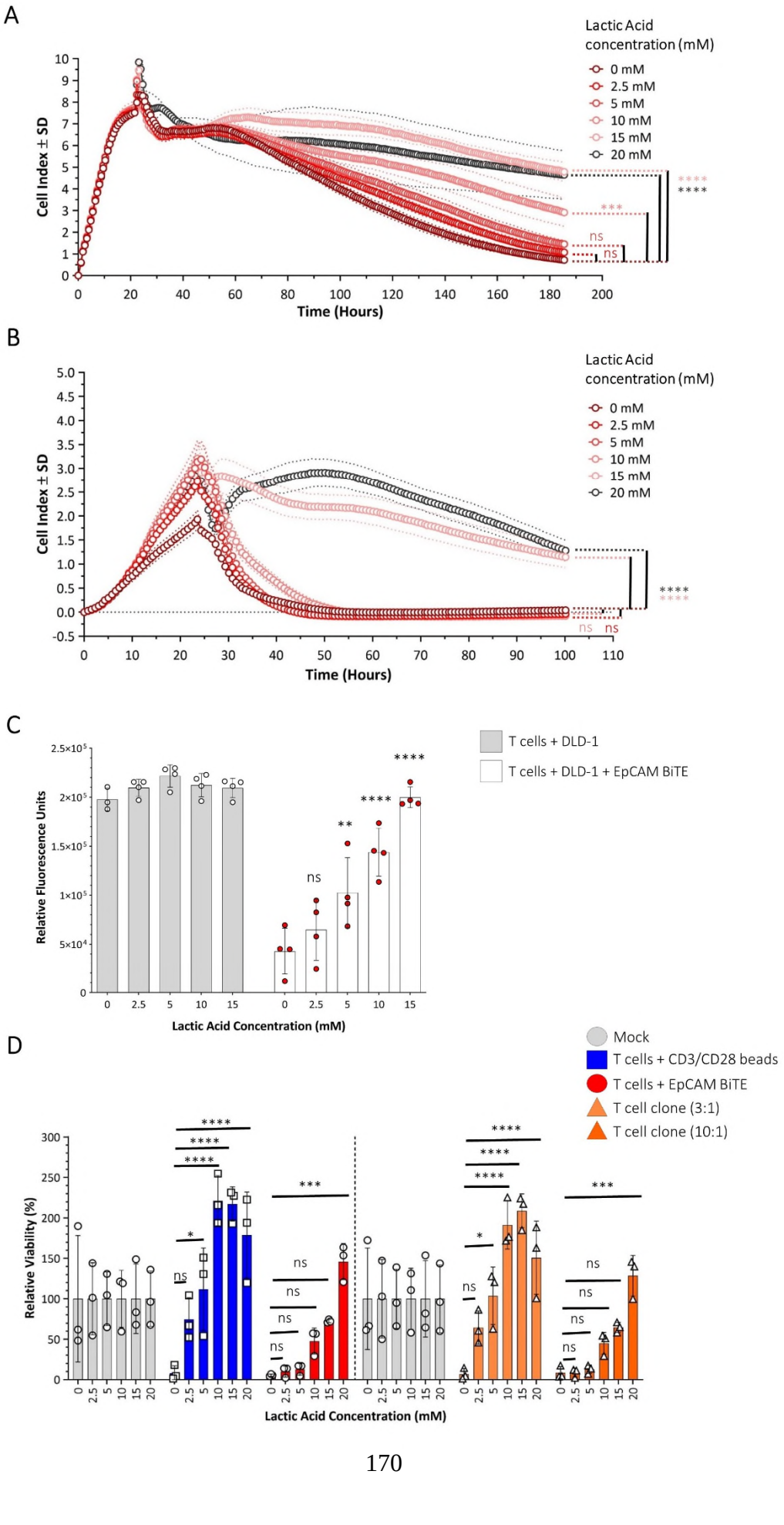

A
Lactic Acid concentration (mM)
0 mM
2.5 mM
5 mM
10 mM
15 mM
20 mM
Cell Index ± SD
Time (Hours)
B
Lactic Acid concentration (mM)
0 mM
2.5 mM
5 mM
10 mM
15 mM
20 mM
Cell Index ± SD
Time (Hours)
C
T cells + DLD-1
T cells + DLD-1 + EpCAM BiTE
Relative Fluorescence Units
Lactic Acid Concentration (mM)
D
Mock
T cells + CD3/CD28 beads
T cells + EpCAM BiTE
T cell clone (3:1)
T cell clone (10:1)
Relative Viability (%)
Lactic Acid Concentration (mM)

Figure 4.7 Tumour cell cytotoxicity induced by T cells following activation is inhibited in lactic acid medium. An xCELLigence based assay was used to assess the viability of SKOV-3 cells **(A)** and DLD-1 cells **(B)** after treatment with $CD3^+$ T cells and EpCAM BiTE at 24 hours. Cytotoxicity was assessed in medium with 0 – 20 mM lactic acid. Electrical impedance was measured at 15 minute intervals. Each condition was measured in biological quadruplicate and represented as the mean ± SD (dashed lines). **(C)** EpCAM BiTE was added to a co-culture of $CD3^+$ T cells and DLD-1 cells (5:1). After 24 hours, DLD-1 cell viability was measured using PrestoBlue cell viability reagent. Data show the mean ± SD of biological quadruplicates. **(D)** HCT116 cell viability was measured using the absolute $EGFR^+$ cell count as determined by flow cytometry after 72 hours in co-culture with PBMC-derived $CD3^+$ T cells, in the presence of CD3/CD28 beads or the EpCAM BiTE, or with a $CD8^+$ T cell clone at an E:T ratio of 3:1 or 10:1. Cultures were set up in medium containing 0 – 20 mM lactic acid. The percentage of relative viability is the total number of $EGFR^+$ cells quantified using counting beads as described in section 2.4.4, divided by the total cell count of HCT116 cells alone (mock in grey) in the different culture mediums tested, multiplied by 100. Data show the mean ± SD of biological triplicates. (A-B) Statistical significance was assessed by a one-way ANOVA test with Dunnett's post-hoc analysis, each treatment being compared to the "0 mM" control condition at 185 hours in (A) and 100 hours in (B). (C, D) Statistical significance was assessed by a two-way ANOVA test with Dunnett's post-hoc analysis, each treatment being compared to the "0 mM" control condition (*, $p < 0.05$; **, $p < 0.01$; ***, $p < 0.001$; ****, $p < 0.0001$; ns, non-significant).

4.2.5 Inhibition of BiTE-mediated T cell activation by lactic acid can be partially reversed with HEPES addition

The literature indicates that T cell inhibition by lactic acid is a widely reported observation, however the precise mechanism is unknown. Here, we wanted to assess if it was the lactate salt itself or the low pH induced by the accumulation of protons from lactic acid that was responsible for inhibition of BiTE-induced T cell activation. Media containing lactic acid was prepared with HEPES, a strong buffer used to stabilise the pH to physiological levels independent of changes in CO_2 (Michl, Park, and Swietach 2019). Buffered media and its acidic equivalent were used to characterise T cell activation and cytolytic potential after EpCAM BiTE or CD3/CD28 bead addition using flow cytometry as described in sections 2.5.5 and 2.5.6.

Figure 4.8A shows the pH in media made with increasing lactic acid with and without addition of 30 mM HEPES. Previously we observed the count of live $CD3^+$ T cells decreased dramatically in RPMI medium with 25 mM lactic acid (Figure 4.1C), however the presence of HEPES appeared to prevent that cytotoxic effect. Instead, the number of T cells increased with

increasing amounts of lactic acid in buffered media (Figure 4.8B). Figures 4.8C and D both show the percentage of CD25-expressing T cells in the absence or presence of immune activators in medium with or without HEPES buffer. In medium without HEPES, the presence of 20 mM lactic acid inhibited expression of CD25 by more than 50%. This effect was abrogated in the presence of 30 mM HEPES.

Expression of IFNγ was analysed in medium without HEPES after addition of either CD3/CD28 beads or EpCAM BiTE. The percentage of IFNγ-expressing T cells decreased over the lactic acid range used from 7.1% and 4.3% for the BiTE and beads, respectively, in complete medium without acid to 0.8% and 1.1% in medium with 20 mM acid. Lower IFNγ expression was seen with as little as 5 mM acid (Figure 4.8C). Although HEPES addition partially mitigated the effect of the acid, IFNγ levels in BiTE-activated T cells nonetheless decreased from 5.8% to 3.3%. Interestingly in complete HEPES-buffered medium, activation with CD3/CD28 beads led to relatively low levels of IFNγ even in the absence of lactic acid, and increased amounts of lactic acid did not further inhibit expression. It therefore appears that the presence of HEPES may affect bead-mediated T cell activation (Figure 4.8D).

Although HEPES partially reversed lactic acid-mediated inhibition observed in T cells when activated with either CD3/CD28 beads or the EpCAM BiTE, the reversal was not complete. This is likely because the HEPES buffering capacity was insufficient to completely restore the pH to physiological levels at the highest concentrations of lactic acid. Activation and function of T cells appears to be extremely pH-sensitive, though this method could not properly discriminate between the influence of the salt form of lactic acid and culture medium pH.

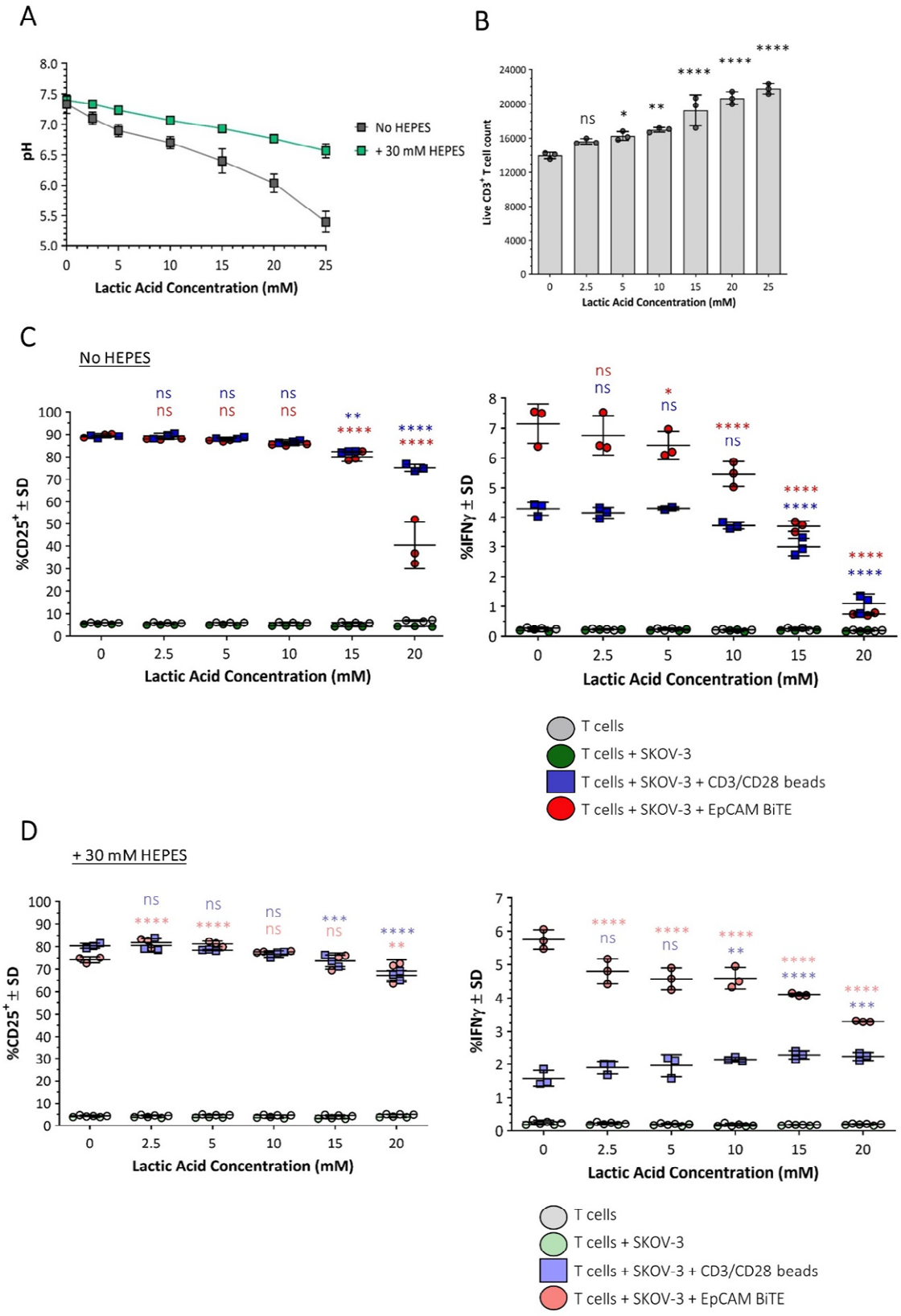

A
pH
Lactic Acid Concentration (mM)
No HEPES
+ 30 mM HEPES
B
Live CD3+ T cell count
Lactic Acid Concentration (mM)
C
No HEPES
%CD25+ ± SD
%IFNγ ± SD
Lactic Acid Concentration (mM)
T cells
T cells + SKOV-3
T cells + SKOV-3 + CD3/CD28 beads
T cells + SKOV-3 + EpCAM BiTE
D
+ 30 mM HEPES
%CD25+ ± SD
%IFNγ ± SD
Lactic Acid Concentration (mM)
T cells
T cells + SKOV-3
T cells + SKOV-3 + CD3/CD28 beads
T cells + SKOV-3 + EpCAM BiTE

Figure 4.8 HEPES buffer addition to lactic acid medium partially restores T cell activation. (A) RPMI 1640 medium was prepared with incremental amounts of 0 – 25 mM lactic acid from a 1 M lactic acid stock in RPMI 1640 medium. Medium was left or buffered with 30 mM HEPES. pH values were measured using a pH meter and probe. **(B)** Live $CD3^+$ T cells were analysed by flow cytometry after 24 hours in culture with lactic acid medium containing HEPES buffer. SKOV-3 ovarian cancer cells were co-cultured with T cells in lactic acid medium without **(C)** and with HEPES **(D)**. T cells were activated with either CD3/CD28 beads or the EpCAM BiTE. At 24h post-activation, the percentage of CD25 expression on T cells was measured and after 6 hours the percentage of IFNγ expression was measured. Data show mean ± SD of biological triplicates. Statistical significance was assessed by a two-way ANOVA test with Dunnett's post-hoc analysis, each treatment being compared to the "0 mM" control condition (B-D) (*, $p < 0.05$; **, $p < 0.01$; ***, $p < 0.001$; ****, $p < 0.0001$; ns, non-significant).

4.2.6 Complete neutralisation of low pH caused by lactic acid accumulation fully restores BiTE activity

As 30 mM HEPES was insufficient to buffer and maintain a physiological pH in medium with high amounts of lactic acid, we used sodium hydroxide (NaOH) to completely neutralise acidic medium before its use in these co-culture experiments. This allowed for complete removal of the effect of low pH on the characterisation of activation, cytolytic potential and cytotoxicity after treatment with the EpCAM BiTE (Figure 4.9A).

The count of total T cells remained essentially unchanged in neutralised medium despite the addition of up to 25 mM lactic acid (Figure 4.9B). To assess whether neutralisation of pH could also reverse the ability of lactic acid to inhibit T cell activation, the percentage of T cells expressing CD25 or IFNγ was measured in neutralised medium after activation with CD3/CD28 beads or the EpCAM BiTE. Under these conditions the presence of lactic acid had no effect on the percentage of CD25-expressing CD4-positive cells after activation with CD3/CD28 beads but a slight decrease was observed after activation using the BiTE (Figure 4.9C). The opposite effect was seen in CD8a cytotoxic T cells, with no effect of lactic acid on CD25 expression after BiTE activation but a slight decrease after bead-mediated activation. Full neutralisation of the lactic acid-mediated acidification prevented any lactic acid-induced changes in IFNγ expression in either T cell subset following activation with the EpCAM BiTE or the CD3/CD28 beads (Figure 4.9D).

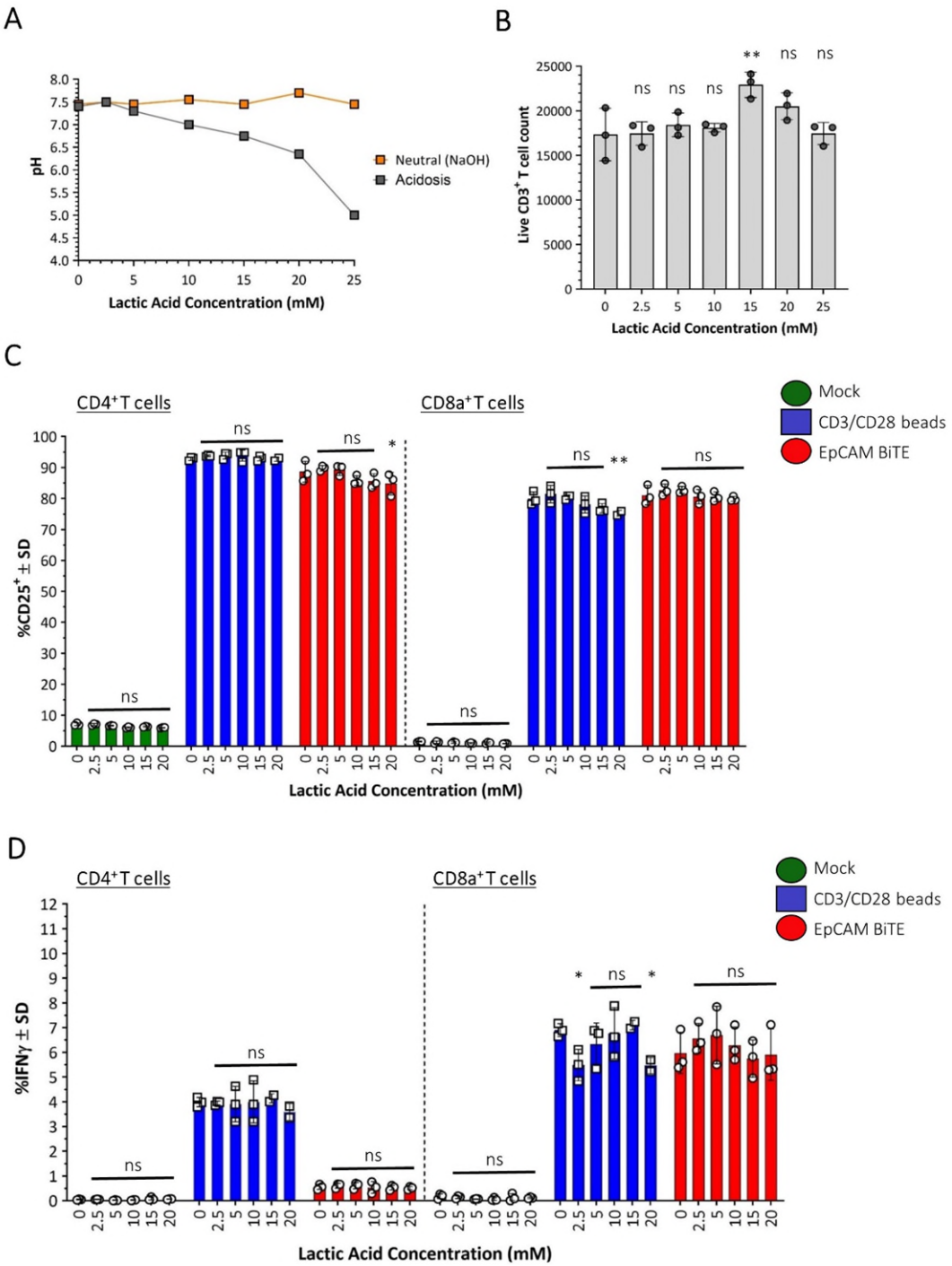


Figure 4.9 Neutralisation of lactic acid medium restores complete T cell activation and cytotoxic potential by the EpCAM BiTE. (A) RPMI 1640 medium was prepared with incremental amounts of 0 – 25 mM lactic acid from a 1 M lactic acid stock in RPMI 1640 medium. Medium was left or neutralised to pH 7.5 before being sterilised and added as culture medium. **(B)** Live $CD3^+$ T cells were analysed by flow cytometry after 24 hours in culture with neutralised lactic acid medium. SKOV-3 ovarian cancer cells were co-cultured with T cells in neutralised lactic acid medium alone or treated with CD3/CD28 beads or the EpCAM BiTE. The percentage of CD25 expression on each T cell subset was measured after 24 hours **(C)**. IFNγ expression **(D)** was measured after 6 hours. Data show mean ± SD of biological triplicates. Statistical significance was assessed by a two-way ANOVA test with Dunnett's post-hoc analysis, each treatment being compared to the "0 mM" control condition (B-D) (*, $p < 0.05$; **, $p < 0.01$; ***, $p < 0.001$; ****, $p < 0.0001$; ns, non-significant).

After confirming that neutralisation of the pH of lactic acid-containing medium essentially removed its ability to inhibit T cell activation, we assessed whether EpCAM BiTE-mediated killing was also restored. Using the xCELLigence assay described in section 2.6.5, we showed that neutralised medium with higher amounts of lactic acid resulted in more rapid tumour cell death compared to culture in neutralised complete medium without lactic acid. This effect was more apparent with SKOV-3 cells, where the kinetics of T cell-mediated cytotoxicity is slower (Figure 4.10A), but the same trend was observed with DLD-1 cells (Figure 4.10B).

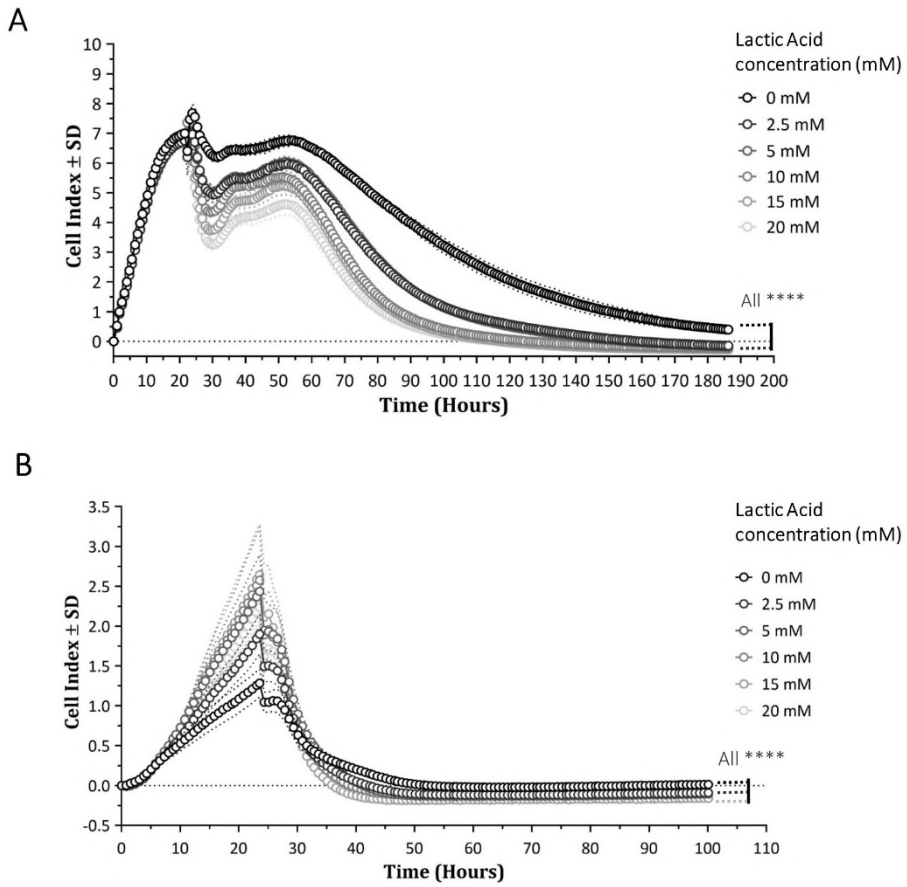


Figure 4.10 Neutralised lactic acid medium restores EpCAM BiTE induced T cell-dependent cytotoxicity of tumour cells. xCELLigence was used to assess the viability of SKOV-3 cells **(A)** and DLD-1 cells **(B)** after treatment with $CD3^+$ T cells and EpCAM BiTE at 24 hours. Cytotoxicity was assessed in lactic acid medium 0 – 20 mM that had been neutralised to pH 7.5 with NaOH before being added to the treatment wells. Electrical impedance was measured at 15 minute intervals. Each condition was measured in biological quadruplicate and represented as the mean ± SD (dashed lines). Statistical significance was assessed by a one-way ANOVA test with Dunnett's post-hoc analysis, each treatment being compared to the "0 mM" control condition at 187 hours in (A) and 100 hours in (B) (*, $p < 0.05$; **, $p < 0.01$; ***, $p < 0.001$; ****, $p < 0.0001$; ns, non-significant).

Restoration of neutral pH by adding NaOH could result in significant changes in osmolality due to the introduction of an osmolyte (Na^+). To account for changes in osmolality, T cell activation was characterised in three different media: medium with lactic acid; medium prepared with the salt form of lactic acid, sodium lactate; and medium made with sodium chloride to osmotically compensate for the addition of Na^+ in the equivalent molar quantities of either lactic acid or its salt form. Figure 4.11A shows the pH values recorded for each of the media prepared. Lactic acid media had a lower pH than sodium lactate or sodium chloride media, which maintained a neutral pH. Total cell counts for CD3-positive cells decreased in medium with 20 mM and 25 mM acid, whereas T cell counts in medium made with the lactate salt or sodium chloride remained at the same level, irrespective of the amount of added lactate salt or sodium chloride (Figure 4.11B). When cultured together with SKOV-3 cells and EpCAM BiTE, the percentage of CD25-expressing T cells decreased in medium with 10 mM acid (pH 7.0). This decrease was completely abrogated in medium with at least 10 mM of the sodium lactate salt or sodium chloride (pH 7.6) (Figure 4.11C).

Together these data show that T cell inhibition results from the low pH reduced by lactic acid accumulation and not by the presence of lactate itself.

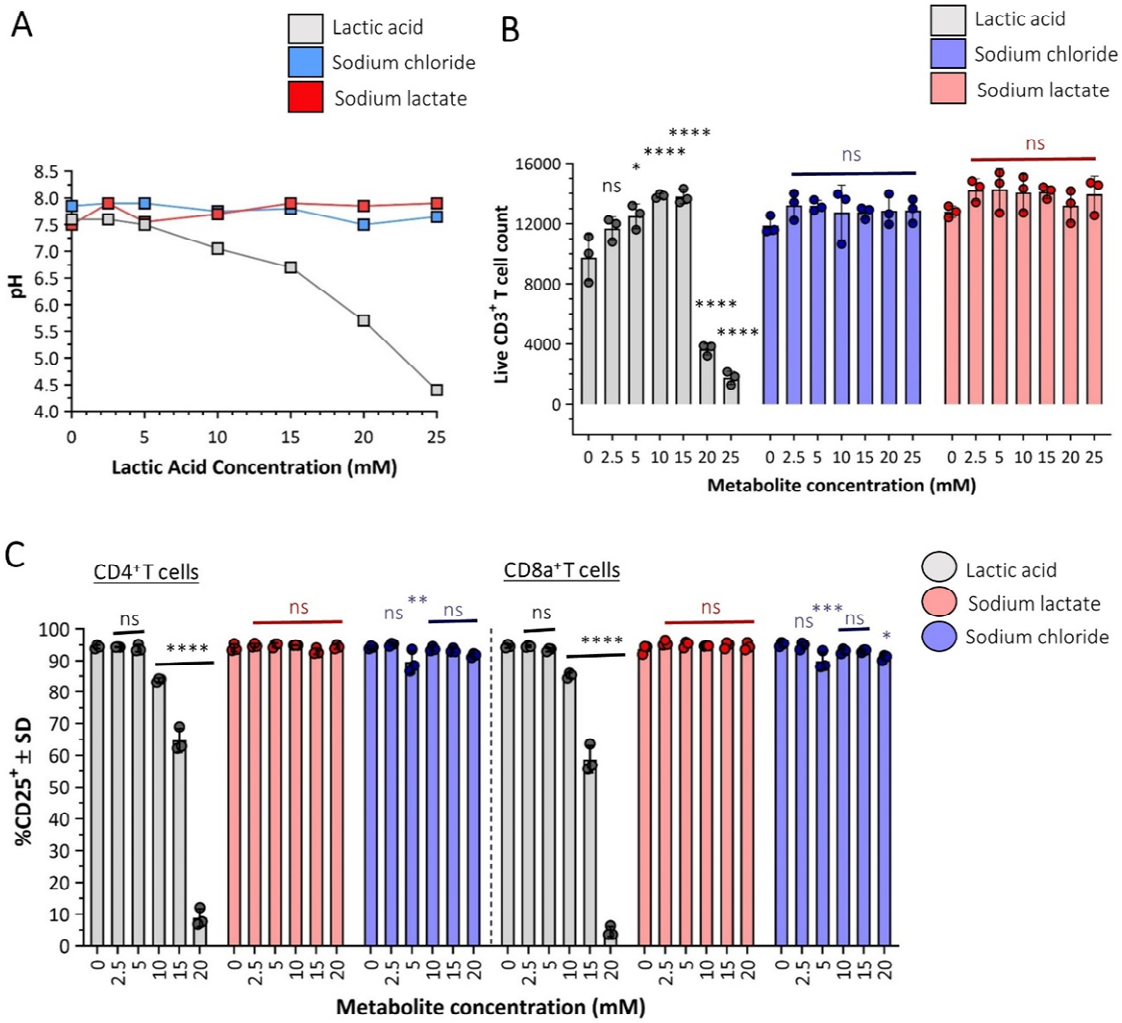


Figure 4.11 Medium prepared from lactic acid, the lactate salt and sodium chloride account for osmolality changes and show inhibition is due to low pH in medium not lactate itself. (A) RPMI 1640 medium was prepared with incremental amounts of 0 – 25 mM lactic acid, sodium lactate or sodium chloride from 1 M stocks prepared in RPMI 1640 medium. **(B)** Live $CD3^+$ T cells were analysed by flow cytometry after 24 hours in culture in each medium made with a different metabolite. Lactic acid in grey, sodium lactate in red and sodium chloride in blue. **(C)** SKOV-3 cells were co-cultured with $CD3^+$ T cells and treated with EpCAM BiTE. The percentage of CD25 expression was measured on CD4 and CD8 T cells after 24 hours. Data show mean ± SD of biological triplicates. Statistical significance was assessed by a two-way ANOVA test with Dunnett's post-hoc analysis, each treatment being compared to the "0 mM" control condition (*, $p < 0.05$; **, $p < 0.01$; ***, $p < 0.001$; ****, $p < 0.0001$; ns, non-significant).

4.2.7 HCl-induced low pH diminished EpCAM BiTE-induced T cell activation

To confirm our findings that low pH is responsible for inhibition of EpCAM BiTE- or CD3/CD28 bead-mediated T cell activation, we examined whether the effect held true for acids other than lactic acid. We used increasing amounts of HCl to match the pH values tested with lactic acid in the previous sections, and the activation and biomarkers of cytolytic potential of T cells were analysed after culturing with immune activators and either SKOV-3 cells or DLD-1 cells using flow cytometry as described in sections 2.5.5 and 2.5.6.

The percentage of CD25-expressing T cells was quantified following activation by EpCAM BiTE in media of different pHs. Figures 4.12A and B shows a significant fall in CD25 activation in medium with a pH of 6.8 or lower in both T cell subsets, independent of the tumour cell type used in the co-culture. CD3/CD28 bead activation of T cell subsets decreased significantly only at a pH of 6.4 and below, in agreement with data above showing that bead-mediated activation was less sensitive to pH changes than EpCAM BiTE-driven activation (Figure 4.6B). In a co-culture with SKOV-3 cells or DLD-1 cells and activation with either CD3/CD28 beads or EpCAM BiTE, the percentage of IFNγ-expressing T cells decreased in medium with a pH of 6.2 or lower in all cases (Figures 4.13A and B). Together, these data confirm our results that T cell activation decreases after treatment with the EpCAM BiTE due to the low pH of the media and not the lactate salt itself.

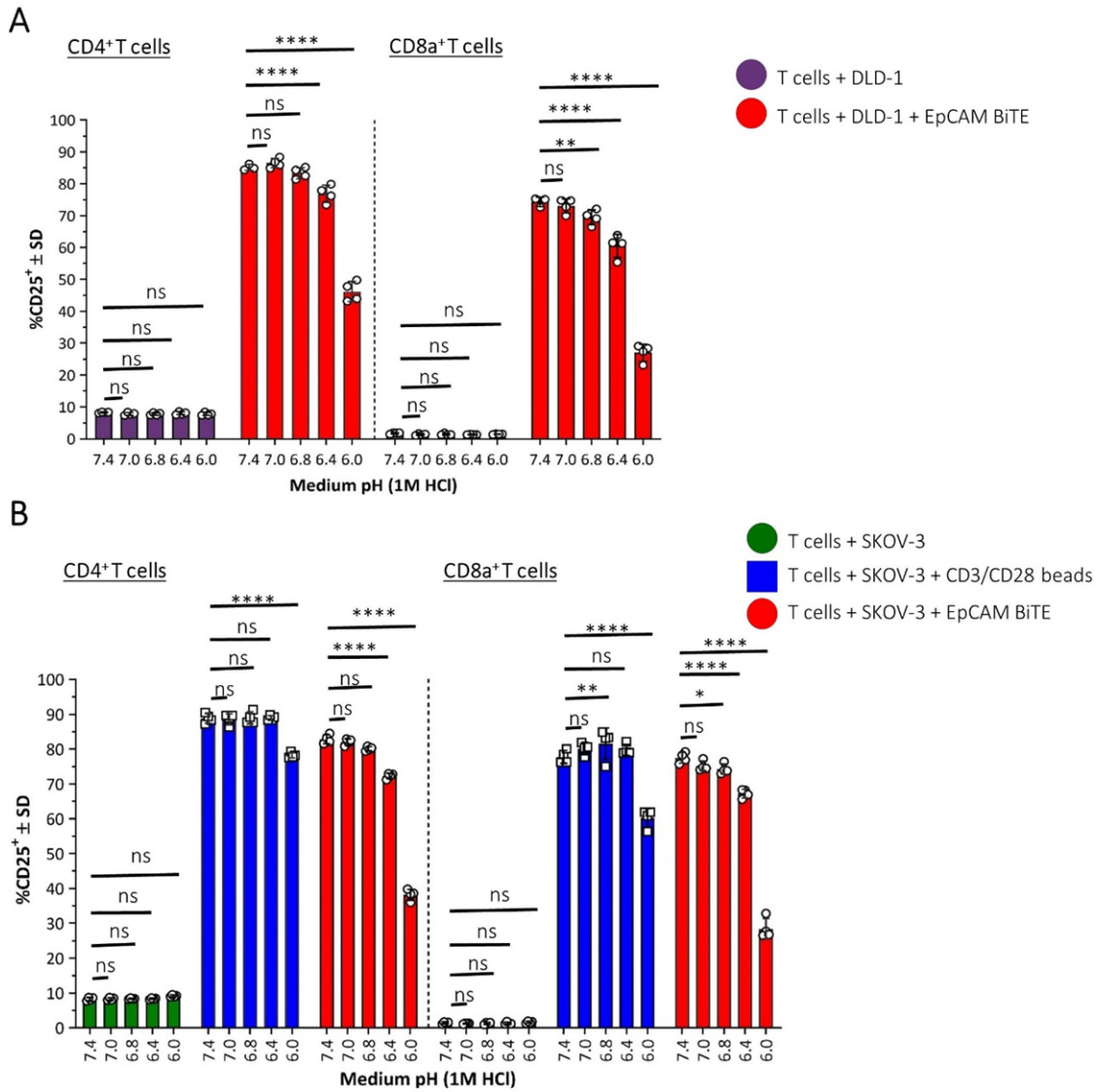


Figure 4.12 Acidosis induced by HCl inhibits T cell activation by the EpCAM BiTE. (A) DLD-1 cells were co-cultured with T cells in low pH medium, created by adding 1 M HCl to reach required pH values. Wells were treated with the EpCAM BiTE and T cell subsets were analysed after 24 hours by flow cytometry for the percentage of T cells expressing CD25. **(B)** SKOV-3 cells were co-cultured with T cells in low pH medium. Wells were treated with the EpCAM BiTE or CD3/CD28 beads and T cell subsets were analysed after 24 hours by flow cytometry for the percentage of CD25. Data show mean ± SD of biological quadruplicates. Statistical significance was assessed by a two-way ANOVA test with Dunnett's post-hoc analysis, each treatment being compared to the "pH 7.4" normal medium control (A-B) (*, $p < 0.05$; **, $p < 0.01$; ***, $p < 0.001$; ****, $p < 0.0001$; ns, non-significant).

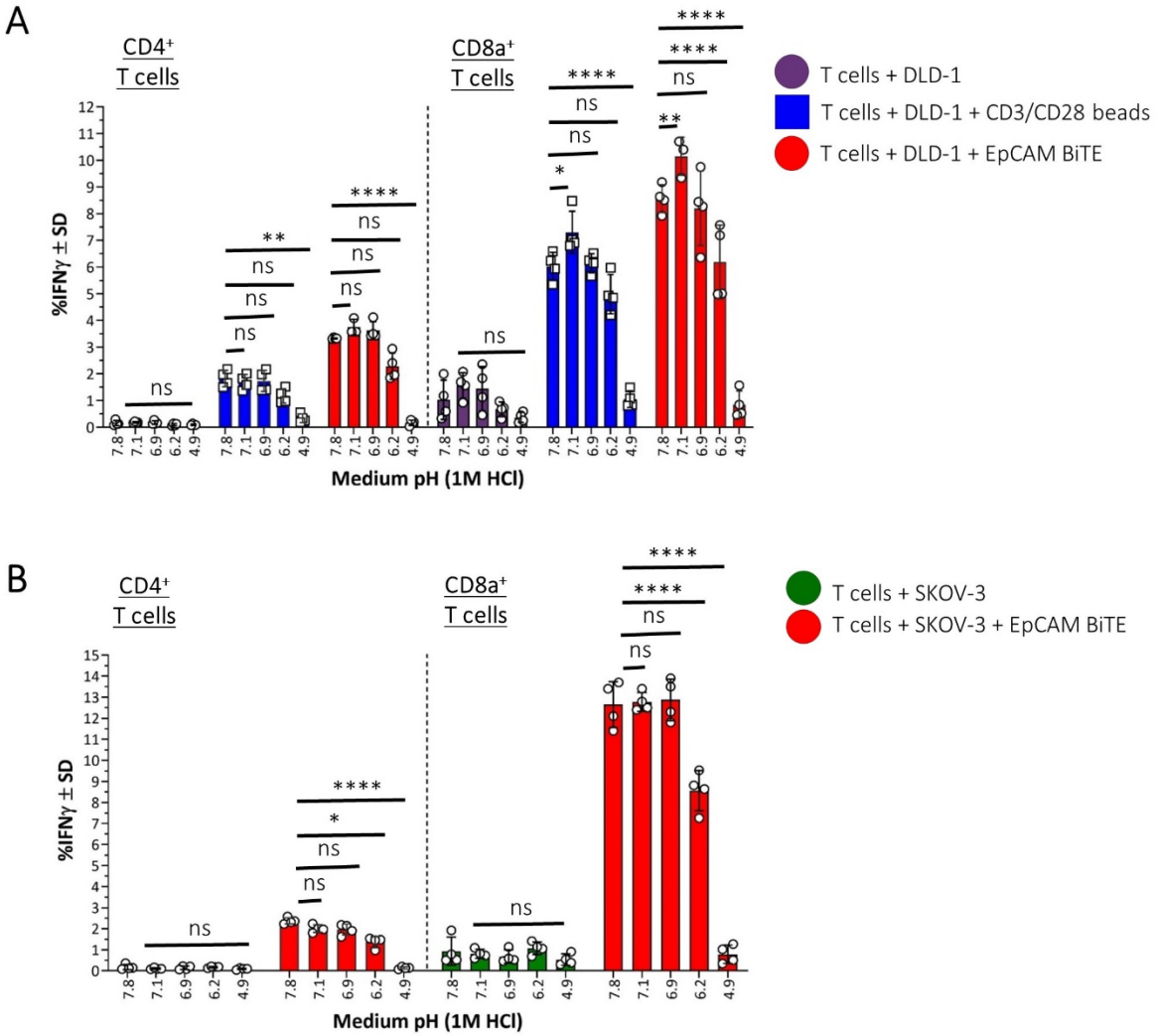


Figure 4.13 Acidosis induced by HCl inhibits T cell cytotoxic potential by the EpCAM BiTE at lower pH values than induced by lactic acid. (A) Low pH medium was prepared by adding 1 M HCl acid to RPMI 1640. DLD-1 cells were co-cultured with T cells in low pH medium. Wells were treated with CD3/CD28 beads or EpCAM BiTE. After 6 hours, T cells were harvested and each T cell subset was analysed for IFNγ expression by flow cytometry. **(B)** SKOV-3 cells were co-cultured with T cells and the EpCAM BiTE in low pH medium. After 6 hours, T cells were analysed for IFNγ expression. Data show mean ± SD of biological quadruplicates. Statistical significance was assessed by a two-way ANOVA test with Dunnett's post-hoc analysis, each treatment being compared to the "pH 7.8" normal medium control (A-B) (*, $p < 0.05$; **, $p < 0.01$; ***, $p < 0.001$; ****, $p < 0.0001$; ns, non-significant).

4.2.8 Binding of EpCAM BiTE constructs to EpCAM$^+$ tumour cells and CD3$^+$ T cells changes in acidic conditions

To determine whether disrupted binding of the EpCAM BiTE could be the reason for the reduction in activation and cytolysis during lactic acidosis, a binding assay was used as described in section 2.4.5. We analysed binding of the EpCAM BiTE to EpCAM-expressing SKOV-3 and DLD-1 tumour cells and CD3-expressing T cells in acidic conditions.

About 25% of SKOV-3 cells stained positively for the αHis-Tag (a component of the BiTE) in cells incubated with the EpCAM BiTE in all media, whereas cells without the BiTE showed no staining, confirming binding assay function. Intriguingly, both the percentage and relative density of αHis-Tag expression increased when cultured in medium with increasing acid concentrations, suggesting increased binding at lower pH (Figure 4.14A). The expression levels of the αHis-Tag in SKOV-3 cells were as expected as this cell line has been shown to have lower levels of EpCAM surface expression compared to DLD-1 tumour cells for example (Freedman et al. 2017).

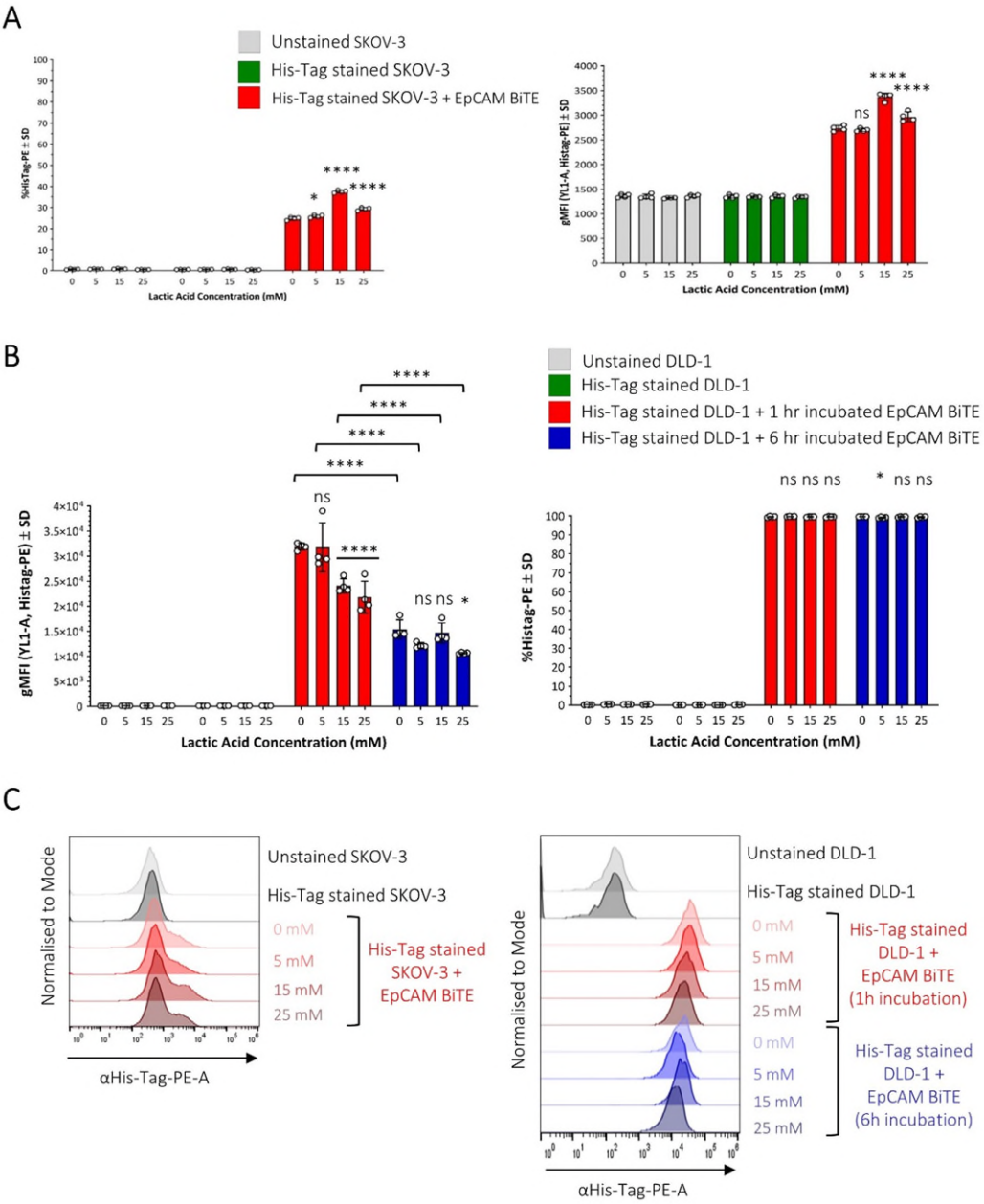


Figure 4.14 EpCAM BiTE binding analysis via its HisTag shows binding to SKOV-3 cells is unaffected but binding in DLD-1 cells may decrease. (A) SKOV-3 cells were left unstained (grey), stained with an α-HisTag Ab (to account for non-specific background staining) (green) or cultured in acidic medium for 1 hour with the EpCAM BITE before being stained with the αHis-Tag Ab (red). The percentage of live cells expressing αHis-Tag, and therefore bound to the EpCAM BiTE, and absolute expression of αHis-Tag in live cells (gMFI) was measured by flow cytometry. **(B)** DLD-1 cells were cultured for 1 hour with EpCAM BiTE in acidic medium (red) or the EpCAM BiTE was incubated in acidic medium for 5 hours prior to addition to cells in the same medium for the additional 1 hour (blue). DLD-1 cells were then stained and analysed by flow cytometry for αHis-Tag binding. **(C)** Representative histograms of αHis-Tag-PE expression on live SKOV-3 and DLD-1 cells after culture with the EpCAM BiTE in medium with increasing amounts of lactic acid. Data is represented as the mean ± SD of biological quadruplicates. Significance was assessed by a two-way ANOVA test with Tukey's post-hoc analysis, each treatment was compared to the "0 mM" control condition (A-B) or in (C) each treatment after 1 hour was compared to the same treatment after 6 hours (*, $p < 0.05$; **, $p < 0.01$; ***, $p < 0.001$; ****, $p < 0.0001$; ns, non-significant).

Binding of the BiTE to DLD-1 tumour cells was also assessed, with EpCAM BiTE incubated in medium with lactic acid for 0h or 5h at 4 ˚C before addition to DLD-1 cells in the same acidic medium for 1 hour prior to staining. Under these conditions 100% of cells stained positively for αHis-Tag and this did not change even after treatment of the BiTE for 6h, though the relative density of molecules (gMFI) decreased in medium with 15 mM and 20 mM lactic acid. Interestingly, the gMFI of αHis-Tag binding decreased two-fold after incubation of the EpCAM BiTE for 6h even in complete medium with no acid (Figure 4.14B). Representative histograms of αHis-Tag-PE expression when EpCAM BiTE was bound in medium containing lactic acid are shown in Figure 4.14C. Binding of EpCAM BiTE to CD3-positive T cells also increased in acidic medium, as measured by the percentage and gMFI of T cells positive for αHis-Tag (Figure 4.15A); representative histograms are shown in Figure 4.15B. In these experiments, T cells remained viable in all acidic media tested (Figure 4.15C).

Whereas the quantity of EpCAM BiTE binding to SKOV-3 cells seemed unaffected by medium containing lactic acid, binding to DLD-1 cells was decreased. This was indicated by the density of αHis-Tag measured (gMFI) but not the percentage of cells positive for αHis-Tag binding, though the decrease in gMFI of wells containing BiTE still far exceeded control wells containing no BiTE. The decrease in gMFI after incubation of the BiTE in complete or acidic medium for 6h suggests the BiTE is unstable even in complete medium when no target cells are present. Together, the results suggest binding to tumour cells is unperturbed in acid but binding to $CD3^+$ T cells increases. This increase does not correlate with CD3 expression on T cells and therefore indicates either increased BiTE binding to the target CD3 antigens or non-specific binding.

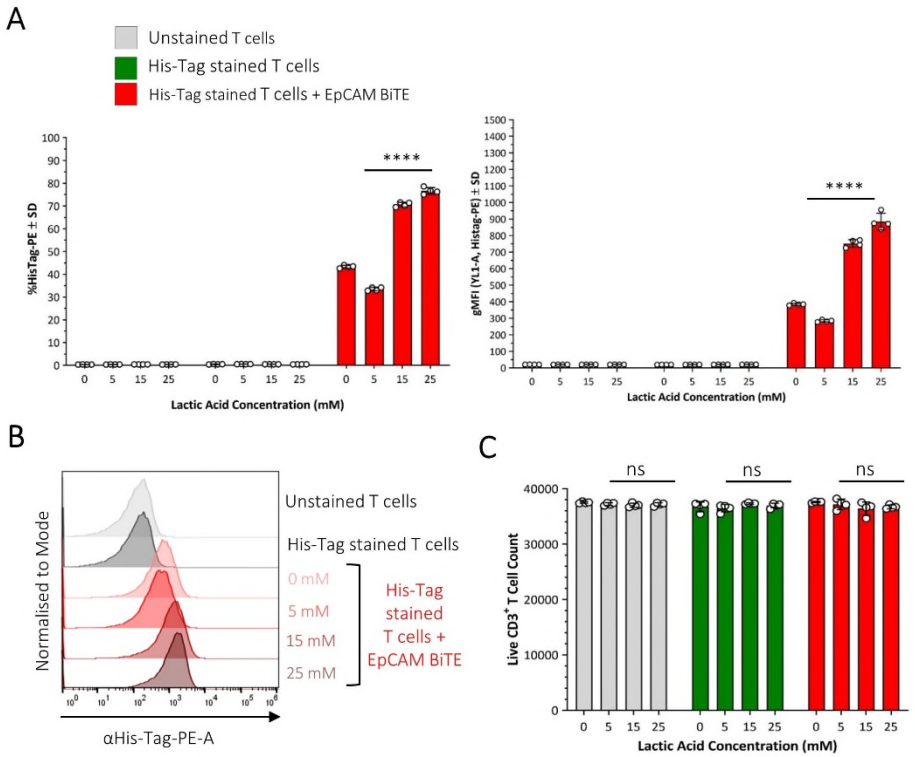


Figure 4.15 EpCAM BiTE binding analysis via the HisTag shows binding to live T cells increases in acidic medium. (A) $CD3^+$ T cells were left unstained (grey), stained with an αHisTag Ab (to account for non-specific background staining) (green) or cultured in acidic medium for 1 hour with the EpCAM BiTE before being stained with the αHisTag Ab (red). The percentage of live T cells expressing αHisTag, and therefore bound to the EpCAM BiTE, or absolute expression (gMFI) of the αHisTag in live cells was measured. **(B)** Representative histograms of αHisTag-PE expression on live T cells after culture with the EpCAM BiTE in increasing amounts of lactic acid medium. **(C)** Live T cells were analysed by flow cytometry using the Viobility 488/520 stain and cell count was analysed after one hour in acidic medium before staining. Data is represented as the mean ± SD of biological quadruplicates. Significance was assessed by a two-way ANOVA test with Tukey's post-hoc analysis, each treatment was compared to the "0 mM" control condition (A, C). Data is represented as the mean ± SD of biological triplicates. Significance was assessed by a one-way ANOVA test with Dunnett's post-hoc analysis, each treatment was compared to the "0 mM" control condition (D) (*, $p < 0.05$; **, $p < 0.01$; ***, $p < 0.001$; ****, $p < 0.0001$; ns, non-significant).

4.2.9 Multiple BiTE constructs are negatively influenced by low pH

Given that the EpCAM BiTE, CD3/CD28 beads and HLA-dependent cytotoxic functions were all inhibited upon lactic acid accumulation in culture medium, acidity presumably affects T cells activated by a number of different mechanisms, as reflected by the literature. However,

our results showed that EpCAM BiTE binding to T cells and DLD-1 cells was influenced by lactic acid. Therefore, we examined whether BiTE constructs with alternative antigen binding targets (PD-L1-OKT3) or epitopes for CD3ε (EpCAM-OKT3) representing differing spatial arrangement possiblities could overcome this inhibition and achieve full functionality compared to the EpCAM BiTE used in this thesis (EpCAM-L2K) (Figure 4.16A).

All BiTEs were used at relative concentrations required to achieve the same EC_{50} value as EpCAM-L2K BiTE; 27.6 pM (EpCAM OKT3; 8.86 pM, PD-L1 OKT3; 2.87 pM). DLD-1 cells were used to compare BiTEs as it expresses both EpCAM and PD-L1. BiTEs were tested in acidic medium with lactic acid and NaOH-neutralised medium with lactic acid. Culture in medium with 10 mM lactic acid resulted in decreased expression of CD25 in CD4-positive T cells activated with any of the three BiTEs, while CD8a-positive T cells were inhibited in 5 mM acid (Figure 4.16B). NaOH-neutralised medium (Figure 4.16C) abrogated the observed inhibition and increased the percentage of CD25-expressing T cells.

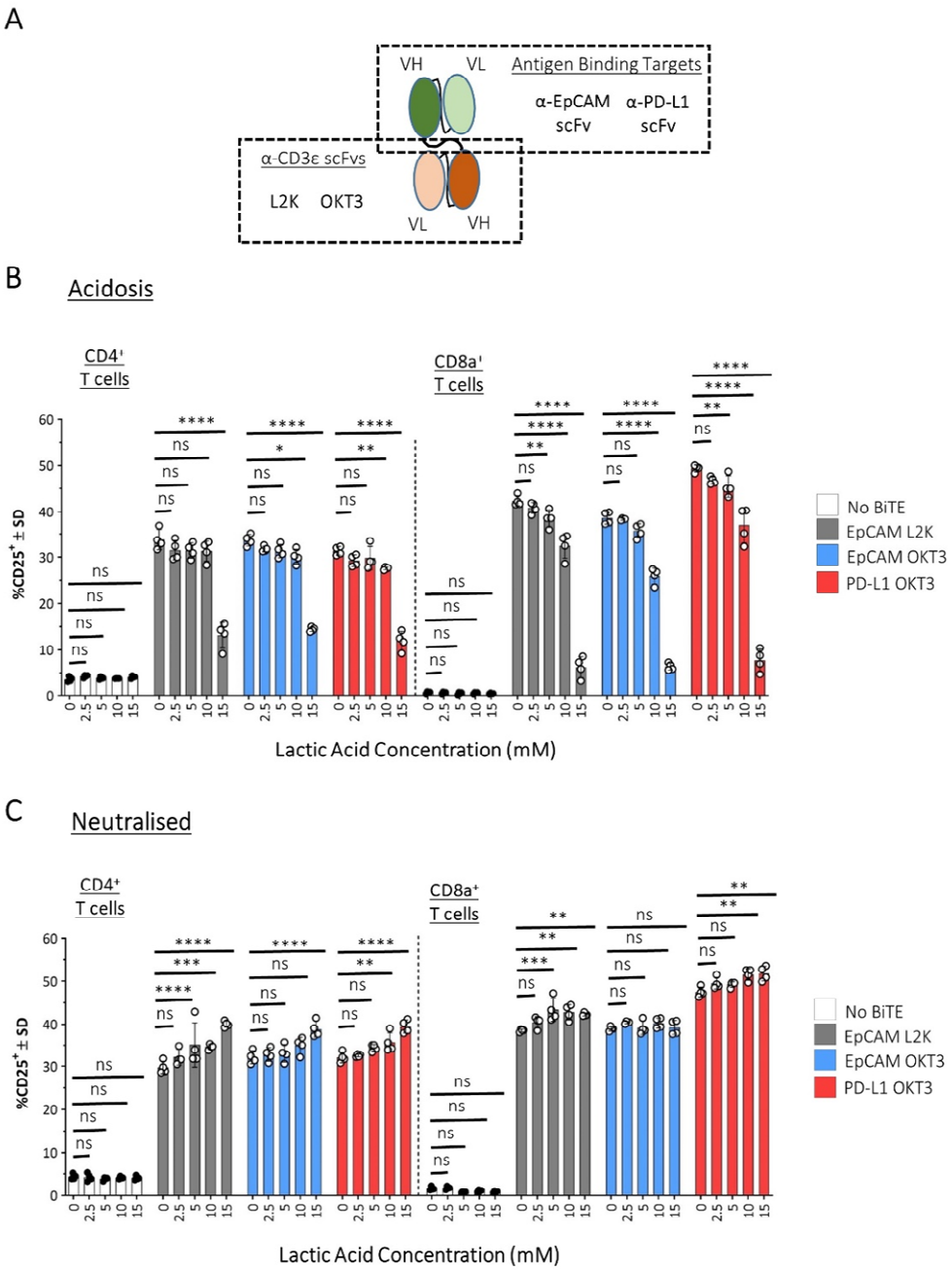


Figure 4.16 Activation of T cells by multiple BiTE constructs is inhibited in the same manner in acidic medium. (A) A schematic of the two different target receptor BiTEs and two different clones of anti-CD3ε scfv. **(B)** DLD-1 cells were co-cultured with $CD3^+$ T cells and left untreated or treated with one of three different BiTEs. Wells were treated with lactic acid medium (acidosis) **(B)** or with lactic acid medium neutralised with NaOH **(C)** for 24 hours. T cells were harvested and stained for CD4, CD8a and CD25 surface expression. Data is represented as the mean ± SD of biological quadruplicates. Significance was assessed by a two-way ANOVA test with Tukey's post-hoc analysis, each treatment was compared to the "0 mM" control condition (B-C) (*, $p < 0.05$; **, $p < 0.01$; ***, $p < 0.001$; ****, $p < 0.0001$; ns, non-significant).

A biomarker for T cell cytolytic potential following activation was analysed for all BiTE constructs in lactic acid-containing and NaOH-neutralised medium after six hours (Figures 4.17A and B respectively). Interestingly no change was observed in the percentage of IFNγ expressed by CD4-positive cells after addition of the BiTEs in either acidic or neutral medium. In CD8-positive T cells, IFNγ expression decreased, most prominently in both BiTEs targeting EpCAM, which induced higher IFNγ expression in complete medium than the PD-L1 BiTE. Although neutralisation led to a decrease of only 1.6% and 1.8% in the percentage of IFNγ-expressing CD8-positive cells treated with the EpCAM-L2K BiTE or the EpCAM-OKT3 BiTE respectively, expression was still partially reduced.

To assess cytotoxicity directly we next measured the ability of the BiTEs to induce cytolysis in DLD-1 cells in acidic or neutralised medium using PrestoBlue as described in section 2.6.3. As shown previously, viability of DLD-1 tumour cells in 20 mM (pH 6.2) and 25 mM (pH 5.2) lactic acid was reduced by more than 50% (Figure 4.1E and Figure 4.2B); therefore, only lactic acid concentrations between 0 (pH 7.5) and 15 mM (pH 6.6) were used. In complete medium without acid, all BiTE constructs reduced tumour cell viability by at least 75%. Viability steadily returned to 100% with increasing amounts of lactic acid, with slight increases in viability observed even in medium with 2.5 mM (pH 7.2) or 5 mM acid (pH 7.0). Significant reductions in cytotoxicity were observed for medium with 10 mM (pH 6.8) or 15 mM acid (pH 6.6). In neutralised medium, cytotoxicity remained unchanged compared to complete medium without acid for all three BiTEs, although viability increased from 20% to 30% for the EpCAM-L2K BiTE (Figure 4.17C).

This data shows BiTE-dependent T cell activation and cytotoxicity are inhibited in the same manner by lactic acid, regardless of the targeted ligand on tumour cells or anti-CD3 targeting domain. It is important to note neutralisation could not fully restore cytokine expression in this case, though this variability could arise due to the use of T cells from different donors.

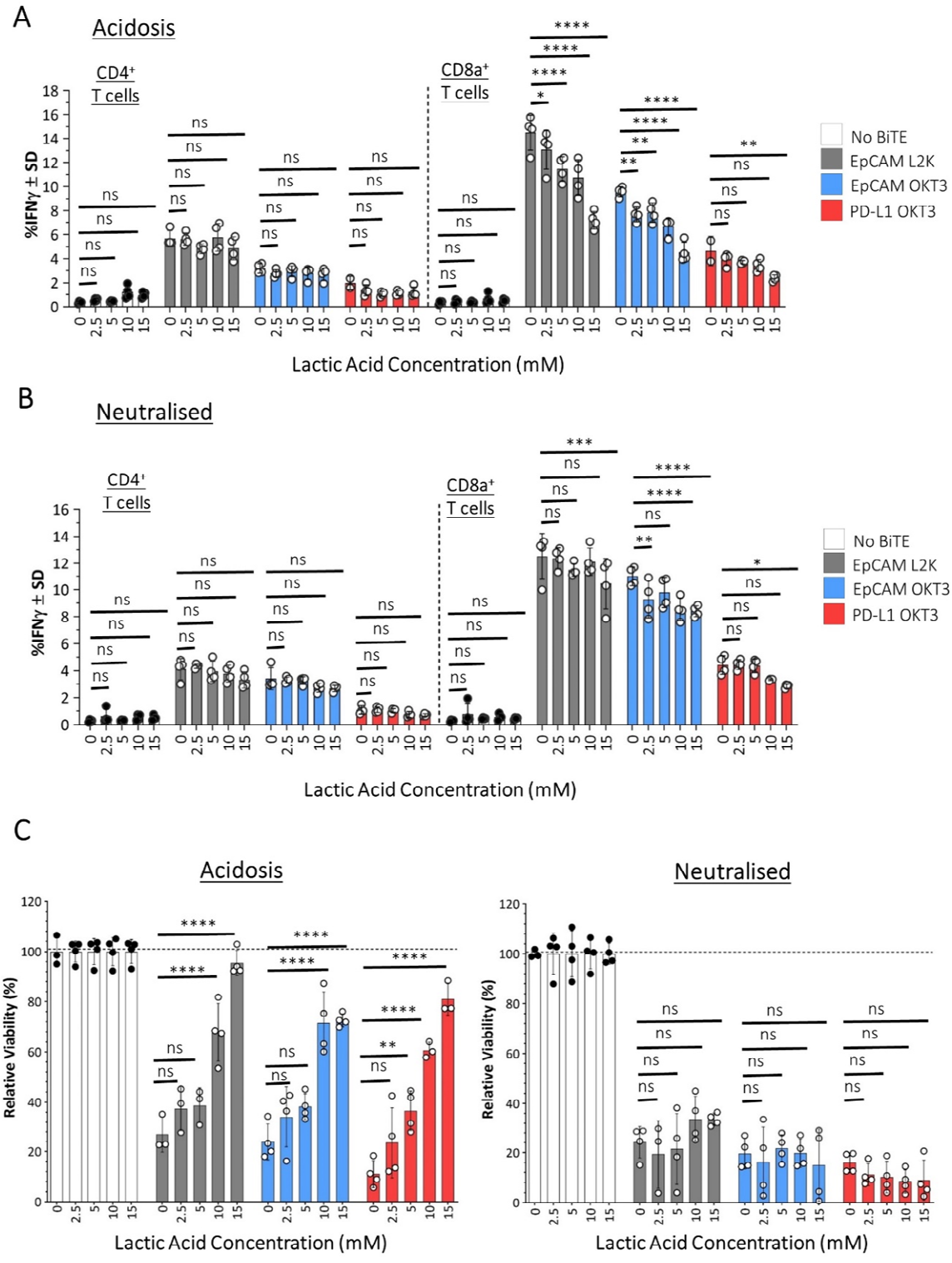

A
Acidosis
CD4+ T cells
CD8a+ T cells
%IFNγ ± SD
Lactic Acid Concentration (mM)
No BiTE
EpCAM L2K
EpCAM OKT3
PD-L1 OKT3
B
Neutralised
CD4+ T cells
CD8a+ T cells
%IFNγ ± SD
Lactic Acid Concentration (mM)
No BiTE
EpCAM L2K
EpCAM OKT3
PD-L1 OKT3
C
Acidosis
Neutralised
Relative Viability (%)
Lactic Acid Concentration (mM)

Figure 4.17 T cell-dependent cytotoxicity induced by multiple BiTE constructs is inhibited in acidic medium. (A) DLD-1 cells were co-cultured with $CD3^+$ T cells and left untreated or treated with one of three different BiTEs. Wells were treated in lactic acid medium (acidosis) or lactic acid medium neutralised with NaOH **(B)** for 6 hours. T cells were harvested and analysed for surface CD4 and CD8a and intracellular IFNγ expression. **(C)** BiTEs were added to a co-culture of $CD3^+$ T cells and DLD-1 cells (5:1). After 24 hours, DLD-1 cell viability was measured using PrestoBlue cell viability reagent. Relative viability (%) was normalised to the viability of the "No BiTE" (untreated) control wells containing DLD-1 cells and T cells only in each medium being tested. Data is represented as the mean ± SD of biological quadruplicates. Significance was assessed by a two-way ANOVA test with Tukey's post-hoc analysis, each treatment was compared to the "0 mM" control condition (A-C) (*, $p < 0.05$; **, $p < 0.01$; ***, $p < 0.001$; ****, $p < 0.0001$; ns, non-significant).

4.2.10 Generation and production of PD-L1 targeting nanoBiTEs

We confirmed that multiple BiTE constructs containing scFvs for different target receptors and linked with scFvs targeting alternative epitopes for CD3ε, all struggled to activate T cells in lactic acid-induced acidosis. However, other antibody formats exist alongside bispecific antibodies. Nanobodies (VHH) for instance have no light chains, they are smaller and are reported to have a higher tolerance to extreme conditions, including non-physiological pH ranges (Chanier and Chames 2019; Jovčevska and Muyldermans 2020). We reasoned that, although acidosis hampers activation by scFv BiTEs, nanoBiTEs may be able to overcome this inhibition. A PD-L1 bispecific light T cell engager (LiTE), consisting of a VHH nanobody against PD-L1 (clone KN035) linked to a scFv specific for CD3ε (clone OKT3) was tested alongside nanoBiTEs, which were formulated from nanobody fragments against both PD-L1 and CD3ε, to test their susceptibility to acidosis-induced inhibition. A diagram of both the LiTE and nanoBiTE tested are pictured in Figure 4.18A.

We engineered two PD-L1-targeting nanoBiTEs with a VHH nanobody targeting CD3ε (clone 60E11) joined by a flexible glycine-serine linker (GGGGS) to a VHH nanobody against PD-L1 (clone KN035). Two constructs were made to represent both orientations: PD-L1-CD3ε or CD3ε-PD-L1. Both BiTEs contained a signal peptide at the N-terminus for secretion and a deca-histidine tag at the C-terminus to allow for detection and quantification following expression

(Figure 4.18B). Engineered constructs were cloned into a mammalian expression vector, pSF-CMV-AMP, downstream of the CMV immediate-early promoter (Figure 4.18C).

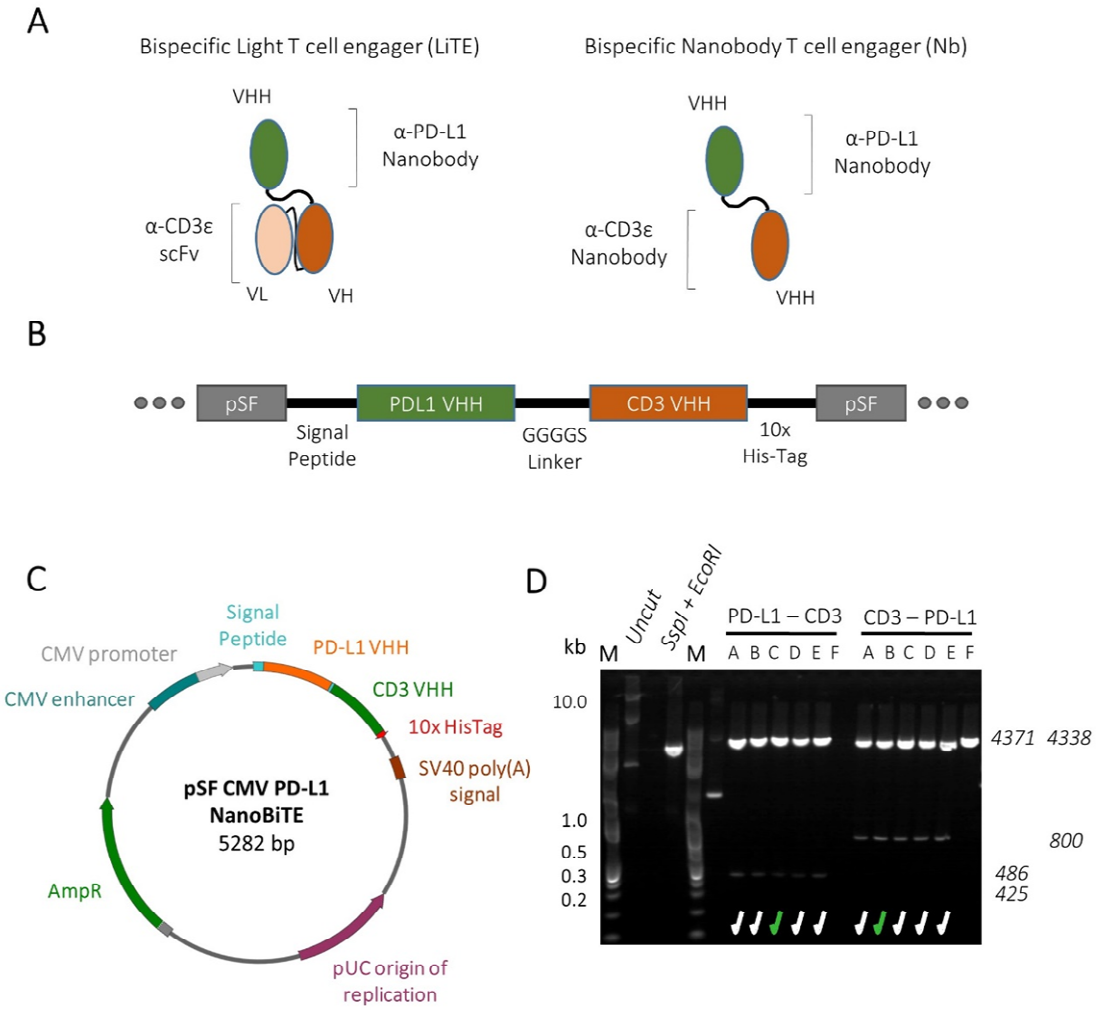


Figure 4.18 Generation of mammalian expression plasmids capable of expressing nanoBiTEs. **(A)** A schematic of a LiTE consisting of a PD-L1 VHH (nanobody) and an anti-CD3 scFv and a nanoBiTE consisting of a PD-L1 VHH (nanobody) and a CD3ε VHH (nanobody). **(B)** The nanoBiTE consists of a signal peptide at the N-terminus of a PD-L1 VHH domain linked to a CD3ε VHH domain with a glycine-serine linker followed by a decahistidine tag at the C-terminus. **(C)** The fragment in (B) was cloned into the pSF-CMV-Amp mammalian expression plasmid under the control of the CMV immediate-early promoter. A schematic of the engineered plasmid is shown. AmpR, ampicillin resistance cassette; SV40, Simian vacuolating virus 40. **(D)** BiTE fragment insertion into pSF-CMV-Amp was confirmed by diagnostic restriction digest with SspI and EcoRI. Predicted band sizes are in *italics*. Colonies with successful insertion are indicated with white ticks; selected colonies for downstream expression work are indicated with green ticks.

Successful expression and secretion of nanoBiTEs into the supernatant following transfection of expression plasmids into 293Ad cells was determined using western blot (Figure 4.19A). NanoBiTE concentrations were determined using a His-Tag ELISA comparing samples of unknown concentration to a standard curve generated from a His-tagged protein standard of known concentration (Figure 4.19B). Concentrations are listed in Table 4.1. NanoBiTE functionality and EC_{50} values were quantified using dose response curves where DLD-1 viability was assessed after treatment with BiTEs and T cells using an MTS assay as described in section 2.6.2. Both engineered nanoBiTEs triggered T cell-dependent cytotoxicity of PD-L1^{+} tumour cells (Figure 4.20A). All BiTEs had EC_{50} values in the picomolar range (Table 4.2).

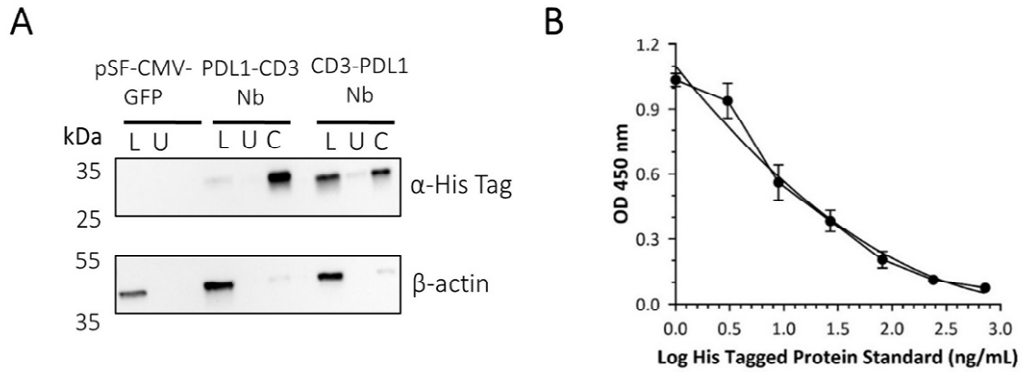


Figure 4.19 NanoBiTE expression confirmation and quantification. (A) BiTE expression plasmids and a pSF-CMV-GFP control expression plasmid were transfected into 293Ad cells, after 48 hours medium and cells were collected. Medium was clarified by centrifugation and concentrated 40-fold. Samples of unconcentrated and concentrated supernatants were kept and cell lysates were treated with RIPA cell lysis buffer. Western blot analysis of all samples was performed and blots were probed with an anti-HisTag primary antibody (mouse) followed by a HRP-conjugated anti-mouse secondary antibody (goat) then reprobed with a HRP-conjugated anti-β actin primary antibody. L, lysate; U, unconcentrated supernatant; C, concentrated supernatant; kDa, kilodaltons. **(B)** A His-tagged protein standard of known concentration was diluted and analysed using a competitive ELISA kit. GraphPad Prism v8 software was used to generate a standard curve of absorbance (OD 450 nm) vs. Log of the protein concentration (ng/mL).

Designed and engineered nanoBiTEs were expressed and functionally active against DLD-1 tumour cells in co-culture with T cells. Dilutions of 1 in 1000 of the EpCAM BiTE (L2K) and the PD-L1 LiTE were enough to drive DLD-1 cell apoptosis whereas the same dilutions of both nanoBiTEs resulted in incomplete killing (Figure 4.20B). Based on the dose response curves, approximately ten times more nanoBiTE than PD-L1 LiTE or EpCAM BiTE was used in comparison experiments.

Table 4.1 BiTE construct concentrations quantified using a standard curve generated from a HisTag ELISA kit. A HisTag ELISA kit was used to quantify unknown His-Tagged BiTE concentrations against a standard curve of known His-Tagged protein standard. The Promega Biomath calculator was used to calculate the molar concentration using quantified BiTE concentration in ng/mL and the estimated molecular weight (kDa) of proteins expressed.

BiTE Construct	Diluted concentration (1/10) Log (ng/mL)	Diluted concentration (ng/mL)	Concentration (ug/mL)	Molecular weight (kDa)	Concentration (nM)
EpCAM L2K	2.67	468	4.68	56.5	82.8
PDL1 OKT3	2.34	218	2.18	56.4	38.6
PDL1 OKT3 (LiTE)	2.38	242	2.42	43.5	55.6
PDL1-CD3 Nb	2.52	331	3.31	28.9	115
CD3-PDL1 Nb	2.46	287	2.87	30.3	94.7

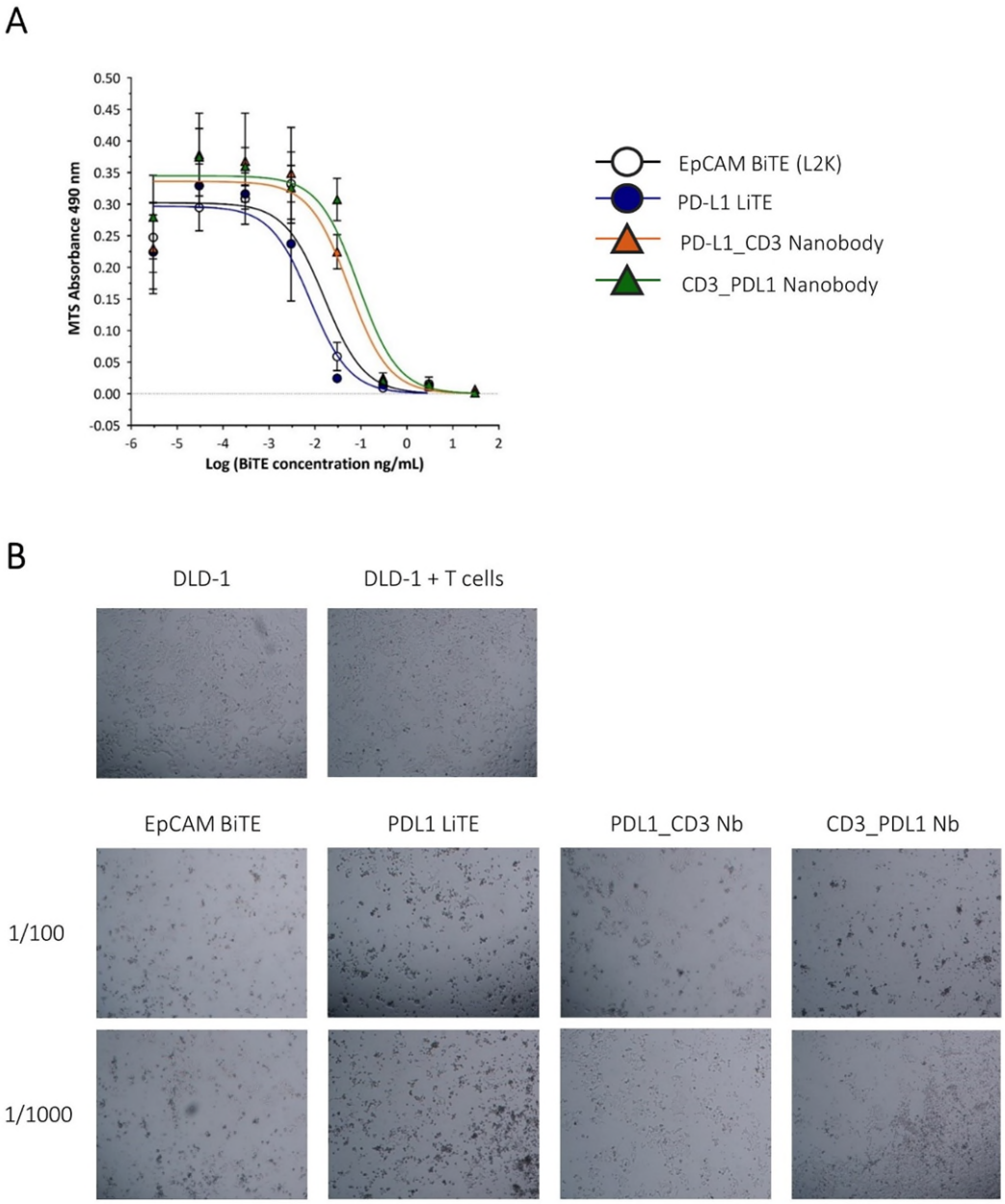


Figure 4.20 NanoBiTEs induce tumour cell death via T cells but are less potent than the EpCAM BiTE and the PD-L1 BiTE. (A) DLD-1 cytotoxicity was measured using an MTS viability assay, absorbance measured at 490 nm. DLD-1 cells were co-cultured with $CD3^+$ T cells in the presence or absence of serially diluted EpCAM BiTE, PD-L1 LiTE or the PD-L1 nanoBiTEs for 48 hours. EC_{50} values were calculated using non-linear fit sigmoidal dose response analysis in Graph Pad Prism v8 software. **(B)** Representative brightfield microscopy images show DLD-1 cell cytotoxicity in diluted BiTE cultures compared to a DLD-1 cell only control and a DLD-1 and T cell only control. After 48 hours, cells were imaged using a Zeiss Axiovert 25 microscope.

Table 4.2 EC_{50} values of BiTE-induced cytotoxicity calculated from dose response curves using an MTS assay. MTS assays were used to create dose response curves for cytotoxicity of DLD-1 cells inferred by BiTE constructs. EC_{50} values were calculated using sigmoidal dose response analysis in Graph Pad Prism v8 software. The EC_{50} in pM was calculated using the Promega Biomath calculator converting EC_{50} in ng/mL using the BiTEs estimated molecular weight (kDa).

BiTE Construct	Log EC50 (ng/mL)	EC50 (ng/mL)	R squared	Molecular weight (kDa)	EC50 (pM)
EpCAM L2K	-1.795	0.0160	0.876	56.5	0.28
PDL1 OKT3 (LiTE)	-2.106	0.0078	0.864	43.5	0.14
PDL1-CD3 Nb	-1.259	0.0551	0.850	28.9	1.91
CD3-PDL1 Nb	-1.060	0.0872	0.842	30.3	2.88

4.2.11 A biomarker of T cell cytotoxicity potential induced by a PD-L1 nanoBiTE or a PD-L1 LiTE remains inhibited during lactic acidosis

The percentage of EpCAM BiTE-induced IFNγ-expressing CD8a-positive T cells decreased 2.0-fold in medium with 15 mM acid (pH 6.9) compared to medium with no acid, while IFNγ expression following treatment with PD-L1 LiTE and PD-L1 nanoBiTE decreased 2.6-fold and 2.3-fold, respectively (Figure 4.21A). Culture in neutralised medium did not reverse inhibition, with the percentage of CD8-positive T cells expressing IFNγ still being reduced by 1.3-fold, 1.5-fold and 2.0-fold for the EpCAM BiTE, PD-L1 LiTE, and PD-L1 nanoBiTE respectively (Figure 4.21B). The percentage of CD4-positive T cells expressing IFNγ was overall much lower as seen previously (Figure 4.6C). A significant reduction was observed in CD4-positive T cells activated with either EpCAM BiTE or PD-L1 nanoBiTE in medium with acid and neutralised medium (Figure 4.21B).

The nanoBiTEs were not able to overcome the T cell inhibition by acidosis. Together with the knowledge that multiple BiTE constructs are affected in the same manner and that CD3/CD28

beads and HLA-dependent activation are also disrupted, the results here suggest that low pH negatively affects T cell function directly, independent of the mode of activation.

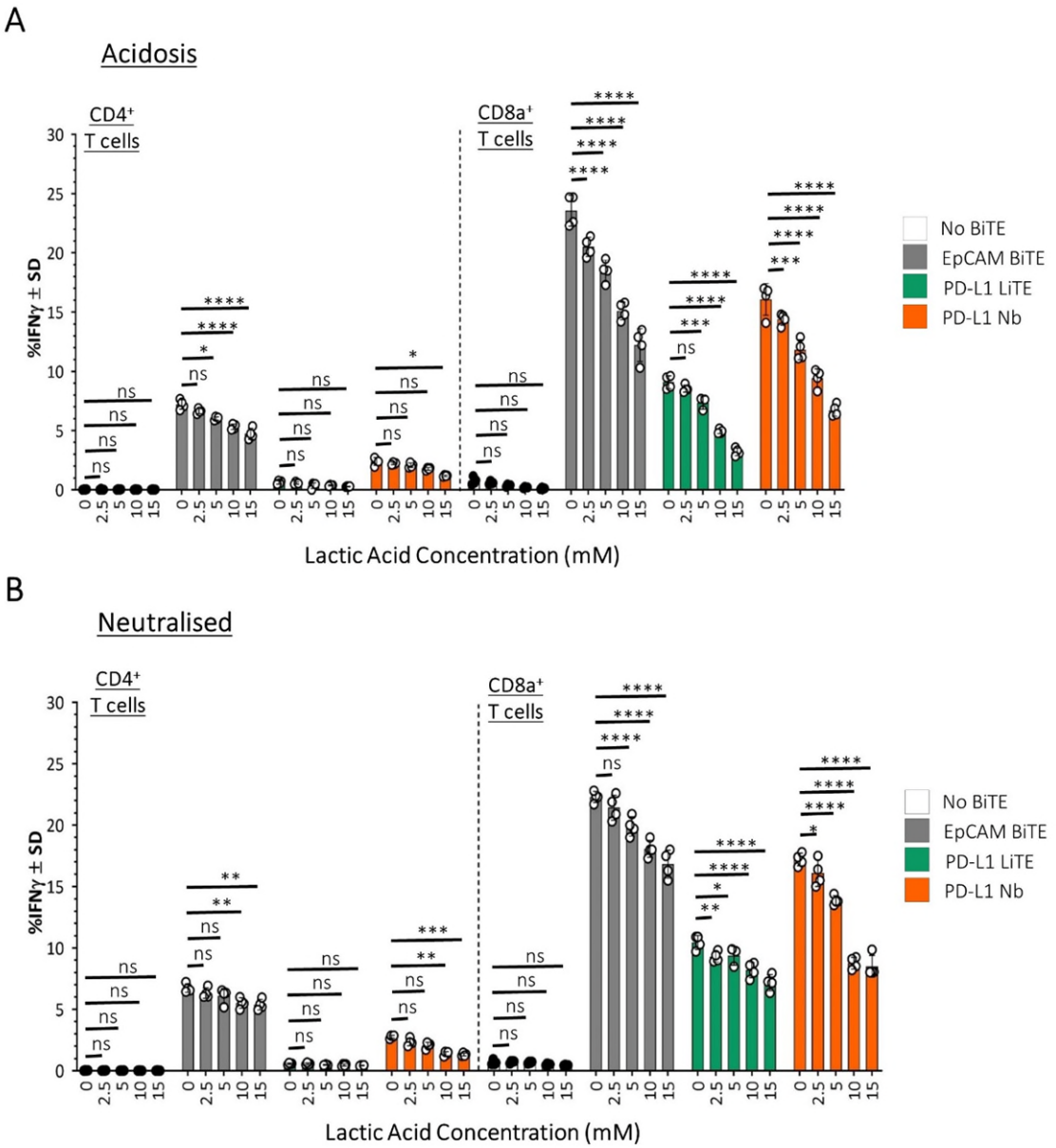


Figure 4.21 T cell-dependent cytotoxicity induced by the PD-L1 LiTE and PD-L1 nanoBiTE (N-PD-L1-CD3-C) is inhibited in acidic medium and partially in neutralised medium. DLD-1 cells were co-cultured with $CD3^+$ T cells and left untreated or were treated with EpCAM BiTE, PD-L1 LiTE or the PD-L1 nanoBiTE (Nb). Wells were treated in lactic acid medium (acidosis) **(A)** or lactic acid medium neutralised with NaOH **(B)** for 6 hours. T cells were harvested and analysed for surface CD4 and CD8a and intracellular IFNγ expression. Data is represented as the mean ± SD of biological quadruplicates. Significance was assessed by a two-way ANOVA test with Tukey's post-hoc analysis, each treatment was compared to the "0 mM" control condition (A-B) (*, $p < 0.05$; **, $p < 0.01$; ***, $p < 0.001$; ****, $p < 0.0001$; ns, non-significant).

4.3 Conclusions

The conclusions of this chapter were:

1. Inhibition of EpCAM-targeted BiTE induced activation of T cells occurred in media containing increasing amounts of lactic acid reaching a pH of 6.1,
2. Reduction in activation and cytotoxicity of T cells results from low pH and not lactate itself,
3. Multiple BiTE constructs targeting either EpCAM or PD-L1 and with different epitopes to target CD3ε were equally affected by acidosis,
4. Treatment with nanoBiTEs did not improve low pH-dependent T cell inhibition.

4.4 Discussion

In this chapter, we explored whether the EpCAM BiTE, a T cell activating platform, would be sufficient to overcome the immunosuppressive power of lactic acid, reported to be a driver of T cell suppression in many solid tumour types (Allison, Coomber, and Bridle 2017; Chiche, Brahimi-horn, and Pouysségur 2010). The differential signalling pathways and 'super activatory' nature of BiTEs led us to hypothesise that the mechanisms behind T cell inhibition *via* lactate or proton build up may not be as potent following a non-canonical form of activation, such as BiTEs, relative to a HLA-dependent form of activation.

We found that T cells could not be activated by the BiTE in medium with lactic acid. Inhibition was mediated by the low pH of medium with lactic acid as opposed to the build-up of the salt form, lactate (Figures 4.3 – 4.13). These results are in agreement with multiple reports that implicate acidity as the regulator for cytokine release and cytotoxicity and not lactate itself (Huber et al. 2017). Not only did we observe this effect on the EpCAM BiTE but also with

BiTEs targeting PD-L1 and nanoBiTE constructs targeting PD-L1 that are reported to be more stable in extreme conditions (Figures 4.16 - 4.17 and 4.21). We did not, however, test an exhaustive list of bispecific formats. As other formats exist, including those that simultaneously target multiple stimulatory domains on T cells, and as the signalling pathways behind acidic inhibition have not yet been conclusively identified, it is entirely possible that a more potent antibody using an alternative format could overcome the observed T cell inhibition by low pH (Ellerman 2019; Smith-Garvin, Koretzky, and Jordan 2009).

In our investigation, we compared acidification-induced inhibition of T cell activation and cytotoxicity following activation with a BiTE, CD3/CD28 beads, or HLA-dependent activation using an antigen-specific T cell clone. We found that activation by the BiTEs (binding to CD3 alone) was more sensitive to low pH than activation by CD3/CD28 beads (Figures 4.4 and 4.6). However, T cell cytokine release and induced target cell cytotoxicity was inhibited for all modes of activation in low pH medium (Figures 4.6 and 4.7). T cell function is therefore likely to remain suppressed at low pH irrespective of the mode of activation.

Our results are supported by recent findings from Wu *et al* (Wu et al. 2020), who observed that lymph nodes contain acidic niches in order to control T cells and their effector functions. Using *in vivo* fluorescence and MRI they showed that lymph nodes have acidic paracortical zones that disappear in lymphodepleted mice, indicating a role for T cells in the acidification process. They also showed that acid inhibition of MCTs results in the negative feedback on the glycolytic rate of T cells by lactate and intracellular proton accumulation, demonstrating that this phenomenon does not interfere with initial activation but rather downstream effector functions, such as cytokine release. This physiological role of regulating T cell activation protects the lymph nodes from premature T cell activation. Many different groups have suggested roles for acid-sensing receptors such as GPR65 and GPR68, acid-mediated ligand interactions such as VISTA binding to P-selectin glycoprotein ligand-1 as well as acid-sensing

channels in the mechanism for acid suppression of T cells (Erra Díaz, Dantas, and Geffner 2018; Pilon-Thomas et al. 2016). However, the knockout studies in the Wu *et al* publication demonstrated that the acid effect did not involve any of these mechanisms and was instead a consequence of enhanced glycolysis and the negative feedback on both MCTs and glycolytic enzymes. However, this study induced a low pH environment by adding HCl and not lactic acid, and used both anti-CD3 and anti-CD28 antibodies to drive T cell activation. Although the acidic niches of lymph nodes were shown to be a result of lactic acid accumulation, the study did not replicate this accumulation and instead replicated pH levels only. The studies presented in this thesis indicated differences in sensitivity to low pH induced by HCl or lactic acid, particularly in IFNγ expression after BiTE- and CD3/CD28 bead-mediated activation (Figures 4.6 and 4.12- 4.13). Together, this emphasises the exquisite control of lactic acid accumulation on T cells.

In light of the findings in this chapter, we conclude that BiTE technology cannot overcome the power of suppression induced by acidification. TME acidification is a common feature across a broad range of tumour types and a likely obstacle to any immunotherapies involving T cell stimulation. Taking into account the findings in Wu *et al*, we speculate that TME acidification could be yet another mechanism usurped by cancer from nature. In the following and final experimental chapter of this thesis, we attempt to provide a solution to acidification-induced T cell suppression in the TME.

5 Assessing the potential of targeting acidosis using armed oncolytic adenoviruses

5.1 Introduction and chapter aims

5.1.1 Introduction

In the previous chapter, we found that the functional activity of multiple scFv-based BiTEs and nanobody-based BiTEs was abolished in lactic acid-induced low pH. Extracellular acidity is hypothesised to be one of the major barriers to immune-based therapies in the TME and correlates with poor prognosis in patients. It is predicted to be responsible for the limited efficacy of checkpoint therapies, the most promising immunotherapeutics of the last decade (Martens et al. 2016; Damuzzo et al. 2016; Weide et al. 2016).

Strategies to target acidity in the TME currently include: small molecule inhibitors capable of disrupting lactic acid production and export, glycolysis inhibitors that block the shift to Warburg metabolism, and proton transport inhibitors targeting V-ATPases, NHEs and CAs (Lacroix et al. 2018). Alternatively, systemic buffering using alkaline supplementation, *e.g.* sodium bicarbonate, has been reported to improve checkpoint blockade therapies in murine models (Pilon-Thomas et al. 2016). Although promising in combination with checkpoint inhibitors and cellular therapies, there are limitations to the anti-acidity compounds currently in clinical trials. Current compounds have detrimental effects on T cell function, and other effector immune cells, by targeting the same components of the glycolytic pathway used by both cancer cells and T cells to reach their maximum activation potential (Doherty and Cleveland 2013; Ippolito et al. 2018).

OVs offer an alternative strategy to deliver therapeutics and avoiding off-target effects, by delivering the therapy directly to the tumour site and replicating, thereby increasing the dose *in-situ* (Scott et al. 2017). Approaches to improve the potency and selectivity of oncolytic therapies have increasingly taken advantage of the RNAi pathway to silence genes that hamper virus efficacy (Brachtlova and van Beusechem 2018). Using this method of interference, components involved in extracellular acidification may be selectively targeted with shRNAs. Viral vectors can be encoded to express shRNAs driven by the Pol III U6 promoter, which is well characterised, small in size, and provides high levels of expression and gene silencing in multiple cell types (Giering et al. 2008). Furthermore, shRNAs can be designed from commercially available siRNA sequences previously validated for efficient knockdown (Barøy, Sørensen, and Mari 2010).

In this chapter, we assessed the potential for arming the OAdV EnAd with shRNA constructs for the targeted knockdown of proteins that modulate glycolysis-induced acidity of culture medium, LDHA and MCT-4 (Doherty and Cleveland 2013). To investigate this, a two-pronged approach was undertaken. We first studied the ability of siRNAs targeting LDHA and MCT-4 to induce changes in a relevant cell line model representative of acidosis observed in the TME. Next we evaluated the impact of acidity on the replicative and cytotoxic properties of the well-studied and clinically-relevant OAdV EnAd, to determine its suitability as a platform for shRNA expression (Illingworth et al. 2017). Finally, we engineered EnAd to express shRNAs based on the validated siRNA constructs and assessed the ability of shRNA-encoding viruses to i) replicate; ii) lyse tumour cells and, iii) silence target genes.

5.1.2 Chapter aims

The aims of this chapter were to:

1. Establish a model to represent the acidosis of the TME using tumour conditioned medium,
2. Quantify the extent of pH modulation that can be achieved using siRNAs targeting LDHA and MCT-4,
3. Characterise the EnAd life cycle during lactic acidosis and after treatment with LDHA, LDHB and MCT-4 siRNAs resulting in aberrant host cell metabolism,
4. Engineer EnAd to express shRNA against LDHA and MCT-4,
5. Assess the oncolytic and replicative properties of EnAd-encoding shRNAs and evaluate shRNA activity following infection.

5.2 Results

5.2.1 Conditioned medium from DLD-1 tumour cell cultures inhibits T cell activation by EpCAM BiTE

In the previous chapter we observed that BiTEs are unable to activate T cells efficiently in medium that had a pH between 6.8 and 6.4 (10-15 mM lactic acid respectively). A549 and DLD-1 cells both rely on glycolysis for sufficient growth and proliferation. As glycolysis is the main source of lactic acid, we deduced that conditioned medium from these cell types would cause T cell inhibition. To test this hypothesis, we cultured A549 cells or DLD-1 cells for 48 hours and 72 hours respectively in 2% RPMI, then harvested the medium from those cells (conditioned medium, CM). We then used the different CM to set up a T cell activation assay: a co-culture of DLD-1 cells and T cells with or without EpCAM BiTE.

When compared to a 2% RPMI medium alone control (Ctrl), CD25 activation in both $CD4^+$ T cells and $CD8a^+$ T cell subsets was reduced in CM from both A549 cells and DLD-1 cells, with

the latter having a bigger effect on reduction (Figure 5.1A). We measured the lactate concentration in the CM (Figure 5.1B) and confirmed lactic acid accumulation. These results show that culture medium from tumour cells can inhibit T cells, and this is due to the buildup of lactic acid in the CM.

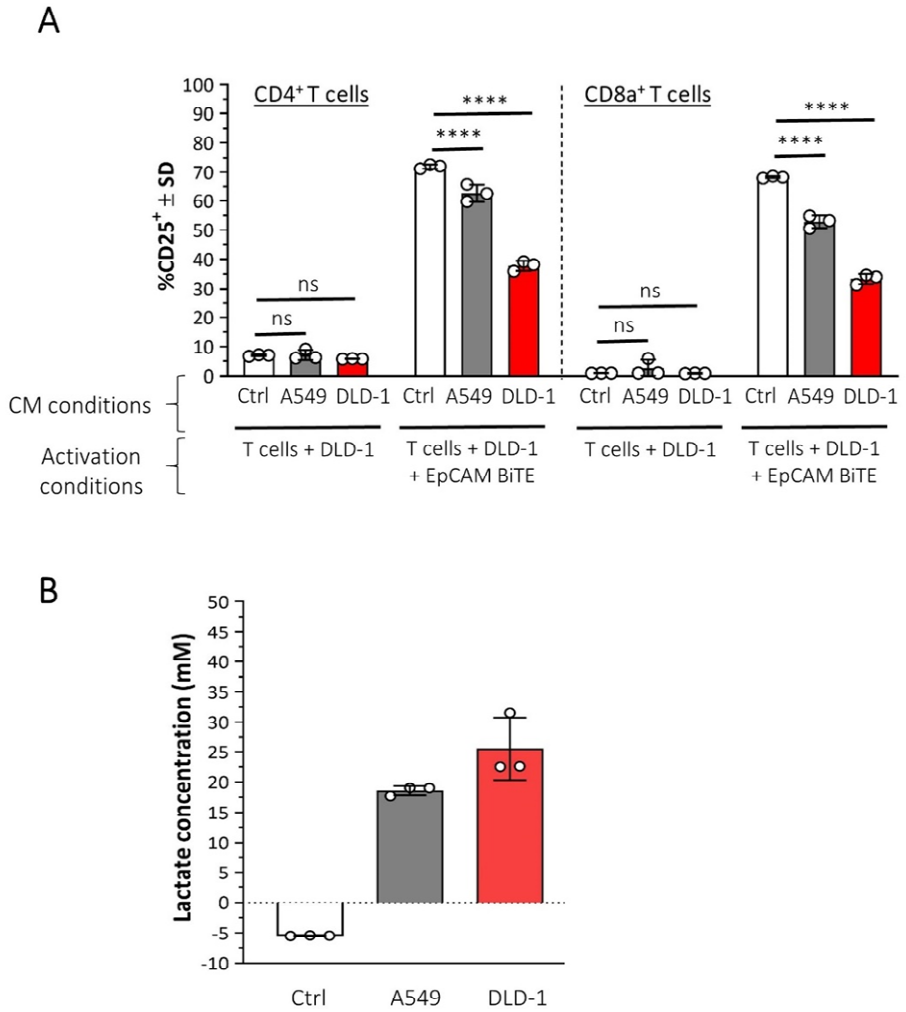


Figure 5.1 T cell activation is decreased the most after culture with CM from DLD-1 tumour cells, associated with lowered pH and not increased lactate. (A) A549 and DLD-1 cells were seeded in 10% RPMI then medium was changed 24 hours later to 2% RPMI. A549 cells were left for 48 hours while DLD-1 cells were left for 72 hours. After the relevant culture time medium was harvested and centrifuged to clear it of tumour cells. Co-cultures of DLD-1 cells and $CD3^+$ T cells were prepared in the presence or absence of the EpCAM BiTE in control (Ctrl) medium, 2% RPMI, or in CM taken from tumour cells. T cells were harvested after 24 hours and activation was measured by analysing for surface expression of CD25 on separate T cell subsets. Data show the mean ± SD of biological triplicates. Significance was assessed by a two-way ANOVA test with Tukey's post-hoc analysis comparing experimental conditions with the "Ctrl" condition. **(B)** 2 µL of the CM used for the T cell activation assay in (A) was diluted 1 in 50 in DPBS before the lactate content was measured using the Lactate-Glo assay kit. Data show the mean ± SD of biological triplicates.

5.2.2 Culturing cells in high glucose increases the level of acidification, recreating the environment more likely observed in patient tumours

Since we had found that, lactic acid accumulates in the CM after culture of DLD-1 cells, we next wanted to establish a model in which the pH would mimic the acidic environment in a tumour (Edmondson et al. 2014). We sought to design a model which would have environmental pH values low enough to inhibit T cell activation (pH 6.8), and that would recapitulate the tumour masses found in patients (Calcinotto et al. 2012). The principal source of lactic acid in the TME is glycolysis, therefore we reasoned that the availability of glucose in RPMI (11 mM) in the current system could be the limiting factor for the extent of acidification observed. In view of this we added incremental amounts of glucose to 293Ad cells, DLD-1 cells, A549 cells and SKOV-3 cells and measured the pH values to determine the glucose concentration required for relevant pH values for T cell inhibition.

The cells were cultured in either RPMI (Figure 5.2A) or DMEM (Figure 5.2B) media over 7 days. By day 4 the media had started to acidify (indicated by phenol red colour changes). On day 7 the pH of the media was measured and wells were imaged. In RPMI containing 20 mM glucose the pH fell in A549, DLD-1, and 293Ad cells, all cells which display a glycolytic phenotype. SKOV-3 cells, a quiescent cell type, remained neutral with a pH of approximately 7.8. In DMEM, higher supplementation of glucose, approximately 40 – 60 mM, was required to reach the lowest pH values recorded. Interestingly, medium from A549 cells cultured in both media types did not reach a pH lower than 7.0.

Culturing glycolytic cells lines in a 2D monolayer in DMEM or RPMI medium supplemented with 60 mM glucose resulted in acidified medium with a pH of approximately 6.6. This pH level is in line with the range of pH conditions recorded in different types of tumour masses

and is also known to be inhibitory to T cell activation by BiTEs (Figure 4.6) (Webb et al. 2011; Robert J Gillies et al. 2002).

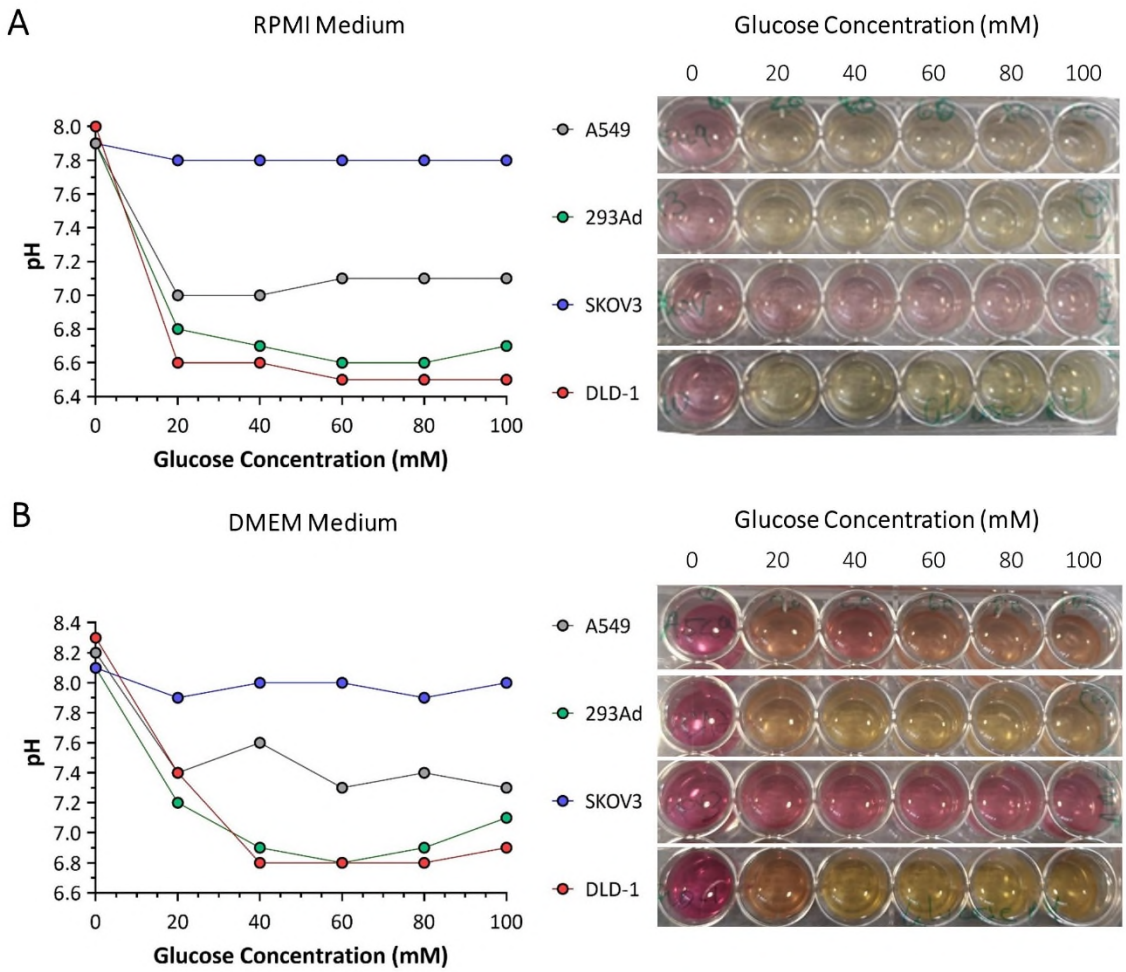


Figure 5.2 Glucose addition to RPMI and DMEM medium in DLD-1 cells, not SKOV-3 cells, results in lactic acid induced pH changes. A549 cells, DLD-1 cells, 293Ad cells and SKOV-3 cells were cultured for 72 hours in RPMI 1640 **(A)** or in DMEM **(B)** media supplemented with 2% FBS and increasing concentrations of glucose, medium was harvested and the pH was measured using a pH probe and meter (Jenway 3610). Phenol red indicator in media changes from pink to yellow, colour change was monitored each day. Images here were taken at 72 hours post glucose addition.

5.2.3 Conditioned medium from EnAd-infected tumour cells does not worsen inhibition of T cells in medium from uninfected tumour cells

All adenoviruses increase glucose uptake, glycolysis and therefore lactic acid secretion upon infection of tumour cells. Although EnAd has been reported to activate the immune response against tumour cells *in vivo* it could be reasoned that, due to increasing the lactic acid output of cells, it may inhibit T cells indirectly (Dyer et al. 2019). As a first step in assessing if EnAd can be used as a platform for the modulation of the pH in the TME, we tested whether infection of cells with EnAd might generate more lactic acid and interfere with the intended pH modulation. Using the normal glucose (11 mM) and high glucose (60 mM) models we described in section 5.2.2, we carried out a CM experiment using three cells line: A549, SKOV-3 and DLD-1. We cultured each cell type in normal and high glucose for 24 hours and subsequently infected them with EnAd at an MOI of 5. A549 cells were incubated for 48 hours, SKOV-3 cells for 144 hours, and DLD-1 cells for 72 hours; these timepoints were chosen as the timepoint at which most cells were actively infected but few had started to die using the xCELLigence assay as described in section 2.6.5 (Figure 5.3). We then used the CM collected to set up T cell co-culture experiments with DLD-1 cells with and without EpCAM BiTE and measured T cell activation 24 hours later.

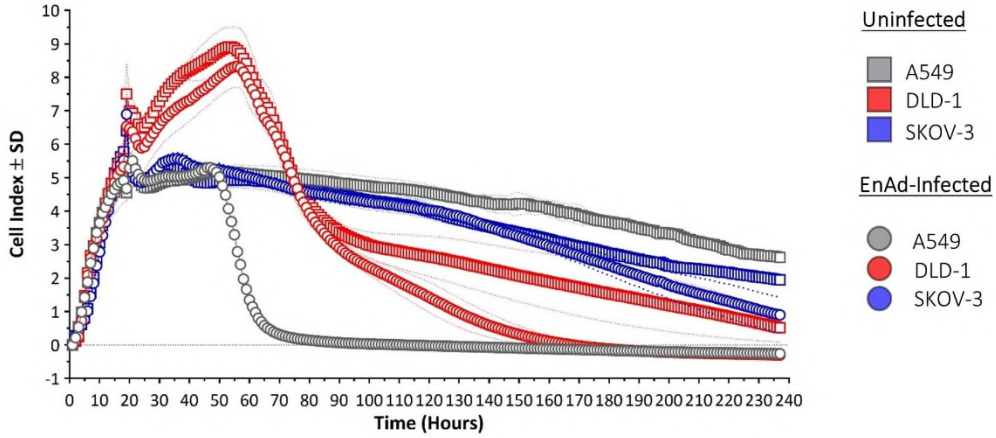


Figure 5.3 EnAd-induced tumour cell lysis in SKOV-3 cells, DLD-1 cells and A549 cells to determine point of CM harvest. 1.5 x 10^4 cells, SKOV-3 (blue), DLD-1 (red) and A549 (grey) were left untreated or infected with EnAd at MOI 5. Cell viability was monitored over 240 hours**.** Electrical impedance was measured at 15 minute intervals, each condition was measured in biological quadruplicate and represented as the mean ± SD (dashed lines).

In normal glucose conditions (Figure 5.4A), conditioned medium from uninfected DLD-1 cells significantly reduced the percentage of CD25-positive T cells, both the CD4-positive and CD8-positive populations. CM from uninfected DLD-1 cells reduced the percentage of CD25-positive T cells by nearly 50%, while CM from uninfected SKOV-3 cells reduced it by only 8%. This was the case for both T cell subsets. CM from uninfected A549 cells caused no significant effect. The presence or absence of infection did not change the effect of the CM media on the percentage of CD25-positive CD4 T cells for any cell type. However, there were slight reductions in CD25-positive CD8 T cells when infected A549 CM or infected DLD-1 CM was used (only 9% and 6%, respectively).

In high glucose conditions, the inhibition of T cell activation was much more pronounced for both T cell subsets when CM from DLD-1 cells was used; this was independent of whether those cells had been infected (Figure 5.4B). The results presented here concur with those displayed in Figure 5.4A; CM from uninfected SKOV-3 cells reduced the CD25-postive

percentage of T cells slightly for both T cells subsets while the CM from uninfected A549 cells had no impact.

A slight decrease in T cell activation was observed when CM is used from cells infected with EnAd, however this is deemed negligible compared to the reduction seen when CM is used from highly glycolytic DLD-1 cells especially when glucose is not a limiting factor (i.e. in high glucose medium).

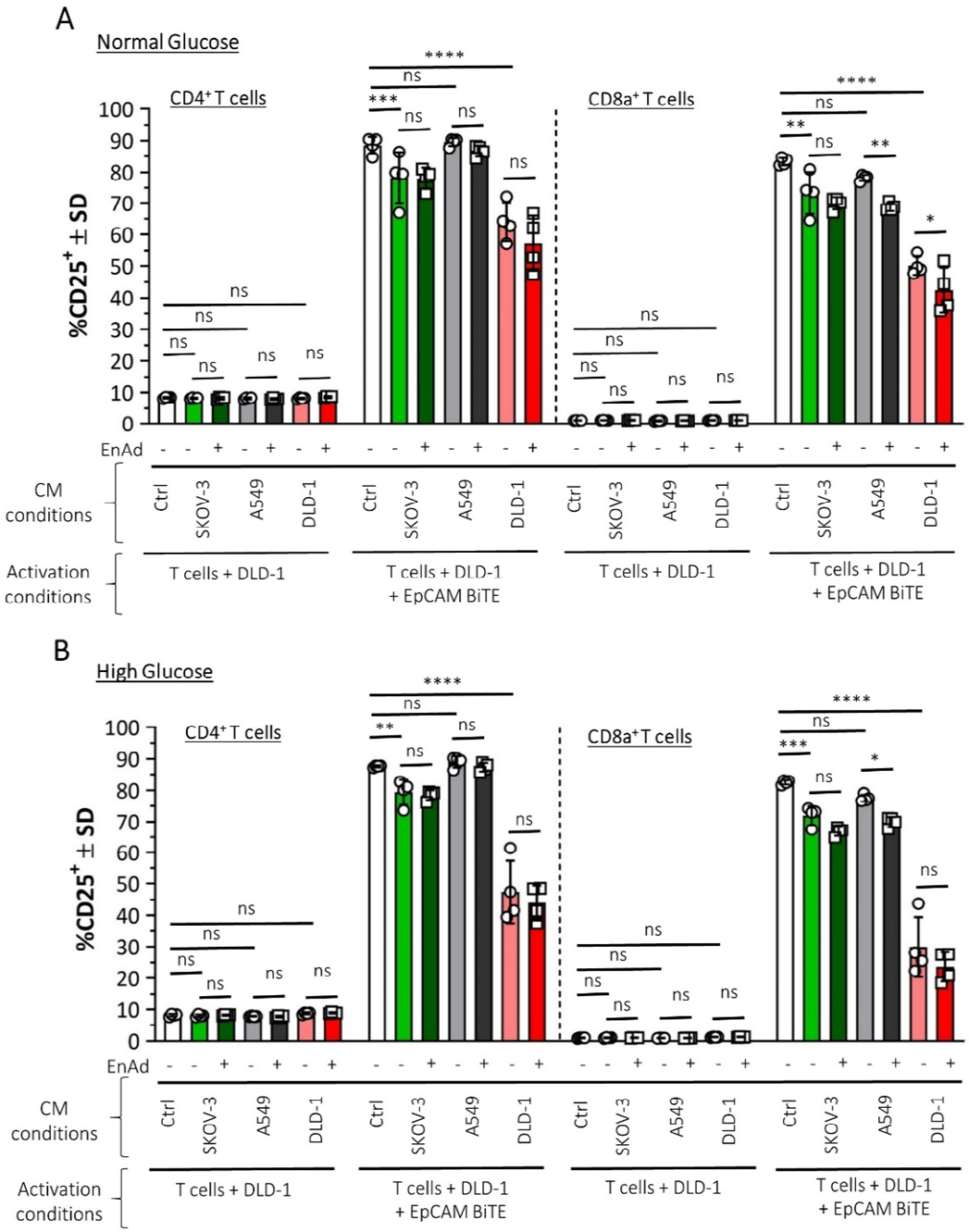


Figure 5.4 T cell activation is decreased more in CM from DLD-1 cells cultured with high concentrations of glucose. A549, SKOV-3 and DLD-1 cells were left untreated or infected with EnAd at an MOI of 5 in 2% RPMI with 11 mM glucose (RPMI 1640) **(A)** or supplemented with 50 mM glucose (total glucose concentration: 61 mM) **(B)**. At different timepoints following infection, 48 hours (A549), 144 hours (SKOV-3) and 72 hours (DLD-1), CM was harvested and filtered through an Amicon centrifugal filter unit MWCO 100 kDa to remove any virus particles. Co-cultures of DLD-1 cells and $CD3^+$ T cells were prepared in the presence or absence of the EpCAM-BiTE in control (Ctrl) medium (normal (A) or high (B) glucose RPMI with 2% FBS), or in CM taken from uninfected or infected tumour cells in normal (A) or high (B) glucose. T cells were harvested after 24 hours and activation was measured by analysing for surface expression of CD25 on separate T cell subsets. Data show the mean ± SD of biological quadruplicates. Significance was assessed by a two-way ANOVA test with Tukey's post-hoc analysis comparing experimental conditions with either the "Ctrl" condition or by comparing the uninfected and infected conditions within each condition medium tested (*, $p < 0.05$; **, $p < 0.01$; ***, $p < 0.001$; ****, $p < 0.0001$; ns, non-significant).

5.2.4 Transfection of siRNA targeting LDHA and MCT-4 does not improve T cell activation in glucose-mediated acidosis

To try to overcome the inhibition of T cell activation induced by lactic acid production from DLD-1 cells, we next explored whether targeting LDHA and MCT-4, two components required for lactic acid efflux, with siRNAs, could modulate glucose-induced acidification of CM. siRNAs targeted towards LDHB were also tested as the LDHB component of LDH enzymes may additionally contribute to acidosis via the other LDH isoforms.

Three synthetic siRNAs were tested for their knockdown activity against each of the two targets: LDHA and MCT-4. Knockdown was assessed by western blot. Transfection of each siRNA into A549 cells and DLD-1 cells resulted in the successful knockdown of LDHA and MCT-4 relative to untransfected or non-target siRNA transfected controls (Figure 5.5A). Knockdown was less efficient in SKOV-3 cells. Increasing doses of siRNAs were used to transfect A549 cells and dose dependent LDHB and LDHA knockdown was observed (Figure 5.5B). In addition, LDHA knockdown by siRNAs was observed to last for over five days post-transfection of A549 cells (Figure 5.5C). Images of A549 cells transfected with siRNAs targeting MCT-4 show acidity of the culture medium is reduced (indicated by phenol red colour change to pink) following transfection with siMCT4 A (s17416) (Figure 5.5D).

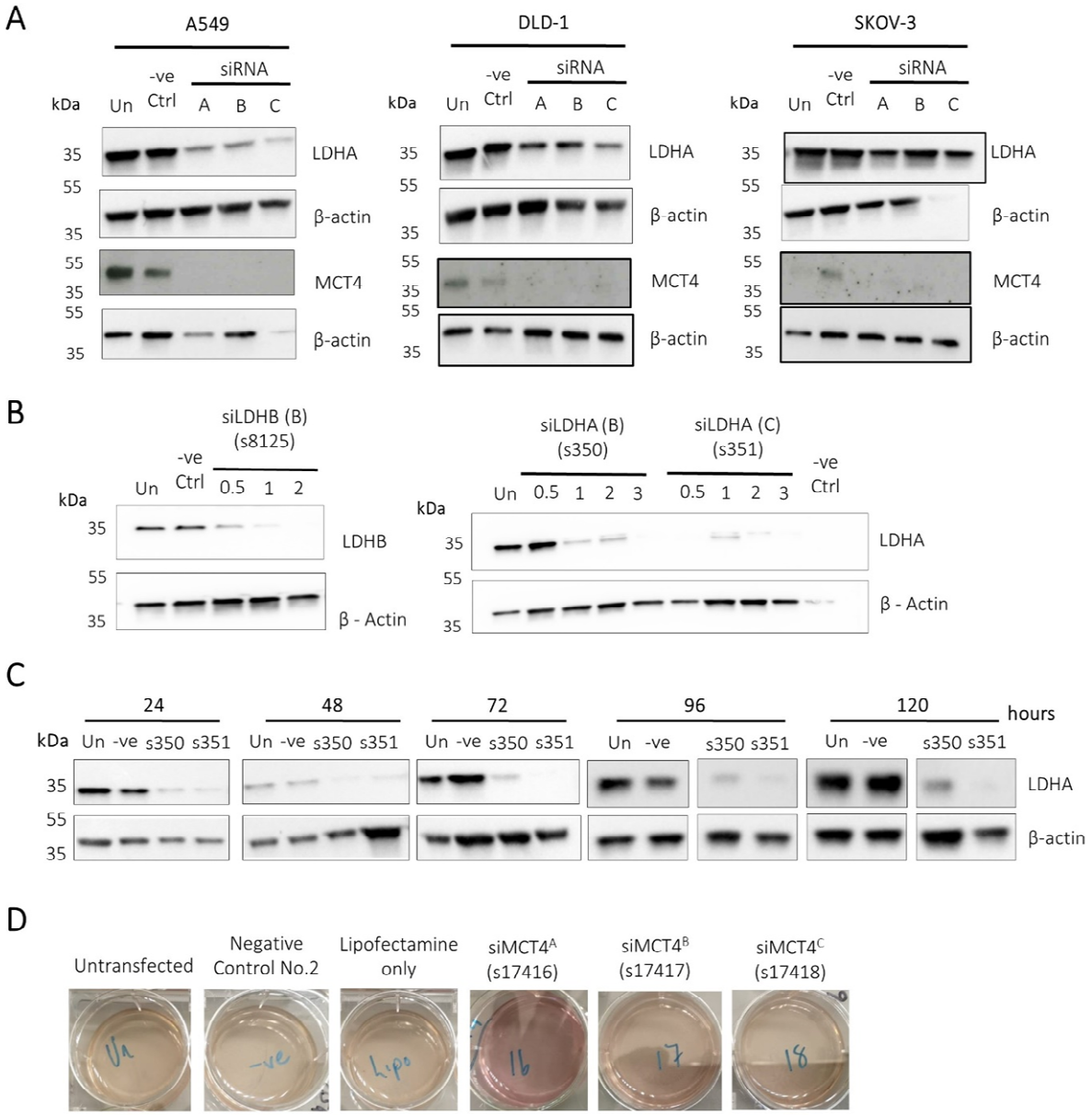


Figure 5.5 LDHA, LDHB and MCT-4 protein expression is reduced following transfection with siRNA's specifically targeting LDHA, LDHB and MCT-4 mRNA. (A) A549 cells, DLD-1 cells and SKOV-3 cells were transfected with three different siRNAs targeting LDHA and MCT-4 (400 nM) or a negative (-ve) siRNA control (No. 2) diluted in opti-MEM. Three days later cells were harvested, and lysates analysed for LDHA (37 kDa) and MCT-4 (43 kDa) expression using western blot analysis. β actin (42 kDa) was used as a loading control. **(B)** Transfections were repeated as above with varying dilutions of LDHA and LDHB siRNA (where 0.5; 200 nM, 1; 400 nM, 2; 800 nM, 3; 1200 nM siRNA) and lysates were analysed for LDHB (37 kDa) and LDHA using western blot analysis. **(C)** A549 cells were transfected with two siRNAs (siRNA B; s350 and siRNA C; s351) (400 nM) targeting LDHA and cells were harvested at 24, 48, 72, 96 and 120 hours post transfection. Lysates were analysed for LDHA by western blot analysis. **(D)** Images taken of phenol red indicator changes in RPMI medium three days post transfection of A549 cells with three different siRNAs targeting MCT-4.

Based on the promising knockdown of targets and the colour change observed in culture media, we next set up T cell activation assays using CM from untransfected DLD-1 cells or from DLD-1 cells that had been transfected with a negative control (no. 2) siRNA or siRNAs targeting either LDHA or MCT-4. Transfections were performed in normal glucose (Figure 5.6A) and high glucose (Figure 5.6B) conditions. A reduction in the percentage of CD25-positive T cells was observed in all samples treated with CM from DLD-1 cells relative to a control sample treated with 2% RPMI. The reduction was greatest for the CD8a-positive T cell subset, agreeing with results obtained previously, where high glucose DLD-1 CM reduced T cell activation more than normal glucose DLD-1 CM. Unfortunately, the CM taken from cells transfected with various siRNAs still reduced activation of T cells and did not reverse the observed suppression. However, a slight increase was seen in activation when CM from cells treated with LDHA s350 siRNA was used compared to the untransfected CM used in Figure 5.6A. The same increase however was not observed in the high glucose experiments (Figure 5.6B), where the biggest increase in activation compared to the untransfected CM control was the samples with CM from the DLD-1 cells transfected with the negative control (no. 2) siRNA.

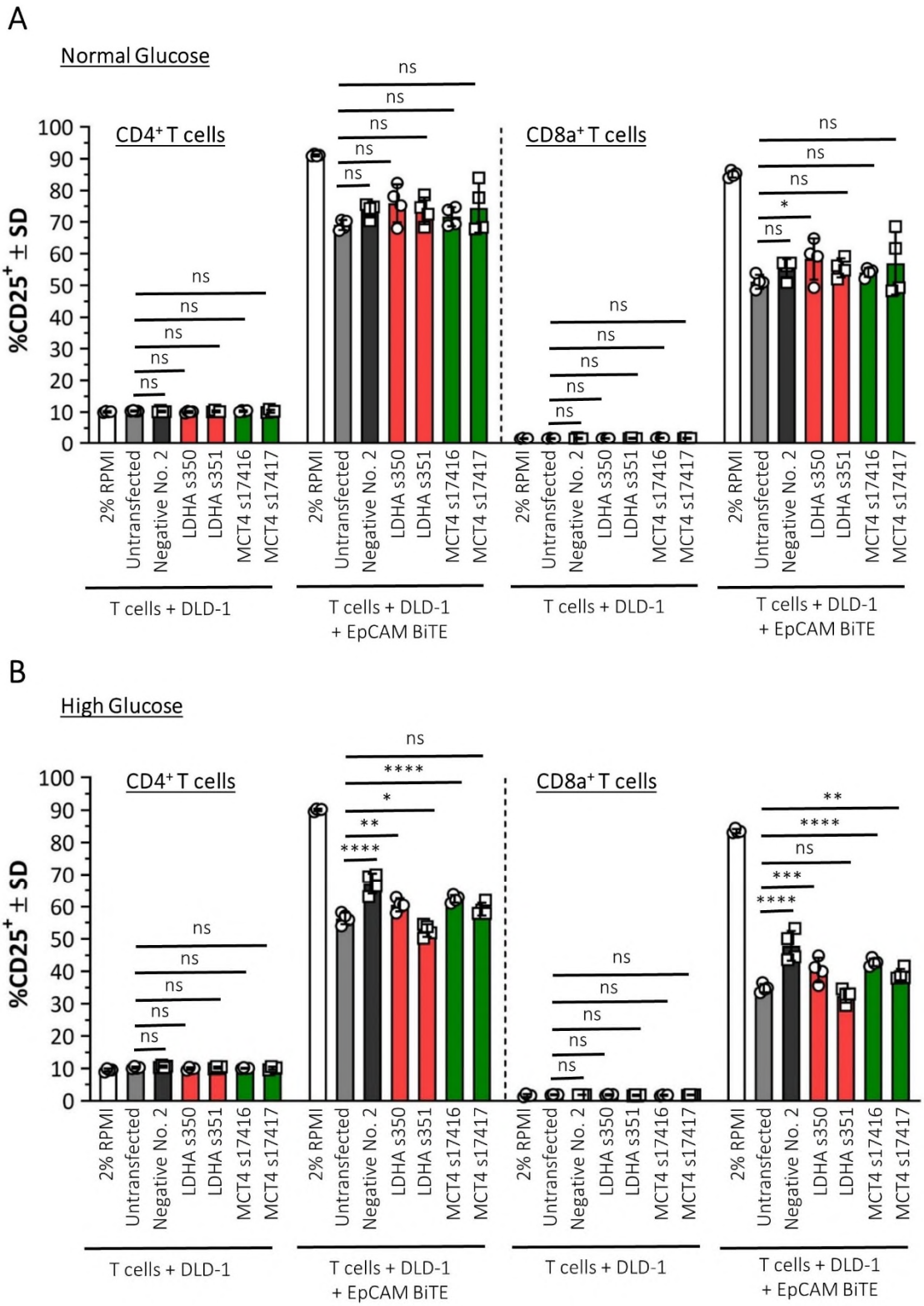

A
Normal Glucose
CD4+ T cells
CD8a+ T cells
%CD25+ ± SD
2% RPMI
Untransfected
Negative No. 2
LDHA s350
LDHA s351
MCT4 s17416
MCT4 s17417
T cells + DLD-1
T cells + DLD-1 + EpCAM BiTE
B
High Glucose

Figure 5.6 CM from DLD-1 cells treated with siRNAs targeting LDHA and MCT-4 do not reverse T cell suppression observed in CM from DLD-1 tumour cells. DLD-1 cells were left untreated or transfected with negative no. 2 siRNA, LDHA siRNAs (s350 and s351) and MCT-4 siRNAs (s17416 and s17417) in 2% RPMI with 11 mM glucose (RPMI 1640) **(A)** or supplemented with 50 mM glucose (total glucose concentration: 61 mM) **(B)**. After 72 hours CM was harvested and filtered through an Amicon centrifugal filter unit MWCO 100 kDa to clarify supernatants. Co-cultures of 2.0 x 10^5 DLD-1 cells and 1 x 10^6 $CD3^+$ T cells were prepared in the presence or absence of the EpCAM-BiTE in control (Ctrl) medium (normal (A) or high (B) glucose RPMI with 2% FBS), or in CM taken from transfected tumour cells in normal (A) or high (B) glucose. T cells were harvested after 24 hours and activation was measured by analysing for surface expression of CD25 on separate T cell subsets. Data show the mean ± SD of biological quadruplicates. Significance was assessed by a two-way ANOVA test with Tukey's post-hoc analysis comparing experimental conditions with either the untransfected conditioned medium wells (*, $p < 0.05$; **, $p < 0.01$; ***, $p < 0.001$; ****, $p < 0.0001$; ns, non-significant).

All three siRNAs tested were successful in targeting LDHA and MCT-4 for knockdown in relevant glycolytic cell lines. Knockdown occurs even at low doses of siRNA and for LDHA knockdown the effects were observed over five days until the experiments end. However, despite successful knockdown of targets, the pH of the CMs remained unchanged (measured using a pH probe, data not shown) and target knockdown did not rescue the negative impact on T cell activation. Transfection of siRNAs into DLD-1 cells may not be sufficient to mediate an effect on pH. Firstly, most knockout studies were based on transfection of A549 cells in Figure 5.5, and although transfection of DLD-1 cells with siRNAs did show some knock down of target proteins, it could be that the extent of knockdown was insufficient and enough functional target protein remained being expressed so as to negate any affect. Secondly, the efficiency of transfection using Lipofectamine 2000 of many cell lines is not optimal. Transfection efficiencies of only 20% for SKOV-3 cells and less than 50% for most other cells lines tested have been reported (ThermoFisher Scientific 2020). Based on the successful knockdown of targets in cells despite low transfection efficiencies, we reasoned that siRNA delivery rather than activity was the principal barrier to modulation of the pH of the CM. Therefore we decided to pursue the use of these siRNAs in future experiments in which EnAd would be used for the targeted expression of siRNAs in cells, providing a far more efficient method of delivery of the relevant interfering RNAs. For example, it is known that infection of DLD-1 cells with EnAd

results in over 70% of cells being infected and therefore potentially expressing RNAs (shown through reporter GFP expression assays, Figure 3.18).

5.2.5 The activity of EnAd in an acidic cellular environment is affected more in glycolytic cells than cells that rely on oxidative phosphorylation

To be able to mediate acidosis in the TME, EnAd must be able to infect and replicate in that same environment containing lactic acid. To test EnAd's efficacy as a platform we quantified viral replication, viral progeny production, and the expression of reporter proteins and OV-armed transgenes encoded in the EnAd genome after infection in medium with lactic acid. We measured the same parameters of viral infection in medium with sodium lactate and medium with sodium chloride to determine if any changes observed were due to low pH or the lactate anion itself.

EnAd-SA-GFP genomes were quantified after infection of A549 cells and SKOV-3 cells in lactic acid supplemented medium; infections were performed as the lactic acid supplemented medium was placed onto adherent cells. These two cell types have very different permissivities to EnAd infection, which is reflected in their differing metabolism. While A549 cells have a classical 'Warburg' phenotype supporting a rapid viral lifecycle, in SKOV-3 cells glycolysis is coupled to OXPHOS and the cells support a much slower adenovirus infectious cycle (Dyer et al. 2019). Viral genome replication in A549 cells was reduced in medium with 15 mM lactic acid; however, in SKOV-3 cells replication was unchanged (Figure 5.7A). Interestingly, viral replication in SKOV-3 cells was slightly reduced in medium containing sodium lactate and sodium chloride (Figure 5.7B). Infectious virus particles in the media from the same SKOV-3 cell genome replication assay were titred using the $TCID_{50}$ assay described in section 2.8.8. The number of infectious viral particles released into the supernatant after successful replication and cell lysis did not change when infections were performed in medium with 15 mM lactic acid,

sodium lactate or sodium chloride compared with the control medium with no lactic acid (Figure 5.7C).

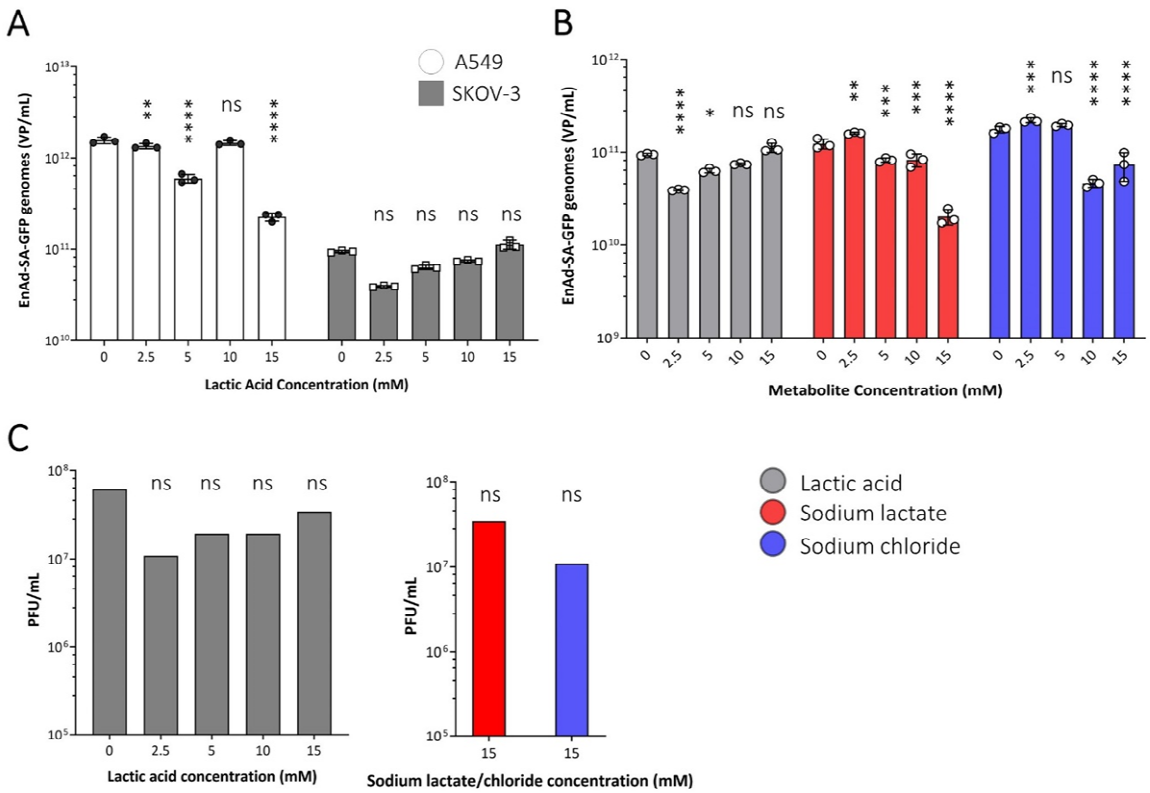


Figure 5.7 EnAd genome replication and infectious viral progeny release is unchanged after SKOV-3 cell infection with EnAd during acidosis. (A) A549 and SKOV-3 cells were exposed to medium prepared with lactic acid and infected with MOI 1 of EnAd-SA-GFP for A549 cells and an MOI 10 of the same virus for SKOV-3 cells. Three days later EnAd genome replication was measured using qPCR primers and a probe against the EnAd hexon gene. **(B)** SKOV-3 cells were infected with lactic acid medium in addition to medium supplemented with the same concentrations of either sodium lactate or sodium chloride and EnAd genome replication was measured. **(C)** Infectious medium was obtained from the same experiment three days post-infection and titred using a $TCID_{50}$ method. Each condition was measured in triplicate and represented as mean ± SD (A-B). Statistical significance was assessed by two-way ANOVA with Tukey's post-hoc analysis with each condition compared to the "0 mM metabolite" control (A-B). $TCID_{50}$ statistical significance was assessed by one-way ANOVA with Dunnett's post-hoc analysis within lactic acid treatment group alone comparing to the "0 mM metabolite" control or between treatments groups comparing each at 15 mM (C) (*, $p < 0.05$; **, $p < 0.01$; ***, $p < 0.001$; ****, $p < 0.0001$; ns, non-significant).

Protein expression was measured using a GFP reporter gene driven by either a CMV promoter or an MLP promoter through an SA site. CMV driven expression provides an indirect measurement of immediate expression following delivery of the viral DNA to the nucleus,

while the MLP links expression of the reporter to expression of the late virus genes so that GFP expression is only observed in cells in which the virus is actively replicating. Addition of lactic acid caused a reduction in GFP expression during infection of A549 cells with reporter viruses EnAd-CMV-GFP or EnAd-SA-GFP. The count of live GFP-positive cells was reduced by 50% in medium with 15 mM lactic acid in both cases (Figure 5.8A). The reporter viruses were also used to infect SKOV-3 cells in medium supplemented with increasing concentrations of lactic acid, sodium lactate or sodium chloride. Slight decreases were observed in cells infected with EnAd-CMV-GFP in both lactic acid and sodium chloride, the osmolality control. A significant drop was observed in medium with 15 mM lactic acid after infection with EnAd-SA-GFP, however this was still a comparable level of GFP expression compared to controls in both sodium lactate and sodium chloride (Figure 5.8B and 5.8C).

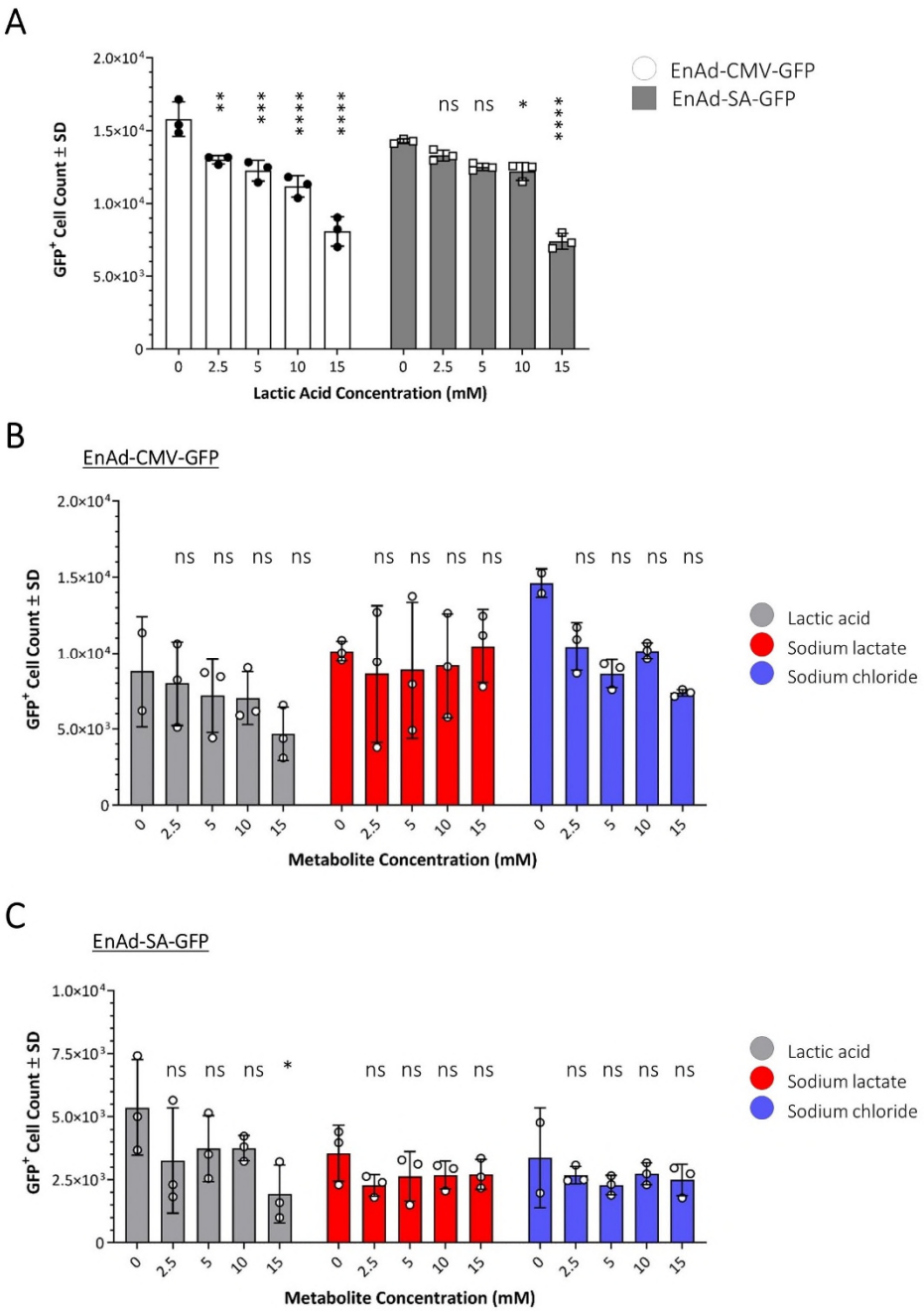


Figure 5.8 Protein expression is reduced in infected A549 cells but not in infected SKOV-3 cells during lactic acidosis. (A) A549 cells were exposed to lactic acid medium and infected with MOI 1 of either EnAd-CMV-GFP or EnAd-SA-GFP. Three days later cells were harvested and analysed for GFP expression and viability (with a LIVE/DEAD Near-IR stain) using flow cytometry. Statistical significance was assessed by two-way ANOVA with Sidak's post-hoc analysis with each condition being compared to the "0 mM lactic acid" control. SKOV-3 cells were cultured in medium supplemented with lactic acid, sodium lactate or sodium chloride and infected with MOI 10 of either EnAd-CMV-GFP **(B)** or EnAd-SA-GFP **(C)**. Three days later cells were harvested and analysed for GFP expression and viability. Each condition was measured in biological triplicate and represented as mean ± SD (A-C). Statistical significance was assessed by two-way ANOVA with Tukey's post-hoc analysis with each condition being compared to the "0 mM metabolite" control (B, C). (*, $p < 0.05$; **, $p < 0.01$; ***, $p < 0.001$; ****, $p < 0.0001$; ns, non-significant).

As exemplified above using the reporter gene GFP, the CMV promoter or the MLP (SA) promoter can also be used to drive the expression of the EpCAM BiTE, a therapeutically relevant protein in oncolytic virotherapy. We wanted to examine if the same effect of decreased protein expression observed in A549 cells would occur following infection of DLD-1 cells with an EnAd variant encoding the EpCAM BiTE. Importantly, DLD-1 cells are similar to A549s in that they are permissive to EnAd infection and display a glycolytic phenotype. Analysis of BiTE expression following infection of cells with EnAd-CMV-EpCAM showed reduced BiTE protein levels in medium with 15 mM lactic acid (Figure 5.9A). Following infection of DLD-1 cells with EnAd-SA-EpCAM, BiTE protein level signal was slightly reduced in medium with 10 and 15 mM lactic acid (Figure 5.9B).

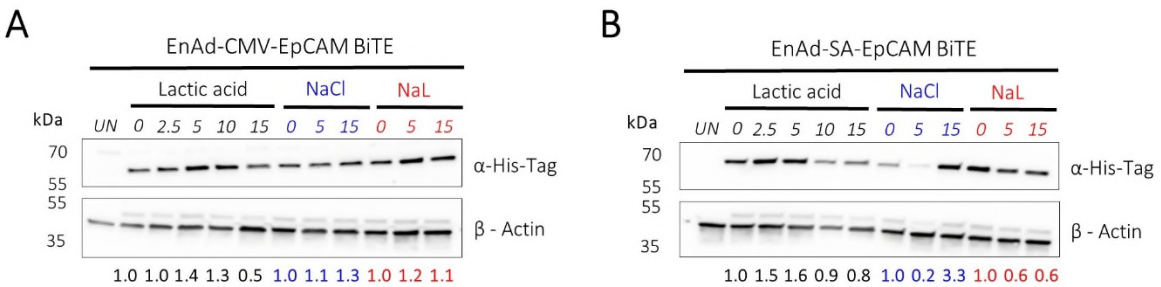


Figure 5.9 EnAd expressing EpCAM BiTE from either the CMV promoter or the MLP promoter during acidosis. DLD-1 cells (6.5 x 10^4) cultured in medium supplemented with lactic acid, sodium chloride and sodium lactate were infected with EnAd-CMV-EpCAM BiTE **(A)** or EnAd-SA-EpCAM BiTE **(B)** at 100 vp/cell determined by the PicoGreen Assay. Lysates were harvested 72 hours post infection and subjected to HisTag (57 kDa) detection by western blot to determine BiTE expression. Relative expression of the His-Tagged BiTEs was determined by comparison to the loading control β-actin (42 kDa) and normalised against expression in the "0 mM" metabolite control condition using ImageLab 6.0.1.

Changes in concentration of lactic acid have a greater effect on viral replication in glycolytic cells such as A549 and DLD-1 cells than in cells with an oxidative phenotype such as SKOV-3 cells. Lactic acid is a direct by-product of aerobic glycolysis associated with the Warburg phenotype. When high concentrations of lactic acid accumulate in the extracellular

environment, the lactic acid concentration gradient reverses, reducing the rate of efflux of lactic acid out of the cell. This results in the accumulation of the inhibitory molecule intracellularly. This causes cellular stress and is likely to downregulate global rates of protein translation which are required for expression of the virally encoded transgene. It should be noted however that despite the inhibition by lactic acid of replication and protein expression in glycolytic cells, the kinetics of viral infection in these cell types remains more rapid than the kinetics of infection in cells that rely on OXPHOS, such as SKOV-3 cells.

5.2.6 The cytolytic activity of EnAd decreased in accumulating lactic acid

The replication kinetics of EnAd are reduced in glycolytic cells but not in OXPHOS reliant cells. We next wanted to see if this delay in replication and expression would be reflected in the ability for EnAd armed with EpCAM BiTE to induce tumour cell death. Lysis of SKOV-3 cells and DLD-1 cells was quantified using the xCELLigence cytotoxicity assay described in section 2.6.5. The oncolytic activity of EnAd alone or EnAd armed with EpCAM BiTE was measured in the presence or absence T cells.

In SKOV-3 cells, a steady decrease in oncolytic activity was observed in medium with increasing amounts of lactic acid, with the most significant reduction in medium with 10 mM and 15 mM acid. The presence of T cells induced death in more than 85% tumour cells seven days earlier than with EnAd alone. In agreement with previous results, T cell activation by the BiTE in medium with acid was inhibited, resulting in a 40-hour delay in medium with 10 mM acid and complete inhibition in medium with 15 mM acid. However, as expected the kinetics of target cell lysis in 15 mM acid was faster for EnAd armed with EpCAM BiTE than EnAd alone (Figure 5.10A). A similar trend was observed with DLD-1 cells. The addition of T cells resulted in lysis of more than 85% of cells 24 hours earlier than virus alone. Medium with 2.5 – 10 mM lactic acid slowed EpCAM BiTE-mediated tumour cell death; this delay was

significant in medium with 15 mM acid. Virus activity in the absence of T cells also decreased significantly in medium with lactic acid, with cytolysis slowed by 24 – 40 hours.

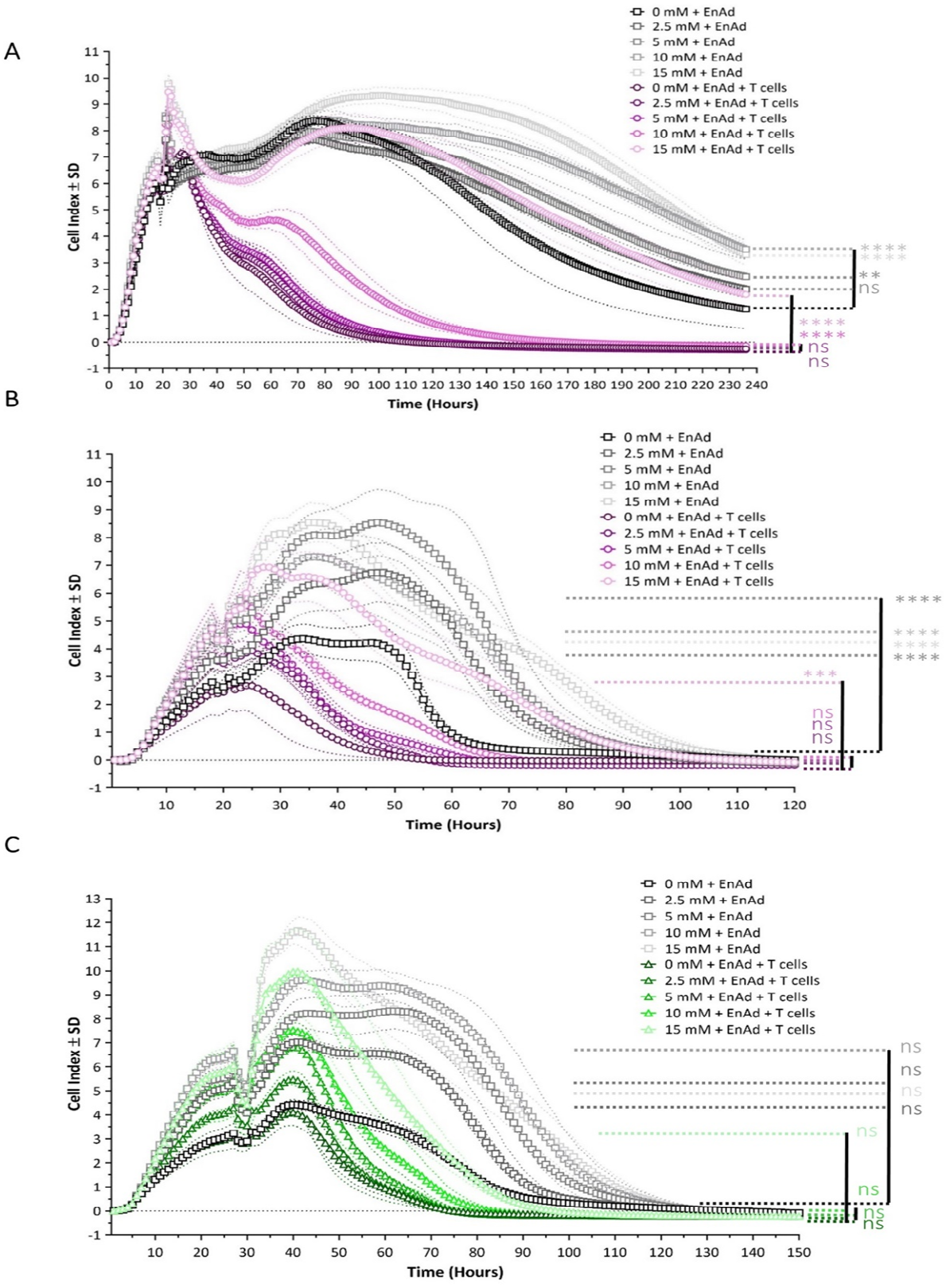


Figure 5.10 EnAd-induced tumour cell lysis is slower in lactic acidosis, and EpCAM BiTE induced lysis following expression from EnAd is inhibited in 15 mM lactic acid. (A) SKOV-3 cell viability was monitored over 240 hours, 1.0 x 10^4 cells were infected at 100 vp/cell with EnAd-CMV-EpCAM BiTE in the presence (purple) or absence (grey) of 5.0 x 10^4 T cells (5:1). EnAd lysis activity and EpCAM induced T cell dependent lysis activity were assessed in lactic acid supplemented medium. **(B)** DLD-1 cell viability was monitored over 120 hours, 1.5 x 10^4 cells were infected at 100 vp/cell with EnAd-CMV-EpCAM BiTE in the presence or absence of 7.5 x 10^4 T cells (5:1). EnAd lysis activity and EpCAM induced T cell dependent lysis activity were assessed in lactic acid supplemented medium. **(C)** DLD-1 cell viability was monitored over 150 hours, 1.5 x 10^4 cells were infected at 100 vp/cell with EnAd-SA-EpCAM BiTE in the presence or absence of 7.5 x 10^4 T cells (5:1) and activity was assessed during culture with lactic acid supplemented medium. Electrical impedance was measured at 15 minute intervals, each condition was measured in biological quadruplicate and represented as the mean ± SD (dashed lines). Statistical significance was assessed using a one-way ANOVA test with Tukey's post-hoc analysis. Significance presented was the experimental condition with or without T cells compared to the "0 mM" control at the timepoint where the control condition had killed > 95% cells. (A) Significance was assessed at 100 hours for T cell presence conditions and 240 hours for T cell absence conditions in SKOV-3 cells. (B) Significance was assessed for both T cell presence and absence at 60 hours for DLD-1 cells infected with EnAd-CMV-EpCAM. (C) Significance was assessed for T cell presence conditions at 80 hours and at 100 hours for T cell absence for DLD-1 cells infected with EnAd-SA-EpCAM (*, $p < 0.05$; **, $p < 0.01$; ***, $p < 0.001$; ****, $p < 0.0001$; ns, non-significant).

Importantly, this decrease in killing activity could be due to an increase in the number of DLD-1 cells in culture with lactic acid, as indicated by the increase in cell index (a proxy for confluency) at 30 hours post-seeding (Figure 5.10B). Similar results were observed between EnAd-CMV-EpCAM BiTE and EnAd-SA-EpCAM BiTE, including an increase in cell index and observed inhibition of virus and BiTE-mediated cell killing in the presence of increasing amounts of lactic acid (Figure 5.10C).

The cytolytic activity of EnAd is reduced in both glycolytic cells and cells that rely on OXPHOS due to an increase in lactic acid concentration. Despite previous observations that BiTE expression after viral infection of glycolytic cells with EnAd-SA-BiTE or EnAd-CMV-BiTE was reduced by lactic acid, BiTE expression levels alongside the presence of T cells was sufficient to accelerate the onset of death in DLD-1 cells by 12 hours. This effect is even more apparent in SKOV-3 cells where the EpCAM BiTE drastically improves cytolysis (by seven days) compared to EnAd alone, due to the fact that SKOV-3 cells are very poorly permissive to adenovirus infection.

5.2.7 Gene knockdown of LDHA and MCT-4 do not affect EnAd genome replication, cell permissiveness or infectious particle release

Part of EnAd's selectivity towards cancer cells is based on preferences towards certain metabolic phenotypes, as exemplified by its efficient replication in glycolytic cells compared to those that use OXPHOS. We hypothesised that if we were to disrupt the cellular metabolism we could modify EnAd's ability to infect, replicate and release more infectious progeny in certain cell types. We therefore tested whether disruption of the lactic acid pathway by knockdown of LDHA, LDHB or MCT-4 would hinder EnAd infection. We transfected siRNAs into A549 cells (the more efficiently transfected cell type) 24 hours prior to infection with EnAd-SA-GFP (Figure 5.11A). We then measured viral replication and reporter gene expression (GFP) using qPCR and flow cytometry respectively. To quantify infectious particle release we infected transfected cells with EnAd-SA-FLuc and used a luminescence based assay described in section 2.8.11.

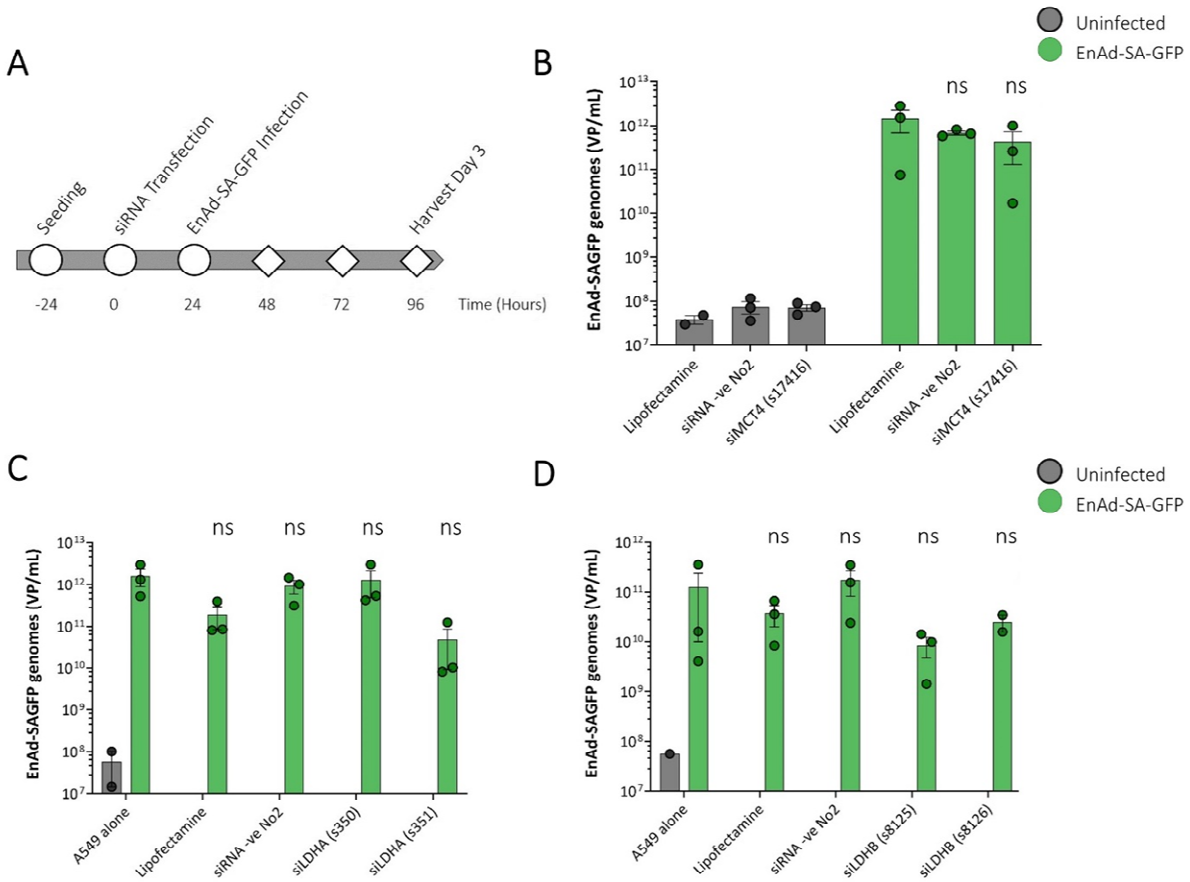


Figure 5.11 EnAd genome replication is unchanged after A549 cells were transfected with siRNA. **(A)** A549 cells were seeded, then 24 hours later, transfected with siRNAs targeting LDHA, LDHB or MCT-4 (400 nM) or with a negative (-ve) control (No.2). After another 24 hours cells were infected with EnAd-SA-GFP at MOI 5. Three days later cells were harvested and EnAd genome replication was measured using qPCR with primers and a probe against the hexon gene. Genome replication was measured after treatment with siRNA targeting MCT-4 **(B)**, with siRNAs targeting LDHA **(C)** and with siRNAs targeting LDHB **(D)**. Each condition was measured in triplicate and represented as mean ± SD (B-D). Statistical significance was assessed by one-way ANOVA with Dunnett's post-hoc analysis with each condition compared to the "A549 alone infected" control (B-D) (*, $p < 0.05$; **, $p < 0.01$; ***, $p < 0.001$; ****, $p < 0.0001$; ns, non-significant).

Viral genome replication did not change in cells transfected with siRNAs targeting MCT-4 (Figure 5.11A), whereas a ten-fold reduction in replication following knockdown with one siRNA (s351) targeting LDHA and two targeting LDHB (s8125 and s8126) was observed (Figures 5.11C and D). Reporter gene, GFP, expression was increased in A549 cells after transfection with siRNAs targeting LDHA (Figure 5.12A), while expression of GFP decreased 2-fold after transfection with the siRNA (s8126) targeting LDHB (Figure 5.12B). Interestingly, the decrease following LDHB siRNA transfection was not significant, however, a clear second

population of GFP positive cells was observed when analysing single cells by flow cytometry (Figure 5.12D). No change in GFP expression was observed when A549 cells were transfected with siRNAs targeting MCT-4 before infection (Figure 5.12C).

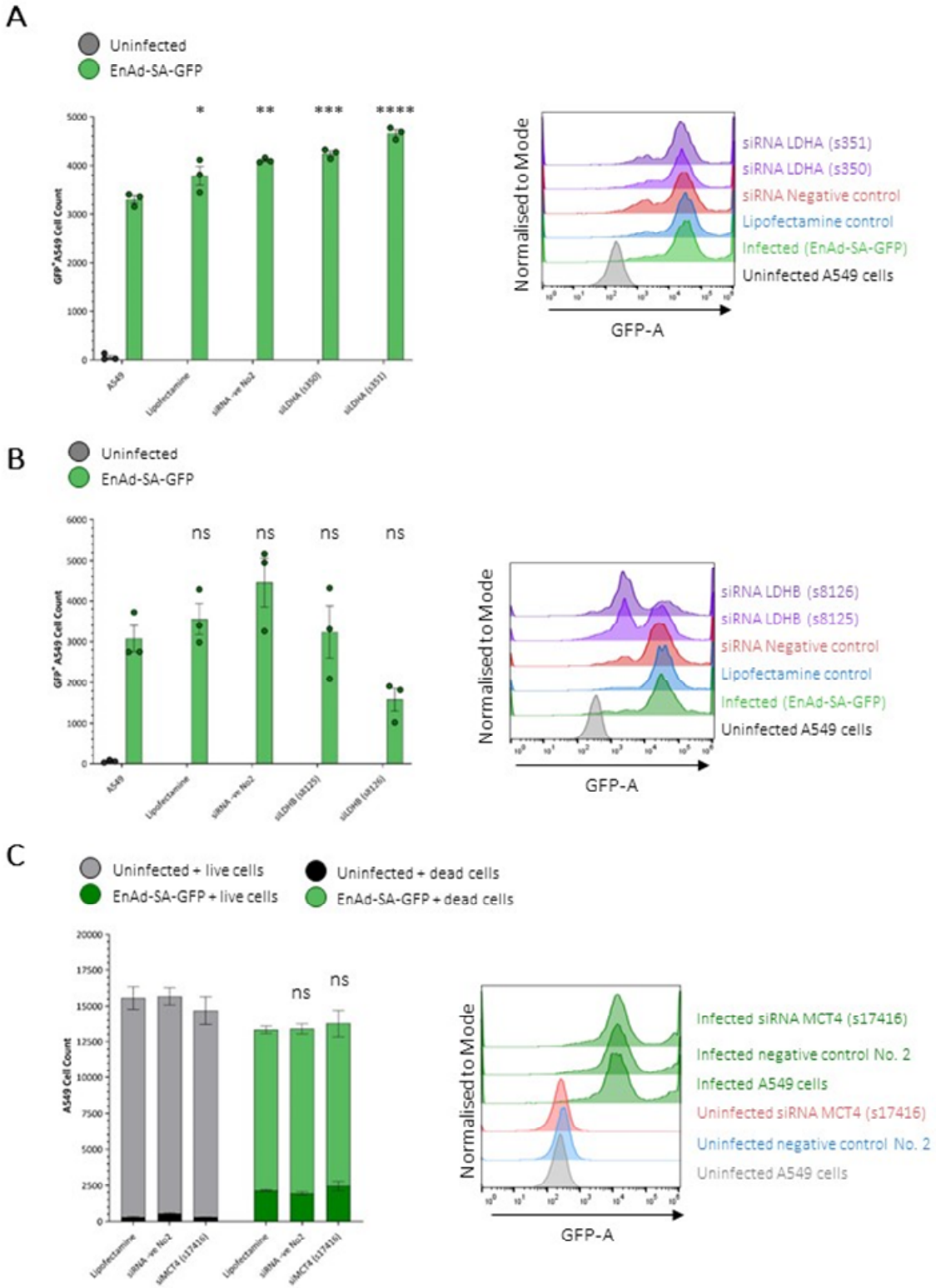

A
Uninfected
EnAd-SA-GFP
GFP+A549 Cell Count
*
**
***
****
A549
Lipofectamine
siRNA -ve No2
siLDHA (s350)
siLDHA (s351)
Normalised to Mode
siRNA LDHA (s351)
siRNA LDHA (s350)
siRNA Negative control
Lipofectamine control
Infected (EnAd-SA-GFP)
Uninfected A549 cells
GFP-A
B
Uninfected
EnAd-SA-GFP
GFP+A549 Cell Count
ns
ns
ns
ns
A549
Lipofectamine
siRNA -ve No2
siLDHB (s8125)
siLDHB (s8126)
Normalised to Mode
siRNA LDHB (s8126)
siRNA LDHB (s8125)
siRNA Negative control
Lipofectamine control
Infected (EnAd-SA-GFP)
Uninfected A549 cells
GFP-A
C
Uninfected + live cells
EnAd-SA-GFP + live cells
Uninfected + dead cells
EnAd-SA-GFP + dead cells
A549 Cell Count
ns
ns
Lipofectamine
siRNA -ve No2
siMCT4 (s17416)
Lipofectamine
siRNA -ve No2
siMCT4 (s17416)
Normalised to Mode
Infected siRNA MCT4 (s17416)
Infected negative control No. 2
Infected A549 cells
Uninfected siRNA MCT4 (s17416)
Uninfected negative control No. 2
Uninfected A549 cells
GFP-A

Figure 5.12 Protein expression is increased in A549 cells transfected with LDHA siRNA, decreased after transfection with LDHB siRNA and is unchanged in those transfected with MCT-4 siRNA. A549 cells were seeded then 24 hours later transfected with siRNAs targeting LDHA **(A)**, LDHB **(B)**, or MCT-4 **(C)** (400 nM) or with a negative control (No.2) then after another 24 hours cells were infected with EnAd-SA-GFP at MOI 5. Three days later cells were harvested and analysed for GFP expression (GFP^+ A549 cell count) using flow cytometry. For each siRNA target a representative flow cytometric histogram of GFP expression following infection with EnAd-SA-GFP is shown. Each condition was measured in triplicate and represented as mean ± SD (A,C,E). Statistical significance was assessed by one-way ANOVA with Tukey's post-hoc analysis with each condition compared to the "A549 alone infected" control (*, $p < 0.05$; **, $p < 0.01$; ***, $p < 0.001$; ****, $p < 0.0001$; ns, non-significant).

Viral progeny released after infection of transfected cells was measured in PFU per mL of infection medium tested. The number of PFU/mL increased over 3 days for all transfected conditions tested, however the numbers recorded at 72 hours for LDHB siRNA transfected cells were too high to analyse accurately with the standard curve used. Within each time point when compared to the untransfected A549 control, no reduction in the number of PFU was observed after transfection with LDHA (Figure 5.13A) or MCT-4 targeting siRNAs (Figure 5.13B). For cells that had been transfected with LDHB targeting siRNAs, a reduction in PFU/mL was observed, but this was at 48 hours and a similar trend at 48 hours was observed for LDHA siRNA transfected cells. A further experiment would be needed to verify this (Figure 5.13C).

EnAd viral replication and progeny release will not be inhibited by the targeted knockdown of LDHA or MCT-4. In fact, LDHA knockdown may even improve infection of glycolytic cells shown through increased GFP expression. LDHB knockdown however may result in reduced expression of GFP (Figure 5.12B) and reduced viral replication, although these results were not significant and would need to be verified.

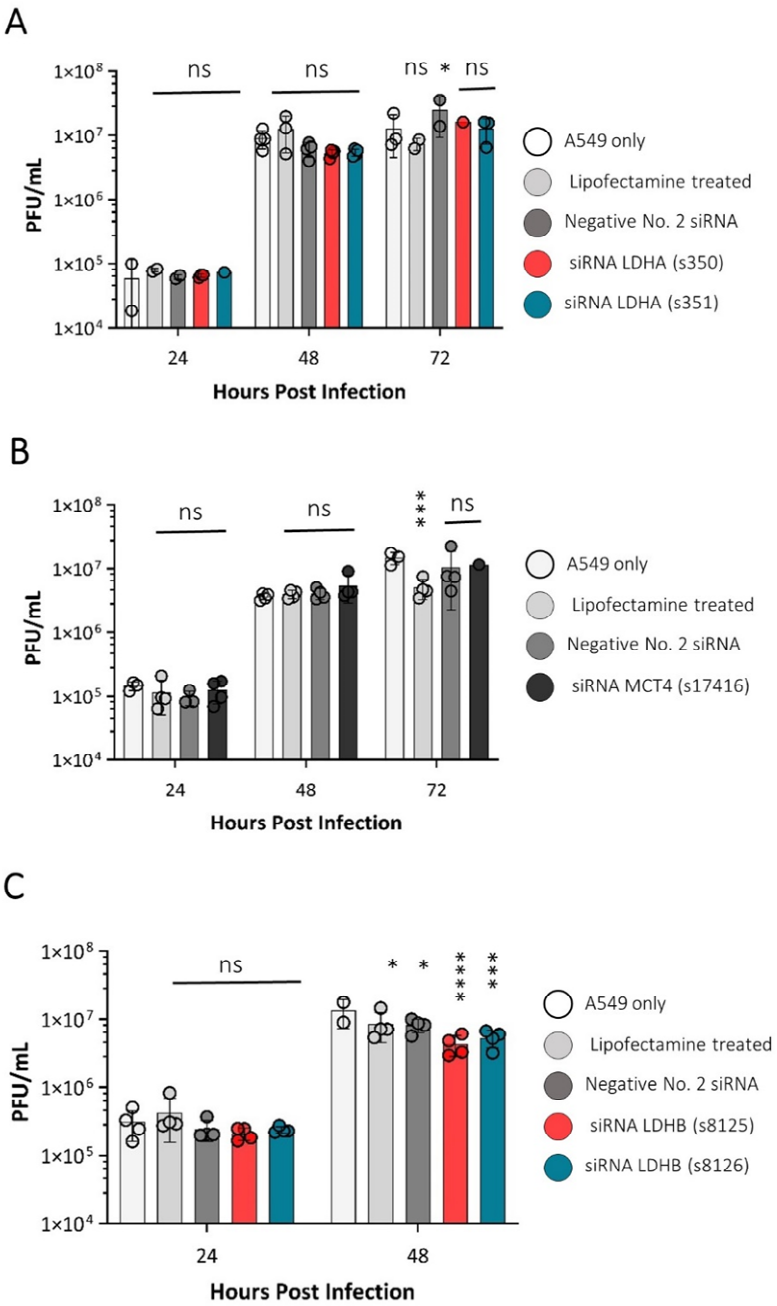


Figure 5.13 Infectious viral progeny release is not affected by decreased LDHA, LDHB or MCT-4 expression. A549 cells were seeded then 24 hours later transfected with siRNAs targeting LDHA, LDHB, or MCT-4 (400 nM) or with a negative control (No.2), then after another 24 hours cells were infected with EnAd-SA-FLuc at MOI 5. At 24 hours, 48 hours and 72 hours medium was removed and stored at -80 ˚C. **(A)** Transfected with siRNAs targeting LDHA. **(B)** Transfected with siRNA targeting MCT-4. **(C)** Transfected with siRNAs targeting LDHB. Each condition was measured in biological triplicate and represented as mean ± SD (B-D). Statistical significance was assessed by two-way ANOVA with Dunnett's post-hoc analysis where each condition was compared to the "A549 only infected" control (*, $p < 0.05$; **, $p < 0.01$; ***, $p < 0.001$; ****, $p < 0.0001$; ns, non-significant).

5.2.8 Design of hairpin siRNAs that target LDHA, LDHB and MCT-4 silence target proteins after DNA transfection

Targeting LDHA and MCT-4 does not alter EnAd's ability to replicate, express proteins and produce infectious progeny. Although we had not seen the desired result of pH mediation by siRNAs following transfection of DLD-1 cells, we hoped that efficiency of EnAd infection would improve knockdown enough to induce a change in the pH in DLD-1 cells in high glucose medium. Whilst siRNA transfection may be useful for transient knockdown of proteins in cells, shRNAs must be designed in order to be encoded in the EnAd genome.

The shRNA constructs were designed based on siRNA candidates tested in previous sections of this chapter. We designed a forward oligomer containing the sense and antisense strands of the siRNA interspaced by a loop sequence, and containing a termination signal at the 5' terminus (T_5). A reverse oligomer of complementary sequence was also synthesised. Additionally, a scramble shRNA sequence kindly provided by David Sabatini was synthesised to use as a negative control. The no. 2 siRNA used as a negative control in the siRNA transfection studies could not be used in this application since the sequence of this siRNA is proprietary information and is therefore not supplied by ThermoFisher. All oligomers ordered are detailed in Table 5.1. Oligomers were annealed to produce a double-stranded product and ligated into a linearised shuttle vector downstream of a human U6 promoter (Figure 5.14).

Table 5.1 Oligomers ordered to form the hairpins to target lactic acid pathway components. Hairpins were designed after validation of synthetic siRNAs targeting proteins for knockdown. The forward strands encode a sense strand (purple) and an antisense strand (green) either side of a loop sequence (red). The reverse strands are complementary to allow for annealing and insertion into a plasmid. *The scramble shRNA oligomers (blue) were designed based on a plasmid created by David Sabatini (Addgene plasmid #1864;http://n2t.net/addgene:1864 ; RRID:Addgene_1864).

Target Gene	Assay ID (ThermoFisher)	Orientation	IDT Oligo Order (Sense Loop Antisense)
LDHA[B]	s350	Fwd	CCGGAACCAGCGTAACGTGAACATATTCAAGAGATATGTTCACGTTACGCTGGTTTTTG
		Rev	AATTCAAAAACCAGCGTAACGTGAACATATCTCTTGAATATGTTCACGTTACGCTGGTT
LDHA[C]	s351	Fwd	CCGGAACAGTGGATATCTTGACCTATTCAAGAGATAGGTCAAGATATCCACTGTTTTTG
		Rev	AATTCAAAAACAGTGGATATCTTGACCTATCTCTTGAATAGGTCAAGATATCCACTGTT
LDHB[B]	s8125	Fwd	CCGGAAGTATGTTACCTGGAAACTATTCAAGAGATAGTTTCCAGGTAACATACTTTTTG
		Rev	AATTCAAAAAGTATGTTACCTGGAAACTATCTCTTGAATAGTTTCCAGGTAACATACTT
LDHB[C]	s8126	Fwd	CCGGAACAGTCCTGATTGCATCATATTCAAGAGATATGATGCAATCAGGACTGTTTTTG
		Rev	AATTCAAAAACAGTCCTGATTGCATCATATCTCTTGAATATGATGCAATCAGGACTGTT
MCT4[A]	s17416	Fwd	CCGGAATCAAGGAGCTCATACAGGATTCAAGAGATCCTGTATGAGCTCCTTGATTTTTG
		Rev	AATTCAAAAATCAAGGAGCTCATACAGGATCTCTTGAATCCTGTATGAGCTCCTTGATT
Scramble*	N/A	Fwd	CCGGAACCTAAGGTTAAGTCGCCCTCGCTCGAGCGAGGGCGACTTAACCTTAGGTTTTTG
		Rev	AATTCAAAAACCTAAGGTTAAGTCGCCCTCGCTCGAGCGAGGGCGACTTAACCTTAGGTT

To test the ability of constructed hairpins to knockdown their targets we transfected A549 cells with either the siRNA or the corresponding U6-shRNA shuttle vector. As shown in Figure 5.15A, transfection of U6-shLDHB (s8125) showed greater knockdown efficiency of LDHB than the siLDHB three days after transfection of A549 cells. The U6-shMCT4 (s17416) vector knocked down MCT-4 to the same extent as siMCT4. No knockdown of LDHA, neither by transfection of the U6-shLDHA vector or of the corresponding siRNAs was observed. Increasing amounts of the U6-LDHB, U6-LDHA and U6-MCT4 plasmids encoding the hairpins were transfected into A549 cells and knockdown was measured 3 days post-transfection (Figure 5.15B). In a second experiment, fewer A549 cells were plated and

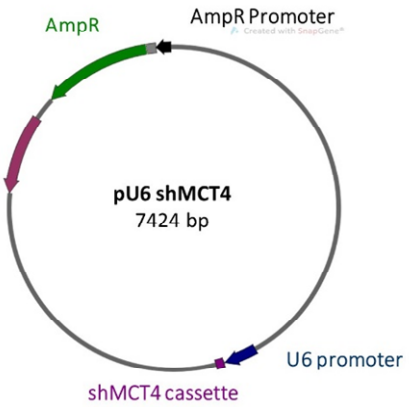


Figure 5.14 The plasmid map for expression of the U6 promoter hairpin (shRNA) cassettes. A schematic of the final U6-shRNA plasmid cloned, and used to transfect tumour cells to silence target genes. Diagram made using SnapGene.

transfections of both the U6-shRNA plasmids targeting LDHA were repeated. Knockdown was observed for both plasmids compared to untransfected and Lipofectamine 2000 treated A549 controls (Figure 5.15C). All shRNA formats knocked down the relevant target protein after transfection into A549 cells. The shRNA based on the siRNA-s351 format was able to more efficiently knockdown LDHA in the dose experiments (Figure 5.15B).

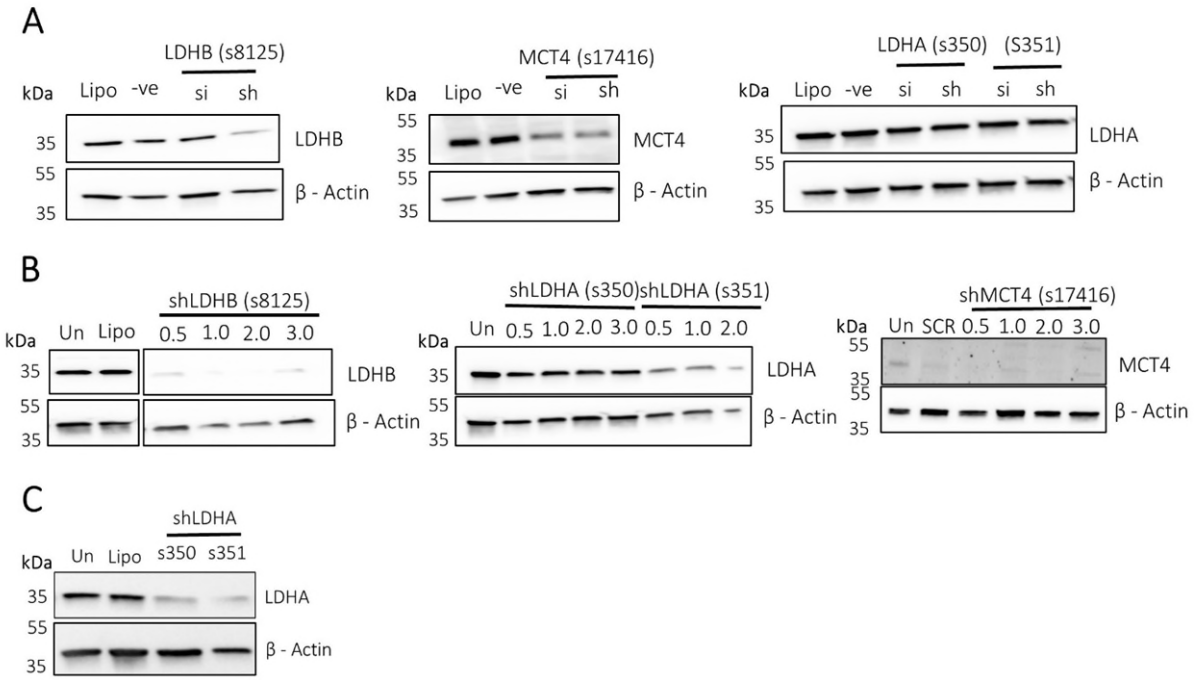


Figure 5.15 LDHA, LDHB and MCT-4 protein expression are reduced in A549 cells following DNA transfection with expression plasmids containing shRNA against each target's mRNA. (A) A549 cells were transfected with either siRNA (400 nM) or their corresponding expression plasmids (U6-shRNA; 0.8 μg) targeting LDHB, LDHA and MCT-4. Three days later cells were harvested and lysates analysed for LDHB (37 kDa), LDHA (37 kDa) and MCT-4 (43 kDa) expression using western blot analysis. β actin (42 kDa) was used as a loading control. Transfections were repeated as above with varying dilutions of U6 shRNA expression plasmids (where 0.5; 0.4 μg, 1; 0.8 μg, 2; 1.6 μg, 3; 2.4 μg DNA) **(B)** or using fewer numbers of A549 cells per well **(C)** and lysates were analysed for LDHB, LDHA and MCT-4 using western blot analysis. Lipo, Lipofectamine 2000 treated control; -ve, Negative No.2 transfected control; si, siRNA transfected; sh, shRNA-containing plasmid transfected; Un, untransfected control; SCR, transfected with the pSF plasmid containing the scramble cassette.

5.2.9 Cloning strategy to generate OVs containing hairpins against LDHA, LDHB and MCT-4 and a GFP reporter

Arming EnAd with shRNAs against LDHA and MCT-4 will mean that they are expressed selectively inside tumour cells. This reduces the probability of off-target effects that are currently reported for small molecule inhibitors against both LDHA and MCT-4 (J Akhenblit and D Pagel 2016). In addition, OVs self-amplify *in-situ* meaning shRNA expression will also amplify saving on any repeated dosing required. We successfully constructed shRNAs against LDHA and MCT-4, capable of knockdown after DNA transfection, we next sought to encode

them into the EnAd genome (kindly provided by Psioxus therapeutics, Oxford, UK) alongside a GFP reporter in order to track modified viruses.

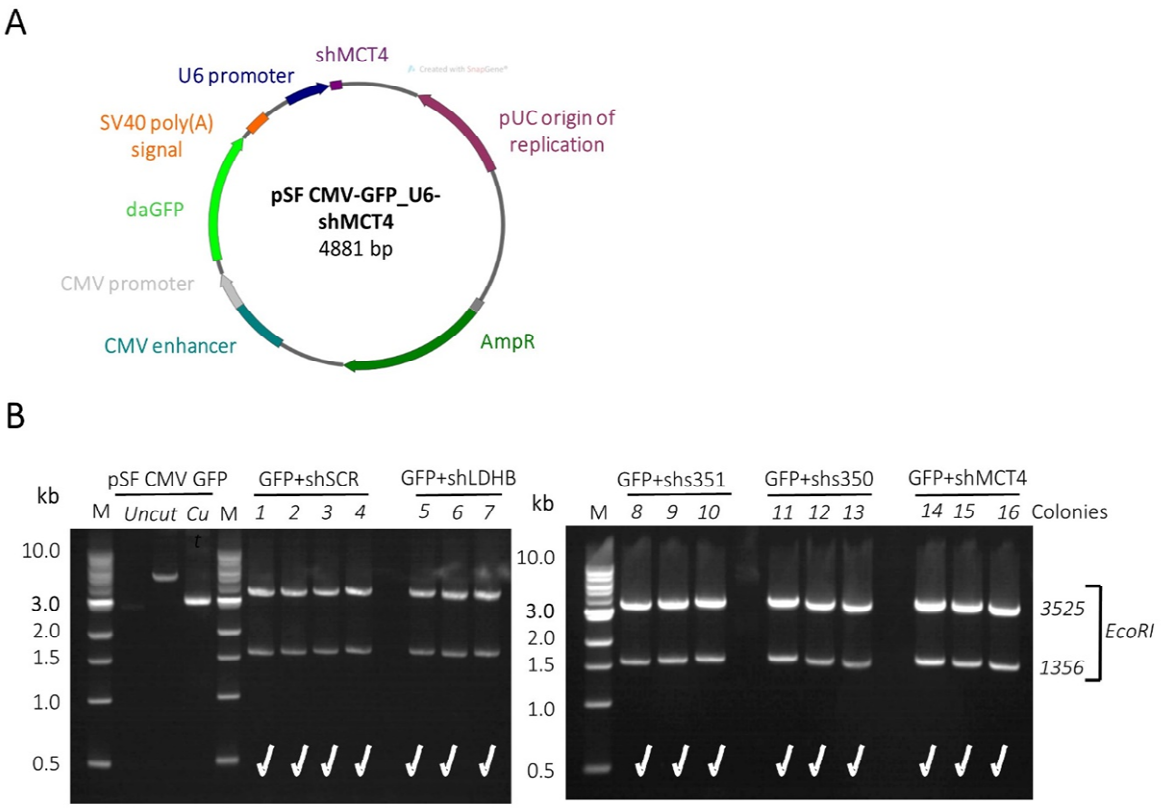


Figure 5.16 Generation of the CMV-GFP_U6-shRNA cassettes to enable reporter virus generation. (A) A schematic of the engineered pSF-CMV-GFP_U6-shRNA expression plasmids cloned. SV40, Simian vacuolating virus 40; p(A) signal, polyadenylation signal; U6 promoter, U6 RNA polymerase III promoter; shMCT4, shRNA hairpin targeting MCT-4; AmpR, ampicillin resistance; CMV, cytomegalovirus; daGFP, green fluorescent protein. **(B)** Transgene insertion was confirmed by diagnostic restriction digest with EcoRI and DNA fragments were resolved on a 1% agarose gel. Predicted band sizes are in *italics*. All colonies picked had successful insertion, indicated with white ticks. Diagram of expression plasmid made using SnapGene.

Gibson assembly was used to clone a GFP reporter gene driven by a CMV promoter alongside hairpins driven by U6, the resulting engineered plasmid is shown in Figure 5.16A. Successful insertion of the U6-shRNA constructs into the backbone of a plasmid containing CMV-GFP was confirmed by diagnostic digests with EcoRI (Figure 5.16B). A549 cells were transfected with the sequenced CMV-GFP_U6-shRNA expression plasmids, then harvested to assess for

knockdown of target proteins, LDHB, LDHA and MCT-4. All plasmids (pSF) knocked down target proteins, and in the case of LDHB and LDHA knock down was more efficient with the pSF plasmid than the U6-shRNA shuttle vectors used in Figure 5.15. Although pSF plasmids also downregulated the loading control, β-actin (Figure 5.17).

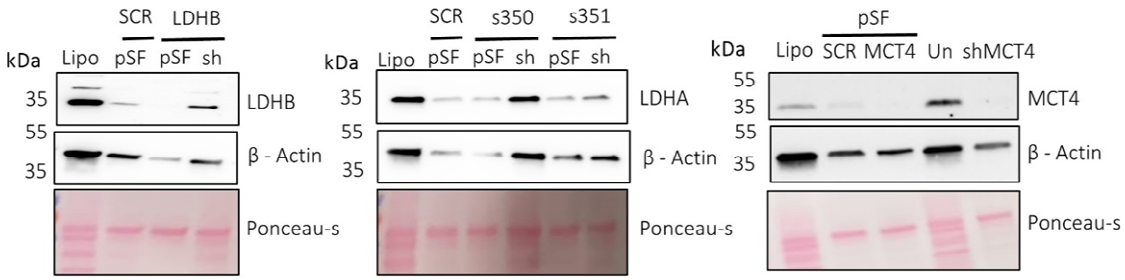


Figure 5.17 LDHA, LDHB and MCT-4 protein expression are reduced in A549 cells following DNA transfection with expression plasmids containing CMV-GFP and U6-shRNA against each target's mRNA. A549 cells were transfected with either U6 expression plasmids (U6-shRNA) or with pSF expression plasmids (pSF-CMV-GFP_U6-shRNA) targeting LDHB, LDHA and MCT4. Three days later cells were harvested and lysates analysed for LDHB (37 kDa), LDHA (37 kDa) and MCT4 (43 kDa) expression using western blot analysis. β actin (42 kDa) was used as a loading control and ponceau-S stains are shown here as a second loading control. Lipo, Lipofectamine 2000 treated control; sh, transfected with U6-shRNA plasmids; Un, untransfected control; SCR, transfected with the pSF plasmid containing the scramble cassette; pSF, transfected with pSF expression plasmids.

After confirming pSF expression plasmids could still knockdown target proteins, the CMV-GFP_U6-shRNA cassettes were amplified out of the expression plasmids using PCR and inserted into linearised EnAd2.4 vector, using Gibson assembly. Successful cassette insertion into the virus genome backbone was confirmed by Sanger sequencing and diagnostic digests with AsiSI or SbfI and AscI shown in Figure 5.18. EnAd vectors with successfully inserted GFP and shRNAs constructs were linearised with AscI then transfected into 293Ad cells. Successful infection was confirmed by monitoring GFP expression two days post-transfection using fluorescent microscopy and comparing transfected linearised modified EnAd to linearised parental EnAd or untransfected 293Ad controls (Figure 5.19).

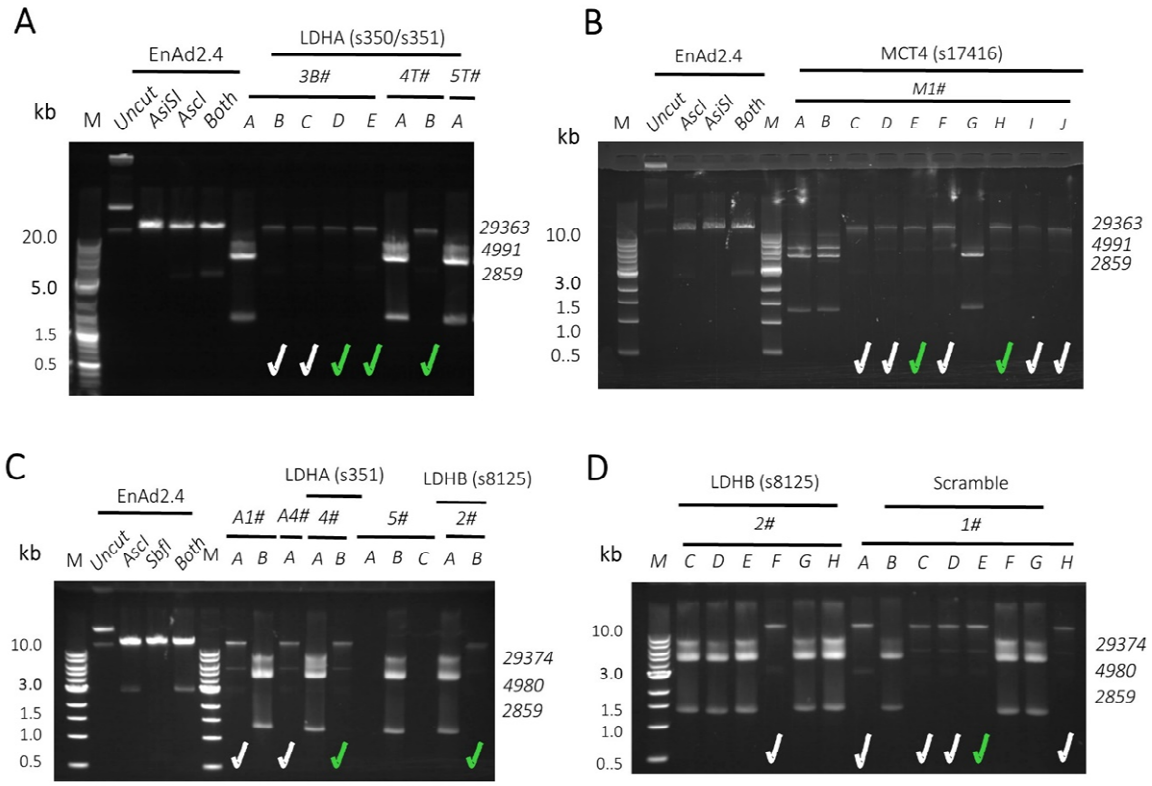


Figure 5.18 CMV-GFP_U6-shRNA cassette insertion into EnAd 2.4 vector backbones was confirmed using diagnostic digests. Transgene insertion was confirmed by diagnostic restriction digests with AsiSI and AscI **(A, B)** or with AscI and SbfI **(C, D)**. EnAd2.4 vectors containing LDHA shRNA are in (A) and in (C). Those containing MCT-4 shRNA are in (B) and those containing LDHB shRNA are in (C) and in (D). DNA fragments were resolved on 0.8% agarose gels and predicted band sizes are in *italics*. Colonies with successful insertion are indicated with white ticks, the colonies chosen to take forward are indicated with green ticks.

The 293Ad cells displaying GFP expression were collected along with culture medium. This crude virus preparation contained a mixture of both the modified virus and the unmodified parental virus, in addition to the transfection reagents used. To isolate single clones of modified viruses, plaque purification was used as described in section 2.8.4, the process of plaque purification is exemplified for EnAd-shMCT4 viruses shown in Figure 5.20. The A549 cells used to amplify the virus after the first iteration of plaque purification were harvested in order to assess the shRNA-induced target protein knockdown after infection with each virus plaque.

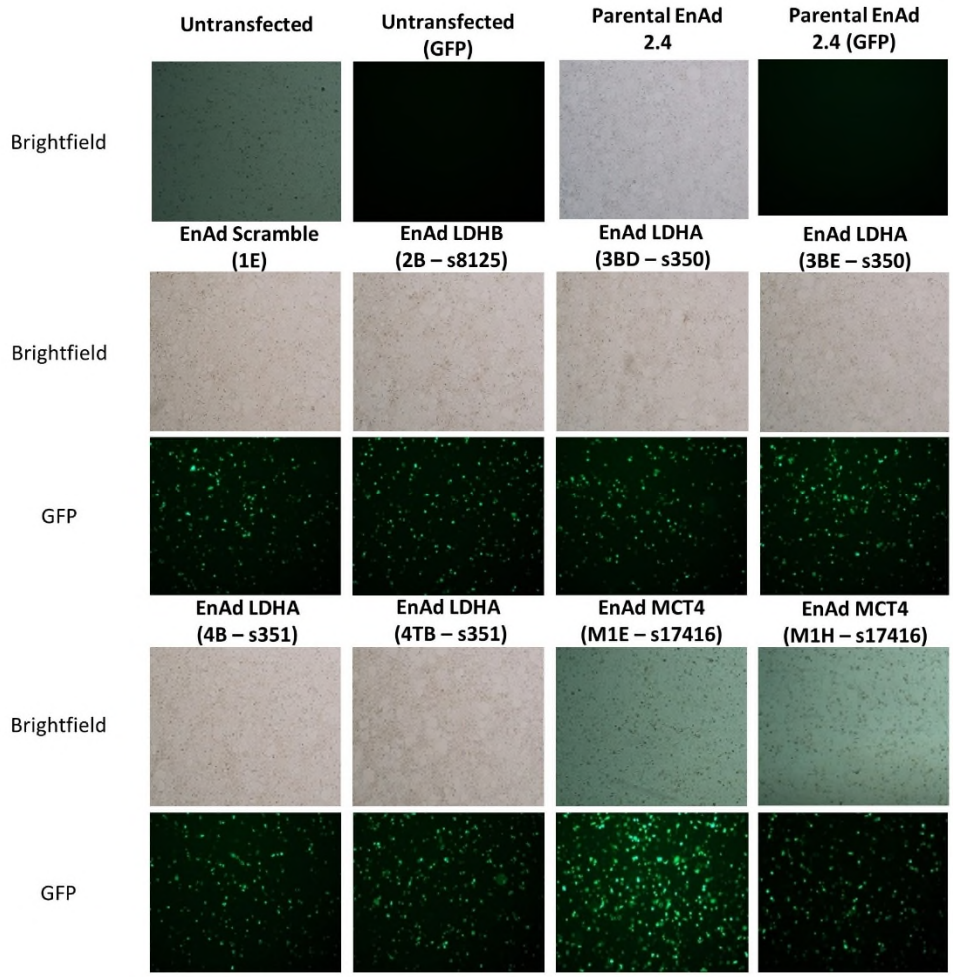


Figure 5.19 GFP expression confirmed following transfection with linearised engineered GFP_shRNA viruses. Engineered EnAd vectors were linearised with AscI, purified using isopropanol precipitation and transfected into adherent 293 cells. Two days after transfection wells were imaged by brightfield or fluorescent microscopy.

U6-shRNA cassettes were successfully cloned into pSF expression plasmids containing GFP under the control of the CMV promoter. All modified plasmids expressed GFP following transfection (data not shown) and all knocked down their relevant target protein with respect to the loading control. CMV-GFP_U6-shRNA cassettes were successfully cloned into the genome of EnAd, the parental oncolytic adenovirus. All modified EnAd viruses were transfected into 293Ad cells, they all expressed GFP and induced significant CPE.

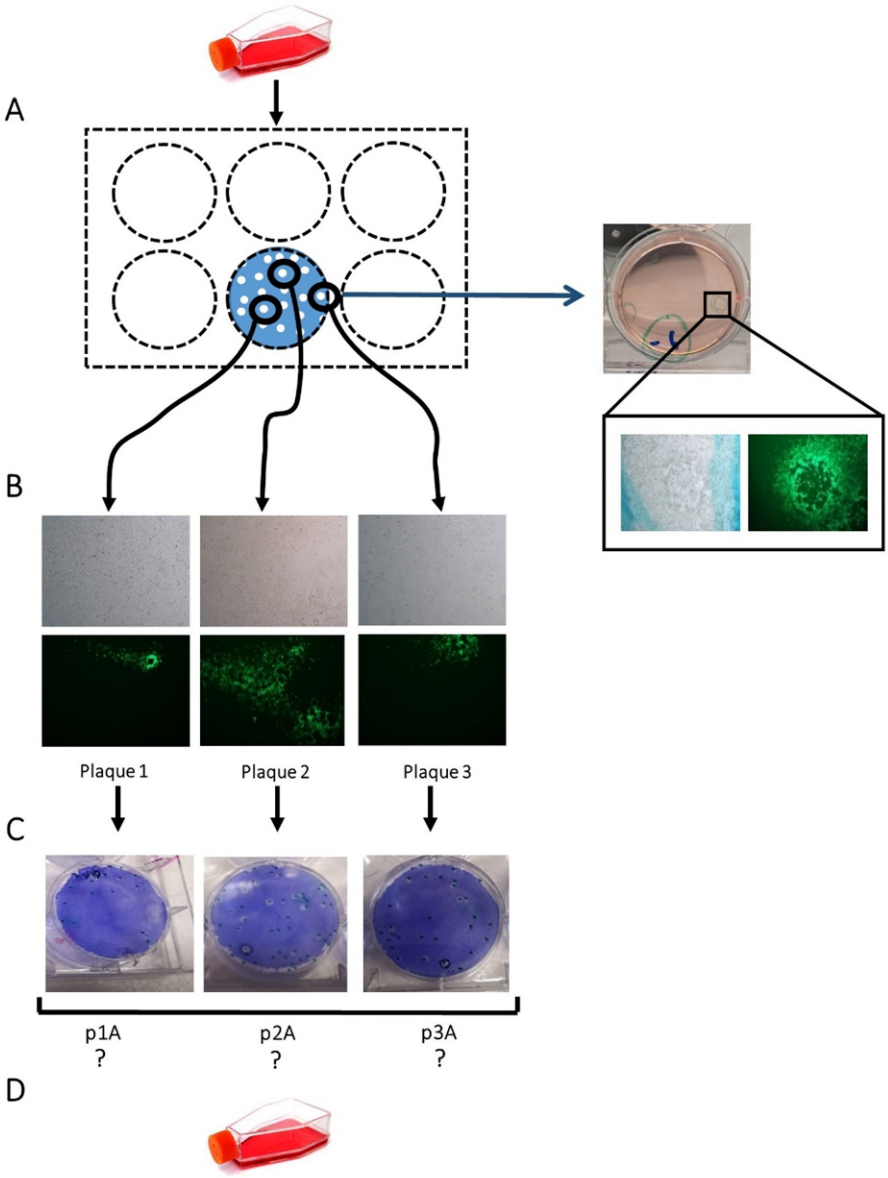


Figure 5.20 EnAd expressing GFP-shRNA cassettes were subject to two rounds of plaque purification. Crude virus preparations following transfection with GFP-shRNA expressing EnAd vectors were purified by isolating single clones of shRNA armed viruses by two rounds of plaque purification. Single virus plaques (p1, p2, p3) were isolated **(A)** from one well and expanded on A549 cells **(B)**, supernatants were harvested upon observation of > 60% CPE and used to set up a further round of plaque purification **(C)**. Single plaques were isolated (p1A, p2A, p3A) and aspirated into medium to infect 293Ad cells **(D)**. Following the observation of extensive CPE, cells and medium were collected and virus was extracted from cells using freeze/thaw cycles, centrifugation and filtration.

5.2.10 Engineered EnAd viruses with hairpins knock down lactic acid pathway target proteins

All three plaques chosen following the first round of plaque purification (Figure 5.20B) were examined for knockdown of LDHA and MCT-4 mRNA and protein expression, visualising knockdown with RT-PCR and western blot respectively. A549 cells were infected at an MOI of 1 using the same virus-containing medium used to set up the second plaque purification round (Figure 5.20C). The dose was calculated based on the PFU/mL titre calculated from the end of the second plaque purification. This would enable us to choose the virus clone with the best knockdown activity to be carried forward in the following amplification step (Figure 5.20D).

We measured the levels of target mRNAs using an RT-PCR approach. RNA was extracted from cells, reverse transcribed into cDNA and target sequences were detected using specific primers. Amplified cDNA was visualised by electrophoresis on a 1% agarose gel. We measured expression of LDHA (Figure 5.21A), MCT-4 (Figure 5.21B) and LDHB (Figure 5.21C) as well as the housekeeping gene β-actin, following infection with either the parental EnAd or those modified to express hairpins and GFP.

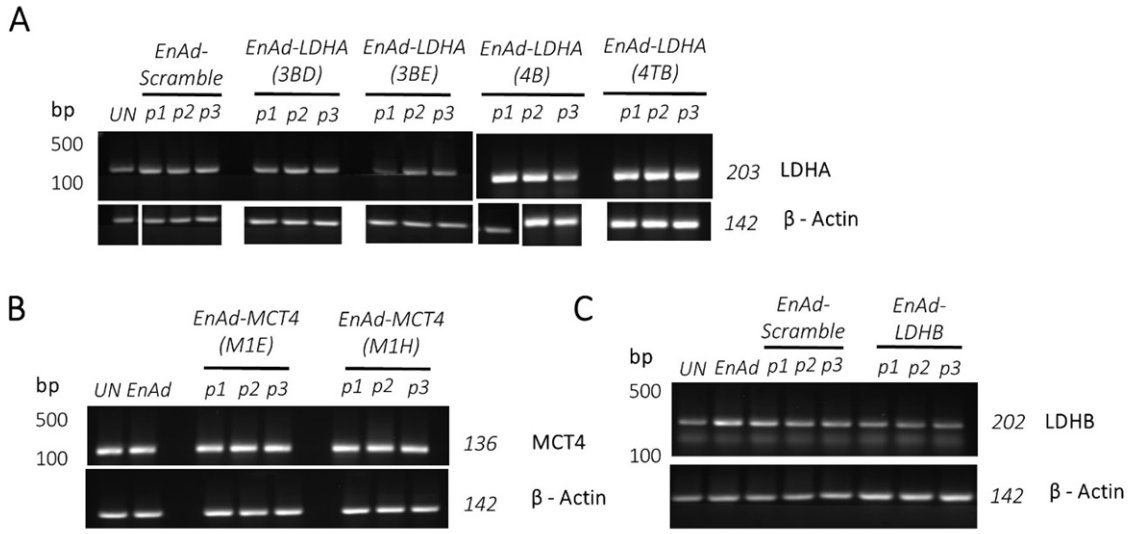


Figure 5.21 shRNA expressing EnAd clones were selected after cDNA analysis using RT-PCR. A549 cells were infected with three single virus plaques. Plaques were isolated from one round of plaque purification and expanded on A549 cells, medium was collected and used to set up a second round of plaque purification. Virus titres of each plaque were determined based on the second round and A549 cells for RT-PCR were infected at an MOI of 1. Cells were lysed when > 75% cells were GFP positive based on fluorescence microscopy visualisation using the Luna® Cell Ready One-Step RT-qPCR kit. During the same reaction any mRNA isolated was reverse-transcribed into cDNA and specific cDNA for LDHA **(A)**, MCT-4 **(B)** and LDHB **(C)**, were amplified by PCR using specific target forward and reverse primers. Predicted cDNA band sizes are in *italics*. β-actin was used as a endogenous control.

Plaque 1 of both the EnAd-LDHA modified viruses with an s350-based hairpin (3BE) had less LDHA cDNA than the uninfected control (Figure 5.21A). Plaque 3 of EnAd-LDHA modified virus with an s351-based hairpin (4B) was observed to have less LDHA mRNA than the uninfected control (Figure 5.21A). No plaques picked for EnAd-MCT4 modified viruses (M1E and M1H; s17416) decreased mRNA expression (Figure 5.21B). All three plaques appear to reduce mRNA expression following infection with EnAd-LDHB (2B; s8125) compared to the uninfected control (Figure 5.21A). However, the EnAd-scramble viruses also appear to knock down LDHB, suggesting that this might not be a specific effect mediated by the shRNA transgene.

Protein expression was determined from A549 lysates following expansion of modified virus plaques picked after a first round of plaque purification. The virus titre in the media used to

infect the cells was unknown however, meaning the results are not directly comparable to the RT-PCR results. Analysis of the expression of target protein LDHA agreed with RT-PCR results, showing that plaque 1 of EnAd-LDHA (3BE) knocked down LDHA successfully. Infection with the EnAd-scramble virus, which served as a negative control, did not result in any knockdown of LDHA (Figure 5.22A). Analysis of LDHB protein expression agrees with RT-PCR results, that all three virus plaques knocked the protein down, however, the EnAd-scramble viruses also knocked down LDHB suggesting the effect may be unrelated to the expression of the shRNAs (Figure 5.22C). Analysis of MCT-4 protein expression showed successful knockdown of the target protein after infection with all three plaques of EnAd-MCT4 viruses. For both viruses (M1E and M1H; s17416), this effect was greatest when using plaque 3, despite the RT-PCR results showing no change in mRNA expression. The EnAd-scramble viruses partially decrease MCT-4 expression but not to the extent of virus plaque 3 of EnAd-MCT4 viruses (Figure 5.22D).

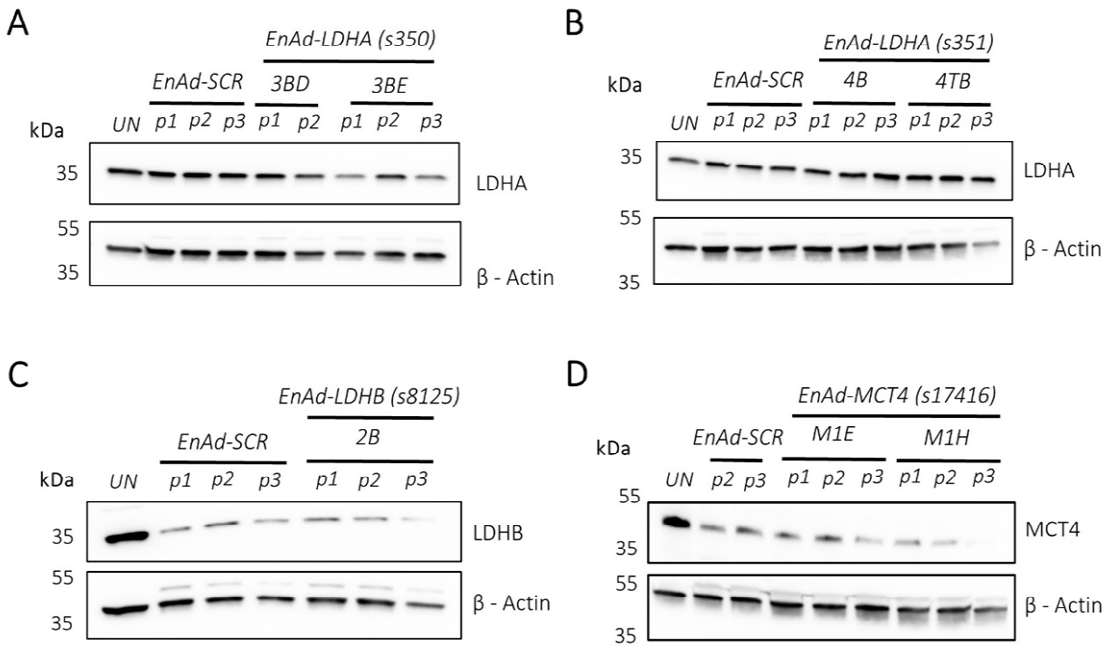


Figure 5.22 shRNA expressing EnAd clones were selected after analysis using western blotting. A549 cells were infected with medium aspirated with picked plaques (p1, p2, p3) of unknown virus titres. Upon the observation of > 60% CPE virus-containing medium was harvested and used to set up a second round of plaque purification whilst cells were harvested and lysates analysed for LDHA (37 kDa) **(A,B)**, LDHB (37 kDa) **(C)** and MCT4 (43 kDa) **(D)** expression using western blot analysis. β actin (42 kDa) was used as a loading control.

For analysis of oncolytic viral activity of the EnAd viruses modified with hairpins we chose to take forward the plaques displaying the greatest efficiencies of target protein knockdown. Plaques 3 (based on Figure 5.21 only) and 1 were chosen for EnAd-LDHA 3BD and 3BE respectively (s350), plaque 3 was chosen for EnAd-LDHA with the alternative shRNA format (4B, s351). Plaque 3 was chosen for EnAd-MCT4 (M1H, s17416), plaque 2 was chosen for EnAd-LDHB (2B, s8125) and plaque 3 for the control EnAd-scramble.

5.2.11 Viral genome replication and oncolytic activities of hairpin-armed EnAd viruses is slightly reduced compared to parental EnAd

The chosen plaques were used to infect A549 cells to amplify viruses on a small scale then those batches were plaque assayed to quantify their PFU/mL (Table 2.11). The replication

kinetics and oncolytic properties of these virus batches were then assessed and compared with parental EnAd; qPCR was used to quantify viral genomes produced over the course of 72 hours and an MTS assay was used to quantify cytolysis of DLD-1 cells after infection with different doses of the viruses as described in sections 2.8.10 and 2.6.2 respectively.

Plaque assays revealed that the EnAd-scramble and EnAd-LDHB viruses were far less concentrated with 100-1000 fold fewer infectious viral particles than the other plaques chosen and amplified. This meant these modified viruses had to be used sparingly and therefore their genome replication was quantified only at the 72 hour timepoint.

Infection of DLD-1 cells with parental EnAd or the modified GFP-shRNA EnAd viruses (MOI 1) yielded similar amounts of viral genomes at 24 hours post-infection. There were however substantial differences in genome titres at 72 hours. While parental EnAd yields 8.8 x 10^{13} genomes/well, EnAd-MCT4 and EnAd-LDHA (3BD, s350) yielded 3.4 x 10^{13} and 1.3 x 10^{13} genomes/well respectively. While EnAd-LDHA (4B, s351) only yielded 9.7 x 10^{11}, 100-fold

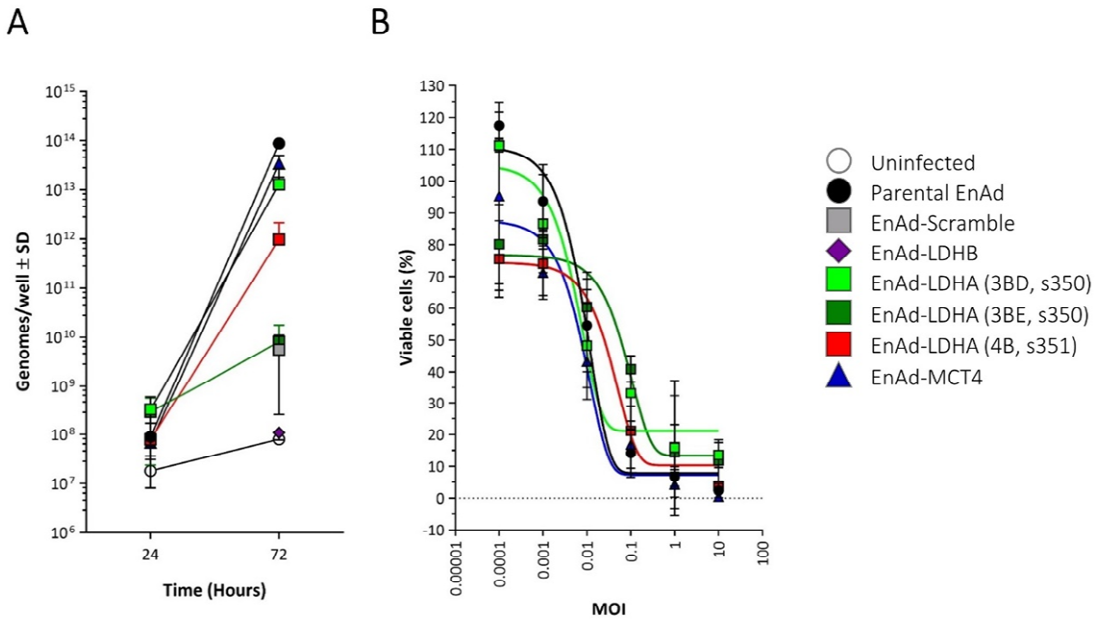


Figure 5.23 Viral genome replication and oncolytic activity of EnAd-expressing shRNA viruses were compared with parental EnAd. (A) DLD-1 cells were infected with parental EnAd or recombinant viruses (MOI 1). Entire wells were harvested at 24 hours or 72 hours into DPBS. Genome replication was assessed by using qPCR primers and a probe against Ad11 hexon. Each condition was measured in technical triplicates and represented as mean ± SD. **(B)** DLD-1 cells were infected with EnAd or recombinant viruses at increasing MOIs of virus. DLD-1 cytotoxicity was measured using an MTS assay after five days of incubation. Each condition was measured in biological triplicate and represented as mean ± SD.

less than parental EnAd and EnAd-LDHA (3BE, s350) yielded 8.1 x 10^9, 10,000-fold less. Both EnAd-LDHB and EnAd-scramble yielded the least genomes/well, 1.1 x 10^8 and 5.6 x 10^9 genomes/well, worryingly only 10- and 100-fold more than the uninfected control (Figure 5.23A). These results indicate that for the EnAd-scramble, EnAd-LDHB, EnAd-LDHA 3BE and EnAd-LDHA 4B viruses, the inclusion of a GFP and shRNA cassette interferes with EnAd's replication kinetics, yet viruses were able to be rescued. This interference was only minor in the context of EnAd-MCT4 and EnAd-LDHA 3BD infections.

The viability DLD-1 cells infected with parental EnAd or the modified viruses at increasing MOIs was measured with MTS five days post-infection. EnAd-MCT4 and EnAd-LDHA 3BD both exhibited cytotoxic activity indistinguishable from the parental EnAd virus, indicating that genetic modification did not alter the intrinsic oncolytic activity of these viruses. However

EnAd-LDHA 3BE and EnAd-LDHA 4B both displayed decreased cytolytic ability, with a 10-fold increase in MOI being required to reduce viability by 50% (Figure 5.23B). These cytotoxicity profiles are consistent with the replication kinetics described above.

Assessment of the replication and oncolytic properties of the modified viruses has shown that EnAd-MCT4 and EnAd-LDHA 3BD (s350) both retain the properties of parental EnAd. However EnAd-LDHA 3BE (s350) and EnAd-LDHA 4B (s351) have slower replication kinetics and a decreased cytolytic effect.

5.2.12 EnAd-expressing shRNA against LDHA successfully knocks down expression of LDHA after infection

We wanted to assess whether the modified viruses were still able to knockdown mRNA expression of LDHA and MCT-4. We infected DLD-1 cells at an MOI of 1 with parental EnAd or with the modified viruses. We then harvested cells at 96 hours post-infection and measured the relative expression of the target genes by comparing them to an uninfected DLD-1 cell control. We used RT-qPCR analysis to quantify target expression normalised to a housekeeping gene and expressed as a fraction of the uninfected control. The method used is described in sections 2.3.7.

We serially diluted template from the uninfected control to create a standard curve to use to calculate a relative abundance of template in test samples by linear regression. We made standard curves for each target gene, LDHA and MCT-4 and standard curves for an endogenous control, β-actin. This allowed us to normalise all samples to the endogenous control. Parental EnAd infection significantly reduced the expression of LDHA compared to the uninfected control (by 20%), however all three viruses encoding the hairpins against LDHA reduced the expression of LDHA further, with those viruses encoding the s350 hairpin displaying the most

efficient knockdown (Figure 5.24A). Surprisingly, when analysing MCT-4 expression in infected samples the parental EnAd decreased the amount of MCT-4 the most by more than 70%. The modified viruses EnAd-LDHA 4B (as a non-specific control) and EnAd-MCT4 samples both had increased levels of MCT-4 expression (Figure 5.24A).

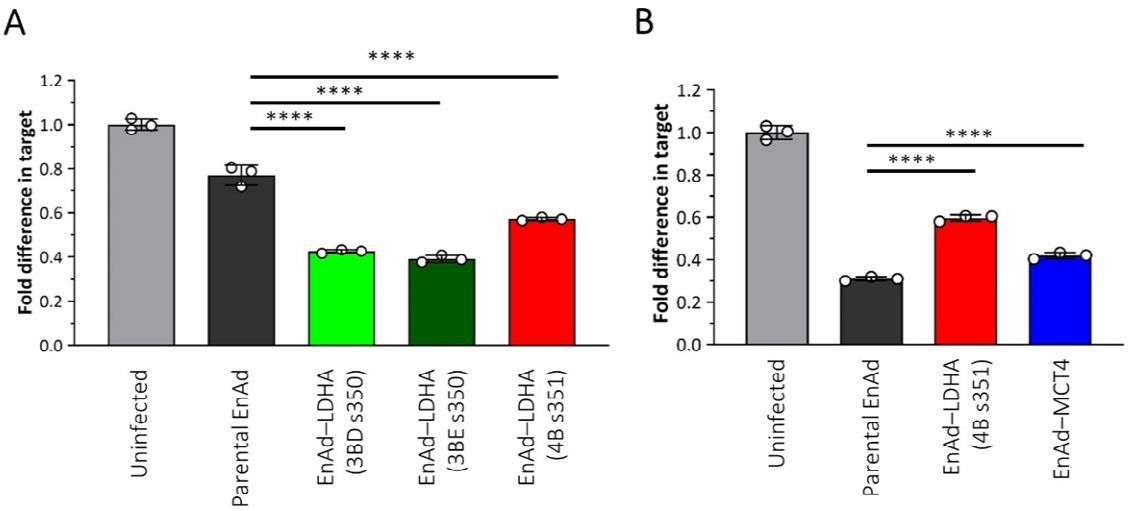


Figure 5.24 The expression of LDHA and MCT4 following infection with EnAd-expressing shRNA viruses was assessed using RT-qPCR. (A) DLD-1 cells were infected with parental EnAd or recombinant viruses (MOI 1). Entire wells were harvested at 96 hours using the RNAeasy plus mini kit. 800 ng total RNA was reverse transcribed to cDNA using the Quantitect kit and 25 ng total cDNA (assuming 100% conversion) was used in a qPCR reaction with primers against LDHA and β-actin. **(B)** The same experiment as in (A) was performed using a primer set against MCT4 and β-actin. Each condition was measured in technical triplicates and represented as mean ± SD. Statistical significance was assessed by one-ANOVA with Dunnett's post-hoc analysis where each condition was compared to the parental EnAd infected control (*, $p < 0.05$; **, $p < 0.01$; ***, $p < 0.001$; ****, $p < 0.0001$; ns, non-significant).

Both of the modified LDHA EnAd viruses using s350 as the shRNA knocked down LDHA mRNA by 50%. The virus encoding the s351 shRNA decreased LDHA RNA levels by 37.5%. Therefore the EnAd-LDHA 3BD virus displays both the best target knockdown efficiency and the best replication kinetics, making it the preferred candidate to take forward and test further. Interestingly, parental EnAd infection resulted in the largest decrease in MCT-4 expression and surprisingly, the modified EnAd-MCT4 virus appeared to increase MCT-4 expression. Cells were harvested at 96 hours post-infection, at which point many cells had died, this could

contribute towards MCT-4 dropping across all samples. Therefore assessing RNA levels at an earlier time point could prove more informative in assessing the silencing ability of EnAd-MCT-4 compared to parental EnAd.

To assess the functional capacity of the EnAd-LDHA 3BD modified virus to modulate the pH of CM, we would next need to infect cells with various MOIs and monitor pH changes. If pH modulation is observed, we could then use culture medium in a CM experiment with T cells to assess whether infection with modified viruses helps to alleviate inhibition of T cells following activation in acidic medium.

5.3 Conclusions

The conclusions of this chapter are:

1. Transfection of siRNAs against LDHA and MCT-4 are not sufficient to restore a neutral pH in conditioned medium with DLD-1 tumour cells,
2. Tumour cell lysis by EnAd is kinetically slower in culture with lactic acid,
3. shRNAs targeted against LDHA and MCT-4 were successfully expressed by engineered EnAd viruses,
4. The replicative and cytolytic capacities of modified EnAd viruses were reduced in two viruses expressing LDHA targeted shRNA,
5. EnAd-expressing LDHA targeted shRNA knocked down mRNA expression of LDHA following infection.

5.4 Discussion

In this chapter, we established a CM model in which we could directly test the effects of tumour cell metabolism on T cells; focusing on the output of lactic acid as a major contributor to low pH in the TME that is known to inhibit the T cell activating therapy, EpCAM BiTE (Chapter 4). We found that DLD-1 cells were highly glycolytic and capable of reducing the activation of cytotoxic T cells by EpCAM BiTE by more than 50% (Figure 5.3). We next explored whether we could reduce the inhibitory effect of medium from DLD-1 cells by exploiting the ability of RNAi to knockdown two key mediators of the lactic acid pathway, LDHA and MCT-4.

We found that although significant effects on protein expression were observed after using siRNA transfection (Figure 5.5), this was not reflected in a functional response to transiently modulate the pH of culture medium of transfected DLD-1 cells (Figure 5.6). We deduced that the efficiency of transfection of DLD-1 cells using Lipofectamine 2000 could be the limiting factor in this functional response; if less than 50% of DLD-1 cells were transfected, there may not have been an observable significant change in pH. Therefore, we hypothesised that we could increase knockdown by encoding shRNAs into an adenoviral vector that would increase efficiency of RNAi delivery in our studies (C. B. Moore et al. 2010). EnAd is an effective dual-mechanism platform for encoding therapeutics and delivery and expression of shRNAs from an OV and would be a proof-of-concept of pH modulation of the TME with a cancer-selective virus. The selectivity of EnAd means that off-target effects will be minimal, which is particularly relevant for small molecule inhibitors currently being tested against LDHA and MCTs (Doherty and Cleveland 2013). Since T cells share the same glycolysis requirement as cancer cells, off-target effects of small molecule inhibitors of LDHA and MCTs often effect this cell type, resulting in decreased immune functionality (Romero-Garcia et al. 2016; Ippolito et al. 2018).

To test this proof-of-concept approach, we first determined whether parental EnAd could successfully replicate in the immunosuppressive acidic conditions that we aimed to reverse. The production of EnAd virions was not reduced in an acidic environment and, despite slightly reduced expression of encoded therapeutics, the ability for EnAd to complete its replication cycle, albeit more slowly, was apparent even in medium with 15 mM lactic acid (Figures 5.7 - 5.10). With this in mind, it can still be concluded that slower kinetic killing of tumour cells would actually help our approach. The longer tumour cells remain alive and infected, the more shRNA is expressed, which could improve knockdown efficiency of the target mRNA and therefore enable pH modulation in the TME.

Constructs containing shRNAs targeting LDHA and MCT-4 were tested alone and were encoded alongside GFP in expression plasmids, for transfection into tumour cells. All constructs knocked down target proteins more efficiently than the original siRNA formats (Figures 5.15 and 5.17). After sequence confirmation, cassettes containing CMV-GFP_U6-shRNA were encoded into the EnAd genome. All EnAd-LDHA viruses knocked down LDHA mRNA (Figure 5.24A) and protein expression (Figure 5.22A). EnAd-LDHA 3BD (s350) knocked down LDHA and retained its replicative and oncolytic properties, making it the most promising candidate (Figure 5.23). However, these viruses need further testing and optimisation to properly assess their functionality to modulate pH of the TME. Moreover these viruses only represent a proof-of-principle and would require further modifications in order for them to be clinically translatable. EnAd is a group B AdV which uses CD46 to gain entry into cells. This is expressed in all nucleated cells and therefore when hairpin expression is driven from a ubiquitous U6 promoter it means that any cell the virus gains entry to will express the hairpins. This would result in knockdown of target proteins in non-target cells; to avoid this virus-specific promoters like MLP should be used or tumour-selective promoters. Unanswered issues with the negative EnAd-scramble control virus also need to be addressed, as EnAd-scramble virus

knocked down both LDHB and MCT-4; suggesting that EnAd itself may influence expression of these key metabolic genes. However according to work done by Yen Rong Fu *et al* (Fu et al. 2017) LDHA, LDHB and MCT-4 protein expression are all slightly increased by Ad5 infection, this would be in contrast to what we have seen with EnAd. Therefore future work will address this limitation in our studies.

The use of RNAi in viral therapy has only really taken off in the last decade and still faces challenges in effective design and implementation. With improvements in design, the favourable and predictable mechanisms of action of various shRNAs could very well improve a strategy like the one exemplified in this chapter. The combinatorial approach with OVs used here to target LDHA and MCT-4 could be applied to other proteins. For example, CD147 is the co-chaperone protein required for translocation and maintenance of MCTs to the plasma membrane. CD147 silencing could be a more attractive candidate for modulating the effects of MCTs as it could lead to the inhibition of all MCTs. This would be beneficial since it is likely that redundancy in lactic acid metabolism would mean that loss of activity due to knockdown of just one MCT, such as MCT-1, will be compensated for by the other MCTs such as MCT-4. Incidences like this have been reported by AstraZeneca in their studies of small molecule inhibitors (Ippolito et al. 2018). Moreover recent findings by Cheng *et al* (Cheng et al. 2019) showed that overexpression of Aurora A kinase in tumour cells promotes tumour growth. This kinase phosphorylates LDHB at serine 162, resulting in the relief of substrate inhibition by pyruvate and modulation of glycolysis to allow LDHB to reduce pyruvate to lactate, rather than its usual route of oxidising lactate back to pyruvate. This represents another mechanism by which tumour cells could avoid potential targeting of the Warburg effect. Oncolytic adenoviruses are an effective platform for shRNA expression and delivery, allowing them to selectively target many pathways that are currently inaccessible due to adverse off-target effects experienced by patients when given systemic treatment (C. B. Moore et al. 2010).

To the best of our knowledge, the approach used in this chapter of encoding shRNAs against LDHA and MCT-4 in OVs has not been reported before. EnAd does not depend on glycolysis, and is only mildly affected by the acidic conditions expected in the TME of some tumour types. It is an ideal candidate for expression of modulators of pH of the TME, but further investigation is required to determine the optimal mode of modulation. If successful, a more alkaline extracellular TME will not only serve to improve T cell-based immunotherapies through reversal of immune suppression, but may also help reverse tolerance in other pro-tumour immune cells, such as DCs and TAMs and tumour-promoting mechanisms, such as the lactate-shuttle hypothesis and the roles in pro-angiogenic and pro-metastatic signalling.

6 Final conclusions and discussion

6.1 Overview of the thesis

The metabolic landscape of tumours exerts a profound influence over the activities of both malignant and non-malignant cells within the TME. In particular, nutrient depletion and lactic acid accumulation contribute towards the establishment of an immune-suppressive environment, in which immune cells are tolerogenic and the positive signals required for innate and adaptive immune activation are dampened. Up-regulated markers of these metabolic features such as IDO, MCT-4 and LDHA are indicators of poor prognosis in patients (summarised in (Nakajima and Houten 2013; Munn and Mellor 2016; J. Y. Lee et al. 2016)).

Cancer immunotherapies have enjoyed remarkable success in recent years, and are becoming another pillar of treatment alongside traditional methods, however, they have still not exhausted their potential. This is partly because of the important influence of the TME, hence the proper understanding of how altered metabolism in the TME can hamper immunotherapeutics is

essential for furthering their progress as therapies (Cascone et al. 2018; Ganapathy-Kanniappan 2017). In this study, we have endeavored to identify whether certain metabolic components of the TME may limit the efficacy of an early-phase OV, namely EnAd, or BiTEs, T cell-activating therapies (H. Li, Er Saw, and Song 2020; M. Zheng et al. 2019). While EnAd has two modes of action; direct cancer cell lysis after viral replication and indirect immune stimulation with DAMPs and PAMPs after ischemic cell death (Dyer et al. 2017), BiTEs rely on T cell functionality alone to induce target cell killing.

As described in Chapter 3, EnAd infection/replication was inhibited when cells were cultured in nutrient-depleted media or malignant ascites, relative to nutrient-rich media. However, we did report that, after prolonged culture in one fluid, a colorectal cancer cell line became more susceptible to EnAd infection. This was evidenced by higher levels of viral replication, cell lysis and viral progeny release (Figures 3.18 and 3.19). By contrast, BiTE functionality in conditions of nutrient depletion, both in amino acid-depleted medium and ascites models, remained stable (Chapter 3). This work suggests that OVs may be more susceptible to nutrient deprivation than T cell engager-based therapies, and underlines the importance of using models that accurately represent the predicted conditions of the TME when developing cancer therapeutics.

The ability of the EpCAM BiTE to trigger T cell activation despite nutrient deprivation suggested that this therapeutic approach may also be resistant to other metabolic stressors such as lactic acid. However, we found this not to be the case (Chapter 4). We established that the EpCAM BiTE lost its functional capacity in conditions of lactic acid, and so too did multiple other BiTE constructs. To the best of our knowledge, these results represent a novel finding and one that is of significant importance to other research teams advancing BiTE therapies. In addition, we observed that T cells activated with anti-CD3/CD28 beads and an antigen-specific T cell clone both lost their cytolytic capabilities in conditions of acidosis. This demonstrated

that it was the T cells themselves that were unable to activate under high lactic acid stress, regardless of the activator. It therefore stands to reason that any therapy requiring T cells to respond in the acidic milieu of a tumour will fall short when met with this hurdle (Chapter 4). The final chapter of this thesis therefore was committed to exploring a solution to this problem, which perhaps represents an extensive barrier to immunotherapies.

Targeting metabolism in the TME as a potential therapeutic approach faces several challenges. Most notably, lactic acid-producing (*i.e.* glycolytic) tumour cells use the same major metabolic pathway for their bioenergetic profile as do most if not all stimulated immune cells (Buck et al. 2017). Glycolysis is favoured by anti-tumour macrophages, neutrophils, DCs, NK cells, and in effector T cells, $CD4^+$ helper T cells and $CD8^+$ cytotoxic T cells (Renner et al. 2017). Targeting any component of this pathway, including those that result in the efflux of lactic acid such as LDHA and MCTs, may have unintended consequences for the immune response. OVs offer an advantageous strategy to overcome this hurdle as they can be engineered to express anti-cancer agents selectively within the tumour and also facilitate delivery and dosage (Seymour and Fisher 2016). In Chapter 5, we investigated whether EnAd could provide a suitable platform for targeting lactic acidosis. EnAd itself is unperturbed by lactic acid accumulation and, although minor decreases of viral parameters including cytolysis were observed following infection of glycolytic tumour cells in acid, they were still able to infect these cells more efficiently than cells with a less permissive oxidative phenotype. EnAd was engineered to express shRNAs targeting LDHA and MCT-4, which both mediate efflux of lactic acid. Importantly, silencing of the intended target genes had no negative ramifications for EnAd replication. The oncolytic activity of one virus engineered with a shRNA targeting LDHA retained its oncolytic and replicative properties and was able to successfully knockdown its target gene. Further work is required to assess whether this action will be sufficient to modulate

the pH effectively, or whether additional targets that contribute to acidification in the TME should be tested.

Although encoding shRNAs in OVs is becoming ever more popular, with successes in targeting the cell cycle, p53 and survival genes in tumour cells with OV-encoded shRNAs (Brachtlova and van Beusechem 2018; Setten, Rossi, and Han 2019), the approach of targeting the lactic acid pathway with OV encoded shRNAs is novel. There are still unanswered questions concerning the efficacy of this approach, but nevertheless this work serves to highlight the potential of using OVs to target metabolic pathways and reinvigorate hampered TILs in an acidic TME, whilst also delivering immune cell activating therapies such as BiTEs.

6.2 Final discussion

The ability to arm OVs represents a powerful strategy to combine distinct therapies each with their own anti-tumour mechanism. In this way, a single agent can exert multiple modes of action, offering the possibility to target multiple hallmarks of cancer. As stated by Hanahan and Weinberg, such an approach may be key to improving the efficacies of therapies and achieving durable results (Hanahan and Weinberg 2011). Targeting the acidity of a tumour, alongside the expression of T-cell activating therapies using an OV represents such a multi-modal approach. In a phase I clinical trial (NCT02053220), systemic delivery of EnAd was observed to increase the number of T cells infiltrating a tumour following administration (Garcia-Carbonero et al. 2017). An increase in T cell influx may improve the efficacy of T-cell activating therapies, such as BiTEs. Importantly, BiTEs would not only redirect T cells that are tumour-specific but also those that are anti-viral, possibly improving the longevity and spread of the OV (Scott et al. 2017). Furthermore, reducing the acidity by targeting lactic acid would reverse immune suppression in the TME, influencing not only T cells but also NK cells and pro-tumoural

immune cells like M2 macrophages. Additionally, limiting the release of lactate, a key signalling molecule itself, has the potential to interfere with several hallmarks of cancer. Those known to be influenced by either acidification or lactate are angiogenesis, invasion and metastasis, deregulating cellular energetics as well as resisting cell death (de la Cruz-López et al. 2019).

As discussed in Chapter 3, the TME and the metabolites associated with it represent a considerable challenge for EnAd replication. Yet surprisingly we did find that one malignant ascites fluid from a patient (Asc2) was able to potentiate viral activity. The levels of glutamine in this ascites fluid was found to be 0.44 mM, the fluid was used at 50% concentration resulting in 0.22 mM on cells. Previous work from our laboratory indicates that this concentration is low enough to inhibit virus activity (Dyer et al. 2019). The finding that cells cultured in Asc2 increased in susceptibility or adapted to potentiate EnAd activity was therefore surprising. A limitation in our study is that we could only measure amino acids; other metabolites in the fluids may be modulating this effect and would need to be elucidated using a combination of mass spectrometry and HPLC. Alternatively, measuring properties of the tumour cell following culture in these ascites fluids may expose the vulnerability that improves virus replication, for instance a change in expression of receptors for viral entry, CD46 or DSG-2 (Sirena et al. 2004; H. Wang et al. 2011). Furthermore, the determination of changes to receptor expression i.e. CD46, during periods of nutrient deprivation and low pH would be important to include in our studies into how these factors can affect adenovirus infection.

Interestingly, directed evolution (Kuhn et al. 2008), as used in the original development of EnAd, may be of use here. If it is known, for example, that EnAd suffers from amino acid depletion in the TME, it may be feasible to direct the evolution of an OV that is less susceptible to this effect. An alternative might be mTOR. It is a known regulator of metabolism, and its activation is known to be mimicked by adenoviral E4-ORF1 and E4-ORF4 proteins (O'Shea et

al. 2005; Kleinberger 2020), EnAd however has lost its E4-ORF4 gene through a deletion and therefore it may be possible to genetically engineer a virus to upregulate mTOR activity which is often downregulated in conditions of nutrient depletion. This may help to overcome the decrease in viral replication observed in these media. Using realistic models such as ascites fluids can help to identify the weaknesses in OVs; however even ascites fluids do not exactly replicate the acidic conditions in the TME, despite their ability to recapitulate LDH levels (Paul Chubb and Williams 2018).

The influence of lactic acid on EnAd was much less extreme than that of nutrient depletion. However, 15 mM lactic acid (pH ~6.6) slowed the cytolytic ability of EnAd considerably, most likely due to an extracellular build up of lactate interfering with the 'Warburg' phenotype that makes cells more permissive to EnAd infection (Dyer et al. 2019). EnAd was shown to rely more heavily on glutamine than glucose (Dyer et al. 2019), and the same effect has also been reported for other OVs; NDV (Deng et al. 2014), reovirus (Kennedy et al. 2019), and VACV (Fontaine, Camarda, and Lagunoff 2014). To strategically target acidosis in the TME, another OV may be preferable. NDV has been shown to synergise with multiple agents targeting glycolysis, as well as to dysregulate glycolysis itself by inhibition of pyruvate dehydrogenase kinase (PDK). This has the effect of reducing acidification by lowering lactic acid production. These studies include a report that 2-DG and NDV synergise to kill breast cancer cells through inhibition of GAPDH and PDK, respectively (Al-Shammari et al. 2019). DCA, another inhibitor of PDK improves NDV viro-immunotherapy of hepatocellular carcinoma in a mouse model. This study also showed improvement in anti-tumour immune responses by reducing; lactate, activated STAT3, IDO and MDSC infiltration (Meng et al. 2019). Finally, a report by Al Ziaydi *et al* (Al-Ziaydi et al. 2020) demonstrated that hexokinase inhibition with D-mannoheptulose enhanced oncolysis by NDV when targeting breast cancer cells, and increased the pH of cancer cell culture medium. No studies have yet involved encoding anti-glycolysis

agents into NDV, though NDV has been used to express ICIs, T cell agonists and immunostimulatory cytokines (Vijayakumar, McCroskery, and Palese 2019), and has an insertion capacity of 6 kb (Lundstrom 2018).

Other than LDHA and MCT-4, a number of other components play a role in controlling acidification in the TME, for instance those that act to regulate pH homeostasis in tumour cells to avoid intracellular acid-induced death (Huber et al. 2017). These pathways offer further opportunities for reducing tumour acidification. As discussed above in the case of NDV, targeting glycolysis itself may also provide a more effective method of neutralising the TME. A limitation of our study was that it lacked a comparison of different modes of acidity inhibition. For example we could compare small molecule inhibitors currently used to target MCTs or their chaperone CD147, with the siRNAs we used in our approach to target LDHA and MCT-4. It would also be of interest to confirm whether targeting the source of lactic acid, namely LDHA, would be more effective than targeting proton exporters. It may in fact be preferable to target multiple transporters at once; this could also avoid the acquisition of resistance by tumour cells to one therapeutic approach (Polanski et al. 2014). Other groups have addressed the issue of acidity by targeting proton pumps and CAs or by neutralising acidity with a buffer like sodium carbonate (reviewed in (Lacroix et al. 2018)). Specific examples include the use of bicarbonate therapy to improve α-PD-L1, α-CTLA-4 antibody therapy and ACT in mouse models (Pilon-Thomas et al. 2016), however these positive results have not yet been translated to clinical use mostly due to challenges with oral dosing of bicarbonate causing discomfort (NCT01350583, NCT01198821). Moreover PPIs, such as esomeprazole, have had some success in mouse models in combination with ACT (Calcinotto et al. 2012).

One potential advantage of allowing glycolysis to continue unperturbed but concentrating targeting efforts on those components further downstream, such as MCT-4 or other proton-exporters, is that this will result in the buildup of lactic acid inside the cell. This lactic acid

buildup will lead to the dysregulation of pH homeostasis and the correction of the reversed pH gradient that tumour cells use to their advantage (Persi et al. 2018). On the other hand, glycolysis inhibition may be the only way to modulate the pH sufficiently quickly, before those cells succumb to lysis by the OV. In fact, this is a key point to consider when using an OV to encode transgenes. Encoding an agent that is secreted as opposed to targeting the cell intracellularly may be preferred, as its effect can extend throughout the tumour. For example, Patgiri *et al* (Patgiri et al. 2020) used an engineered bacterial enzyme, lactate oxidase in combination with catalase to alleviate reductive stress. This technology could be secreted from OVs to convert extracellular lactate to water, though its effect on extracellular pH has not yet been tested.

A striking observation from our work was the differential susceptibility of BiTE-activated T cells to amino acid-depleted medium and acidic medium (Chapters 3 and 4). Due to the incomplete knowledge of signalling pathways upon BiTE activation it is hard to decipher why this might be. However, we know that the number of clustering events possible between an EpCAM BiTE and TCRs on a T cell surface implies the stimulus would be strong, inducing a rapid response (C. Y. Ma et al. 2020). It is possible that, while the strength of this stimulus can override potential amino acid sensing, it cannot overcome the consequences of acid on T cells. This is not unsurprising considering results from recent studies finding that lactic acid T cell suppression was a natural mechanism used in the lymph node to avoid premature T cell cytolytic activity that has been usurped by the TME (Wu et al. 2020). In this study cytokine production and cytolysis were overwhelmed by the acidity due to its influence on glycolysis, the metabolic pathway required for optimal effector T cell activation. Walton *et al* (Walton et al. 2018) found that acid in murine T cells inhibits mTORC1 by scattering lysosomes and therefore disrupting the association of Ras homology enriched in brain (RHEB) with mTOR at the lysosomal surface, a specific physical change that doesn't occur during conditions of

nutrient depletion. Instead, amino acids are sensed through the Ras-related (RAG) guanosine triphosphate (GTP)-binding protein pathway (Saxton and Sabatini 2017).

A limitation of this work is that BiTEs activate without the need for CD28 co-stimulation at extreme rates that may bypass those metabolic checkpoints required for fully functional and responsive T cell activity (Figure 3.6). This may leave T cells activated by BiTEs open to anergy and exhaustion once the BiTE has dissipated, while still left in metabolic stress conditions (Y. Zheng et al. 2009). Possibly one of the most important components of future work to understand the ability of BiTEs to induce sorely required long-term immune responses is to measure the ability of T cells to be restimulated following initial BiTE activation. Furthermore, an understanding of the metabolic state of T cells during this dormant period will allow researchers to decipher if any development of memory T cell populations or loss of function and viability occurred following original activation. We imagine that uncovering the intricacies behind BiTE signalling cascades and T cell phenotypes following activation may help to inform decisions on their future design and further measures needed to induce the desired response. For example, next generation bispecifics in the format of TriTEs with a third antigen specific for co-stimulation could enhance T cell function and overcome any issues with exhaustion if they are observed (Scott et al. 2019). Next-generation CAR-T cells with co-stimulatory activating domains, such as CD137/4-1BB (Long et al. 2015), could also be used. Likewise, Rivadeneira *et al* (Rivadeneira et al. 2019) have shown leptin expression from an oncolytic VACV can overcome metabolic insufficiencies of T cells in the TME, promoting a T cell memory response upon tumour rechallenge in mouse models.

6.3 Concluding remarks

This thesis identified major barriers in the TME resulting in inhibition of BiTE-mediated T cell cytotoxicity and OV-mediated target cell lysis, two therapies currently being trialled for the treatment of cancer both as monotherapies and combination therapies. We identified acidosis as a major barrier to BiTE functionality, completely diminishing its cytolytic activities whilst only partially inhibiting the cytolytic ability of EnAd. These data prompted us to engineer an EnAd variant encoding shRNAs targeting LDHA and MCT-4, proteins responsible for lactic acidosis in the TME. Although the potential of the modified viruses was not fully assessed, LDHA was knocked down with a modified EnAd virus that retained its oncolytic abilities. Furthermore, the ability to encode a wide range of transgenes using EnAd as a platform, as exemplified in this study and previous works by our research group, offers the opportunity to compare a range of anti-acidic approaches that could be tailored to specific cancer contexts.

With accumulating evidence that metabolism is at the heart of the longevity of immune responses, is a hallmark of cancer, and could be a dominant factor in OV tropism, we envisage that further understanding of these pathways will result in more effective design of engineered OVs. It is possible to imagine a successful strategy that targets many of these components using a highly specific, well-chosen OV to deliver carefully designed agents to overcome major metabolic barriers. By potentiating immune-stimulation, we can provide a dominant multi-modal treatment targeting complex solid tumours to generate long-term anti-tumour immunity in patients.

7 Appendices

Appendix I Materials

Table 7.1 Reagents used in tissue culture medium.

Reagent	Catalogue Number	Manufacturer
Glucose	G8270	Sigma Aldrich
Lactic acid	L6402	Sigma Aldrich
Sodium hydroxide	72068-100 mL	Sigma Aldrich
Sodium L-Lactate	L7022	Sigma Aldrich
Sodium chloride	S9625	Honeywell
L-Arginine hydrochloride	A5131	Sigma Aldrich
L-Asparagine (anhydrous)	0210079425	MP Biomedicals UK
L-Aspartic acid	0210236925	MP Biomedicals UK
L-Cysteine.2HCl	0219464625	MP Biomedicals UK
L-Glutamic acid	0219467780	MP Biomedicals UK
L-Glutamine	25030081	Gibco
Glycine	G8898	Sigma Aldrich
L-Histidine hydrochloride	H8125	Sigma Aldrich
Hydroxy-L-Proline	H5534	Sigma Aldrich
L-Isoleucine	I2752	Sigma Aldrich
L-Leucine	L8000	Sigma Aldrich
L-Lysine hydrochloride	L5626	Sigma Aldrich
L-Methionine	M9625	Sigma Aldrich
L-Phenylalanine	P2126	Sigma Aldrich
L-Proline	0210273025	MP Biomedicals UK
L-Serine	0210287305	MP Biomedicals UK
L-Threonine	T8625	Sigma Aldrich
L-Tryptophan	T0254-1G	Sigma Aldrich
L-Tyrosine.2Na.2H_2O	0210318350	MP Biomedicals UK
L-Valine	V0500	Sigma Aldrich
Amino acid standard solution	AAS18	Sigma Aldrich
L-Kynurenine	K8625-25MG	Sigma Aldrich
MEM Non-essential amino acids solution (100x)	11140035	Life Technologies

Table 7.2 Recipes for buffers used for multiple applications. SDS, Sodium dodecyl sulphate; BSA, bovine serum albumin; Na_2HPO_4, sodium phosphate dibasic; $Na_2B_4O_7$, sodium tetraborate; H_3PO_4, phosphoric acid; CsCl, caesium chloride.

Buffer	Application	Recipe
0.5 M EDTA	Agarose gel electrophoresis	186 g EDTA (#E5134, Sigma Aldrich) in 1 L dH_2O, adjust to pH 8.0
TAE buffer (50x)	Agarose gel electrophoresis	242 g Tris (#10708976001, Roche), 100 mL 0.5 M EDTA, 57.1 mL acetic acid (#A6283, Sigma Aldrich) in 1 L H_2O
SDS running buffer (10x)	SDS Page gel electrophoresis	19.8 g Tris, 86.4 g glycine, 6 g SDS (#L3771, Sigma Aldrich), dH_2O up to 1 L
Transfer buffer (10x)	Western blotting	30.29 g Tris, 144 g glycine, dH_2O up to 1 L
Transfer buffer (1x)	Western blotting	100 mL Transfer buffer (10x), 200 mL methanol (#34860, Sigma Aldrich) and 700 mL dH_2O
PBST buffer	Western blotting	1 mL Tween® 20 (#P1379, Sigma Aldrich) in 1 L 1x PBS
0.2 M EDTA	Virus banding and flow cytometry	7.44 g EDTA in 100 mL dH_2O adjust to pH 8.0
MACs buffer	Flow cytometry	2.5 g BSA (#A3059, Sigma Aldrich), 5 mL 0.2 M EDTA in 500 mL 1x DPBS
1 M HEPES	Culture medium	119.1 g HEPES (#H3375, Sigma Aldrich) in 500 mL dH_2O
T cell medium	T cell clone maintenance	50 mL FBS, 5 mL P/S (#15140122, Gibco™), 5 mL L-glutamine, 5 mL 1x MEM non-essential amino acids, 5 mL sodium pyruvate (#11360070, Gibco™), 5 mL 1 M HEPES in 500 mL RPMI 1640 (#R8758)
Mobile Phase A	HPLC (Amino acid analysis)	1.4 g Na_2HPO_4 (#255793, Sigma Aldrich), 3.8 g $Na_2B_4O_7 \cdot 10H_2O$ (#S9640, Sigma Aldrich) and dH_2O up to 1 L, adjust to pH 8.2
Mobile Phase B	HPLC (Amino acid analysis)	450 mL acetonitrile (#271004, Sigma Aldrich), 450 mL methanol, 100 mL dH_2O (45:45:10, v/v/v)
Injection diluent	HPLC (Amino acid analysis)	100 mL Mobile Phase A, 0.4 mL H_3PO_4 (#P5811, Sigma Aldrich)
2x DMEM	Plaque assay	2x DMEM powder in 500 mL dH_2O supplemented with 12.5 mL 1 M HEPES, 5 mL P/S and 20 mL FBS
1.4% low melting point agarose	Plaque assay	1.4 g low melting point agarose (#16520050, Invitrogen™) in 100 mL dH_2O
Agarose-DMEM	Plaque assay	1:1 mixture of 2x DMEM and 1.4% low melting point agarose
n-Butanol	Virus banding	20 mL n-Butanol (#B7906, Sigma Aldrich) is added to 20 mL dH_2O (the top layer is water-saturated n-Butanol)
0.5 M Tris-HCl	Virus banding	7.88 g Trizma® hydrochloride (#T5941, Sigma Aldrich) in 100 mL dH_2O, adjust to pH 7.9
1:32 ρ CsCl	Virus banding	192 g CsCl (#C4036, Sigma Aldrich), 367.2 mL of dH_2O, 40.8 mL of 0.5 M Tris-HCl (pH 7.9)
1:45 ρ CsCl	Virus banding	307.5 g CsCl, 387 mL of dH_2O, 43.5 mL of 0.5 M Tris-HCl (pH 7.9)
40% glycerol	Virus banding	165 mL glycerol (#G6279, Sigma Aldrich), 10 mL of 0.5 M Tris-HCl (pH 7.9), 2.5 mL 0.2 M EDTA (pH 8.0), dH_2O up to 500 mL
TE buffer	Picogreen assay	5 mL 1 M Tris-HCl (pH 8), 1 mL 0.5 M EDTA (pH 8.0), dH_2O up to 500 mL

Appendix II DNA and amino acid sequences

Table 7.3 Oligonucleotides used for genetic engineering and Sanger sequencing.

Primer ID	Target	Primer	Tm (°C)
1-Sigpep CD3 Nano F	N term - CD3 domain	AATTCAAAGGAGGTACCCACCATGGGCTGGTCTTGTATTATCCTTTTCCTGGTGGCA ACCGCGACCGGGGTCCACTCCGAAGTGCAGCTGGTGGAAAG	88
12-Sigpep CD3 Nano R	N term - CD3 domain	GTTGGACTTGGCTTCCACCACCTCCTGAAGAAACTGTGACGAG	79
13-PDL1 Nano His F	C term - PD-L1 domain	AGTTTCTTCAGGAGGTGGTGGAAGCCAAGTCCAACTCCAAGAGAG	79
4-PDL1 Nano His R	C term -PD-L1 domain	GGAGACAACTTCTAGAAACCCTAATGGTGATGGTGGTGATGGTGATGGTGATGTG AGACAGTGACCTGCGTC	83
5-Sigpep PDL1 Nano F	N term - PD-L1 domain	AATTCAAAGGAGGTACCCACCATGGGCTGGTCTTGTATTATCC	77
6-Sigpep PDL1 Nano R	N term - PD-L1 domain	GCTGCACTTCGCTTCCACCACCTCCTGAGACAGTGACCTGCGTC	83
9-CD3 Nano His F	C term - CD3 domain	CACTGTCTCAGGAGGTGGTGGAAGCGAAGTGCAACTCGTGGAAAG	80
10-CD3 Nano His R	C term - CD3 domain	GGAGACAACTTCTAGAAACCCTAATGGTGATGGTGGTGATGGTGATGGTGATGTG AAGAAACTGTGACGAG	81
14-U6-shRNA F	U6-shRNA cassette	TAGTCGTCAGCTATCCTGCATGCAGGTGCCAGAACATTTC	77
15-U6-shRNA R	U6-shRNA cassette	AAATCGAGAGATCGCCTGCACTGCCTTGGGAAAAGCGC	80
16-U6-shRNA R	U6-shRNA cassette	AAATCGAGAGATCGCCTGCACGCATGCTCCAGACTGCC	80
Lenti Seq. 1	Sanger seq.	GACTATCATATGCTTACCGT	53
F2-CMVAMP BITE	Sanger seq.	TGTCGATCCTACCATCCA	53
22-F1	Sanger seq.	TGCAGGCGATCTCTCGATTTC	53
23-F2	Sanger seq.	AGTAAACTTGGTCTGACAGTTACC	59
24-F3	Sanger seq.	AAAGCATCTTACGGATGGCATGAC	61
27-R1	Sanger seq.	TTTCGTTCCACTGAGCGTCAGAC	61
28-R2	Sanger seq.	TCTGAGAATAGTGTATGCGGCG	61
29-R3	Sanger seq.	AAAGGTAAGCTGACGATAGCTGAC	61
25-F4b	Sanger seq.	CGTATGTTCCCATAGTAACGCC	60
26-F5b	Sanger seq.	GCCCTCGATTCTGTATATTCTCC	60
30-R4b	Sanger seq.	TTTCCGCAAGATATGCCCGTC	60
31-R5b	Sanger seq.	CTACCCGGTAGTATCGATTGTAAG	60
32-Fibre Site F	Sanger seq.	CGTATAACTTGGTCCTGGA	59
33-Fibre Site R	Sanger seq.	GCTGTGCGTGGGGAGAGA	67
34-SbfI F	CMV-GFP_U6-shRNA cassette	TTTGCGATCGCTACCCTGCAGGTCATTAGTTCATAGCCC	77
35-SbfI R	CMV-GFP_U6-shRNA cassette	CAAATAAACAAGTTCCTGCACTACCCGGTAGTATCGATTG	73

Signal peptide (DNA sequence)

ATGGGCTGGTCTTGTATTATCCTTTTCCTGGTGGCAACCGCGACCGGGGTCCACTC
C

Signal peptide (Amino acid sequence)

MGWSCIILFLVATATGVHS

HisTag (DNA sequence)

CACCACCATCACCACCACCATCACCATCAT

HisTag (Amino acid sequence)

HHHHHHHHHH

PD-L1_CD3 NanoBiTE (DNA sequence)

CAAGTCCAACTCCAAGAGAGCGGGGGCGGATTGGTGCAACCAGGGGGAAGTTTG
CGCCTCTCTTGTGCAGCCTCCGGGAAGATGAGTAGTCGCAGGTGCATGGCCTGGT
TCCGCCAAGCGCCTGGTAAAGAACGGGAGCGGGTGGCTAAACTGCTTACAACGT
CAGGTTCAACTTACCTTGCCGACTCTGTCAAAGGACGATTCACTATAAGTCAGAA
TAATGCGAAAAGTACCGTTTACCTGCAGATGAACTCATTGAAACCCGAAGACACC
GCAATGTATTATTGCGCTGCAGATAGCTTCGAGGACCCGACTTGTACGTTGGTAA
CCAGTTCAGGCGCGTTTCAATATTGGGGGCAGGGGACGCAGGTCACTGTCTCAGG
AGGTGGTGGAAGCGAAGTGCAACTCGTGGAAAGTGGTGGAGGATTGGTACAACC
GGGTGGAAGTTTGAGGCTGTCATGTGCGGCTTCCGGCGATATCTACAAATCCTTC
GATATGGGTTGGTACCGACAGGCACCGGGAAAGCAGAGAGATTTGGTTGCTGTA
ATTGGGTCAAGGGGTAACAACAGGGGCCGAACTAATTATGCGGACTCCGTGAAA
GGTCGCTTCACCATTTCAAGGGACGGAACTGGCAATACAGTGTATCTCCTGATGA
ATAAACTGCGCCCGGAAGATACAGCCATATATTATTGTAATACTGCCCCGTTGGT
TGCTGGAAGACCGTGGGGTCGGGGCACTCTCGTCACAGTTTCTTCA

PD-L1_CD3 NanoBiTE (Amino acid sequence)

QVQLQESGGGLVQPGGSLRLSCAASGKMSSRRCMAWFRQAPGKERERVAKLLTTSG
STYLADSVKGRFTISQNNAKSTVYLQMNSLKPEDTAMYYCAADSFEDPTCTLVTSSG
AFQYWGQGTQVTVSGGGGSEVQLVESGGGLVQPGGSLRLSCAASGDIYKSFDMGW
YRQAPGKQRDLVAVIGSRGNNRGRTNYADSVKGRFTISRDGTGNTVYLLMNKLRPE
DTAIYYCNTAPLVAGRPWGRGTLVTVSS

CD3_PD-L1 NanoBiTE (DNA sequence)

GAAGTGCAACTCGTGGAAAGTGGTGGAGGATTGGTACAACCGGGTGGAAGTTTG
AGGCTGTCATGTGCGGCTTCCGGCGATATCTACAAATCCTTCGATATGGGTTGGT
ACCGACAGGCACCGGGAAAGCAGAGAGATTTGGTTGCTGTAATTGGGTCAAGGG
GTAACAACAGGGGCCGAACTAATTATGCGGACTCCGTGAAAGGTCGCTTCACCAT
TTCAAGGGACGGAACTGGCAATACAGTGTATCTCCTGATGAATAAACTGCGCCCG
GAAGATACAGCCATATATTATTGTAATACTGCCCCGTTGGTTGCTGGAAGACCGT
GGGGTCGGGGCACTCTCGTCACAGTTTCTTCAGGAGGTGGTGGAAGCCAAGTCCA
ACTCCAAGAGAGCGGGGGCGGATTGGTGCAACCAGGGGGAAGTTTGCGCCTCTC
TTGTGCAGCCTCCGGGAAGATGAGTAGTCGCAGGTGCATGGCCTGGTTCCGCCAA
GCGCCTGGTAAAGAACGGGAGCGGGTGGCTAAACTGCTTACAACGTCAGGTTCA
ACTTACCTTGCCGACTCTGTCAAAGGACGATTCACTATAAGTCAGAATAATGCGA
AAAGTACCGTTTACCTGCAGATGAACTCATTGAAACCCGAAGACACCGCAATGTA

TTATTGCGCTGCAGATAGCTTCGAGGACCCGACTTGTACGTTGGTAACCAGTTCA
GGCGCGTTTCAATATTGGGGGCAGGGGACGCAGGTCACTGTCTCA

CD3_PD-L1 NanoBiTE (Amino acid sequence)

EVQLVESGGGLVQPGGSLRLSCAASGDIYKSFDMGWYRQAPGKQRDLVAVIGSRGN
NRGRTNYADSVKGRFTISRDGTGNTVYLLMNKLRPEDTAIYYCNTAPLVAGRPWGR
GTLVTVSSGGGGSQVQLQESGGGLVQPGGSLRLSCAASGKMSSRRCMAWFRQAPGK
ERERVAKLLTTSGSTYLADSVKGRFTISQNNAKSTVYLQMNSLKPEDTAMYYCAAD
SFEDPTCTLVTSSGAFQYWGQGTQVTVS

Appendix III HPLC amino acid standard curves

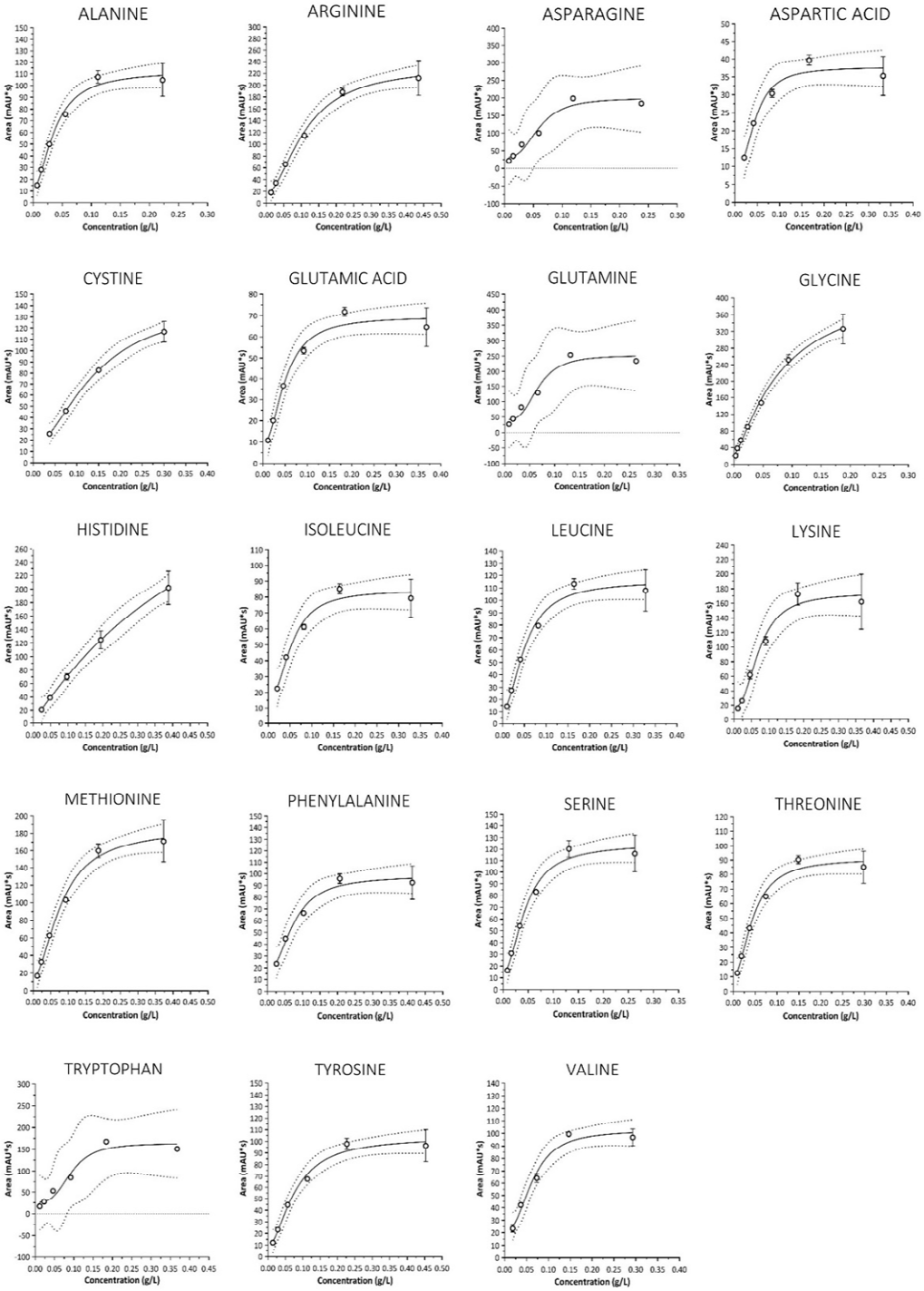


Figure 7.1 Standard curves formed from two-fold serial dilutions of known concentrations of amino acids following HPLC analysis.

8 References

Aalipour, Amin, Fabrice Le Boeuf, Matthew Tang, Surya Murty, Federico Simonetta, Alexander X Lozano, Travis M Shaffer, John C Bell, and Sanjiv S Gambhir. 2020. “Viral Delivery of CAR Targets to Solid Tumors Enables Effective Cell Therapy.” *Molecular Therapy: Oncolytics* 17 (June): 232–40. https://doi.org/10.1016/j.omto.2020.03.018.

Achard, Carole, Abera Surendran, Marie-eve Wedge, Guy Ungerechts, John Bell, and Carolina S Ilkow. 2018. “Lighting a Fire in the Tumor Microenvironment Using Oncolytic Immunotherapy.” *EBioMedicine* 31: 17–24. https://doi.org/10.1016/j.ebiom.2018.04.020.

Aduen, Javier, Wendy K. Bernstein, Terrance Khastgir, Joann Miller, Roger Kerzner, Asha Bhatiani, Lindsay Davison, Jack Lustgarten, Avtar S. Bassin, and Bart Chernow. 1994. “The Use and Clinical Importance of a Substrate-Specific Electrode for Rapid Determination of Blood Lactate Concentrations.” *JAMA: The Journal of the American Medical Association* 272 (21): 1678–85. https://doi.org/10.1001/jama.1994.03520210062033.

Al-Shammari, Ahmed Majeed, Amer Hasan Abdullah, Zainab Majid Allami, and Nahi Y. Yaseen. 2019. “2-Deoxyglucose and Newcastle Disease Virus Synergize to Kill Breast Cancer Cells by Inhibition of Glycolysis Pathway Through Glyceraldehyde3-Phosphate Downregulation.” *Frontiers in Molecular Biosciences* 6 (90): 1–13. https://doi.org/10.3389/fmolb.2019.00090.

Al-Ziaydi, Ahmed Ghdhban, Ahmed Majeed Al-Shammari, Mohammed I Hamzah, Haider Sabah kadhim, and Majid Sakhi Jabir. 2020. “Hexokinase Inhibition Using D-Mannoheptulose Enhances Oncolytic Newcastle Disease Virus-mediated Killing of Breast Cancer Cells.” *Cancer Cell International* 20 (420): 1–10. https://doi.org/10.1186/s12935-020-01514-2.

Alberts, P, Andra Tilgase, Agnija Rasa, Katrina Bandere, and Dite Venskus. 2018. “The Advent of Oncolytic Virotherapy in Oncology: The Rigvir Story.” *European Journal of Pharmacology* 837: 117–26. https://doi.org/10.1016/j.ejphar.2018.08.042.

Allison, Katrina E., Brenda L. Coomber, and Byram W. Bridle. 2017. “Metabolic Reprogramming in the Tumour Microenvironment: A Hallmark Shared by Cancer Cells and T Lymphocytes.” *Immunology* 152 (2): 175–84. https://doi.org/10.1111/imm.12777.

Altomonte, Jennifer, Sabrina Marozin, Enrico N De Toni, Antonia Rizzani, Irene Esposito, Katja Steiger, Annette Feuchtinger, Claus Hellerbrand, Roland M Schmid, and Oliver Ebert. 2013. “Antifibrotic Properties of Transarterial Oncolytic VSV Therapy for Hepatocellular Carcinoma in Rats With Thioacetamide-Induced Liver Fibrosis.” *YMTHE* 21 (11): 2032–42. https://doi.org/10.1038/mt.2013.181.

Amend, Sarah R., and Kenneth J. Pienta. 2015. “Ecology Meets Cancer Biology: The Cancer Swamp Promotes the Lethal Cancer Phenotype.” *Oncotarget* 6 (12): 9669–78. https://doi.org/10.18632/oncotarget.3430.

Ananieva, Elitsa A., and Adam C. Wilkinson. 2018. “Branched-Chain Amino Acid Metabolism in Cancer.” *Current Opinion in Clinical Nutrition and Metabolic Care* 21 (1): 64–70. https://doi.org/10.1097/MCO.0000000000000430.

Anderson, Michael, Anna Moshnikova, Donald M Engelman, Yana K Reshetnyak, and Oleg A Andreev. 2016. “Probe for the Measurement of Cell Surface PH in Vivo and Ex Vivo.” *PNAS* 113 (29): 8177–81. https://doi.org/10.1073/pnas.1608247113.

Angelin, Alessia, Gil-de-Gomez, Satinder Dahiya, Jing Jiao, Lili Guo, Matthew H Levine, Zhonglin Wang, et al. 2017. “Foxp3 Reprograms T Cell Metabolism to Function in Article Foxp3 Reprograms T Cell Metabolism to Function in Low-Glucose , High-Lactate Environments.” *Cell*

Metabolism 25: 1282–93. https://doi.org/10.1016/j.cmet.2016.12.018.

Appleman, Leonard J, and Vassiliki A Boussiotis. 2003. "T Cell Anergy and Costimulation." *Immunological Reviews* 192: 161–80.

Arruebo, Manuel, Nuria Vilaboa, Berta Sáez-gutierrez, and Julio Lambea. 2011. "Assessment of the Evolution of Cancer Treatment Therapies," 3279–3330. https://doi.org/10.3390/cancers3033279.

Baker, Alexander T, Carmen Aguirre-Hernandez, Gunnel Hallden, and Alan L Parker. 2018. "Designer Oncolytic Adenovirus: Coming of Age." *Cancers* 10 (201): 1–39. https://doi.org/10.3390/cancers10060201.

Baker, Lillian E. 1928. "The Chemical Nature of the Substances Required for Cell Multiplication." *Journal of Experimental Medicine*, 163–82.

Baker, Lillian E, and Alexis Carrel. 1926. "EFFECT OF THE AMINO ACIDS AND DIALYZABLE CONSTITUENTS OF EMBRYONIC TISSUE JUICE ON THE GROWTH OF FIBROBLASTS." *Journal of Experimental Medicine* xliii (591): 397–407.

Balkwill, Frances R, Melania Capasso, and Thorsten Hagemann. 2012. "The Tumor Microenvironment at a Glance." *Journal of Cell Science* 125: 5591–96. https://doi.org/10.1242/jcs.116392.

Bar-Peled, Liron, and David M. Sabatini. 2014. "Regulation of MTORC1 by Amino Acids." *Trends in Cell Biology* 24 (7): 400–406. https://doi.org/10.1016/j.tcb.2014.03.003.

Barøy, Tuva, Kirsten Sørensen, and Mona Mari. 2010. "ShRNA Expression Constructs Designed Directly from SiRNA Oligonucleotide Sequences," 116–20. https://doi.org/10.1007/s12033-010-9247-8.

Bartee, Mee Y, Katherine M Dunlap, and Eric Bartee. 2017. "Tumor-Localized Secretion of Soluble PD1 Enhances Oncolytic Virotherapy" 77 (11): 2952–64. https://doi.org/10.1158/0008-5472.CAN-16-1638.

Bauzon, Maxine, and Terry Hermiston. 2014. "Armed Therapeutic Viruses – a Disruptive Therapy on the Horizon of Cancer Immunotherapy." *Frontiers in Immunology* 5 (74): 1–10. https://doi.org/10.3389/fimmu.2014.00074.

Bergstrom, J, P Furst, L O Noree, and E Vinnars. 1974. "Intracellular Free Amino Acid Concentration in Human Muscle Tissue." *Journal of Applied Physiology* 36 (6).

Beusechem, Victor W Van, Petra B Van Den Doel, Jacques Grill, Herbert M Pinedo, and Winald R Gerritsen. 2002. "Conditionally Replicative Adenovirus Expressing P53 Exhibits Enhanced Oncolytic Potency 1," 6165–71.

Bhutia, Yangzom D., Ellappan Babu, Sabarish Ramachandran, and Vadivel Ganapathy. 2015. "Amino Acid Transporters in Cancer and Their Relevance to 'Glutamine Addiction': Novel Targets for the Design of a New Class of Anticancer Drugs." *Cancer Research* 75 (9): 1782–88. https://doi.org/10.1158/0008-5472.CAN-14-3745.

Bianchi, Valentina. 2016. "Molecular and Cellular Basis of T-Cell Responses to Melanoma Antigens." Cardiff University. http://orca.cf.ac.uk/92547/2/2016BianchiVPhD.pdf.

Bonuccelli, Gloria, Diana Whitaker-Menezes, Remedios Castello-Cros, Stephanos Pavlides, Richard G. Pestell, Alessandro Fatatis, Agnieszka K. Witkiewicz, et al. 2010. "The Reverse Warburg Effect: Glycolysis Inhibitors Prevent the Tumor Promoting Effects of Caveolin-1 Deficient Cancer Associated Fibroblasts." *Cell Cycle* 9 (10): 1960–71. https://doi.org/10.4161/cc.9.10.11601.

Brachtlova, Tereza, and Victor W van Beusechem. 2018. "Unleashing the Full Potential of Oncolytic Adenoviruses against Cancer by Applying RNA Interference: The Force Awakens." *Cells* 7 (228): 1–21. https://doi.org/10.3390/cells7120228.

Brand, Almut, Katrin Singer, Gudrun E. Koehl, Marlene Kolitzus, Gabriele Schoenhammer, Annette Thiel, Carina Matos, et al. 2016. "LDHA-Associated Lactic Acid Production Blunts Tumor Immunosurveillance by T and NK Cells." *Cell Metabolism* 24: 657–71. https://doi.org/10.1016/j.cmet.2016.08.011.

Bridle, Byram W, Kyle B Stephenson, Jeanette E Boudreau, Sandeep Koshy, Natasha Kazdhan, Eleanor Pullenayegum, Jérôme Brunellière, Jonathan L Bramson, Brian D Lichty, and Yonghong Wan. 2010. "Potentiating Cancer Immunotherapy Using an Oncolytic Virus." *Molecular Therapy* 18 (8): 1430–39. https://doi.org/10.1038/mt.2010.98.

Brinkmann, Ulrich, and Roland E Kontermann. 2017. "The Making of Bispecific Antibodies." *MABS* 9 (2): 182–212. https://doi.org/10.1080/19420862.2016.1268307.

Brischwein, Klaus, Larissa Parr, Stefan Pflanz, Jo Volkland, John Lumsden, Matthias Klinger, Mathias Locher, et al. 2007. "Strictly Target Cell-Dependent Activation of T Cells by Bispecific Single-Chain Antibody Constructs of the BiTE Class" 30 (8): 798–807.

Brischwein, Klaus, Bernd Schlereth, Benjamin Guller, Carola Steiger, Andreas Wolf, Ralf Lutterbuese, Sonja Offner, et al. 2006. "MT110 : A Novel Bispecific Single-Chain Antibody Construct with High Efficacy in Eradicating Established Tumors" 43: 1129–43. https://doi.org/10.1016/j.molimm.2005.07.034.

Brisson, Lucie, Piotr Bański, Martina Sboarina, Coralie Dethier, Pierre Danhier, Marie Joséphine Fontenille, Vincent F. Van Hée, et al. 2016. "Lactate Dehydrogenase B Controls Lysosome Activity and Autophagy in Cancer." *Cancer Cell* 30 (3): 418–31. https://doi.org/10.1016/j.ccell.2016.08.005.

Bröer, Stefan. 2018. "Amino Acid Transporters as Disease Modifiers and Drug Targets." *SLAS Discovery* 23 (4): 303–20. https://doi.org/10.1177/2472555218755629.

Bröer, Stefan, and Angelika Bröer. 2017. "Amino Acid Homeostasis and Signalling in Mammalian Cells and Organisms." *Biochemical Journal* 474 (12): 1935–63. https://doi.org/10.1042/BCJ20160822.

Brooks, George A., and L. Bruce Gladden. 2003. *The Metabolic Systems: Anaerobic Metabolism (Glycolytic and Phosphagen). Exercise Physiology: People and Ideas, Ed. Tipton CM, Chap. 8*. https://doi.org/10.1016/B978-019512527-6.50009-X.

Browne, Kylie A, Elizabeth Blink, Vivien R Sutton, Christopher J Froelich, David A Jans, and Joseph A Trapani. 1999. "Cytosolic Delivery of Granzyme B by Bacterial Toxins : Evidence That Endosomal Disruption , in Addition to Transmembrane Pore Formation , Is an Important Function of Perforin" 19 (12): 8604–15.

Bruggen, P van der, C Traversari, P Chomez, C Lurquin, E de Plaen, B van den Eynde, A Knuth, and T Boon. 1991. "A Gene Encoding an Antigen Recognized by Cytolytic T Lymphocytes on a Human Melanoma." *Science* 254 (December): 1643–47.

Buck, Michael D., Ryan T. Sowell, Susan M. Kaech, and Erika L. Pearce. 2017. "Metabolic Instruction of Immunity." *Cell* 169 (4): 570–86. https://doi.org/10.1016/j.cell.2017.04.004.

Burgos-Panadero, Rebeca, Federico Lucantoni, Esther Gamero-Sandemetrio, Luis de la Cruz-Merino, Tomás Álvaro, and Rosa Noguera. 2019. "The Tumour Microenvironment as an Integrated Framework to Understand Cancer Biology." *Cancer Letters* 461 (July): 112–22. https://doi.org/10.1016/j.canlet.2019.07.010.

Calcinotto, Arianna, Paola Filipazzi, Matteo Grioni, Manuela Iero, Angelo De Milito, Alessia Ricupito, Agata Cova, et al. 2012. "Modulation of Microenvironment Acidity Reverses Anergy in Human and Murine Tumor-Infiltrating T Lymphocytes." *Cancer Research* 72 (11): 2746–56. https://doi.org/10.1158/0008-5472.CAN-11-1272.

Caplen, Natasha J, Susan Parrish, Farhad Imani, Andrew Fire, and Richard A Morgan. 2001. "Specific

Inhibition of Gene Expression by Small Double-Stranded RNAs in Invertebrate and Vertebrate Systems." *PNAS* 98 (17): 9742–47.

Carelle, Nadege, Estelle Piotto, Agnes Bellanger, Jerome Germanaud, Alain Thuillier, and David Khayat. 2002. "Changing Patient Perceptions of the Side Effects Of." *Cancer* 95 (1): 155–63. https://doi.org/10.1002/cncr.10630.

Carette, Jan E., Harm C.A. Graat, Frederik H.E. Schagen, Mohamed A.I. Abou El Hassan, Winald R. Gerritsen, and Victor W. van Beusechem. 2005. "Replication-Dependent Transgene Expression from a Conditionally Replicating Adenovirus via Alternative Splicing to a Heterologous Splice-Acceptor Site." *The Journal of Gene Medicine* 7: 1053–62. https://doi.org/10.1002/jgm.754.

Carette, Jan E, M Overmeer, Frederik H E Schagen, Ramon Alemany, Oleg A Barski, Winald R Gerritsen, and Victor W Van Beusechem. 2004. "Conditionally Replicating Adenoviruses Expressing Short Hairpin RNAs Silence the Expression of a Target Gene in Cancer Cells." *Cancer Research* 64: 2663–67.

Cascone, Tina, Jodi A. McKenzie, Rina M. Mbofung, Simone Punt, Zhe Wang, Chunyu Xu, Leila J. Williams, et al. 2018. "Increased Tumor Glycolysis Characterizes Immune Resistance to Adoptive T Cell Therapy." *Cell Metabolism* 27 (5): 977-987.e4. https://doi.org/10.1016/j.cmet.2018.02.024.

Chanier, Timothée, and Patrick Chames. 2019. "Nanobody Engineering: Toward Next Generation Immunotherapies and Immunoimaging of Cancer." *Antibodies* 8 (1): 13. https://doi.org/10.3390/antib8010013.

Chaurasiya, Shyambabu, Yuman Fong, and Susanne G Warner. 2020. "Optimizing Oncolytic Viral Design to Enhance Antitumor Efficacy: Progress and Challenges." *Cancers* 12 (1699).

Chen, Lin, Dongfeng Chen, Mouchun Gong, Manli Na, Linfang Li, Hongping Wu, Lihua Jiang, Yanzhen Qian, Guoen Fang, and Xuchao Xue. 2009. "Concomitant Use of Ad5 / 35 Chimeric Oncolytic Adenovirus with TRAIL Gene and Taxol Produces Synergistic Cytotoxicity in Gastric Cancer Cells." *Cancer Letters* 284 (2): 141–48. https://doi.org/10.1016/j.canlet.2009.04.026.

Chen, Liu Qi, and Mark D Pagel. 2015. "Evaluating PH in the Extracellular Tumour Microenvironment Using CEST MRI and Other Imaging Methods." *Advanced Radiology*. https://doi.org/10.1016/j.physbeh.2017.03.040.

Chen, Qi, Yueqin Liu, Xiao Lan Zhu, Fan Feng, Hui Yang, and Wenlin Xu. 2019. "Increased NHE1 Expression Is Targeted by Specific Inhibitor Cariporide to Sensitize Resistant Breast Cancer Cells to Doxorubicin in Vitro and in Vivo." *BMC Cancer* 19 (1): 1–13. https://doi.org/10.1186/s12885-019-5397-7.

Cheng, Aoxing, Peng Zhang, Bo Wang, Dongdong Yang, Xiaotao Duan, Yongliang Jiang, Tian Xu, et al. 2019. "Aurora-A Mediated Phosphorylation of LDHB Promotes Glycolysis and Tumor Progression by Relieving the Substrate-Inhibition Effect." *Nature Communications*, 1–16. https://doi.org/10.1038/s41467-019-13485-8.

Chiavenna, S M, J P Jaworski, and A Vendrell. 2017. "State of the Art in Anti-Cancer MAbs." *Journal of Biomedical Science* 24 (15): 1–12. https://doi.org/10.1186/s12929-016-0311-y.

Chiche, Johanna, M Christiane Brahimi-horn, and Jacques Pouysségur. 2010. "Tumour Hypoxia Induces a Metabolic Shift Causing Acidosis : A Common Feature in Cancer." *Journal of Cellilar and Molecular Medicine* 14 (4): 771–94. https://doi.org/10.1111/j.1582-4934.2009.00994.x.

Chiche, Johanna, Jean-ehrland Ricci, and Jacques Pouysségur. 2013. "Tumor Hypoxia and Metabolism – Towards Novel Anticancer Approaches." *Annales d'Endocrinologie* 74 (2): 111–14. https://doi.org/10.1016/j.ando.2013.02.004.

Choi, Eun Kyung, Im-ryung Kim, Oliver Chang, Danbee Kang, Seok-jin Nam, Jeong Eon Lee, Se Kyung Lee, et al. 2014. "Impact of Chemotherapy-Induced Alopecia Distress on Body Image,

Psychosocial Well-Being, and Depression in Breast Cancer Patients." *Psycho-Oncology* 23: 1103–10.

Choi, Joung Woo, Soo Jung Jung, Dayananda Kasala, June Kyu Hwang, Jun Hu, You Han Bae, and Chae Ok Yun. 2015. "PH-Sensitive Oncolytic Adenovirus Hybrid Targeting Acidic Tumor Microenvironment and Angiogenesis." *Journal of Controlled Release* 205: 134–43. https://doi.org/10.1016/j.jconrel.2015.01.005.

Choi, SY, H Xue, R Wu, L Fazli, D Lin, CC Collins, ME Gleave, PW Gout, and Y Wang. 2016. "The MCT4 Gene : A Novel , Potential Target for Therapy of Advanced Prostate Cancer." *Clinical Cancer Research* 22 (11): 2721–33. https://doi.org/10.1158/1078-0432.CCR-15-1624.

Cibrián, Danay, and Francisco Sánchez-madrid. 2017. "CD69: From Activation Marker to Metabolic Gatekeeper." *European Journal of Immunology* 47 (6): 946–53. https://doi.org/10.1002/eji.201646837.CD69.

Clemente, C, M Mihm Jr, R Bufalino, S Zurrida, P Collini, and N Cascinelli. 1996. "Prognostic Value of Tumor Infiltrating Lymphocytes in the Vertical Growth Phase of Primary Cutaneous Melanoma." *Cancer* 77: 1303–10.

Cohen, Sivan, Keiko Danzaki, and Nancie J MacIver. 2017. "Nutritional Effects on T-Cell Immunometabolism." *European Journal of Immunology* 47 (2): 225–35. https://doi.org/10.1002/eji.201646423. Nutritional.

Coley, William B. 1909. "The Treatment of Inoperable Sarcoma by Bacterial Toxins (the Mixed Toxins of the Streptococcus Erysipelas and the Bacillus Prodigiosus)." *Surgical Section* July 13.

Comito, G, A Iscaro, A Bacci, A Morandi, L Ippolito, M Parri, I Montagnani, et al. 2019. "Lactate Modulates CD4+ T-Cell Polarization and Induces an Immunosuppressive Environment, Which Sustains Prostate Carcinoma Progression via TLR8 / MiR21 Axis." *Oncogene* 38: 3681–95. https://doi.org/10.1038/s41388-019-0688-7.

Conry, Robert M, Brian Westbrook, Svetlana Mckee, Timothy Graham, Robert M Conry, Brian Westbrook, Svetlana Mckee, et al. 2018. "Talimogene Laherparepvec : First in Class Oncolytic Virotherapy." *Human Vaccines & Immunotherapeutics* 14 (4): 839–46. https://doi.org/10.1080/21645515.2017.1412896.

Counillon, Laurent, Yann Bouret, Ibtissam Marchiq, and Jacques Pouysségur. 2016. "Na+/H+ Antiporter (NHE1) and Lactate/H+ Symporters (MCTs) in PH Homeostasis and Cancer Metabolism." *Biochimica et Biophysica Acta - Molecular Cell Research* 1863 (10): 2465–80. https://doi.org/10.1016/j.bbamcr.2016.02.018.

Critchlow, Susan E, Gareth Hughes, Anna Staniszewska, Matt King, Filippos Michopoulos, Lorna Hopcroft, Martin R Brown, et al. 2019. "Reversing Lactate-Driven Immunosuppression Using the Novel, Potent and Selective MCT4 Inhibitor AZD0095 [Abstract]." In *Proceedings of the American Association for Cancer Research Annual Meeting 2019; 2019 Mar 29-Apr 3; Atlanta, GA. Philadelphia (PA): AACR; Cancer Res*, 79 (13 Suppl).

Curiel, T, G Coukos, L Zou, X Alvarez, C Pui, P Mottram, M Evdemon-Hogan, et al. 2004. "Specific Recruitment of Regulatory T Cells in Ovarian Carcinoma Fosters Immune Privilege and Predicts Reduced Survival." *Nature Medicine* 10 (9): 942–49.

Dahlén, Eva, Niina Veitonmäki, and Per Norlén. 2018. "Bispecific Antibodies in Cancer Immunotherapy." *Therapeutic Advances in Vaccines and Immunotherapy* 6 (1): 3–17. https://doi.org/10.1177/2515135518763280.

Damuzzo, V, S Solito, L Pinton, E Carrozzo, S Valpione, J Pigozzo, R Arboretti Giancristofaro, V Chiarion-Sileni, and S Mandruzzato. 2016. "Clinical Implication of Tumor-Associated and Immunological Parameters in Melanoma Patients Treated with Ipilimumab." *Oncoimmunology* 5

(12).

Davola, Maria Eugenia, and Karen Louise Mossman. 2019. “Oncolytic Viruses: How ‘Lytic’ Must They Be for Therapeutic Efficacy?” *OncoImmunology* 8 (6): 1–7. https://doi.org/10.1080/2162402X.2019.1596006.

Decker, WK, RF da Silva, MH Sanabria, LS Angelo, F Guimaraes, BM Burt, F Kheradmand, and S Paust. 2017. “Cancer Immunotherapy : Historical Perspective of a Clinical Revolution and Emerging Preclinical Animal Models.” *Frontiers in Immunology* 8 (829). https://doi.org/10.3389/fimmu.2017.00829.

Dehne, Nathalie, Javier Mora, Dmitry Namgaladze, Andreas Weigert, and Bernhard Brüne. 2017. “Cancer Cell and Macrophage Cross-Talk in the Tumor Microenvironment.” *Current Opinion in Pharmacology* 35: 12–19. https://doi.org/10.1016/j.coph.2017.04.007.

Deng, Xiaoyu, Yanlong Cong, Renfu Yin, Guilian Yang, Chan Ding, Shengqing Yu, Xiufan Liu, Chunfeng Wang, and Zhuang Ding. 2014. “Proteomic Analysis of Chicken Peripheral Blood Mononuclear Cells after Infection by Newcastle Disease Virus.” *Journal of Veterinary Science* 15 (4): 511–17. https://doi.org/10.4142/jvs.2014.15.4.511.

Dereziński, Paweł, Agnieszka Klupczynska, Wojciech Sawicki, Jerzy A. Pałka, and Zenon J. Kokot. 2017. “Amino Acid Profiles of Serum and Urine in Search for Prostate Cancer Biomarkers: A Pilot Study.” *International Journal of Medical Sciences* 14 (1): 1–12. https://doi.org/10.7150/ijms.15783.

Di, Y, L Seymour, and K Fisher. 2014. “Activity of a Group B Oncolytic Adenovirus (ColoAd1) in Whole Human Blood.” *Gene Therapy* 21: 440–43. https://doi.org/10.1038/gt.2014.2.

Dock, George. 1904. “THE INFLUENCE OF COMPLICATING DISEASES UPON LEUKAEMIA.” *The American Journal of the Medical Sciences* 127 (4).

Doherty, Joanne R, and John L Cleveland. 2013. “Targeting Lactate Metabolism for Cancer Therapeutics.” *The Journal of Clinical Investigation* 123 (9): 3685–92. https://doi.org/10.1172/JCI69741.transcription.

Draoui, Nihed, and Olivier Feron. 2011. “Lactate Shuttles at a Glance: From Physiological Paradigms to Anti-Cancer Treatments.” *Disease Models & Mechanisms* 4: 727–32. https://doi.org/10.1242/dmm.007724.

Dreier, Torsten, Grit Lorenczewski, Christian Brandl, Patrick Hoffmann, Uwe Syring, Frank Hanakam, Peter Kufer, Gert Riethmuller, Ralf B Bargou, and Patrick A Baeuerle. 2002. “Extremely Potent, Rapid and Costimulation-Independent Cytotoxic T-Cell Response against Lymphoma Cells Catalysed by a Single-Chain Bispecific Antibody.” *International Journal of Cancer* 100: 690–97. https://doi.org/10.1002/ijc.10557.

Duan, Qianqian, Hualing Zhang, Junnian Zheng, and Lianjun Zhang. 2020. “Turning Cold into Hot: Firing up the Tumor Microenvironment.” *Trends in Cancer* 6 (7): 605–18. https://doi.org/10.1016/j.trecan.2020.02.022.

Duffy, Margaret R, Kerry D Fisher, and Len W Seymour. 2017. “Making Oncolytic Virotherapy a Clinical Reality: The European Contribution.” *Human Gene Therapy* 28 (11): 1033–46. https://doi.org/10.1089/hum.2017.112.

Dulbecco, R, and G Freeman. 1959. “A Plaque Assay for the Polyoma Virus.” *Virology* 8: 396–97.

Dunn, Gavin P, Allen T Bruce, Hiroaki Ikeda, Lloyd J Old, and Robert D Schreiber. 2002. “Cancer Immunoediting : From Immuno-Surveillance to Tumor Escape.” *Nature Immunology* 3 (11): 991–98.

Dyer, Arthur, Ying Di, Hugo Calderon, Sam Illingworth, Gray Kueberuwa, Alison Tedcastle, Phil

Jakeman, et al. 2017. “Oncolytic Group B Adenovirus Enadenotucirev Mediates Non-Apoptotic Cell Death with Membrane Disruption and Release of Inflammatory Mediators.” *Molecular Therapy: Oncolytics* 4: 18–30. https://doi.org/10.1016/j.omto.2016.11.003.

Dyer, Arthur, Sally Frost, Kerry D Fisher, and Len W Seymour. 2020. “The Role of Cancer Metabolism in Defining the Success of Oncolytic Viro- Immunotherapy.” *Cytokine and Growth Factor Reviews*. https://doi.org/10.1016/j.cytogfr.2020.07.006.

Dyer, Arthur, Benjamin Schoeps, Sally Frost, Philip Jakeman, Eleanor M. Scott, Joshua Freedman, Egon J. Jacobus, and Leonard W. Seymour. 2019. “Antagonism of Glycolysis and Reductive Carboxylation of Glutamine Potentiates Activity of Oncolytic Adenoviruses in Cancer Cells.” *Cancer Research* 79 (2): 331–45. https://doi.org/10.1158/0008-5472.CAN-18-1326.

Eagle, H. 1959. “Amino Acid Metabolism in Mammalian Cell Cultures.” *Science* 130 (3373): 432–37.

Eagle, Harry. 1955. “Nutrition Needs of Mammalian Cells in Tissue Culture.” *Science* 122 (3168): 501–4.

Edmondson, Rasheena, Jessica Jenkins Broglie, Audrey F. Adcock, and Liju Yang. 2014. “Three-Dimensional Cell Culture Systems and Their Applications in Drug Discovery and Cell-Based Biosensors.” *Assay and Drug Development Technologies* 12 (4): 207–18. https://doi.org/10.1089/adt.2014.573.

Elbashir, Sayda M, Jens Harborth, Winfried Lendeckel, Abdullah Yalcin, Klaus Weber, and Thomas Tuschl. 2001. “Duplexes of 21 ± Nucleotide RNAs Mediate RNA Interference in Cultured Mammalian Cells.” *Letters to Nature* 411: 1–5.

Ellerman, Diego. 2019. “Bispecific T-Cell Engagers: Towards Understanding Variables Influencing the in Vitro Potency and Tumor Selectivity and Their Modulation to Enhance Their Efficacy and Safety.” *Methods* 154 (September 2018): 102–17. https://doi.org/10.1016/j.ymeth.2018.10.026.

Engelman, Jeffrey A, and Jeffrey Settleman. 2008. “Acquired Resistance to Tyrosine Kinase Inhibitors during Cancer Therapy.” *Current Opinion in Genetics and Development* 18: 73–79. https://doi.org/10.1016/j.gde.2008.01.004.

Erra Díaz, Fernando, Ezequiel Dantas, and Jorge Geffner. 2018. “Unravelling the Interplay between Extracellular Acidosis and Immune Cells.” *Mediators of Inflammation* 2018. https://doi.org/10.1155/2018/1218297.

Esaki, Shinichi, Samuel D Rabkin, Robert L Martuza, and Hiroaki Wakimoto. 2016. “Transient Fasting Enhances Replication of Oncolytic Herpes Simplex Virus in Glioblastoma.” *American Journal of Cancer Research* 6 (2): 300–311.

Faget, Julien, Cathy Biota, Thomas Bachelot, Michael Gobert, Isabelle Treilleux, Nadeǵe Goutagny, Isabelle Durand, et al. 2011. “Early Detection of Tumor Cells by Innate Immune Cells Leads to T Reg Recruitment through CCL22 Production by Tumor Cells.” *Cancer Research* 71 (19): 6143–52. https://doi.org/10.1158/0008-5472.CAN-11-0573.

Fajardo, Carlos Alberto, Sonia Guedan, Luis Alfonso Rojas, Rafael Moreno, Marcel Arias-badia, Jana De Sostoa, Carl H June, and Ramon Alemany. 2017. “Oncolytic Adenoviral Delivery of an EGFR-Targeting T-Cell Engager Improves Antitumor Efficacy.” *Therapeutics, Targets, and Chemical Biology* 77 (8): 2052–64. https://doi.org/10.1158/0008-5472.CAN-16-1708.

Farkona, Sofia, Eleftherios P Diamandis, and Ivan M Blasutig. 2016. “Cancer Immunotherapy: The Beginning of the End of Cancer ?” *BMC Medicine* 14 (73): 1–18. https://doi.org/10.1186/s12916-016-0623-5.

Feig, Christine, James O. Jones, Matthew Kraman, Richard J.B. Wells, Andrew Deonarine, Derek S. Chan, Claire M. Connell, et al. 2013. “Targeting CXCL12 from FAP-Expressing Carcinoma-Associated Fibroblasts Synergizes with Anti-PD-L1 Immunotherapy in Pancreatic Cancer.” *PNAS*

110 (50): 20212–17. https://doi.org/10.1073/pnas.1320318110.

Feng, J., H. Yang, Y. Zhang, H. Wei, Z. Zhu, B. Zhu, M. Yang, W. Cao, L. Wang, and Z. Wu. 2017. "Tumor Cell-Derived Lactate Induces TAZ-Dependent Upregulation of PD-L1 through GPR81 in Human Lung Cancer Cells." *Oncogene* 36 (42): 5829–39. https://doi.org/10.1038/onc.2017.188.

Filley, Anna C, and Mahua Dey. 2017. "Immune System, Friend or Foe of Oncolytic Virotherapy?" *Frontiers in Oncology* 7 (106): 1–8. https://doi.org/10.3389/fonc.2017.00106.

Fischer, A. 1948. "Amino-Acid Metabolism of Tissue Cells in Vitro." *Biochemical Journal* 43: 491–97.

Fischer, Karin, Petra Hoffmann, Simon Voelkl, Norbert Meidenbauer, Julia Ammer, Matthias Edinger, Eva Gottfried, et al. 2007. "Inhibitory Effect of Tumor Cell-Derived Lactic Acid on Human T Cells." *Blood* 109 (9): 3812–19. https://doi.org/10.1182/blood-2006-07-035972.

Floch, Renaud Le, Johanna Chiche, Ibtissam Marchiq, Tanesha Naïken, Karine Ilc, Clare M Murray, Susan E Critchlow, Danièle Roux, Marie-Pierre Simon, and Jacques Pouyssegur. 2011. "CD147 Subunit of Lactate/H+ Symporters MCT1 and Hypoxia-Inducible MCT4 Is Critical for Energetics and Growth of Glycolytic Tumors." *PNAS* 109 (40): 16663–68. https://doi.org/10.1073/pnas.1219161109.

Fontaine, Krystal A, Roman Camarda, and Michael Lagunoff. 2014. "Vaccinia Virus Requires Glutamine but Not Glucose for Efficient Replication." *Journal of Virology* 88 (8): 4366–74. https://doi.org/10.1128/JVI.03134-13.

Franchina, Davide G., Feng He, and Dirk Brenner. 2018. "Survival of the Fittest: Cancer Challenges T Cell Metabolism." *Cancer Letters* 412: 216–23. https://doi.org/10.1016/j.canlet.2017.10.014.

Frankel, Stanley R, and Patrick A Baeuerle. 2013. "Targeting T Cells to Tumor Cells Using Bispecific Antibodies." *Current Opinion in Chemical Biology* 17 (3): 385–92. https://doi.org/10.1016/j.cbpa.2013.03.029.

Freedman, Joshua D, Margaret R Duffy, Janet Lei-rossmann, Alice Muntzer, Eleanor M Scott, Joachim Hagel, Leticia Campo, et al. 2018. "An Oncolytic Virus Expressing a T-Cell Engager Simultaneously Targets Cancer and Immunosuppressive Stromal Cells." *Cancer Research* 78 (24): 6852–66. https://doi.org/10.1158/0008-5472.CAN-18-1750.

Freedman, Joshua D, Joachim Hagel, Eleanor M Scott, Ioannis Psallidas, Avinash Gupta, Laura Spiers, Paul Miller, et al. 2017. "Oncolytic Adenovirus Expressing Bispecific Antibody Targets T-cell Cytotoxicity in Cancer Biopsies." *EMBO Molecular Medicine* 9 (8): 1067–87. https://doi.org/10.15252/emmm.201707567.

Friedberg, Jonathan W. 2005. "Unique Toxicities and Resistance Mechanisms Associated with Monoclonal Antibody Therapy." *Hematology*, 329–34.

Fu, Yen Rong, Andrew S. Turnell, Simon Davis, Kate J. Heesom, Vanessa C. Evans, and David A. Matthews. 2017. "Comparison of Protein Expression during Wild-Type, and E1B-55k-Deletion, Adenovirus Infection Using Quantitative Time-Course Proteomics." *Journal of General Virology* 98 (6): 1377–88. https://doi.org/10.1099/jgv.0.000781.

Gallmeier, Eike, Dominik C Bader, Lydia Kriegl, Sabina Berezowska, Hendrik Seeliger, Thomas Kirchner, Christiane Bruns, and Enrico N De Toni. 2013. "Loss of TRAIL-Receptors Is a Recurrent Feature in Pancreatic Cancer and Determines the Prognosis of Patients with No Nodal Metastasis after Surgery." *PLoS ONE* 8 (2): 1–10. https://doi.org/10.1371/journal.pone.0056760.

Galloway, Sarah A.E., Garry Dolton, Meriem Attaf, Aaron Wall, Anna Fuller, Cristina Rius, Valentina Bianchi, et al. 2019. "Peptide Super-Agonist Enhances T-Cell Responses to Melanoma." *Frontiers in Immunology* 10: 1–18. https://doi.org/10.3389/fimmu.2019.00319.

Galon, J, A Costes, F Sanchez-Cabo, A Kirilovsky, B Mlecnik, C Lagorce-Pages, M Tosolini, et al. 2006. “Type, Density, and Location of Immune Cells Within Human Colorectal Tumors Predict Clinical Outcome.” *Science* 313: 1960–65.

Gamper, Christopher J, Jonathan D Powell, David K Finlay, and Trinity College. 2012. “All PI3Kinase Signaling Is Not MTOR : Dissecting MTOR-Dependent and Independent Signaling Pathways in T Cells.” *Frontiers in Immunology* 3 (312): 1–11. https://doi.org/10.3389/fimmu.2012.00312.

Ganapathy-Kanniappan, Shanmugasundaram. 2017. “Taming Tumor Glycolysis and Potential Implications for Immunotherapy.” *Frontiers in Oncology* 7 (36): 1–7. https://doi.org/10.3389/fonc.2017.00036.

Ganeshan, Kirthana, and Ajay Chawla. 2014. “Metabolic Regulation of Immune Responses.” *Annual Review of Immunology* 32 (1): 609–34. https://doi.org/10.1146/annurev-immunol-032713-120236.

Garcia-Carbonero, Rocio, Ramon Salazar, Ignacio Duran, Ignacio Osman-Garcia, Luis Paz-Ares, Juan M Bozada, Valentina Boni, et al. 2017. “Phase 1 Study of Intravenous Administration of the Chimeric Adenovirus Enadenotucirev in Patients Undergoing Primary Tumor Resection.” *Journal for ImmunoTherapy of Cancer* 5 (71): 1–13. https://doi.org/10.1186/s40425-017-0277-7.

Garcia, Vanessa, Ramya Krishnan, Colin Davis, Cory Batenchuk, Fabrice Le Boeuf, Hesham Abdelbary, and Jean Simon Diallo. 2014. “High-Throughput Titration of Luciferase-Expressing Recombinant Viruses.” *Journal of Visualized Experiments* 91 (e51890): 1–8. https://doi.org/10.3791/51890.

Garrido, Federico, Natalia Aptsiauri, Elien M Doorduijn, Angel M Garcia Lora, and Thorbald Van Hall. 2016. “The Urgent Need to Recover MHC Class I in Cancers for Effective Immunotherapy.” *Current Opinion in Immunology* 39: 44–51. https://doi.org/10.1016/j.coi.2015.12.007.

Gatenby, Robert A, and Robert J Gillies. 2004. “Why Do Cancers Have High Aerobic Glycolysis?” *Nature Reviews Cancer* 4: 891–99.

Ge, Yan, Haiyan Wang, Jinghua Ren, Weilin Liu, Lingjuan Chen, Hongqi Chen, Junjie Ye, et al. 2020. “Oncolytic Vaccinia Virus Delivering Tethered IL-12 Enhances Antitumor Effects with Improved Safety.” *Journal for ImmunoTherapy of Cancer* 8: 1–8. https://doi.org/10.1136/jitc-2020-000710.

Geiger, Roger, Jan C. Rieckmann, Tobias Wolf, Camilla Basso, Yuehan Feng, Tobias Fuhrer, Maria Kogadeeva, et al. 2016. “L-Arginine Modulates T Cell Metabolism and Enhances Survival and Anti-Tumor Activity.” *Cell* 167 (3): 829-842.e13. https://doi.org/10.1016/j.cell.2016.09.031.

Gibson, Daniel G., Lei Young, Ray Yuan Chuang, J. Craig Venter, Clyde A. Hutchison, and Hamilton O. Smith. 2009. “Enzymatic Assembly of DNA Molecules up to Several Hundred Kilobases.” *Nature Methods* 6 (5): 343–45. https://doi.org/10.1038/nmeth.1318.

Giering, Jeffery C, Dirk Grimm, Theresa A Storm, and Mark A Kay. 2008. “Expression of ShRNA From a Tissue-Specific Pol II Promoter Is an Effective and Safe RNAi Therapeutic.” *Molecular Therapy* 16 (9): 1630–36. https://doi.org/10.1038/mt.2008.144.

Gillies, R J, and Z Bhujwalla. 1994. “31P-MRS Measurements of Extracellular PH of Tumors Using.” *American Journal of Physiology* 267 (1 Pt 1): C195-203.

Gillies, Robert J, Natarajan Raghunand, Gregory S Karczmar, and Zaver M Bhujwalla. 2002. “MRI of the Tumor Microenvironment” 450: 430–50. https://doi.org/10.1002/jmri.10181.

Goveia, Jermaine, Andreas Pircher, Lena-Christin Conradi, Joanna Kalucka, Vincenzo Lagani, Mieke Dewerchin, Guy Eelen, Ralph J DeBerardinis, Ian D Wilson, and Peter Carmeliet. 2016. “Meta-analysis of Clinical Metabolic Profiling Studies in Cancer: Challenges and Opportunities.” *EMBO Molecular Medicine* 8 (10): 1134–42. https://doi.org/10.15252/emmm.201606798.

Gropper, Yael, Tali Feferman, Tali Shalit, Tomer-meir Salame, Ziv Porat, and Guy Shakhar. 2017.

"Culturing CTLs under Hypoxic Conditions Enhances Their Cytolysis and Improves Their Anti-Tumor Function." *CellReports* 20: 2547–55. https://doi.org/10.1016/j.celrep.2017.08.071.

Guedan, Sonia, Juan José Rojas, Alena Gros, Elena Mercade, Manel Cascallo, and Ramon Alemany. 2010. "Hyaluronidase Expression by an Oncolytic Adenovirus Enhances Its Intratumoral Spread and Suppresses Tumor Growth." *Molecular Therapy* 18 (7): 1275–83. https://doi.org/10.1038/mt.2010.79.

Gupta, Gaorav P, and Joan Massagué. 2006. "Cancer Metastasis : Building a Framework." *Cell* 127: 679–95. https://doi.org/10.1016/j.cell.2006.11.001.

Haas, Robert, Joanne Smith, Vidalba Rocher-Ros, Suchita Nadkarni, Trinidad Montero-Melendez, Fulvio D'Acquisto, Elliot J Bland, et al. 2015. "Lactate Regulates Metabolic and Pro-Inflammatory Circuits in Control of T Cell Migration and Effector Functions." *PloS Biology*, 1–24. https://doi.org/10.1371/journal.pbio.1002202.

Haddad, Dana, and Yuman Fong. 2015. "Molecular Imaging of Oncolytic Viral Therapy." *Molecular Therapy — Oncolytics* 1 (14007): 1–8. https://doi.org/10.1038/mto.2014.7.

Han, Ming Zhi, Shuai Wang, Wen Bo Zhao, Shi Lei Ni, Ning Yang, Yang Kong, Bin Huang, et al. 2019. "Immune Checkpoint Molecule Herpes Virus Entry Mediator Is Overexpressed and Associated with Poor Prognosis in Human Glioblastoma." *EBioMedicine* 43: 159–70. https://doi.org/10.1016/j.ebiom.2019.04.002.

Hanahan, Douglas, and Robert A Weinberg. 2011. "Hallmarks of Cancer: The Next Generation." *Cell* 144 (5): 646–74. https://doi.org/10.1016/j.cell.2011.02.013.

Hao, Guanyu, Zhi Ping Xu, and Li Li. 2018. "Manipulating Extracellular Tumour PH: An Effective Target for Cancer Therapy." *RSC Advances* 8: 22182–92. https://doi.org/10.1039/c8ra02095g.

Harlin, Helena, Yuru Meng, Amy C. Peterson, Yuanyuan Zha, Maria Tretiakova, Craig Slingluff, Mark McKee, and Thomas F. Gajewski. 2009. "Chemokine Expression in Melanoma Metastases Associated with CD8 + T-CeII Recruitment." *Cancer Research* 69 (7): 3077–85. https://doi.org/10.1158/0008-5472.CAN-08-2281.

Hemminki, Otto, Suvi Parviainen, Juuso Juhila, Riku Turkki, Nina Linder, Johan Lundin, Matti Kankainen, et al. 2014. "Immunological Data from Cancer Patients Treated with Ad5 / 3-E2F-Δ24-GMCSF Suggests Utility for Tumor Immunotherapy." *Oncotarget* 6 (6): 4467–81.

Henderson, J. W., and A. Brooks. 2010. "Improved Amino Acid Methods Using Agilent ZORBAX Eclipse Plus C18 Columns for a Variety of Agilent LC Instrumentation and Separation Goals." *Agilent Technologies*, 1–16.

Hensley, Christopher T, Ajla T Wasti, and Ralph J DeBerardinis. 2013. "Glutamine and Cancer: Cell Biology, Physiology, and Clinical Opportunities." *The Journal of Clinical Investigation* 123 (9): 3678–84. https://doi.org/10.1172/JCI69600.3678.

Higgins, Jack P, Michael B Bernstein, and James W Hodge. 2009. "Enhancing Immune Responses to Tumor-Associated Antigens." *Cancer Biology and Therapy* 8 (15): 1440–49. https://doi.org/10.4161/cbt.8.15.9133.Enhancing.

Hodi, Stephen, Steven O'Day, David McDermott, and Robert Weber. 2010. "Improved Survival with Ipilimumab in Patients with Metastatic Melanoma." *The New England Journal of Medicine* 363 (8): 711–23.

Holm, Eggert, Ulrich Staedt, Gerwin Schlickeiser, Hans Leweling, Mehmet Tokus, Egbert Hagmüller, Hans Joachim Gtinther, and Hermann B. Kollmar. 1995. "Substrate Balances across Colonic Carcinomas in Humans." *Cancer Research* 55 (6): 1373–78.

Hou, Weizhou, Padma Sampath, Juan J Rojas, and Steve H Thorne. 2016. "Oncolytic Virus-Mediated

Targeting of PGE 2 in the Tumor Alters the Immune Status and Sensitizes Established and Resistant Tumours to Immunotherapy." *Cancer Cell* 30: 108–19. https://doi.org/10.1016/j.ccell.2016.05.012.

Howie, Duncan, and Nicolas Degauque. 2018. "Regulation of the Immune Response by the Inflammatory Metabolic Microenvironment in the Context of Allotransplantation." *Frontiers in Immunology* 9 (1465): 1–11. https://doi.org/10.3389/fimmu.2018.01465.

Huber, Veronica, Chiara Camisaschi, Angela Berzi, Simona Ferro, Luana Lugini, Tiziana Triulzi, Alessandra Tuccitto, Elda Tagliabue, Chiara Castelli, and Licia Rivoltini. 2017. "Cancer Acidity: An Ultimate Frontier of Tumor Immune Escape and a Novel Target of Immunomodulation." *Seminars in Cancer Biology* 43: 74–89. https://doi.org/10.1016/j.semcancer.2017.03.001.

Huehls, Amelia M, Tiffany A Coupet, and Charles L Sentman. 2015. "Bispecific T-Cell Engagers for Cancer Immunotherapy." *Immunology and Cell Biology* 93: 290–96. https://doi.org/10.1038/icb.2014.93.

Iacobelli-Martinez, Milena, Ronald R. Nepomuceno, Jodi Connolly, and Glen R. Nemerow. 2005. "CD46-Utilizing Adenoviruses Inhibit C/EBPβ-Dependent Expression of Proinflammatory Cytokines." *Journal of Virology* 79 (17): 11259–68. https://doi.org/10.1128/jvi.79.17.11259-11268.2005.

Illingworth, Sam, Ying Di, Maxine Bauzon, Janet Lei, Margaret R. Duffy, Simon Alvis, Brian Champion, et al. 2017. "Preclinical Safety Studies of Enadenotucirev, a Chimeric Group B Human-Specific Oncolytic Adenovirus." *Molecular Therapy - Oncolytics* 5: 62–74. https://doi.org/10.1016/j.omto.2017.03.003.

Ippolito, Luigi, Andrea Morandi, Elisa Giannoni, and Paola Chiarugi. 2018. "Lactate: A Metabolic Driver in the Tumour Landscape." *Trends in Biochemical Sciences* 44 (2): 153–66. https://doi.org/10.1016/j.tibs.2018.10.011.

Iqbal, Nida, and Naveed Iqbal. 2014. "Imatinib: A Breakthrough of Targeted Therapy in Cancer." *Hindawi - Chemotherapy Research and Practice* 2014: 1–9.

J Akhenblit, Paul, and Mark D Pagel. 2016. "Recent Advances in Targeting Tumor Energy Metabolism with Tumor Acidosis as a Biomarker of Drug Efficacy." *Journal of Cancer Science & Therapy* 08 (01): 20–29. https://doi.org/10.4172/1948-5956.1000382.

Jin, Hyung-seung, Da-som Choi, Minkyung Ko, Dongkap Kim, Dong-hee Lee, Soojin Lee, Ah Young, et al. 2019. "Extracellular PH Modulating Injectable Gel for Enhancing Immune Checkpoint Inhibitor Therapy." *Journal of Controlled Release* 315: 65–75. https://doi.org/10.1016/j.jconrel.2019.10.041.

Jovčevska, Ivana, and Serge Muyldermans. 2020. "The Therapeutic Potential of Nanobodies." *BioDrugs* 34: 11–26. https://doi.org/10.1007/s40259-019-00392-z.

Jun, Kyong-hwa, Sepideh Gholami, Tae-jin Song, Joyce Au, Dana Haddad, Joshua Carson, Chun-hao Chen, et al. 2014. "A Novel Oncolytic Viral Therapy and Imaging Technique for Gastric Cancer Using a Genetically Engineered Vaccinia Virus Carrying the Human Sodium Iodide Symporter." *Journal of Experimental and Clinical Cancer Research* 33 (2): 1–7.

June, Carl H, and M Sadelain. 2018. "Chimeric Antigen Receptor Therapy." *The New England Journal of Medicine* 379 (1): 64–73. https://doi.org/10.1056/NEJMra1706169.

Kabanova, Anna, Vanessa Zurli, and Cosima Tatiana Baldari. 2018. "Signals Controlling Lytic Granule Polarization at the Cytotoxic Immune Synapse." *Frontiers in Immunology* 9 (307): 1–13. https://doi.org/10.3389/fimmu.2018.00307.

Kakavand, Hojabr, Louise A Jackett, Alexander M Menzies, Tuba N Gide, Matteo S Carlino, Robyn P M Saw, John F Thompson, James S Wilmott, Georgina V Long, and Richard A Scolyer. 2017.

"Negative Immune Checkpoint Regulation by VISTA : A Mechanism of Acquired Resistance to Anti-PD-1 Therapy in Metastatic Melanoma Patients." *Modern Pathology* 30: 1666–76. https://doi.org/10.1038/modpathol.2017.89.

Kantarjian, H, A Stein, N Gokbuget, A Fielding, A Schuh, JM Ribera, A Wei, et al. 2017. "Blinatumomab versus Chemotherapy for Advanced Acute Lymphoblastic Leukemia." *The New England Journal of Medicine* 376 (9). https://doi.org/10.1056/NEJMoa1609783.

Kato, Yasumasa, Shigeyuki Ozawa, Chihiro Miyamoto, Yojiro Maehata, Atsuko Suzuki, and Toyonobu Maeda. 2013. "Acidic Extracellular Microenvironment and Cancer." *Cancer Cell International* 13 (89): 1–8. https://doi.org/10.1186/1475-2867-13-89.

Kaufman, Howard L., Frederick J. Kohlhapp, and Andrew Zloza. 2015. "Oncolytic Viruses: A New Class of Immunotherapy Drugs." *Nature Reviews Drug Discovery* 14 (9): 642–62. https://doi.org/10.1038/nrd4663.

Kazokaitė, Justina, Ashok Aspatwar, Seppo Parkkila, and Daumantas Matulis. 2017. "An Update on Anticancer Drug Development and Delivery Targeting Carbonic Anhydrase IX." *PeerJ* 2017 (11): 1–31. https://doi.org/10.7717/peerj.4068.

Keefe, Dorothy M K, and Emma H Bateman. 2019. "Potential Successes and Challenges of Targeted Cancer Therapies." *Journal of the National Cancer Institute* 2019 (53): 25–29. https://doi.org/10.1093/jncimonographs/lgz008.

Kennedy, Barry E., John Patrick Murphy, Derek R. Clements, Prathyusha Konda, Namit Holay, Youra Kim, Gopal P. Pathak, Michael A. Giacomantonio, Yassine El Hiani, and Shashi Gujar. 2019. "Inhibition of Pyruvate Dehydrogenase Kinase Enhances the Antitumor Efficacy of Oncolytic Reovirus." *Cancer Research* 79 (15): 3824–36. https://doi.org/10.1158/0008-5472.CAN-18-2414.

Kerr, Matthew D, David A Mcbride, Arun K Chumber, and Nisarg J Shah. 2020. "Expert Opinion on Drug Discovery Combining Therapeutic Vaccines with Chemo- and Immunotherapies in the Treatment of Cancer." *Expert Opinion on Drug Discovery*, 1–12. https://doi.org/10.1080/17460441.2020.1811673.

Kim, Ryungsa, Manabu Emi, and Kazuaki Tanabe. 2007. "Cancer Immunoediting from Immune Surveillance to Immune Escape." *Immunology* 121: 1–14. https://doi.org/10.1111/j.1365-2567.2007.02587.x.

Kirn, David H, Yaohe Wang, Fabrice Le Boeuf, John Bell, and Steve H Thorne. 2007. "Targeting of Interferon-Beta to Produce a Specific , Multi-Mechanistic Oncolytic Vaccinia Virus" 4 (12). https://doi.org/10.1371/journal.pmed.0040353.

Kleinberger, Tamar. 2020. "Biology of the Adenovirus E4orf4 Protein: From Virus Infection to Cancer Cell Death." *FEBS Letters* 594: 1891–1917. https://doi.org/10.1002/1873-3468.13704.

Kleinpeter, Patricia, Laetitia Fend, Christine Thioudellet, Michel Geist, Nathalie Sfrontato, Véronique Koerper, Catherine Fahrner, et al. 2016. "Vectorization in an Oncolytic Vaccinia Virus of an Antibody , a Fab and a ScFv against Programmed Cell Death -1 (PD-1) Allows Their Intratumoral Delivery and an Improved Tumor-Growth Inhibition." *OncoImmunology* 5 (10): 1–14. https://doi.org/10.1080/2162402X.2016.1220467.

Kouidhi, Soumaya, Farhat Ben Ayed, and Amel Benammar Elgaaied. 2018. "Targeting Tumor Metabolism: A New Challenge to Improve Immunotherapy." *Frontiers in Immunology* 9 (353): 1–11. https://doi.org/10.3389/fimmu.2018.00353.

Koukourakis, Michael I, Alexandra Giatromanolaki, Adrian L Harris, and Efthimios Sivridis. 2006. "Comparison of Metabolic Pathways between Cancer Cells and Stromal Cells in Colorectal Carcinomas : A Metabolic Survival Role for Tumor-Associated Stroma." *Cancer Researc* 66 (2): 632–38. https://doi.org/10.1158/0008-5472.CAN-05-3260.

Kowalsky, Stacy J, Zuqiang Liu, Mathilde Feist, Sara E Berkey, Congrong Ma, Roshni Ravindranathan, Enyong Dai, Edward J Roy, Zong Sheng Guo, and David L Bartlett. 2018. “Superagonist IL-15-Armed Oncolytic Virus Elicits Potent Antitumor Immunity and Therapy That Are Enhanced with PD-1 Blockade.” *Molecular Therapy* 26 (10): 2476–86. https://doi.org/10.1016/j.ymthe.2018.07.013.

Kuhn, Irene, Paul Harden, Maxine Bauzon, Cecile Chartier, Julie Nye, Steve Thorne, Tony Reid, et al. 2008. “Directed Evolution Generates a Novel Oncolytic Virus for the Treatment of Colon Cancer.” *PLoS ONE* 3 (6): 1–11. https://doi.org/10.1371/journal.pone.0002409.

Kunimasa, Kei, and Taichiro Goto. 2020. “Immunosurveillance and Immunoediting of Lung Cancer: Current Perspectives and Challenges.” *International Journal of Molecular Sciences* 21 (597).

la Cruz-López, Karen G. de, Leonardo Josué Castro-Muñoz, Diego O. Reyes-Hernández, Alejandro García-Carrancá, and Joaquín Manzo-Merino. 2019. “Lactate in the Regulation of Tumor Microenvironment and Therapeutic Approaches.” *Frontiers in Oncology* 9 (1143): 1–21. https://doi.org/10.3389/fonc.2019.01143.

Laconi, Ezio. 2007. “The Evolving Concept of Tumor Microenvironments.” *BioEssays* 29: 738–44. https://doi.org/10.1002/bies.20606.

Lacroix, Ruben, Elisa A Rozeman, Marina Kreutz, Kathrin Renner, and Christian U Blank. 2018. “Targeting Tumor-Associated Acidity in Cancer Immunotherapy.” *Cancer Immunology, Immunotherapy* 67: 1331–48. https://doi.org/10.1007/s00262-018-2195-z.

Lan, Xiuwen, Sen Li, Hongyu Gao, Abiyasi Nanding, Lina Quan, Chunyan Yang, Shaohua Ding, and Yingwei Xue. 2017. “Increased BTLA and HVEM in Gastric Cancer Are Associated with Progression and Poor Prognosis.” *OncoTargets and Therapy* 10: 919–26. https://doi.org/10.2147/OTT.S128825.

Ledford, Heidi. 2015. “Cancer-Fighting Viruses near Market.” *Nature* 526.

Lee, Jaeryun, Deokbae Park, and Youngki Lee. 2017. “Metformin Synergistically Potentiates the Antitumor Effects of Imatinib in Colorectal Cancer Cells.” *Devlopment & Reproduction* 21 (2): 139–50.

Lee, Ji Yun, Inkyoung Lee, Won Jin Chang, Su Min Ahn, Sung Hee Lim, Su Kim, Kwai Han Yoo, et al. 2016. “MCT4 as a Potential Therapeutic Target for Metastatic Gastric Cancer with Peritoneal Carcinomatosis.” *Oncotarget* 7 (28): 43492–503.

Lee, Peter P, Cassian Yee, Peter A Savage, Lawrence Fong, Dirk Brockstedt, Jeffrey S Weber, Denise Johnson, et al. 1999. “Characterization of Circulating T Cells Specific for Tumor- Associated Antigens in Melanoma Patients.” *Nature Medicine* 5 (6): 677–85.

Li, Heliang, Phei Er Saw, and Erwei Song. 2020. “Challenges and Strategies for Next-Generation Bispecific Antibody-Based Antitumor Therapeutics.” *Cellular and Molecular Immunology* 17 (5): 451–61. https://doi.org/10.1038/s41423-020-0417-8.

Li, Jun, Mark O Malley, Julie Urban, Padma Sampath, Z Sheng Guo, Pawel Kalinski, Steve H Thorne, and David L Bartlett. 2011. “Chemokine Expression From Oncolytic Vaccinia Virus Enhances Vaccine Therapies of Cancer.” *Molecular Therapy* 19 (4): 650–57. https://doi.org/10.1038/mt.2010.312.

Lieu, Elizabeth L, Tu Nguyen, Shawn Rhyne, and Jiyeon Kim. 2020. “Amino Acids in Cancer.” *Experimental & Molecular Medicine*, 15–30. https://doi.org/10.1038/s12276-020-0375-3.

Lin, Aifen, and Wei Hua Yan. 2018. “Heterogeneity of HLA-G Expression in Cancers: Facing the Challenges.” *Frontiers in Immunology* 9 (September): 2164. https://doi.org/10.3389/fimmu.2018.02164.

Liu, Y, Y Komohara, N Domenick, M Ohno, M Ikeura, R Hamilton, H Horbinski, X Wang, S Ferrone, and H Okada. 2012. “Expression of Antigen Processing and Presenting Molecules in Brain Metastasis of Breast Cancer.” *Cancer Immunology, Immunotherapy* 61 (6): 789–801. https://doi.org/10.1007/s00262-011-1137-9.Expression.

Liu, Zuqiang, Yan Ge, Haiyan Wang, Congrong Ma, Mathilde Feist, Songguang Ju, Z Sheng Guo, and David L Bartlett. 2018. “Modifying the Cancer-Immune Set Point Using Vaccinia Virus Expressing Re-Designed Interleukin-2.” *Nature Communications* 9 (4682). https://doi.org/10.1038/s41467-018-06954-z.

Liu, Zuqiang, Roshni Ravindranathan, Jun Li, Pawel Kalinski, Z Sheng Guo, David L Bartlett, Zuqiang Liu, et al. 2016. “CXCL11-Armed Oncolytic Poxvirus Elicits Potent Antitumor Immunity and Shows Enhanced Therapeutic Efficacy.” *OncoImmunology* 5 (3): 1–10. https://doi.org/10.1080/2162402X.2015.1091554.

Long, Adrienne H., Waleed M. Haso, Jack F. Shern, Kelsey M. Wanhainen, Meera Murgai, Maria Ingaramo, Jillian P. Smith, et al. 2015. “4-1BB Costimulation Ameliorates T Cell Exhaustion Induced by Tonic Signaling of Chimeric Antigen Receptors.” *Nature Medicine* 21 (6): 581–90. https://doi.org/10.1038/nm.3838.

Lundstrom, Kenneth. 2018. “Viral Vectors in Gene Therapy.” *Diseases* 6 (42): 1–20. https://doi.org/10.3390/diseases6020042.

Ma, Claire Y, John C Marioni, Gillian M Griffiths, and Arianne C Richard. 2020. “Stimulation Strength Controls the Rate of Initiation but Not the Molecular Organisation of TCR-Induced Signalling.” *ELife* 9 (e53948): 1–27.

Ma, Eric H., Glenn Bantug, Takla Griss, Stephanie Condotta, Radia M. Johnson, Bozena Samborska, Nello Mainolfi, et al. 2017. “Serine Is an Essential Metabolite for Effector T Cell Expansion.” *Cell Metabolism* 25 (2): 345–57. https://doi.org/10.1016/j.cmet.2016.12.011.

Ma, J, X He, W Wang, Y Huang, L Chen, W Cong, J Gu, et al. 2009. “E2F Promoter-Regulated Oncolytic Adenovirus with P16 Gene Induces Cell Apoptosis and Exerts Antitumor Effect on Gastric Cancer.” *Digestive Disease And Sciencesnd Sciences*, 1425–31. https://doi.org/10.1007/s10620-008-0543-0.

Machiels, Jean-pascal, Ramon Salazar, Sylvie Rottey, Ignacio Duran, Luc Dirix, Karen Geboes, Christine Wilkinson-blanc, et al. 2019. “A Phase 1 Dose Escalation Study of the Oncolytic Adenovirus Enadenotucirev , Administered Intravenously to Patients with Epithelial Solid Tumors (EVOLVE).” *Journal for ImmunoTherapy of Cancer* 7 (20): 1–15.

Mader, Emily K, Yoshihiro Maeyama, Yi Lin, Greg W Butler, Holly M Russell, Evanthia Galanis, Stephen J Russell, Allan B Dietz, and Kah-whye Peng. 2009. “Mesenchymal Stem Cell Carriers Protect Oncolytic Measles Viruses from Antibody Neutralization in an Orthotopic Ovarian Cancer Therapy Model.” *Clinical Cancer Research* 15 (23): 7246–56. https://doi.org/10.1158/1078-0432.CCR-09-1292.

Marcus, Assaf, Benjamin G Gowen, Thornton W Thompson, Alexandre Iannello, Michele Ardolino, Weiwen Deng, Lin Wang, Nataliya Shifrin, and David H Raulet. 2014. “Recognition of Tumors by the Innate Immune System and Natural Killer Cells.” *Advances in Immunology* 122: 91–128. https://doi.org/10.1016/B978-0-12-800267-4.00003-1.Recognition.

Marelli, Giulia, Anwen Howells, Nicholas R Lemoine, and Yaohe Wang. 2018. “Oncolytic Viral Therapy and the Immune System: A Double-Edged Sword Against Cancer.” *Frontiers in Immunology* 9 (866): 1–8. https://doi.org/10.3389/fimmu.2018.00866.

Maroun, Justin, Miguel Muñoz-Alía, Arun Ammayappan, Autumn Schulze, Kah Whye Peng, and Stephen Russell. 2017. “Designing and Building Oncolytic Viruses.” *Future Virology* 12 (4): 193–213. https://doi.org/10.2217/fvl-2016-0129.

Martens, Alexander, Kilian Wistuba-Hamprecht, Marnix Geukes Foppen, Jianda Yuan, Michael A Postow, Phillip Wong, Emanuela Romano, et al. 2016. “Baseline Peripheral Blood Biomarkers Associated with Clinical Outcome of Advanced Melanoma Patients Treated with Ipilimumab.” *Clinical Cancer Research* 22 (12): 2908–18. https://doi.org/10.1158/1078-0432.CCR-15-2412.

Martin, G Ray, and Rakesh K Jain. 1994. “Noninvasive Measurement of Interstitial PH Profiles in Normal and Neoplastic Tissue Using Fluorescence Ratio Imaging Microscopy.” *Cancer Research* 54: 5670–74.

Martinez-Outschoorn, Ubaldo E, Maria Peiris-Pagés, Richard G Pestell, Federica Sotgia, and Michael P Lisanti. 2016. “Cancer Metabolism: A Therapeutic Perspective.” *Nature Reviews. Clinical Oncology*, no. May: 1–21. https://doi.org/10.1038/nrclinonc.2016.60.

Mckee, Trevor D, Paola Grandi, Wilson Mok, George Alexandrakis, Numpon Insin, John P Zimmer, Moungi G Bawendi, Yves Boucher, Xandra O Breakefield, and Rakesh K Jain. 2006. “Degradation of Fibrillar Collagen in a Human Melanoma Xenograft Improves the Efficacy of an Oncolytic Herpes Simplex Virus Vector.” *Cancer Research* 66 (5): 2509–14. https://doi.org/10.1158/0008-5472.CAN-05-2242.

Medema, J P, J De Jong, L T C Peltenburg, E M E Verdegaal, A Gorter, S A Bres, K L M C Franken, et al. 2001. “Blockade of the Granzyme B ¯Perforin Pathway through Overexpression of the Serine Protease Inhibitor PI-9/SPI-6 Constitutes a Mechanism for Immune Escape by Tumors.” *PNAS* 98 (20): 11515–20.

Meerten, Tom van, Rozemarijn S van Rijn, Samantha Hol, Anton Hagenbeek, and Saskia B Ebeling. 2006. “Complement-Induced Cell Death by Rituximab Depends on CD20 Expression Level and Acts Complementary to Antibody-Dependent Cellular Cytotoxicity Cancer Therapy : Preclinical Complement-Induced Cell Death by Rituximab Depends on CD20 Expression Level and Act.” *Clinical Cancer Research* 12 (13): 4027–35. https://doi.org/10.1158/1078-0432.CCR-06-0066.

Melero, Ignacio, David M Berman, M Angela Aznar, Alan J Korman, Jose Gracia, and John Haanen. 2015. “Evolving Synergistic Combinations of Targeted Immunotherapies to Combat Cancer.” *Nature Publishing Group* 15 (August): 457–72. https://doi.org/10.1038/nrc3973.

Mendler, Anna N., Bin Hu, Petra U. Prinz, Marina Kreutz, Eva Gottfried, and Elfriede Noessner. 2012. “Tumor Lactic Acidosis Suppresses CTL Function by Inhibition of P38 and JNK/c-Jun Activation.” *International Journal of Cancer* 131 (3): 633–40. https://doi.org/10.1002/ijc.26410.

Meng, Gang, Binghua Li, Anxian Chen, Meihong Zheng, Tiancheng Xu, Hailin Zhang, Jie Dong, Junhua Wu, Decai Yu, and Jiwu Wei. 2019. “Targeting Aerobic Glycolysis by Dichloroacetate Improves Newcastle Disease Virus-Mediated Viro-Immunotherapy in Hepatocellular Carcinoma.” *British Journal of Cancer*, December. https://doi.org/10.1038/s41416-019-0639-7.

Michl, Johanna, Kyung Chan Park, and Pawel Swietach. 2019. “Evidence-Based Guidelines for Controlling PH in Mammalian Live-Cell Culture Systems.” *Communications Biology* 2 (1): 1–12. https://doi.org/10.1038/s42003-019-0393-7.

Mikhail Binnewies, Edward W. Roberts, Kelly Kersten, Vincent Chan, Douglas F. Fearon, Miriam Merad, Lisa M. Coussens, et al. 2018. “Understanding the Tumor Immune Microenvironment (TIME) for Effective Therapy.” *Nature Medicine* 24 (5): 541–50. https://doi.org/10.1038/s41591-018-0014-x.Understanding.

Mittal, Deepak, Matthew M Gubin, Robert D Schreiber, and Mark J Smyth. 2014. “ScienceDirect New Insights into Cancer Immunoediting and Its Three Component Phases — Elimination , Equilibrium and Escape.” *Current Opinion in Immunology* 27: 16–25. https://doi.org/10.1016/j.coi.2014.01.004.

Mølgaard, Kasper, Seandean L Harwood, Marta Compte, Nekane Merino, Jaume Bonet, Ana Alvarez, Cienfuegos Kasper, et al. 2018. “Bispecific Light T-Cell Engagers for Gene-Based

Immunotherapy of Epidermal Growth Factor Receptor (EGFR) -Positive Malignancies." *Cancer Immunology, Immunotherapy* 67 (8): 1251–60. https://doi.org/10.1007/s00262-018-2181-5.

Molon, Barbara, Bianca Calì, and Antonella Viola. 2016. "T Cells and Cancer: How Metabolism Shapes Immunity." *Frontiers in Immunology* 7 (20): 1–7. https://doi.org/10.3389/fimmu.2016.00020.

Moore, Chris B, Elizabeth H Guthrie, Max Tze-han Huang, and Debra J Taxman. 2010. "Short Hairpin RNA (ShRNA): Design, Delivery, and Assessment of Gene Knockdown." *Methods in Molecular Biology* 629: 141–58. https://doi.org/10.1007/978-1-60761-657-3.

Moore, George E, Robert E Gerner, and H Addison Franklin. 1967. "Culture of Normal Human Leukocytes." *The Journal of the American Medical Association* 199 (8).

Morton, Helen J. 1970. "A Survey of Commercially Available Tissue Culture Media." *In Vitro* 6: 89–108.

Munn, David H., and Andrew L. Mellor. 2016. "IDO in the Tumor Microenvironment: Inflammation, Counter-Regulation, and Tolerance." *Trends in Immunology* 37 (3): 193–207. https://doi.org/10.1016/j.it.2016.01.002.

Munn, David H, and Andrew L Mellor. 2007. "Indoleamine-2,3-Dioxygenase and Tumor-Induced Tolerance." *The Journal of Clinical Investigation* 117 (5): 1147–54. https://doi.org/10.1172/JCI31178.effects.

Muñoz-Alvarez, Kim A, Jennifer Altomonte, Iina Laitinen, Sibylle Ziegler, Katja Steiger, Irene Esposito, Roland M Schmid, and Oliver Ebert. 2015. "PET Imaging of Oncolytic VSV Expressing the Mutant HSV-1 Thymidine Kinase Transgene in a Preclinical HCC Rat Model." *Molecular Therapy* 23 (4): 728–36. https://doi.org/10.1038/mt.2015.12.

Murakami, Pete, and Michael T. McCaman. 1999. "Quantitation of Adenovirus DNA and Virus Particles with the Picogreen Fluorescent Dye." *Analytical Biochemistry* 274 (2): 283–88. https://doi.org/10.1006/abio.1999.4282.

Nakajima, Erica C, and Bennett Van Houten. 2013. "Metabolic Symbiosis in Cancer: Refocusing the Warburg Lens." *Molecular Carcinogenesis* 52: 329–37. https://doi.org/10.1002/mc.21863.

O'Shea, Clodagh, Kristina Klupsch, Serah Choi, Bridget Bagus, Conrado Soria, Jerry Shen, Frank McCormick, and David Stokoe. 2005. "Adenoviral Proteins Mimic Nutrient/Growth Signals to Activate the MTOR Pathway for Viral Replication." *The EMBO Journal* 24 (6): 1211–21. https://doi.org/10.1038/sj.emboj.7600597.

Offner, Sonja, Robert Hofmeister, Andrea Romaniuk, Peter Kufer, and Patrick A Baeuerle. 2006. "Induction of Regular Cytolytic T Cell Synapses by Bispecific Single-Chain Antibody Constructs on MHC Class I-Negative Tumor Cells." *Molecular Immunology* 43: 763–71. https://doi.org/10.1016/j.molimm.2005.03.007.

Oishi, Motoi, Shogo Sumitani, and Yukio Nagasaki. 2007. "On-off Regulation of 19F Magnetic Resonance Signals Based on PH-Sensitive PEGylated Nanogels for Potential Tumor-Specific Smart 19F MRI Probes." *Bioconjugate Chemistry* 18 (5): 1379–82. https://doi.org/10.1021/bc7002154.

Pandha, H, A Rigg, J John, and N Lemoine. 2007. "Loss of Expression of Antigen-Presenting Molecules in Human Pancreatic Cancer and Pancreatic Cancer Cell Lines." *Clinical and Experimental Immunology* 148: 127–35. https://doi.org/10.1111/j.1365-2249.2006.03289.x.

Parato, Kelley A, Caroline J Breitbach, Fabrice Le Boeuf, Jiahu Wang, Chris Storbeck, Carolina Ilkow, Jean-simon Diallo, et al. 2012. "The Oncolytic Poxvirus JX-594 Selectively Replicates in and Destroys Cancer Cells Driven by Genetic Pathways Commonly Activated in Cancers." *Molecular Therapy* 20 (4): 749–58. https://doi.org/10.1038/mt.2011.276.

Patel, Manish R, Blake A Jacobson, Yan Ji, Jeremy Drees, Shaogeng Tang, Kerry Xiong, Hengbing Wang, et al. 2015. “Vesicular Stomatitis Virus Expressing Interferon-β Is Oncolytic and Promotes Antitumor Immune Responses in a Syngeneic Murine Model of Non-Small Cell Lung Cancer.” *Oncotarget* 6 (32): 33165–77.

Patgiri, Anupam, Owen S. Skinner, Yusuke Miyazaki, Grigorij Schleifer, Eizo Marutani, Hardik Shah, Rohit Sharma, et al. 2020. “An Engineered Enzyme That Targets Circulating Lactate to Alleviate Intracellular NADH:NAD+ Imbalance.” *Nature Biotechnology* 38 (3): 309–13. https://doi.org/10.1038/s41587-019-0377-7.

Patil, Sandeep S, Ivaylo Gentschev, Marion Adelfinger, Ulrike Donat, Michael Hess, Stephanie Weibel, Ingo Nolte, Alexa Frentzen, and Aladar A Szalay. 2012. “Virotherapy of Canine Tumors with Oncolytic Vaccinia Virus GLV-1h109 Expressing an Anti-VEGF Single-Chain Antibody.” *PLoS ONE* 7 (10): e47472. https://doi.org/10.1371/journal.pone.0047472.

Paul Chubb, S. A., and Robin A. Williams. 2018. “Biochemical Analysis of Pleural Fluid and Ascites.” *Clinical Biochemist Reviews* 39 (2): 39–50.

Pearce, Erika L., and Edward J. Pearce. 2013. “Metabolic Pathways in Immune Cell Activation and Quiescence.” *Immunity* 38 (4): 633–43. https://doi.org/10.1016/j.immuni.2013.04.005.

Persi, Erez, Miquel Duran-Frigola, Mehdi Damaghi, William R. Roush, Patrick Aloy, John L. Cleveland, Robert J. Gillies, and Eytan Ruppin. 2018. “Systems Analysis of Intracellular PH Vulnerabilities for Cancer Therapy.” *Nature Communications* 9 (1). https://doi.org/10.1038/s41467-018-05261-x.

Phillips, Melissa M., Michael T. Sheaff, and Peter W. Szlosarek. 2013. “Targeting Arginine-Dependent Cancers with Arginine-Degrading Enzymes: Opportunities and Challenges.” *Cancer Research and Treatment* 45 (4): 251–62. https://doi.org/10.4143/crt.2013.45.4.251.

Pilon-Thomas, Shari, Krithika N. Kodumudi, Asmaa E. El-Kenawi, Shonagh Russell, Amy M. Weber, Kimberly Luddy, Mehdi Damaghi, et al. 2016. “Neutralization of Tumor Acidity Improves Antitumor Responses to Immunotherapy.” *Cancer Research* 76 (6): 1381–90. https://doi.org/10.1158/0008-5472.CAN-15-1743.

Polanski, Radoslaw, Cassandra L Hodgkinson, Alberto Fusi, Daisuke Nonaka, Lynsey Priest, Paul Kelly, Francesca Trapani, et al. 2014. “Activity of the Monocarboxylate Transporter 1 Inhibitor AZD3965 in Small Cell Lung Cancer.” *Clinical Cancer Research* 20 (4): 926–37. https://doi.org/10.1158/1078-0432.CCR-13-2270.

Pollard, Roy, and Jeffrey W. 2015. “Tumor-Associated Macrophages : From Mechanisms to Therapy.” *Immunity*. 41 (1): 49–61. https://doi.org/10.1016/j.immuni.2014.06.010.Tumor-associated.

Pollizzi, Kristen N, and Jonathan D Powell. 2015. “Regulation of T Cells by MTOR : The Known Knowns and the Known Unknowns.” *Trends in Immunology* 36 (1): 13–20. https://doi.org/10.1016/j.it.2014.11.005.

Prussin, Calman, and Dean D. Metcalfe. 1995. “Detection of Intracytoplasmic Cytokine Using Flow Cytometry and Directly Conjugated Anti-Cytokine Antibodies.” *Journal of Immunological Methods* 188 (1): 117–28. https://doi.org/10.1016/0022-1759(95)00209-X.

Purbhoo, Marco A., Darrell J. Irvine, Johannes B. Huppa, and Mark M. Davis. 2004. “T Cell Killing Does Not Require the Formation of a Stable Mature Immunological Synapse.” *Nature Immunology* 5 (5): 524–30. https://doi.org/10.1038/ni1058.

Purbhoo, Marco A, Deborah H Sutton, Joanna E Brewer, Rebecca E Mullings, Maxine E Hill, Tara M Mahon, Julia Karbach, et al. 2006. “Quantifying and Imaging NY-ESO-1/LAGE-1-Derived Epitopes on Tumor Cells Using High Affinity T Cell Receptors.” *The Journal of Immunology* 176: 7308–16. https://doi.org/10.4049/jimmunol.176.12.7308.

Pusapati, Raju V., Anneleen Daemen, Catherine Wilson, Wendy Sandoval, Min Gao, Benjamin Haley, Andreas R. Baudy, Georgia Hatzivassiliou, Marie Evangelista, and Jeff Settleman. 2016. "MTORC1-Dependent Metabolic Reprogramming Underlies Escape from Glycolysis Addiction in Cancer Cells." *Cancer Cell* 29 (4): 548–62. https://doi.org/10.1016/J.CCELL.2016.02.018.

Qin, Shuang, Linping Xu, Ming Yi, Shengnan Yu, Kongming Wu, and Suxia Luo. 2019. "Novel Immune Checkpoint Targets : Moving beyond PD-1 and CTLA-4." *Molecular Cancer* 18 (155): 1–14.

Ramamonjisoa, Nirilanto, and Ellen Ackerstaff. 2017. "Characterization of the Tumor Microenvironment and Tumor – Stroma Interaction by Non-Invasive Preclinical Imaging." *Frontiers in Oncology* 7 (3): 1–22. https://doi.org/10.3389/fonc.2017.00003.

Randtke, Edward A, Jeffry C Granados, Christine M Howison, Mark D Pagel, and Julio Cardenas-Rodriguez. 2017. "Multislice CEST MRI Improves the Spatial Assessment of Tumor PH." *Magnetic Resonance in Medicine* 78 (1): 97–106. https://doi.org/10.1002/mrm.26348.Multislice.

Ranganathan, Punithavathi, Arulkumaran Shanmugam, Daniel Swafford, Amol Suryawanshi, Pushpak Bhattacharjee, Mohamed S. Hussein, Pandelakis A. Koni, et al. 2018. "GPR81, a Cell-Surface Receptor for Lactate, Regulates Intestinal Homeostasis and Protects Mice from Experimental Colitis." *The Journal of Immunology*, ji1700604. https://doi.org/10.4049/jimmunol.1700604.

Ravishankar, Buvana, Lavanya Adusumilli, Deepa Pookot Pookot, Emily Hunag, Raashi Sreenivasan, Lisa Marshall, Deepika Kaveri, et al. 2019. "Targeting the Stress Response Kinase GCN2 to Restore Immunity in the Tumor Microenvironment." In *Proceedings of the American Association for Cancer Research Annual Meeting 2019; 2019 Mar 29-Apr 3; Atlanta, GA. Philadelphia (PA): AACR; Cancer Res*. Vol. 79. https://doi.org/DOI: 10.1158/1538-7445.AM2019-1104.

Ray, Kevin J., Manon A. Simard, James R. Larkin, James Coates, Paul Kinchesh, Sean C. Smart, Geoff S. Higgins, Michael A. Chappell, and Nicola R. Sibson. 2019. "Tumor PH and Protein Concentration Contribute to the Signal of Amide Proton Transfer Magnetic Resonance Imaging." *Cancer Research* 79 (7): 1343–52. https://doi.org/10.1158/0008-5472.CAN-18-2168.

Reina-Campos, Miguel, Jorge Moscat, and Maria Diaz-Meco. 2017. "Metabolism Shapes the Tumor Microenvironment." *Current Opinion in Cell Biology* 48: 47–53. https://doi.org/10.1016/j.ceb.2017.05.006.

Renner, Kathrin, Katrin Singer, Gudrun E Koehl, Edward K Geissler, Katrin Peter, Peter J Siska, and Marina Kreutz. 2017. "Metabolic Hallmarks of Tumor and Immune Cells in the Tumor Microenvironment." *Frontiers in Immunology* 8 (March): 1–11. https://doi.org/10.3389/fimmu.2017.00248.

Rescigno, Maria, Francesca Avogadri, and Giuseppe Curigliano. 2007. "Challenges and Prospects of Immunotherapy as Cancer Treatment." *Biochimica et Biophysica Acta 1776*, 108–23. https://doi.org/10.1016/j.bbcan.2007.07.003.

Reznik, Ed, Augustin Luna, Bülent Arman Aksoy, Eric Minwei Liu, Konnor La, Irina Ostrovnaya, Chad J. Creighton, A. Ari Hakimi, and Chris Sander. 2018. "A Landscape of Metabolic Variation across Tumor Types." *Cell Systems* 6 (3): 301-313.e3. https://doi.org/10.1016/j.cels.2017.12.014.

Richard, Arianne C., Aaron T.L. Lun, Winnie W.Y. Lau, Berthold Göttgens, John C. Marioni, and Gillian M. Griffiths. 2018. "T Cell Cytolytic Capacity Is Independent of Initial Stimulation Strength." *Nature Immunology* 19 (8): 849–58. https://doi.org/10.1038/s41590-018-0160-9.

Rivadeneira, Dayana B., Kristin DePeaux, Yiyang Wang, Aditi Kulkarni, Tracy Tabib, Ashley V. Menk, Padmavathi Sampath, et al. 2019. "Oncolytic Viruses Engineered to Enforce Leptin Expression Reprogram Tumor-Infiltrating T Cell Metabolism and Promote Tumor Clearance." *Immunity* 51 (3): 548-560.e4. https://doi.org/10.1016/j.immuni.2019.07.003.

Robey, Ian F, Brenda K Baggett, Nathaniel D Kirkpatrick, Denise J Roe, Julie Dosescu, Bonnie F Sloane, Arig Ibrahim Hashim, et al. 2009. "Bicarbonate Increases Tumor PH and Inhibits Spontaneous Metastases." *Cancer Research* 69 (6): 2260–68. https://doi.org/10.1158/0008-5472.CAN-07-5575.

Rofstad, Einar K, Berit Mathiesen, Kristil Kindem, and Kanthi Galappathi. 2006. "Acidic Extracellular PH Promotes Experimental Metastasis of Human Melanoma Cells in Athymic Nude Mice." *Cancer Research* 66 (13): 6699–6708. https://doi.org/10.1158/0008-5472.CAN-06-0983.

Romero-Garcia, Susana, Jose Sullivan Lopez-Gonzalez, José Luis Báez-Viveros, Dolores Aguilar-Cazares, and Heriberto Prado-Garcia. 2011. "Tumor Cell Metabolism An Integral View." *Cancer Biology and Therapy* 12 (11): 939–48.

Romero-Garcia, Susana, María Maximina B. Moreno-Altamirano, Heriberto Prado-Garcia, and Francisco Javier Sánchez-García. 2016. "Lactate Contribution to the Tumor Microenvironment: Mechanisms, Effects on Immune Cells and Therapeutic Relevance." *Frontiers in Immunology* 7 (FEB). https://doi.org/10.3389/fimmu.2016.00052.

Rosenberg, Steven A, James C Yang, Richard M Sherry, Udai S Kammula, Marybeth S Hughes, Giao Q Phan, Deborah E Citrin, et al. 2011. "Durable Complete Responses in Heavily Pretreated Patients with Metastatic Melanoma Using T-Cell Transfer Immunotherapy." *Clinical Cancer Research* 17 (13): 4550–58. https://doi.org/10.1158/1078-0432.CCR-11-0116.

Roy, Dominic Guy, Theresa Falls, Kwame Twumasi-boateng, Lauren Elizabeth St-germain, Monique Marguerie, Vanessa Garcia, Mohammed Selman, et al. 2016. "Oncolytic Vesicular Stomatitis Virus Expressing Interferon- γ Has Enhanced Therapeutic Activity." *Official Journal of the American Society of Gene & Cell Therapy* 3 (December 2015): 16001. https://doi.org/10.1038/mto.2016.1.

Russell, Luke, and Kah-Whye Peng. 2018. "The Emerging Role of Oncolytic Virus Therapy against Cancer." *Physiology & Behavior* 7 (2): 139–48. https://doi.org/10.1016/j.physbeh.2017.03.040.

Rutzky, Lynn P, and Robert W Pumper. 1974. "Supplement to a Survey of Commercially Available Tissue Culture Media (1970)." *In Vitro* 9: 468–69.

Salmon, Héléne, and Emmanuel Donnadieu. 2012. "Within Tumors, Interactions between T Cells and Tumor Cells Are Impeded by the Extracellular Matrix." *OncoImmunology* 1 (6): 992–94. https://doi.org/10.4161/onci.20239.

Sarbassov, Dos D., David A. Guertin, Siraj M. Ali, and David M. Sabatini. 2005. "Phosphorylation and Regulation of Akt/PKB by the Rictor-MTOR Complex." *Science* 307 (5712): 1098–1101. https://doi.org/10.1126/science.1106148.

Saxton, Robert A., and David M. Sabatini. 2017. "MTOR Signaling in Growth, Metabolism, and Disease." *Cell* 168 (6): 960–76. https://doi.org/10.1016/j.cell.2017.02.004.

Schäfer, Simon, Stephanie Weibel, Ulrike Donat, Qian Zhang, Richard J Aguilar, Nanhai G Chen, and Aladar A Szalay. 2012. "Vaccinia Virus-Mediated Intra-Tumoral Expression of Matrix Metalloproteinase 9 Enhances Oncolysis of PC-3 Xenograft Tumors." *BMC Cancer* 12 (366): 1–9. https://doi.org/10.1186/1471-2407-12-366.

Scheubeck, Gabriel, Susanne Berchtold, Irina Smirnow, Andrea Schenk, Julia Beil, and Ulrich M. Lauer. 2019. "Starvation-Induced Differential Virotherapy Using an Oncolytic Measles Vaccine Virus." *Viruses* 11 (7): 614. https://doi.org/10.3390/v11070614.

Schodin, Beth A., Theodore J. Tsomides, and David M. Kranz. 1996. "Correlation between the Number of T Cell Receptors Required for T Cell Activation and TCR-Ligand Affinity." *Immunity* 5 (2): 137–46. https://doi.org/10.1016/S1074-7613(00)80490-2.

Scott, E.M., S. Frost, H. Khalique, J.D. Freedman, L.W. Seymour, and J. Lei-Rossman. 2020. "Use of

Liquid Patient Ascites Fluids as a Preclinical Model for Oncolytic Virus Activity. In: Engeland C. (Eds) Oncolytic Viruses." In *Methods in Molecular Biology*, 2058:261–70. https://doi.org/10.1038/nrc948.

Scott, E, M Duffy, J Freedman, K D Fisher, and L W Seymour. 2017. "Solid Tumor Immunotherapy with T Cell Engager-Armed Oncolytic Viruses." *Macromolecular Bioscience* 1700187: 1–10. https://doi.org/10.1002/mabi.201700187.

Scott, Eleanor M, Egon J Jacobus, Brian Lyons, Sally Frost, Joshua D Freedman, Arthur Dyer, Hena Khalique, et al. 2019. "Bi- and Tri-Valent T Cell Engagers Deplete Tumour-Associated Macrophages in Cancer Patient Samples." *Journal for ImmunoTherapy of Cancer* 7 (320): 1–18.

Setten, Ryan L, John J Rossi, and Si-ping Han. 2019. "The Current State and Future Directions of RNAi-Based Therapeutics." *Nature Reviews Drug Discovery* 18 (June): 421–46. https://doi.org/10.1038/s41573-019-0017-4.

Seymour, Leonard W, and Kerry D Fisher. 2016. "Oncolytic Viruses: Finally Delivering." *British Journal of Cancer* 114: 1–5. https://doi.org/10.1038/bjc.2015.481.

Shen, Wei, Chun-yi Wang, Xue-hu Wang, and Zhong-xue Fu. 2009. "Oncolytic Adenovirus Mediated Survivin Knockdown by RNA Interference Suppresses Human Colorectal Carcinoma Growth in Vitro and in Vivo." *Journal of Experimental and Clinical Cancer Research* 28 (81): 1–11. https://doi.org/10.1186/1756-9966-28-81.

Shi, Tao, Xueru Song, Yue Wang, Fangcen Liu, and Jia Wei. 2020. "Combining Oncolytic Viruses With Cancer Immunotherapy: Establishing a New Generation of Cancer Treatment." *Frontiers in Immunology* 11 (April): 1–13. https://doi.org/10.3389/fimmu.2020.00683.

Sierra, J Rafael, Virna Cepero, and Silvia Giordano. 2010. "Molecular Mechanisms of Acquired Resistance to Tyrosine Kinase Targeted Therapy." *Molecular Cancer* 9 (75): 1–13.

Silva, Ariosto S, Jose A Yunes, Robert J Gillies, and Robert A Gatenby. 2009. "The Potential Role of Systemic Buffers in Reducing Intratumoral Extracellular PH and Acid-Mediated Invasion." *Cancer Rese* 69 (6): 2677–84. https://doi.org/10.1158/0008-5472.CAN-08-2394.

Sirena, Dominique, Benjamin Lilienfeld, Markus Eisenhut, Stefan Kälin, Karin Boucke, Roger R. Beerli, Lorenz Vogt, et al. 2004. "The Human Membrane Cofactor CD46 Is a Receptor for Species B Adenovirus Serotype 3." *Journal of Virology* 78 (9): 4454–62. https://doi.org/10.1128/jvi.78.9.4454-4462.2004.

Sivanandam, Venkatesh, Christopher J Larocca, Nanhai G Chen, Yuman Fong, and Susanne G Warner. 2019. "Oncolytic Viruses and Immune Checkpoint Inhibition : The Best of Both Worlds." *Molecular Therapy: Oncolytics* 13 (June): 93–106. https://doi.org/10.1016/j.omto.2019.04.003.

Sluis, Robert Van, Zaver M Bhujwalla, Natarajan Raghunand, Paloma Ballesteros, Jose Alvarez, Sebastian Cerdan, Jean-Philippe Galons, and Robert J Gillies. 1999. "In Vivo Imaging of Extracellular PH Using 1 H MRSI." *Magnetic Resonance in Medicine* 41: 743–50.

Small, Eric J, Michael A Carducci, James M Burke, Ron Rodriguez, Lawrence Fong, Lynn Van Ummersen, D C Yu, et al. 2006. "A Phase I Trial of Intravenous CG7870 , a Replication-Selective, Prostate-Specific Antigen-Targeted Oncolytic Adenovirus, for the Treatment of Hormone-Refractory, Metastatic Prostate Cancer." *Molecular Therapy* 14 (1): 107–17. https://doi.org/10.1016/j.ymthe.2006.02.011.

Smith-Garvin, Jennifer E, Gary A Koretzky, and Martha S Jordan. 2009. "T Cell Activation." *Annu. Rev. Immunol* 27: 591–619. https://doi.org/10.1146/annurev.immunol.021908.132706.T.

Sonveaux, Pierre, Olivier Feron, Mark W Dewhirst, Pierre Sonveaux, Frédérique Végran, Thies Schroeder, Melanie C Wergin, et al. 2008. "Targeting Lactate-Fueled Respiration Selectively Kills Hypoxic Tumor Cells in Mice Find the Latest Version : Targeting Lactate-Fueled Respiration

Selectively Kills Hypoxic Tumor Cells in Mice." *The Journal of Clinical Investigation* 118 (12): 3930–42. https://doi.org/10.1172/JCI36843.however.

Srivastava, Minu K., Pratima Sinha, Virginia K. Clements, Paulo Rodriguez, and Suzanne Ostrand-Rosenberg. 2010. "Myeloid-Derived Suppressor Cells Inhibit T-Cell Activation by Depleting Cystine and Cysteine." *Cancer Research* 70 (1): 68–77. https://doi.org/10.1158/0008-5472.CAN-09-2587.

Stern, Robert, Svetlana Shuster, Birgit A. Neudecker, and Bent Formby. 2002. "Lactate Stimulates Fibroblast Expression of Hyaluronan and CD44: The Warburg Effect Revisited." *Experimental Cell Research* 276 (1): 24–31. https://doi.org/10.1006/excr.2002.5508.

Svoboda, Petr. 2014. "Renaissance of Mammalian Endogenous RNAi." *FEBS Letters* 588: 2550–56.

Talmadge, James E. 2007. "Clonal Selection of Metastasis within the Life History of a Tumor." *Cancer Research* 67 (24): 11471–76. https://doi.org/10.1158/0008-5472.CAN-07-2496.

Tanaka, Atsushi, and Shimon Sakaguchi. 2017. "Regulatory T Cells in Cancer Immunotherapy." *Cell Research* 27 (1): 109–18. https://doi.org/10.1038/cr.2016.151.

Tannock, Ian F., and Daniela Rotin. 1989. "Acid PH in Tumors and Its Potential for Therapeutic Exploitation." *Cancer Research* 49 (16): 4373–84.

Tau, Gregory Z, Simone N Cowan, Jeffrey Weisburg, Ned S Braunstein, and Paul B Rothman. 2001. "Regulation of IFN-γ Signaling Is Essential for the Cytotoxic Activity of CD8+ T Cells." *Physiology & Behavior* 167 (10): 5574–82.

Teng, Michele W L, Jeremy B Swann, Catherine M Koebel, Robert D Schreiber, and Mark J Smyth. 2008. "Immune-Mediated Dormancy: An Equilibrium with Cancer." *Journal of Leukocyte Biology* 84: 988–93. https://doi.org/10.1189/jlb.1107774.

Thai, Minh, Shivani K. Thaker, Jun Feng, Yushen Du, Hailiang Hu, Ting Ting Wu, Thomas G. Graeber, Daniel Braas, and Heather R. Christofk. 2015. "MYC-Induced Reprogramming of Glutamine Catabolism Supports Optimal Virus Replication." *Nature Communications* 6 (8873): 1–9. https://doi.org/10.1038/ncomms9873.

Theaker, Sarah M, Cristina Rius, Alexander Greenshields-watson, Angharad Lloyd, Andrew Trimby, Anna Fuller, John J Miles, et al. 2016. "T-Cell Libraries Allow Simple Parallel Generation of Multiple Peptide-Specific Human T-Cell Clones." *Journal of Immunological Methods* 430: 43–50. https://doi.org/10.1016/j.jim.2016.01.014.

ThermoFisher Scientific. 2020. "Factors Influencing Transfection Efficiency." 2020. https://www.thermofisher.com/uk/en/home/references/gibco-cell-culture-basics/transfection-basics/factors-influencing-transfection-efficiency.html.

Thistlethwaite, Alan I, Dennis B Leeper, David J Moylan III, and Rudolph E Nerlinger. 1985. "PH Distribution in Human Tumors." *International Journal of Radiation Oncology, Biology and Physics* 11: 1647–52.

Thurber, Greg M, Stefan C Zajic, and K Dane Wittrup. 2007. "Theoretic Criteria for Antibody Penetration into Solid Tumors and Micrometastases." *The Journal of Nuclear Medicine* 48 (6): 995–1000. https://doi.org/10.2967/jnumed.106.037069.

Toniatti, Carlo, Philip Jones, Hilary Graham, Bruno Pagliara, and Giulio Draetta. 2014. "Oncology Drug Discovery: Planning a Turnaround." *Cancer Discovery* 4 (4): 397–404. https://doi.org/10.1158/2159-8290.CD-13-0452.

Topalian, Suzanne L, Linda M Muul, Diane Solomon, and Steven A Rosenberg. 1987. "Expansion of Human Tumor Infiltrating Lymphocytes for Use in Immunotherapy Trials." *Journal of Immunological Methods* 102 (1): 127–41. https://doi.org/10.1016/S0022-1759(87)80018-2.

Trickett, Annette, and Yiu Lam Kwan. 2003. “T Cell Stimulation and Expansion Using Anti-CD3 / CD28 Beads.” *Journal of Immunological Methods* 275: 251–55. https://doi.org/10.1016/S0022-1759(03)00010-3.

Tsang, Julia Y.S., Kit Wing Chan, Yun Bi Ni, Thazin Hlaing, Jintao Hu, Siu Ki Chan, Sai Yin Cheung, and Gary M. Tse. 2017. “Expression and Clinical Significance of Herpes Virus Entry Mediator (HVEM) in Breast Cancer.” *Annals of Surgical Oncology* 24 (13): 4042–50. https://doi.org/10.1245/s10434-017-5924-1.

Turtle, Cameron J, Laïla-aïcha Hanafi, Carolina Berger, Theodore A Gooley, Sindhu Cherian, Michael Hudecek, Daniel Sommermeyer, et al. 2016. “CD19 CAR – T Cells of Defined CD4+: CD8+ Composition in Adult B Cell ALL Patients.” *The Journal of Clinical Investigation* 126 (6): 2123–38. https://doi.org/10.1172/JCI85309.modified.

Uusi-kerttula, Hanni, James A Davies, Jill M Thompson, Phonphimon Wongthida, Laura Evgin, Kevin G Shim, Angela Bradshaw, et al. 2018. “Ad5NULL-A20: A Tropism-Modified, Avb6 Integrin-Selective Oncolytic Adenovirus for Epithelial Ovarian Cancer Therapies.” *Clinical Cancer Research* 24 (17): 4215–25. https://doi.org/10.1158/1078-0432.CCR-18-1089.

Va, Amy L, B Biddlecombe, William M Spees, Joel R Garbow, Dayanjali Wijesinghe, Oleg A Andreev, Donald M Engelman, Yana K Reshetnyak, and Jason S Lewis. 2009. “A Novel Technology for the Imaging of Acidic Prostate Tumors by Positron Emission Tomography.” *Cancer Research* 69 (10): 4510–17. https://doi.org/10.1158/0008-5472.CAN-08-3781.

Vaupel, P, F Kallinowski, and P Okunieff. 1989. “Blood Flow, Oxygen and Nutrient Supply, and Metabolic Microenvironment of Human Tumors: A Review.” *Cancer Research* 49 (23): 6449–65. http://www.ncbi.nlm.nih.gov/pubmed/2684393.

Vavere, Amy L., Gráinne B. Biddlecombe, William M. Spees, Joel R. Garbow, Dayanjali Wijesinghe, Oleg A. Andreev, Donald M. Engelman, Yana K. Reshetnyak, and Jason S. Lewis. 2009. “A Novel Technology for the Imaging of Acidic Prostate Tumors by Positron Emission Tomography.” *Cancer Research* 69 (10): 4510–16. https://doi.org/10.1158/0008-5472.CAN-08-3781.

Vegran, F, R Boidot, C Michiels, P Sonveaux, and O Feron. 2011. “Lactate Influx through the Endothelial Cell Monocarboxylate Transporter MCT1 Supports an NF- k B / IL-8 Pathway That Drives Tumor Angiogenesis.” *Molecular and Cellular Pathobiology* 71 (7): 2550–60. https://doi.org/10.1158/0008-5472.CAN-10-2828.

Velde, Lee-Ann Van de, Xi-Zhi J Guo, Lidija Barbaric, Amber M Smith, Thomas H Ogiun III, Paul G Thomas, and Peter J Murray. 2016. “Stress Kinase GCN2 Controls the Proliferative Fitness and Trafficking of Cytotoxic T Cells Independent of Environmental Amino Acid Sensing.” *Cell Reports* 17 (9): 2247–58.

Vettore, Lisa, Rebecca L Westbrook, and Daniel A Tennant. 2020. “New Aspects of Amino Acid Metabolism in Cancer.” *British Journal of Cancer* 122: 150–56. https://doi.org/10.1038/s41416-019-0620-5.

Vijayakumar, Gayathri, Stephen McCroskery, and Peter Palese. 2019. “Engineering Newcastle Disease Virus as an Oncolytic Vector for Intratumoral Delivery of Immune Checkpoint Inhibitors and Immunocytokines.” *Journal of Virology* 94 (3): 1–14. https://doi.org/10.1128/jvi.01677-19.

Vilalta, M, M Rafat, and E Graves. 2016. “Effects of Radiation on Metastasis and Tumor Cell Migration.” *Cellular and Molecular Life Sciences* 73 (16): 2999–3007.

Vučetić, Milica, Yann Cormerais, Scott K. Parks, and Jacques Pouysségur. 2017. “The Central Role of Amino Acids in Cancer Redox Homeostasis: Vulnerability Points of the Cancer Redox Code.” *Frontiers in Oncology* 7 (December). https://doi.org/10.3389/fonc.2017.00319.

Waickman, Adam T, and Jonathan D Powell. 2012. “MTOR, Metabolism, and the Regulation of T-Cell

Differentiation and Function." *Immunological Reviews* 249: 43–58.

Walenta, Stefan, and Wolfgang F Mueller-Klieser. 2004. "Lactate : Mirror and Motor of Tumor Malignancy." *Seminars in Radiation Oncology* 14 (3): 267–74. https://doi.org/10.1016/j.semradonc.2004.04.004.

Walenta, Stefan, Michael Wetterling, Michael Lehrke, Georg Schwickert, Kolbein Sundfør, Einar K. Rofstad, and Wolfgang Mueller-Klieser. 2000. "High Lactate Levels Predict Likelihood of Metastases, Tumor Recurrence, and Restricted Patient Survival in Human Cervical Cancers." *Cancer Research* 60 (4): 916–21.

Walton, Zandra E., Chirag H. Patel, Rebekah C. Brooks, Yongjun Yu, Arig Ibrahim-Hashim, Malini Riddle, Alessandra Porcu, et al. 2018. "Acid Suspends the Circadian Clock in Hypoxia through Inhibition of MTOR." *Cell* 174 (1): 72-87.e32. https://doi.org/10.1016/j.cell.2018.05.009.

Wang, Bi Yun, Jian Zhang, Jia Lei Wang, Si Sun, Zhong Hua Wang, Lei Ping Wang, Qun Ling Zhang, et al. 2015. "Intermittent High Dose Proton Pump Inhibitor Enhances the Antitumor Effects of Chemotherapy in Metastatic Breast Cancer." *Journal of Experimental and Clinical Cancer Research* 34 (1): 1–12. https://doi.org/10.1186/s13046-015-0194-x.

Wang, Hongjie, Zongyi Li, Ying Liu, Jonas Persson, Ines Beyer, Thomas Möller, Dilara Koyuncu, et al. 2011. "Desmoglein 2 Is a Receptor for Adenovirus Serotypes 3, 7, 11, and 14." *Nature Medicine* 17 (1): 96–104. https://doi.org/10.1038/nm.2270.Desmoglein.

Wang, Ziyu, Xunlong Shi, Yubin Li, Xian Zeng, Jiajun Fan, Yun Sun, Zongshu Xian, et al. 2014. "Involvement of Autophagy in Recombinant Human Arginase-Induced Cell Apoptosis and Growth Inhibition of Malignant Melanoma Cells." *Applied Microbiology and Biotechnology* 98 (6): 2485–94. https://doi.org/10.1007/s00253-013-5118-0.

Warburg, Otto. 1956. "On the Origin of Cancer Cells." *Science* 123 (3191): 309–14. https://doi.org/10.1126/science.123.3191.309.

Warner, Susanne G, Sang-in Kim, Shyambabu Chaurasiya, Michael P O Leary, Jianming Lu, Venkatesh Sivanandam, Yanghee Woo, Nanhai G Chen, and Yuman Fong. 2019. "A Novel Chimeric Poxvirus Encoding HNIS Is Tumor-Tropic , Imageable , and Synergistic with Radioiodine to Sustain Colon Cancer Regression." *Molecular Therapy: Oncolytics* 13 (June): 82–92. https://doi.org/10.1016/j.omto.2019.04.001.

Watanabe, Akiharu, Toshihiro Higashi, Tatsuro Sakata, and Hideo Nagashima. 1984. "Serum Amino Acid Levels in Patients With Hepatocellular Carcinoma." *Cancer* 54: 1875–82.

Webb, Bradley A, Michael Chimenti, Matthew P Jacobson, and Diane L Barber. 2011. "Dysregulated PH: A Perfect Storm for Cancer Progression." *Nature Publishing Group* 11 (September): 671–77. https://doi.org/10.1038/nrc3110.

Weerakkody, Dhammika, Anna Moshnikova, Mak S. Thakur, Valentina Moshnikova, Jennifer Daniels, Donald M. Engelman, Oleg A. Andreev, and Yana K. Reshetnyak. 2013. "Family of PH (Low) Insertion Peptides for Tumor Targeting." *PNAS* 110 (15): 5834–39. https://doi.org/10.1073/pnas.1303708110.

Wei, Jun, Jana Raynor, Thanh Long M. Nguyen, and Hongbo Chi. 2017. "Nutrient and Metabolic Sensing in T Cell Responses." *Frontiers in Immunology* 8 (247): 1–14. https://doi.org/10.3389/fimmu.2017.00247.

Wei, Spencer C, Colm R Duffy, and James P Allison. 2018. "Fundamental Mechanisms of Immune Checkpoint Blockade Therapy." *Cancer Discovery*, 1–18. https://doi.org/10.1158/2159-8290.CD-18-0367.

Wei, Zhe-wei, Jing Wu, Wei-bin Huang, Jin Li, Xiao-fang Lu, Yu-jie Yuan, Wen-jun Xiong, et al. 2020. "Immune-Infiltration Based Signature as a Novel Prognostic Biomarker in Gastrointestinal

Stromal Tumour." *EBioMedicine* 57: 102850. https://doi.org/10.1016/j.ebiom.2020.102850.

Weide, Benjamin, Alexander Martens, Jessica C Hassel, Carola Berking, Michael A Postow, Kees Bisschop, Ester Simeone, et al. 2016. "Baseline Biomarkers for Outcome of Melanoma Patients Treated with Pembrolizumab." *Clinical Cancer Research* 22 (22): 5487–96. https://doi.org/10.1158/1078-0432.CCR-16-0127.

Weitzman, Matthew D., and David A. Ornelles. 2005. "Inactivating Intracellular Antiviral Responses during Adenovirus Infection." *Oncogene* 24 (52): 7686–96. https://doi.org/10.1038/sj.onc.1209063.

Whiteside, Theresa L, Sandra Demaria, Maria E Rodriguez-Ruiz, Hassane M Zarour, and Ignacio Melero. 2016. "Emerging Opportunities and Challenges in Cancer Immunotherapy." *Clinical Cancer Research* 22 (8): 1845–55. https://doi.org/10.1158/1078-0432.CCR-16-0049.

Wise, David R., Ralph J. Deberardinis, Anthony Mancuso, Nabil Sayed, Xiao Yong Zhang, Harla K. Pfeiffer, Ilana Nissim, et al. 2008. "Myc Regulates a Transcriptional Program That Stimulates Mitochondrial Glutaminolysis and Leads to Glutamine Addiction." *PNAS* 105 (48): 18782–87. https://doi.org/10.1073/pnas.0810199105.

Wolf, Evelyn, Robert Hofmeister, Peter Kufer, Bernd Schlereth, and Patrick A Baeuerle. 2005. "BiTEs: Bispecific Antibody Constructs with Unique Anti-Tumor Activity." *Drug Discovery Today* 10 (18): 1237–44.

Wolint, Petra, Michael R. Betts, Richard A. Koup, and Annette Oxenius. 2004. "Immediate Cytotoxicity but Not Degranulation Distinguishes Effector and Memory Subsets of CD8+ T Cells." *Journal of Experimental Medicine* 199 (7): 925–36. https://doi.org/10.1084/jem.20031799.

Wong, P., H. W. Kleemann, and I. F. Tannock. 2002. "Cytostatic Potential of Novel Agents That Inhibit the Regulation of Intracellular PH." *British Journal of Cancer* 87 (2): 238–45. https://doi.org/10.1038/sj.bjc.6600424.

Wu, Hao, Veronica Estrella, Matthew Beatty, Dominique Abrahams, Asmaa El-kenawi, Shonagh Russell, Arig Ibrahim-hashim, et al. 2020. "T-Cells Produce Acidic Niches in Lymph Nodes to Suppress Their Own Effector Functions." *Nature Communications* 11 (4113): 1–13. https://doi.org/10.1038/s41467-020-17756-7.

Wu, Hao, Minfeng Ying, and Xun Hu. 2016. "Lactic Acidosis Switches Cancer Cells from Aerobic Glycolysis Back to Dominant Oxidative Phosphorylation." *Oncotarget* 7 (26): 40621–29. https://doi.org/10.18632/oncotarget.9746.

Xiao, Zhengtao, Jason W. Locasale, and Ziwei Dai. 2020. "Metabolism in the Tumor Microenvironment: Insights from Single-Cell Analysis." *OncoImmunology* 9 (1). https://doi.org/10.1080/2162402X.2020.1726556.

Xu, W, T Neill, Y Yang, Z Hu, E Cleveland, Y Wu, R Hutten, et al. 2015. "The Systemic Delivery of an Oncolytic Adenovirus Expressing Decorin Inhibits Bone Metastasis in a Mouse Model of Human Prostate Cancer." *Gene Therapy* 22: 247–56. https://doi.org/10.1038/gt.2014.110.

Yang, Ming, Chun Sheng, Wenwen Guo, Jianqin Tang, Qian Huang, Shouxin Feng, Aijun Jiang, XiFeng Xu, Guan Jiang, and Yan Qun Liu. 2017. "A Novel Fiber Chimeric Conditionally Replicative Adenovirus-Ad5/F35 for Tumor Therapy." *Cancer Biology and Therapy* 18 (11): 833–40.

Yang, Yuefeng, Weidong Xu, Di Peng, Hao Wang, Xiaoyan Zhang, Hua Wang, Fengjun Xiao, et al. 2019. "An Oncolytic Adenovirus Targeting Transforming Growth Factor b Inhibits Protumorigenic Signals and Produces Immune Activation : A Novel Approach to Enhance Anti-PD-1 and Anti-CTLA-4 Therapy." *Human Gene Therapy* 30 (9): 1117–33. https://doi.org/10.1089/hum.2019.059.

Yao, Tatsuma, and Yuta Asayama. 2017. "Animal-Cell Culture Media: History, Characteristics, and

Current Issues." *Reproductive Medicine and Biology* 16 (2): 99–117. https://doi.org/10.1002/rmb2.12024.

Yao, Xiaosai, Myriam Labelle, Carla R Lamb, John M Dugan, Christina A Williamson, Donna R Spencer, Kimberly R Christ, et al. 2013. "Determination of 35 Cell Surface Antigen Levels in Malignant Pleural Effusions Identifies CD24 as a Marker of Disseminated Tumor Cells." *International Journal of Cancer* 133 (12): 2925–33. https://doi.org/10.1002/ijc.28312.Determination.

Yu, Feng, Xingbing Wang, Z Sheng Guo, David L Bartlett, Stephen M Gottschalk, and Xiao-tong Song. 2014. "T-Cell Engager-Armed Oncolytic Vaccinia Virus Significantly Enhances Antitumor Therapy." *Molecular Therapy* 22 (1): 102–11. https://doi.org/10.1038/mt.2013.240.

Zhang, Lan, and Shengmian Li. 2020. "Lactic Acid Promotes Macrophage Polarization through MCT-HIF1α Signaling in Gastric Cancer." *Experimental Cell Research* 388 (2): 111846. https://doi.org/10.1016/j.yexcr.2020.111846.

Zhao, L, A Dong, J Gu, Z Liu, Y Zhang, W Zhang, Y Wang, et al. 2006. "The Antitumor Activity of TRAIL and IL-24 with Replicating Oncolytic Adenovirus in Colorectal Cancer." *Cancer Gene Therapy* 13: 1011–22. https://doi.org/10.1038/sj.cgt.7700969.

Zheng, Jun-Nian, Dong-Sheng Pei, Fang-Hao Sun, Bao-Fu Zhang, JXin-Yuan Liu, Jin-Fa Gu, Yan-Hua Liu, et al. 2009. "Inhibition of Renal Cancer Cell Growth by Oncolytic Adenovirus Armed Short Hairpin RNA Targeting HTERT Gene." *Cancer Biology and Therapy* 8 (1): 1–8. https://doi.org/10.4161/cbt.8.1.7204.

Zheng, Meijun, Jianhan Huang, Aiping Tong, and Hui Yang. 2019. "Oncolytic Viruses for Cancer Therapy: Barriers and Recent Advances." *Molecular Therapy - Oncolytics* 15 (37): 234–47. https://doi.org/10.1016/j.omto.2019.10.007.

Zheng, Yan, Greg M Delgoffe, Christian F Meyer, Waipan Chan, and Jonathan D Powell. 2009. "Anergic T Cells Are Metabolically Anergic." *Journal of Immunology Research* 183 (10): 6095–6101. https://doi.org/10.4049/jimmunol.0803510. Epub 2009 Oct 19.

Zhou, Yi, Feng Wen, Pengfei Zhang, Ruilei Tang, and Qiu Li. 2016. "Vesicular Stomatitis Virus Is a Potent Agent for the Treatment of Malignant Ascites." *Oncology Reports* 35 (3): 1573–81. https://doi.org/10.3892/or.2015.4522.